SURFACE CHEMICAL AND PHYSICAL BEHAVIOR

OF CHRYSOTILE ASBESTOS IN

NATURAL WATERS AND WATER TREATMENT

Thesis by

Roger Curtis Bales

In Partial Fulfillment of the Requirements

for the Degree of

Doctor of Philosophy

California Institute of Technology

Pasadena, California

1985

(Submitted June 12, 1984)

ACKNOWLEDGEMENTS

iv

District of Southern California facilitated work in the field and
provided important analytical support through their laboratory.
Various individuals at James M. Montgomery freely shared their
knowledge and resources.

My wife, Rebecca Bales, arranged her life to provide me with the
maximum freedom to pursue my studies. With her devotion, pursuing a
thesis program while maintaining spiritual and social health were
possible.

Generous financial support to Caltech and to this research were
provided by the Andrew W. Mellon Foundation through a grant to
Caltech's Environmental Quality Laboratory, and by The Metropolitan
Water District of Southern California. A portion of the Metropolitan
grant was given through the American Water Works Association Research
Foundation.

ABSTRACT

Chrysotile asbestos fibers enter California waters from physical weathering of magnesium-silicate, serpentine rocks in mountains of the northern and central portions of the state. Chrysotile particles, initially positively charged below pH 8.9 because of their magnesium-hydroxide surface, become negatively charged due to dissolution and adsorption of organic matter. Magnesium release from chrysotile dissolving in 0.1 M inorganic electrolyte at pH 7-10 for up to five days is in excess of the 3:2 Mg:Si to silica molar ratio in the solid. The magnesium release rate exhibits a fractional dependence on hydrogen-ion concentration:

$$r = k_1' [H^+]^{0.24}$$

The observed rate constant, k_1', depends on dissolution mechanism, specific surface area of the solid and charge-potential relation at the surface. In terms of a surface site-binding model, the fractional dependence implies that dissolution is limited by a chemical reaction involving less than one adsorbed proton per magnesium ion released. Silica release shows no clear pH dependence.

The rate of magnesium release is independent of the anions NO_3^-, Cl^-, SO_4^{2-}, HCO_3^-, oxalate or catechol. Oxalate inhibited and catechol slightly enhanced silica release at pH 7.5-8.5; other anions had no systematic effect. Chrysotile's dissolution rate ($10^{-15.7}$ mol/cm$^2 \cdot$s at pH 8) is consistent with observations on other magnesium silicates and brucite.

Catechol adsorption onto chrysotile or aluminum oxide (pH 7.5-8.5) does not reach equilibrium but increases over five days. After one day the maximum adsorption density (Langmuir adsorption equation) on chrysotile is 0.7×10^{-9} mol/cm^2 (50×10^{-6} mg C/cm^2), approximately one-third of the estimated density for proton exchange. The maximum adsorption density for natural organic matter was near 30×10^{-6} mg C/cm^2 on both chrysotile and aluminum oxide.

Chrysotile adsorbs sufficient natural organic matter within one day to reverse its surface charge. The extent of reversal is larger than observed on aluminum oxide, because of selective dissolution of chrysotile's outer magnesium-hydroxide layer.

In reservoirs, submicron-sized chrysotile particles coagulate with larger (>2 μm), negatively-charged particles that subsequently settle out. The rate at which freshly-suspended, positively-charged fibers coagulate is at least ten-fold greater than the rate for aged, negatively-charged fibers coagulate. Capture of chrysotile particles in water filtration is enhanced 10-fold or more by incorporating fibers into larger flocs.

TABLE OF CONTENTS

LIST OF FIGURES

LIST OF TABLES

CHAPTER 1

INTRODUCTION

The purpose of the research work described in this thesis is to
develop a better understanding of the chemical behavior and the
influence of surface chemistry on the physical behavior of chrysotile
asbestos particles in natural waters and in water-treatment processes.
Chrysotile particles suspended in lakes and rivers undergo
dissolution, adsorb organic and inorganic ions from solution, and
coagulate with other suspended matter. In water treatment, these
particles also adsorb dissolved ions, serve as nucleation sites for
added coagulant chemicals, coagulate with other particles and deposit
onto sand filter grains. The rate and extent of each of these
processes depends on chemical reactions that occur on the particle
surface. The work described here applies recent developments from the
surface chemistry of well-defined, model systems to a particle of
potential interest in environmental health and engineering.

1.1. MOTIVATION TO STUDY CHRYSOTILE

1.1.1. Asbestos in Drinking Water

Asbestos is found in drinking water as a result of natural
weathering of rocks and soil and due to corrosion of asbestos-cement
pipe. Chrysotile fiber concentrations in the range of 10^8 fibers/L
have been consistently found in drinking waters in Everett, Washington
(Polissar, et al. 1982), California, (Cooper et al., 1978, 1979;
Hayward, 1984), Thetford Mines, Quebec (Lawrence & Zimmermann, 1976)
and Beine Verte, Newfoundland (Toft et al., 1981). Fiber levels above

10^6/L have been found in over 80 of 426 water supplies surveyed in the U.S. (Millette et al., 1979; 1980).

There is no direct evidence to confirm or deny a link between ingestion of water-borne asbestos and disease in humans. However, elevated risks for lung cancer, mesothelioma and gastrointestinal (GI) cancers among occupational groups exposed to high levels of airborne fibers are well documented (Selikoff et al., 1979; Newhouse & Berry, 1979; McDonald & Liddell, 1979; Michaels & Chissick, 1979). Asbestos-related diseases are the leading cause of death among some of these occupational groups. From 13-18 percent of U.S. cancer deaths are asbestos related (Lemen et al., 1980). Although the pathogenesis of asbestos-related disorders such as pleural disease, lung fibrosis and cancer is in general not known, recent medical evidence suggests that asbestos exposure may stimulate or alter certain responses of the immune system (Miller et al., 1983).

An increased incidence of GI cancer due to asbestos inhalation is thought to be directly related to the clearing of fibers from airways and subsequent ingestion. The increased incidence among asbestos workers of peritoneal mesothelioma, a cancer of the lining of the abdomen, is thought to be caused by fibers penetrating intestinal walls. These indirect suggestions that ingested fibers cause disease in humans provide a basis for water-quality concerns (NRC, 1977).

A recent evaluation of dose-response data for GI cancer from inhaled asbestos concluded that drinking water containing 0.11×10^6 fibers/L (adult men) and 0.17×10^6 fibers/L (adult women) may lead to one excess GI-tract cancer per 100,000 persons exposed over a lifetime of 70 years (NRC, 1983). The committee also analyzed epidemiological

studies of groups exposed to asbestos in drinking water and concluded that their estimates of risk are compatible with the results of the studies. However, the expected risks are below levels that can be statistically detected from available data. The committee also concluded that there was no basis for selective regulation based on fiber size. Neither is there a basis for different regulations based on mineral identity. All types of asbestos have been shown to cause high incidences of cancer in humans (IARC, 1977). Although evidence is inconclusive, some investigators have suggested that relative risks for contracting lung cancer from inhaled asbestos fibers may decrease in going from crocidolite to amosite to chrysotile (Walton, 1982).

1.1.2. <u>Chrysotile Minerology</u>

The term "asbestos" is applied to two chemically and structurally different classes of naturally-occurring fibrous silicate minerals that are important for their high strengths and fire resistance -- amphiboles and serpentines. Amphiboles are inosilicates (chain silicates) and form crystals by repeat of the chains -- make of silica and oxides of iron, magnesium, calcium and sodium -- in two directions. Fibers form by shearing small bundles of chains parallel to the chain axis. Serpentine minerals are phyllosilicates (layer silicates); crystals form by repeated alternate stacking of the infinite magnesium-hydroxide and silica sheets. A mismatch in the lattice dimensions between the magnesium-hydroxide and silica sheets that combine to make each layer results in a curved rather than a flat crystal. Ionic substitution, particularly in the octahedral magnesium-hydroxide sheet, may also relieve strain caused by this mismatch (Wicks & Whittaker, 1975). Each layer is electrically

neutral and adjacent layers are held together by van der Waals forces (Hurlbut & Klein, 1977). Hydrogen bonding may also develop between adjacent layers.

Chrysotile fibers can be thought of as about 40 layers of spiral or concentric tubes, as illustrated on Figure 1.1. Of the serpentine minerals (chrysotile, lizardite and antigorite) only chrysotile is commonly fibrous. Not all chrysotile is fibrous, however, and some fibrous material may be antigorite (Wicks, 1979). Antigorite typically forms a wave, corrugated sheet and lizardite forms a flat planar sheet in crystals. The chemical formula for serpentine is $Mg_3Si_2O_5(OH)_4$.

High-resolution electron microscopy observations of one synthetic and five natural chrysotile samples showed fiber diameters ranging from 10-60 nm, depending on conditions of growth (Yada, 1971, 1979). Coalinga, California fiber diameters were log-normally distributed with a mean outer dimension of 280 nm; inner diameter was 8 nm. Both concentric and spiral layer structures were common. Yada (1971) also noted that outer surfaces of fibers in raw ore were generally smooth and clean, suggesting that in fiber bundles, inter-fiber sites are void. Filling of chrysotile fiber centers is uncertain, and thought to be variable (Wicks, 1979a).

In California, serpentine minerals are found primarily in magnesium-silicate ultramafic rocks. Ultramafic rocks form elongate bodies within and adjacent to major fault zones of the Sierra-Nevada foothills; the most abundant component of these bodies is serpentine (Clark, 1960). Large ultramafic bodies are also found in the coastal mountains. The chrysotile deposit of largest commercial importance is
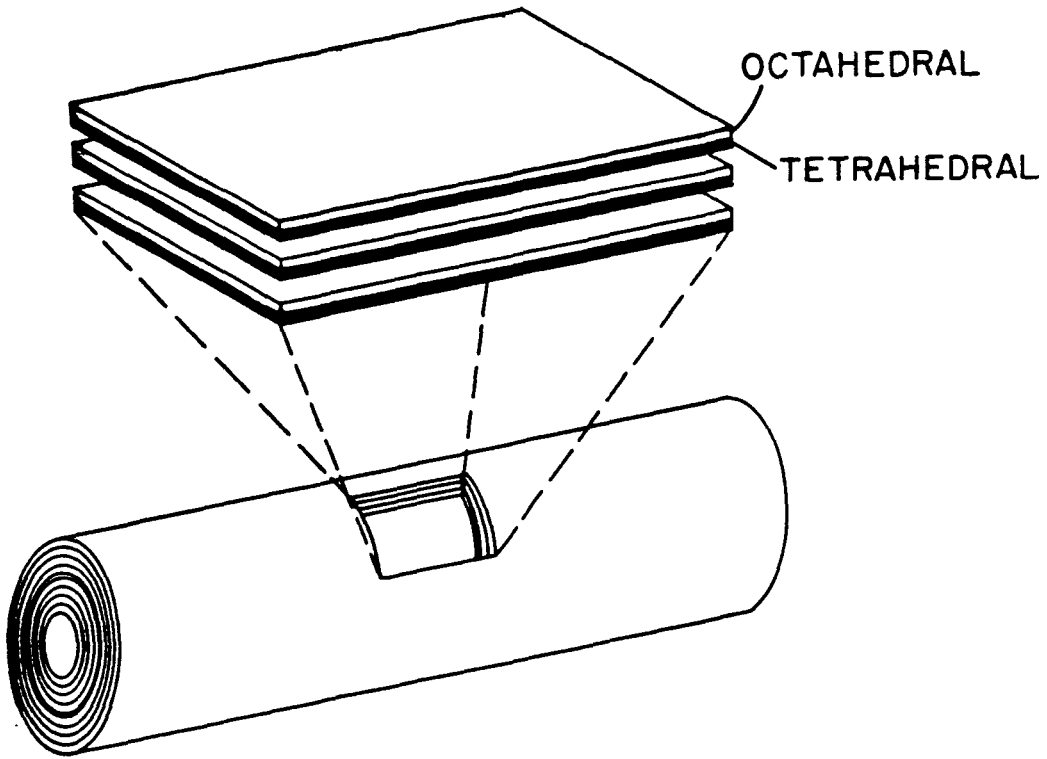
Fig. 1.1. Chrysotile fiber, concentric layer structure; each layer has an outer octahedral sheet of magnesium hydroxide and an inner tetrahedral silica sheet.

in the coastal mountains of central California, near Coalinga (New Idria area).

Asbestos forms other than chrysotile are less common in the Sierra Nevada and the mountains of the Pacific coast, but may be found associated with ultramafics as well. Brucite may occur in fibrous form intimately associated with chrysotile or as platey irregular grains.

The highly-sheared chrysotile ore found in the New Idria area consists of friable masses of matted chrysotile surrounding other rock fragments (Mumpton & Thompson, 1975). The latter associated minerals are most commonly lizardite, brucite and magnetite in these alpine-type ultramafics (Coleman 1971). Most other chrysotile ores consist of veins within massive serpentine rock. Fiber length depends on source. For example, fibers from Globe, Arizona or Quebec may reach several millimeters in length. Those from New Idria are shorter, up to a few microns in length. Recoverable fiber in the New Idria ore is 35-75 percent; in most ores containing veins of chrysotile it is less than ten percent. Chrysotile deposits in the Klamath mountains commonly consist of a small zone of closely-spaced veins up to one inch thick. Fibers are oriented perpendicular to vein walls (Albers, 1966). Antigorite is the predominant serpentine type in other areas in the mountains of California, with little or no lizardite and chrysotile present (Coleman, 1971; Springer, 1974; Olmstead, 1971). However, it has been recently suggested that the majority of California's serpentine rocks are composed of lizardite only or lizardite plus chrysotile (Moody, 1976; Evans, 1977).

The chrysotile content of the principally serpentine, ultramafic areas in California varies from near zero to 100 percent. Ultramafic bodies vary in area from a few square meters to several square kilometers. Most serpentine in California contains insufficient chrysotile to warrant mining. Historically, most mining claims contained less than five percent recoverable chrysotile in the serpentine ore (Rice, 1957), the notable exception being chrysotile in the New Idria area (Wiebelt & Smith, 1959). Essentially all serpentine contains some chrysotile. Thus as noted by Wicks (1979a) and others, naturally-occurring chrysotile will be found in soils, streams and lakes in many localities.

1.1.3. Chrysotile in California Surface Waters

Chrysotile asbestos fibers are introduced into surface waters having their origin in the coastal mountains and western slopes of the Sierra Nevada as a result of natural weathering of the serpentine rock. Tributaries of nearly all the rivers in the northern and central portion of the state that flow to the Pacific ocean or into the Central valley pass through serpentine. Observed and predicted fiber concentrations below major reservoirs range from 10^{10}-10^{11}/L in the northern coast and western Sacramento-valley reservoirs to concentrations on the order of 10^8-10^{10}/L in the Sierra-foothill reservoirs (Table 1.1). Fiber concentrations in water passing through source-water reservoirs of The Metropolitan Water District of Southern California (Metropolitan) decrease as an exponential function of time. For example, the approximate one year of detention in lake Perris on the east branch of the California aquaduct provides a one-log removal of fibers; the three years of

Table 1.1 Summary of fiber concentrations in California surface waters[a].

	Conc. leaving, fibers/ℓ	
Location	Predicted	Observed
North Coast Rivers	10^{11}-10^{12}	10^{11}
Northern & Western Sacramento Valley Rivers	10^9 -10^{11}	10^{10}
Eastern Sacramento Valley Rivers	10^9 -10^{10}	10^8-10^9
Eastern San Joaquin Valley Rivers	0 - 10^9	10^7
Delta Pumping Plants	10^9- 10^{10}	10^8-10^9
California Aqueduct	10^8- 10^{10}	10^9
Metropolitan Source-water	10^6- 10^9	10^6-10^9
Metropolitan Water-treatment Plants	10^5- 10^7	10^5-10^7

[a]Adapted from Bales et al., 1984 (Appendix VI).

detention in lakes Pyramid and Castaic on the west branch provides a three-log removal. These observations are taken from a recent analysis of chrysotile fiber distribution in major surface waters tributary to the California aqueduct and to Metropolitan's water treatment plants (Bales et al., 1984). Other recent reports give concentrations in selected waters of the state (Hayward, 1984; McGuire et al., 1982, 1983; Farrell & Qualley, 1982; Cooper et al., 1978, 1979).

In water filtration, fiber removal depends on particle size and thus on the extent to which fibers coagulate with added chemicals. Approximately two-log removal results for the low coagulant doses (3-5 mg/L alum) used at Metropolitan's water treatment plants.

1.2. SCOPE AND OBJECTIVES

Specific objectives of this work relate to both water-quality engineering and water chemistry. The underlying assumption in this relation is that a better understanding of the basic surface-chemical reactions on chrysotile will contribute to both better insight into the environmental fate of these particles and a better control over particle removal in engineered systems. These objectives are:

1. Determine experimentally the rates at which magnesium and silica are released from the chrysotile surface during dissolution.

2. Interpret the dissolution in terms of coordination-chemical reactions occurring at the surface -- adsorption of protons and adsorption of ligands -- and the accompanying shifts in magnesium-hydroxide versus silica character of the surface.

3. Infer whether or not the observed dissolution behavior of chrysotile is consistent with rates reported for other oxides and silicates, and with suggested dissolution mechanisms.

4. Determine the extent to which adsorption of major inorganic anions found in natural waters influences the dissolution rate and surface charge of chrysotile.

5. Determine the effect on surface charge of adsorbing model organics and natural organic matter onto aged chrysotile particles and onto an aluminum oxide surface.

6. Relate the extent of adsorption and surface-charge development on chrysotile to the rate at which these submicron-sized fibers coagulate with larger particles.

7. Verify experimentally, under a limited set of well-defined conditions, the coagulation efficiency of chrysotile with larger, silica particles.

The scope involves four levels of investigation -- literature review, model calculations, laboratory experiments and field investigations. Primary emphasis is on experimental work supported by model calculations aimed toward meeting the above objectives. The latter level, field investigations, is to better define actual behavior of chrysotile particles in the systems of interest.

CHAPTER 2

BACKGROUND

2.1. MOLECULAR MODEL OF SURFACE

2.1.1. Chrysotile Surface Structure

Each chrysotile fiber is a single crystal, with the external surface of an ideal crystal being magnesium hydroxide. The outer hydroxide ions are in a hexagonal-close-packed arrangement, as illustrated by the two-dimensional molecular picture of the surface on Figure 2.1a. Each magnesium ion is in octahedral coordination with six ions, four hydroxides and two oxides. Three of these hydroxides lie in the particle surface. The remaining three ions lie in a plane beneath the surface, with the two oxides also forming the apices of underlying silica tetrahedra and the hydroxide lying between the apical oxides. Surface hydroxide density for the octahedral layer of chrysotile is the same as for brucite (Whittaker, 1956; Deer et al., 1966), calculated from unit-cell dimensions to be 12 ion/mm^2 (2×10^{-9} mol/cm^2). Each surface hydroxide is coordinated to three of the underlying magnesium ions.

Removing the outermost hydroxide and magnesium ions without further surface rearrangement would leave a surface made up of the apical oxides of the silica tetrahedra and the remaining hydroxide ions that made up the octahedral coordination of magnesium (Figure 2.1b). The combined oxide-hydroxide density for this surface is also 12 ion/mm^2.

During at least the initial one to three days it is suspended in water, chrysotile dissolves with magnesium being released into

a. Magnesium hydroxide surface
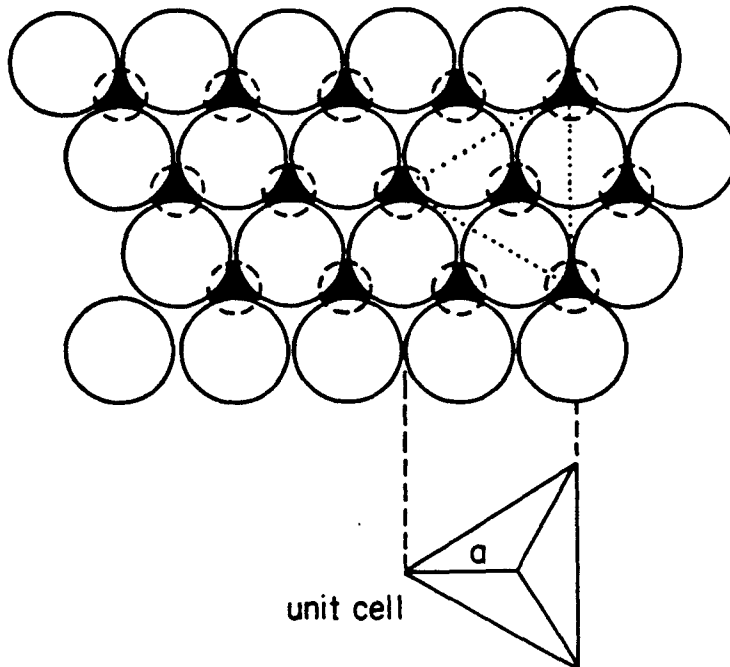
unit cell

b. Silica surface
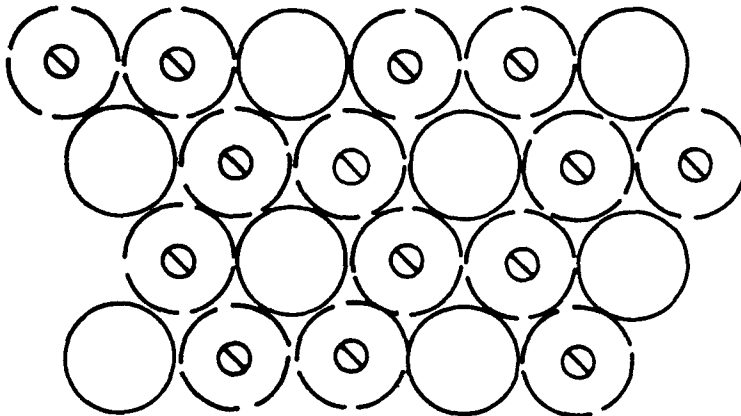
Fig. 2.1. Schematic of chrysotile surface layers;
a) O hydroxide, ● underlying magnesium; unit cell
encompasses 1.5 magnesium ions and 1.5 surface
hydroxides; a = 3.13 Å;
b ◌ oxide, ⊘ underlying silicon.

solution in excess of the 3:2 ratio in pure serpentine ($Mg_3Si_2O_5(OH)_4$) (Luce, 1969; Hostetler & Christ, 1968). This is apparently due to faster dissolution of the outer brucite (magnesium sheet) relative to the immediately-underlying silica sheet making up chrysotile's outer layer, suggesting that the outer surface of a fiber dissolving at or below pH's of natural waters becomes more silica-like (Figure 2.1b) and less magnesium-like (Figure 2.1a) with time.

Each hydroxide on the initial, ideal chrysotile surface is assumed to be a possible adsorption site for protons, other cations or anions. It is further assumed that removal by dissolution of a given number of surface hydroxides coordinated to magnesium ions (>Mg-OH) in the outer sheet results in creation of an equal number of silica surface sites (>Si-OH) by exposure of the immediately-underlying sheet. These are also possible adsorption sites for protons, other cations or anions. Figure 2.2 is a general schematic of adsorption reactions that are assumed to occur at the mixed, magnesium-silicate surface.

Physically, the components lying between the apical oxides on the silica surface (dashed circles on Figure 2.1b) could be either remaining hydroxide ions or adsorbed water molecules replacing hydroxides that were removed with the magnesiums. In terms of the surface structure and surface model this distinction is not important. Rather the assumption is that on the remaining silica surface the surface site density is 12 ion/mm^2 and the sites are alike -- each site has an equal probability of being occupied by an adsorbable ion.

The surface site density calculated for chrysotile is near that reported by others for oxide minerals. For example, the surface site density on TiO_2 (ionizable >OH) was calculated to be 12.2 ion/mm^2

a)

SOLID | WATER   SOLID | WATER

>Mg–OH   >Mg–OH

>Mg–OH + H⁺   ⇌   >Mg–OH₂⁺

>Mg–OH + OH⁻ ⇌   >Mg–O⁻ + H₂O

Si–OH   Si–OH

Si–OH + OH⁻   ⇌   Si–O⁻ + H₂O

b)

>Mg–OH + L²⁻   ⇌   >Mg–L⁻ + OH⁻

>Mg–OH + L²⁻ + H⁺ ⇌   >Mg–LH⁻ + OH⁻

>Mg–OH + C²⁺   ⇌   >Mg–O⁻C²⁺ + H⁺

Si–OH   Si–OH

Si–OH + C²⁺   ⇌   Si–O⁻C²⁺ + H⁺
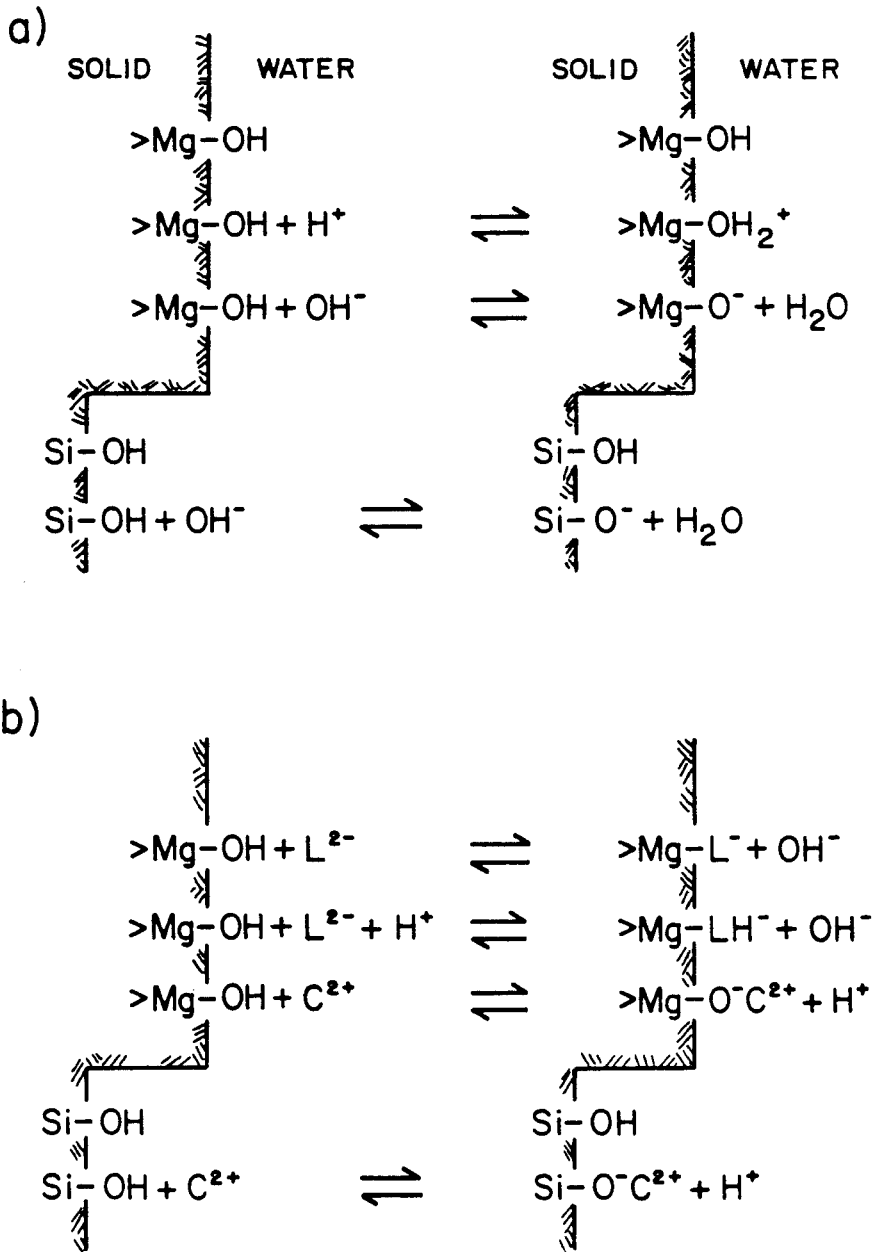
Fig. 2.2.   Schematic of possible adsorption reactions on chrysotile surface; a) proton adsorption and desorption, and b) adsorption of ligands (L²⁻) and cations (C²⁺).

based on a composite of three exposed crystal faces (Jones & Hockey,
1971). Bound H_2O was responsible for a portion of the estimated
density. A higher value, 16.8 ion/nm^2, was estimated by Yates for
α-FeOOH (James & Parks, 1982). The TiO_2 value compares well with the
site density measured by isotopic exchange (Yates et al., 1980).

Fiber ends, which make up approximately two percent of the total
chrysotile particle surface area, are assumed to have the same
adsorption properties as the face. Aside from the relative abundance
of face to edge sites, this may be a necessary assumption in the
surface-chemical model owing to the lack of a method to distinguish
between the two in adsorption experiments. Edge-type sites also arise
due to holes or pits on the surface.

2.1.2. Coordination-Chemical Model

2.1.2.1. Model Development

It is assumed that ions adsorb to both >Mg-OH
sites and >Si-OH sites as inner sphere complexes and that a
constant-capacitance model characterizes surface adsorption (Stumm &
Morgan, 1981). A triple-layer model incorporating elecrolyte binding
could equally-well or better describe adsorption of charged ions on
the surface (Morel et al., 1981). Three factors contributed to the
choice not to use the triple-layer model for chrysotile. First, the
effect on surface charge resulting from changing the ionic strength
within the range of interest, 0.01-0.1 M and pH 7-9, was observed to
be small relative to the variability in the experimental results.
Second, data requirements are more extensive for a triple-layer model.
Third, the additional insight to be gained from estimating parameters
in a triple-layer versus a simple constant-capacitance model is small,

given the uncertainties in formulating surface species for the mixed magnesium-silica surface studied.

Surface charge is assumed to arise due to ion adsorption and be on the surface, in contrast to the space charge due to ionic substitution in the structurally similar aluminum-silicate clay minerals. In the model employed, the following intrinsic equilibrium constants describe proton coordination:

$$K^S_{a1(int)} = \frac{\{>Mg-OH\}\,[H^+]}{\{>Mg-OH_2^+\}}\; e^{-e\psi/kT} \tag{2.1}$$

$$K^S_{a2(int)} = \frac{\{>Mg-O^-\}\,[H^+]}{\{>Mg-OH\}}\; e^{-e\psi/kT} \tag{2.2}$$

$$K^S_{as(int)} = \frac{\{>SiO^-\}\,[H^+]}{\{>SiOH\}}\; e^{-e\psi/kT} \tag{2.3}$$

Concentrations of surface species, in braces, are in mol/cm^2 and solution species, in brackets, are in mol/L. ψ is surface potential (volts), e is the charge on an electron, k is Boltzmann's constant and T is temperature. Surface charge-density (C/cm^2 is given by:

$$\sigma = F(\{>Mg-OH_2^+\} - \{>Mg-O^-\} - \{>SiO^-\}) \tag{2.4}$$

where F is the Faraday.

Surface charge density, determined experimentally, is calculated from a charged ion balance (electroneutrality) in the suspension,

where charge on the surface plus that in solution must equal zero. For chrysotile in the pH range 7-9, the expression is:

$$\sigma = F(C_A - C_B - 2[Mg^{2+}] - [MgOH^+] + [H_3SiO_4^-] + 2[H_2SiO_4^{2-}] + [OH^-]) \quad (2.5)$$

C_A and C_B are the concentrations of acid and base added to hold pH constant.

Mass balance requires that:

$$S_T = \{ >Mg-OH_2^+ \} + \{ >Mg-OH \} + \{ >Mg-O^- \} + \{ >Si-OH \} + \{ >Si-O^- \} \quad (2.6)$$

S_T is the total number of surface sites, assumed to be constant at 12 ion/mm^2 (2×10^{-9} mol/cm^2) as noted above. It is assumed that initially most are magnesium sites, a small fraction are silica sites and additional silica sites arise due to preferential dissolution of magnesium over silica. At any time $S_m + S_s = S_T$ -- the number concentration of magnesium sites plus the concentration of silica sites must sum to S_T. These two quantities are given by the difference between the number of magnesium and silica ions removed from the surface:

$$S_m = S_T - [Mg^{2+}] - [MgOH^+] + 3/2[H_4SiO_4] + 3/2[H_3SiO_4^-] - S_s^0 \quad (2.7)$$

$$S_s = S_T - S_m + S_s^0 \quad (2.8)$$

The 3/2 term on silica reflects the stoichiometric ratio in the solid. S_s^0 is the number of silica sites initially on the surface.

The relation between charge and potential is given by:

$$C = \sigma / \psi \tag{2.9}$$

where C is capacitance, a constant in this model.

The acid-base character of silica surfaces has been studied, recently by Young (1981). There are no similar reports in the literature for a magnesium-hydroxide surface. However, some insight into its expected behavior can be inferred from observations on similar solids. Representative data from the literature that have been evaluated using a constant-capacitance model are listed in Table 2.1.

2.1.2.2. Predicted Chrysotile Surface Speciation

The estimated pH_{zpc} of magnesium hydroxide is ≤ 12.5 (Parks, 1967), suggesting that $>Mg-OH_2^+$ should be the predominant surface species in the pH range of interest in California surface waters, 7.5-8.5. The reported pH_{zpc}'s for silica are variable, but average about 2 (Iler, 1979). At natural-water pH's the surface species $>Si-O^-$ should predominate. Serpentine minerals have an intermediate pH_{zpc}, estimated by Parks (1967) to be 8.9, based on both $>Mg-OH$ and $>SiOH$ being on the surface. Reported values for pH_{iep} for freshly-suspended chrysotile fibers are in the range 10-11.8 (Pundsack, 1955; Martinez & Zucker, 1960). Ahmed (1981) reports a pH_{zpc} of 10 for freshly-suspended fibers.

Constant-capacitance model analyses of silica surface properties have included three additional equilibria that may be important in a chrysotile-water system, those for binding of monovalent cations (sodium or potassium) and magnesium:

Table 2.1. Reported Acid-Base Character of Surfaces; Constant Capacitance Model.

Material	pK_{a1}^s	pK_{a2}^s	ΔpK	pH_{zpc}	S_T, nm^{-2}	Electrolyte	C, [a] $C/V \cdot cm^2$
γ-Al_2O_3[b]	7.2	9.5	2.3	8.3	1.3	0.1M $NaClO_4$	1.3/12.9
γ-Al_2O_3[c]	7.4	10.0	2.6	8.7	1.3	0.1M $NaClO_4$	0.89/2.6
α-$FeOOH$[d]	6.4	9.25	2.85	7.8	4	0.1M $NaClO_4$	1.8/2.9
am-SiO_2[e]	-	7.5	-	-	5	0.1M NaCl	1.25
am-SiO_2[f]	-	6.7	-	-	5	0.1M $NaClO_4$	-
TiO_2[g]	5.4	6.4	1.0	5.9	-	0.1M KCl	-

[a]First number is capacitance observed below pH_{zpc}, second is above pH_{zpc}; units are coulombs/volt $\cdot$ cm^2.

[b]Reference: Hohl & Stumm, 1976.

[c]Reference: Kummert & Stumm, 1980.

[d]Reference: Sigg & Stumm, 1981.

[e]Reference: Young, 1981, capacitance and S_T values assumed rather than observed.

[f]Reference: Schindler, 1981.

[g]Reference: Huang, 1981; data of Bérubé & deBruyn.

$$* K^S_c = \frac{\{>Si-ONa\}[H+]}{\{>Si-OH\}[Na^+]} \qquad (2.10)$$

$$* K^S_{Mg} = \frac{\{>Si-OMg^+\}[H^+]}{\{>SiOH\}[Mg^{2+}]} e^{e\psi/kT} \qquad (2.11)$$

$$* \beta^S_{Mg} = \frac{\{(>Si-O)_2 Mg\}[H^+]^2}{\{>Si-OH\}^2[Mg^{2+}]} \qquad (2.12)$$

Recently-reported values for these constants are $p^* K^S_c$ = 9.5 (Young, 1981), $p^* K^S_{Mg}$ = 7.3 (Schindler, 1981) and $p^* \beta^S_{Mg}$ = 14.7 (Schindler, 1981). The predicted behavior for a magnesium-silicate surface is shown on Figure 2.3, using these reported constants and with $pK_{a1}{}^S$ = 8, $pK_{a2}{}^S$ = 10, $pK_{as}{}^S$ = 7.5, C=4 $C/V \cdot cm^2$ and sa = 48.5 m^2/g. Of the silica sites, the species >Si-O⁻ and >Si-OH predominate. Adsorption of Mg^{2+} is not considered in the analyses that follow.

2.1.3. Magnesium-Anion Complexes

Adsorption of both inorganic and organic anions onto the >Mg-OH surface of chrysotile will alter the surface charge and may influence the rate at which chrysotile dissolves in natural waters. The major anions of interest in California waters are sulfate, chloride, bicarbonate, and the anions of carboxylic and phenolic groups associated with natural organic matter (NOM). The poorly defined and variable character of natural organic matter in California waters introduces a high degree of uncertainty into prediction and evaluation of adsorption characteristics. To a first approximation
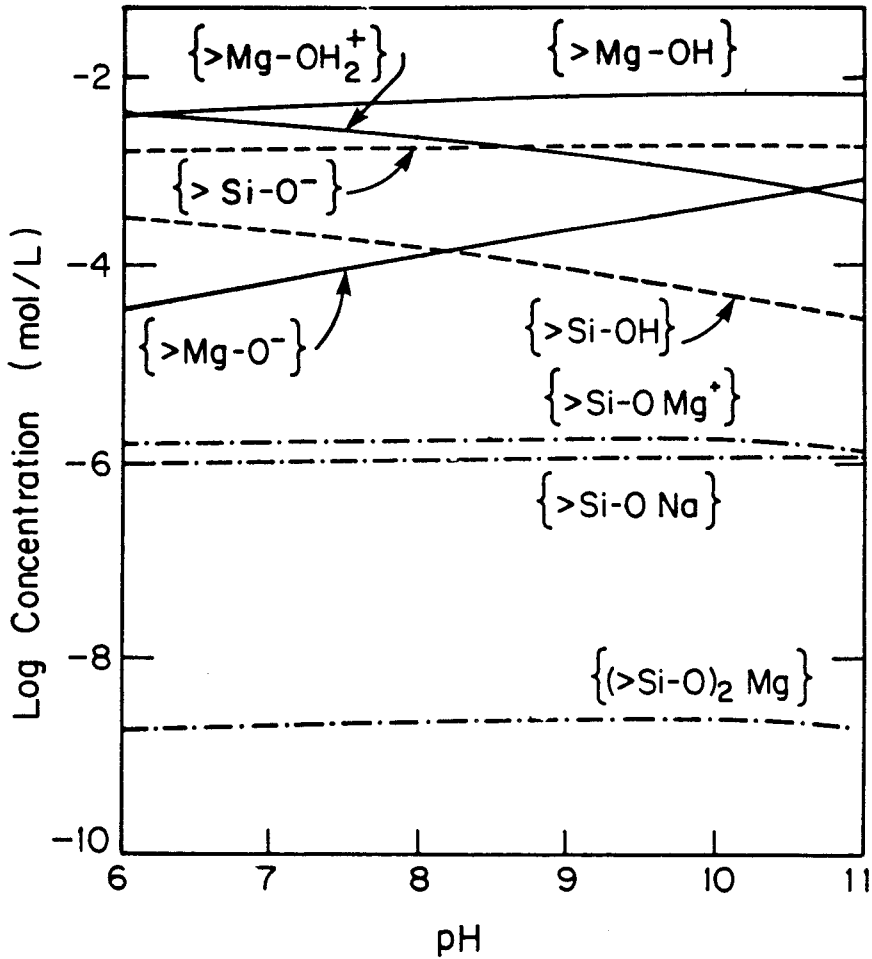
Fig. 2.3. Predicted magnesium-silicate surface speciation; $S_T = 9.7 \times 10^{-3}$ M, $S_m = 0.8\ S_T$, $S_s = 0.2\ S_T$, $pK_{a1}^s = 8$, $pK_{a2}^s = 10$, $pK_{as}^s = 7.5$, $C = 4$ C/V · cm^2, sa = 48.5 m^2/g.

the adsorption behavior of higher molecular weight organic acids such as NOM may resemble that of lower molecular weight carboxylic and phenolic acids. In the analyses that follow, low-molecular weight organic acids are used to model the behavior of NOM; these analyses aid in both predicting and interpreting surface-organic interactions on chrysotile in natural waters.

The relative tendency for specific adsorption of anions on the α-FeOOH and γ-Al$_2$O$_3$ surfaces is observed to be related to the tendency for the respective metal-anion complex to form in solution (Stumm et al., 1980). Comparable equilibria are the tendency of ligands to replace OH$^-$ on the surface and in solution; for example:

$$>Fe-OH + H_2A \rightleftharpoons FeHA + H_2O \qquad *K_1^S \qquad (2.13)$$

$$FeOH^{2+} + H_2A \rightleftharpoons FeHA^{2+} + H_2O \qquad *K_1 \qquad (2.14)$$
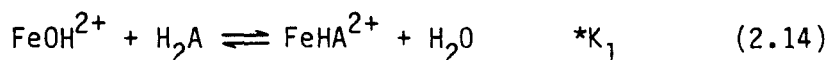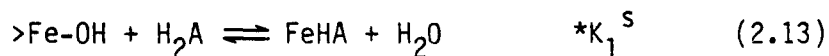
Equilibrium constants for magnesium complexation with various anions are listed in Table 2.2. These equilibria are generally of the form:

$$Mg^{2+} + A^{2-} \rightleftharpoons MgA \qquad (2.15)$$

When combined with the first and second acidity constants for H$_2$A and with the MgOH$^+$ complexation equilibrium constant, this takes the form:

$$MgOH^+ + H_2A \rightleftharpoons MgA + H^+ + H_2O \qquad (2.16)$$
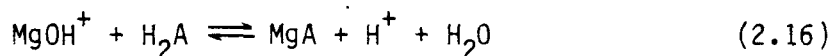
Table 2.2. Magnesium Equilibria at 25 C.

Anion	$\log K^{(a)}$	$\log([MgL^{(2-z)-}][Mg^{2+}]^{-1})^{(b)}$	
		$L_T = 0.1$ M	$L_T = 0.001$ M
EDTA ($N_2C_{10}H_{12}O_8^{4-}$)	8.83	5.38	1.69
Catechol ($C_6H_4O_2^{2-}$)	5.7	-1.56	-3.56
NTA ($NC_6H_6O_6^{2-}$)	5.47	3.02	0.45
Silicate ($H_2SiO_4^{2-}$)	5.37	-5.27	-5.54
Silicate ($H_3SiO_4^{-}$)	1.24	-3.68	-3.95
Salicylate ($C_7H_4O_3^{2-}$)	5.2	-1.15	-3.15
Citrate ($C_6H_5O_7^{3-}$)	3.37	2.34	0.03
Carbonate (CO_3^{2-})	2.85	-	-2.78[c]
Bicarbonate (HCO_3^{-})	0.69	-	-2.59[c]
Oxalate (K_1)($C_2O_2^{2-}$)	2.76	2.17	-0.09
Oxalate (β_2)	4.24	2.87	-1.66
Phosphate (PO_4^{3-})	2.50	1.02	-0.98
Sulfate (SO_4^{2-})	2.28	0.97	-1.03
Hydroxide (OH^{-})	2.21[d]	-	-
Fluoride (F^{-})	1.82	0.82	-1.18
Phthalate ($C_8H_4O_4^{2-}$)	2[e]	0.1	-1.9
Chloride (Cl^{-})	0.91	-0.09	-2.09
Benzoate ($C_7H_4O_2^{-}$)	0.1	-1.1	-3.1
Nitrate (NO_3^{-})	-[f]	-	-

[a] $K = [MgL^{(2-z)-}][Mg^{2+}][L^{z-}]^{-1}$; K's from Martel & Smith (1976).

[b] $Mg_T = 0.001$ M, pH = 8, K_a's from Martel & Smith (1976).

[c] Equil. with $P_{CO_2} = 10^{-3.5}$; under these conditions, $[CO_3^{2-}] = 10^{-5.63}$ and $[HCO_3^{-}] = 10^{-3.28}$; carbonate system K's from Stumm & Morgan (1981).

[d] Source: McGee & Hostetler (1975).

[e] Estimated.

[f] No evidence of complexation.

The relative tendencies for magnesium to form complexes of this sort are compared in Table 2.2 for 0.1 M and 0.001 M total ligand. For example, at pH 8 with 0.1 M concentration of selected ligands the relative tendency for Mg^{2+} complexation is: oxalate > PO_4^{3-} $\simeq$ SO_4^{2-} > F^- > Cl^- > benzoate > catechol > $H_3SiO_4^-$. The order is the same at 0.001 M. At 350 ppm CO_2, HCO_3^- complexes with magnesium to a greater extent than 0.001 M benzoate but less than 0.001 M chloride.

Sulfate and chloride, common in natural waters, show some evidence of complexation with magnesium and thus may coordinate at a >Mg-OH surface and impart some charge. Bicarbonate, silicate and the weak organic acid catechol are expected to less strongly bind to the surface under the conditions stated. Because H_4SiO_4 and catechol are weak acids they are only slightly dissociated at pH 8. The magnesium-anion binding constant (log K of Table 2.2) together with the acidity constants for the anion of interest determine the relative importance of the complex. Oxalate and other carboxylic acids form strong magnesium complexes. No constant was available for coordination with the dicarboxylic phthalic acid. Based on equilibrium data for other cations and ligands, it is estimated that log K for a magnesium-phthalate complex would be about 2. At both 0.1 M and 0.001 M, phthalate would form slightly stronger complexes with magnesium than would chloride.

2.2. DISSOLUTION MODEL

2.2.1. Dissolution Process

Dissolution is a multi-step process involving both redistribution of components in space by diffusion and chemical reactions at the solid-liquid interface that facilitate flux of

components across the interface. Figure 2.4 shows the steps involved in dissolution at the surface of a solid suspended in a moving fluid. Either diffusion (steps a,b,h or i) or chemical reaction (steps c-g) may be rate limiting.

For a reaction-limited process, steps c-g recognize that dissolution occurs preferentially at sites of higher energy, consistent with the accepted terrace-ledge-kink (TLK) model of growing or subliming solid surfaces (Boudart, 1975). For example, it is suggested that cation release from an oxide may proceed similarly to vaporization of metal in vacuum or anodic dissolution of metal (Valverde & Wagner, 1976):

$$Me^{Z+}(kink) \rightleftharpoons Me^{Z+}(step) \rightleftharpoons Me^{Z+}(ads) \rightleftharpoons Me^{Z+}(aq)$$
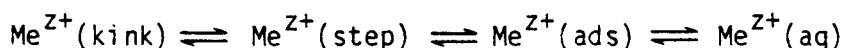
Electron-transfer, ion-exchange or complexation reactions may alter the rate of cation transfer from kink sites to bulk solution by slowing or speeding a surface-chemical reaction or changing the rate of diffusion. For example, Stumm et al. (1983) suggest that protonation of surface >MOH groups and ligand exchange -- formation of suitable inner-sphere complexes of the form >ML -- weaken remaining metal-oxide bonds and enhance detachment of the >M-L or $>M-OH_2$ group. Alternately, specifically-adsorbing solutes may block access to surface sites and prevent proton or ligand attack.

The rate of a surface reaction may be limited by both the total surface area and the number of reactive sites per unit area that are available for reaction (Wadsworth, 1975). In laboratory experiments, the initial concentration of kink sites, or sites of higher energy, may be different from the steady-state number present at later stages of dissolution. Size reduction by grinding the parent material

(a) Transport

(b) Bdy.-layer diffusion

(c) Surface diffusion

(d) Complexation

(e) Activated cpx. formation

(f) Detachment

(g) Surface diffusion

(h) Bdy.-layer diffusion

(i) Transport

(j) Solution complexation
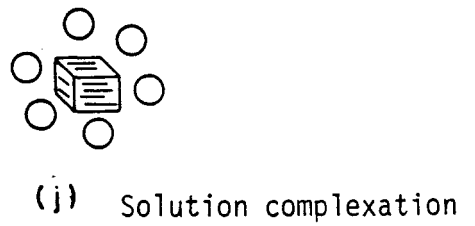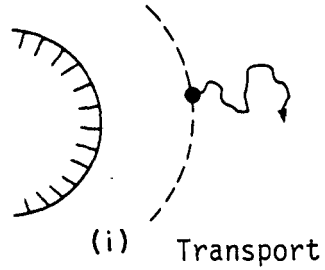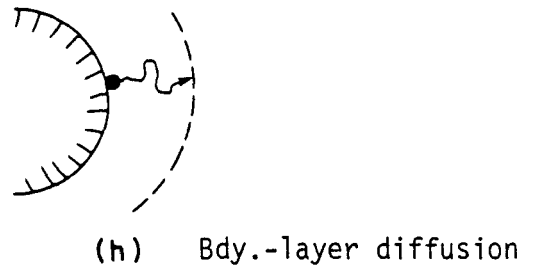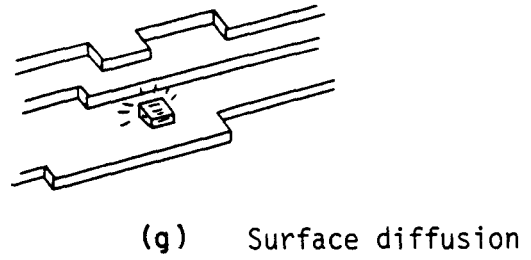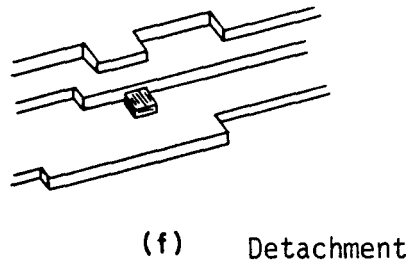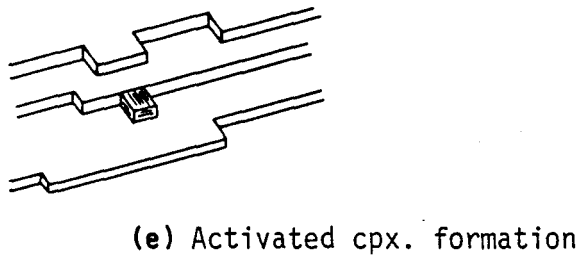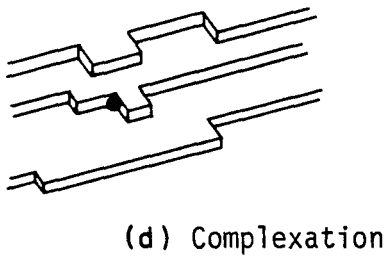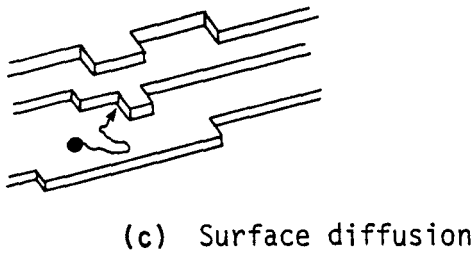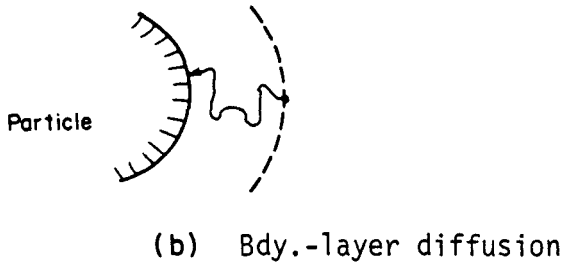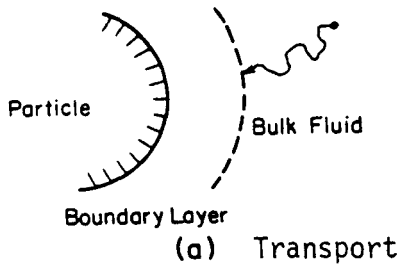
Fig. 2.4. Dissolution process.

creates fresh surfaces; the distribution of energy levels of surface sites will depend on the relative number of cracks, tips and dislocations formed and on the particle-size distribution. These surface properties are determined by the intensity and duration of grinding. The dissolution rate for freshly-ground material typically decreases over several hours or days to a steady-state value, whereas pre-weathered material exhibits steady-state dissolution from the outset (Holdren & Berner, 1979; Schott et al., 1981; Stumm et al., 1983).

Where dissolution is limited by surface reaction, large well-developed etch pits are observed to form at points of excess energy such as surface dislocations. For transport-controlled dissolution, attack is more rapid and more uniformly distributed over the surface (Berner, 1981).

Dissolution may be diffusion limited, either in bulk solution (Rickard & Sjöberg, 1983; Zutic & Stumm, 1982), or through a surface precipitate or leached layer that forms when some solid components are released into solution at a faster rate than are others (Wadsworth, 1975; Luce et al., 1972). A surface leached layer could result from selective exchange of cations for H^+ (or H_3O^+); a surface precipitate could result from reformation of surface material as selective ions are removed, or from precipitation of less-soluble, amorphous material as a well-ordered crystal dissolves. In addition to the sequence of Figure 2.4, two additional steps would occur: b.2) diffusion of reactive species through the surface layer and b.3) diffusion of dissolved species away, through the surface layer.

2.2.2. Chrysotile Dissolution

Chrysotile dissolves according to the overall reaction:

$$Mg_3Si_2O_5(OH)_4(s) + 6H^+ \rightleftharpoons 3Mg^{2+} + 2SiO_2(aq) + 5H_2O$$
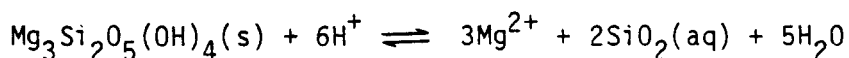
Past studies of chrysotile dissolution have found that magnesium is released into solution in excess of the 3:2 ratio in pure chrysotile. This was observed for dissolution of a significant fraction of the solid at acidic pH (Morgan et al., 1973) and during at least the initial one to three days of dissolution near netural pH (Luce, 1969; Hostetler & Christ, 1968). Selective removal of the outer brucite $(Mg(OH)_2)$ layer could account for the greater magnesium release at short times. Continued release of magnesium at a higher rate could result in build-up of a silica surface layer. A surface gel or leached layer may form on chrysotile under natural-water conditions in at least two situations. First, at low to neutral pH, Mg^{2+} may be undersaturated and removed to solution while released silica precipitates as an amorphous surface layer due to oversaturation. Second, the chemical affinity for dissolution may be sufficient to enable forming a new lower-entropy surface phase by rearrangement of components remaining after the more-soluble Mg^{2+} is removed, forming a surface leached layer. Recent experimental evidence on feldspars, amphiboles and pyroxenes suggests that these do not occur to an extent sufficient to control reaction rate. Rather, chemical reaction at the mineral-water interface controls dissolution (Aagaard & Helgeson, 1982; Berner & Schott, 1982; Berner & Holdren, 1979; Berner, 1978). Evidence on serpentines is inconclusive (Thomassin et al., 1977).

Berner (1978) observed that for selected minerals there is a reasonably good correlation between the solubility of a mineral and

the rate-controlling mechanism by which it dissolves. Minerals with solubilities on the order of 10^{-3} mol/L or lower (pH 8 in water) tend to be limited by surface reaction and those more soluble are limited by transport. Surface-reaction limited dissolution is generally slower than dissolution limited by transport in solution. This correlation would be true if precipitation, the reverse of dissolution, involved a rate-limiting chemical step that was common to several different minerals and that occurred at approximately the same rate in different minerals. For a reversible reaction $k_{diss} = K_{eq}k_{prec}$, where k_{diss} and k_{prec} are the rate constants for dissolution and precipitation respectively and K_{eq} is the equilibrium solubility product. If k_{prec} is of similar magnitude for different minerals, then k_{diss} is proportional to K_{eq}. If the rate-limiting step in precipitation involves loss of one or more water molecules, analogous to solution complexation (Morel, 1983), then it is unlikely that k_{prec} for a variety of minerals could be approximately equal. Water exchange rates for different cations vary by several orders of magnitude. Concepts of common rate-limiting steps or quantitative relations between K_{eq} and k_{diss} on k_{prec} have not been incorporated into theories of nucleation and crystal growth.

Based on the correlation between solubility and dissolution mechanism, brucite dissolution should be transport limited and silica dissolution, reaction-rate limited. This suggests that chrysotile should be either reaction limited or a mix of reaction and transport limited.

Experimental results on chrysotile dissolution in strong acid can be interpreted as being either transport or reaction-rate limited.

For example, from 25 to 250 hours is required to release into solution 70 percent of the total magnesium from chrysotile suspended in 1 M HCl (Morgan et al., 1973). As a function of the original surface area (assuming 50 m^2/g) the average dissolution rate is on the order of 10^{-13}-10^{-12} mol/cm^2·s. The amount of magnesium released in these experiments was proportional to the square root of time, which is consistent with a transport-controlled reaction (Luce et al., 1972). Electron micrographs of the fresh and magnesium-leached material showed little change in fiber morphology, suggesting that both reactants (protons) and products (magnesium ions) diffused through an outer, porous silica layer that became progressively thicker as dissolution proceeded (Morgan et al., 1973). It is not known if the silica remained as a leached layer due to slow dissolution or dissolved and reprecipitated from a saturated solution. Chowdhury (1975) observed release rates for magnesium from chrysotile on the order of 10^{-15} mol/cm^2s at pH 7 and 37 C, which is considerably lower than the rate in strong acid. (Surface area of the material was not reported in his experiments, so a value of 50 m^2/g was assumed.)

The calculated diffusion coefficient from the data of Morgan et al. (1973), estimated following Luce et al. (1972), is on the order of 10^{-16} cm^2/s. This is near the 10^{-17} cm^2/s estimated for magnesium leaching from chrysotile in 0.1 N oxalic acid (Thomassin et al., 1977).

Ionic diffusion coefficients in silicate minerals are in general not known, and may range from 10^{-10} to 10^{-30} cm^2/s (Petrovic, 1976) versus the 10^{-5} cm^2/s for ionic diffusion in water (Sherwood et al., 1975). Values for a surface-leached layer will depend on the

structure of the pores, or diffusion channels, through the solid. Petrovic suggests that diffusion through an amorphous aluminum hydroxide precipitate in feldspars should proceed with diffusion coefficients comparable to those for diffusion through comparably-sized porous solids, on the order of 10^{-9}-10^{-6} cm^2/s. That is, dissolution that implies diffusion rates much smaller than these is too slow to be diffusion controlled.

These order-of-magnitude comparisons fail to suggest whether chrysotile dissolution in strong acid is reaction-rate or diffusion limited. The diffusion limitation could be in a surface-leached layer rather than a precipitate coating. Observations do, however, provide an upper bound on the expected dissolution rate in low pH media such as stomach acids -- 10^{-12}-10^{-13} mol/cm$^2 \cdot$s, which corresponds to complete dissolution of a single fiber within a few days.

2.2.3. Reaction Kinetics

2.2.3.1. Theory

Mineral dissolution involves simultaneous, multi-step chemical processes that transform solid species into solution species and also rearrange species remaining in the solid phase. For example, release of cations from an oxide may involve surface attack by protons, water dipoles and coordinating ligands at the same or different types of surface sites (e.g. edge vs. face sites), with each reaction occurring at a different rate. In many cases a single process at a single type of site will dominate.

The overall reaction rate for dissolution can be defined as:

$$r = -\frac{1}{S}\frac{dn}{dt} = -\frac{\nu}{S}\frac{d\xi}{dt} \tag{2.17}$$

which has units of mol $cm^{-2} \cdot s^{-1}$. n is the amount of reactant in the system (mol), S is the amount of surface area in the system (cm^2), ξ is the reaction progress variable, ν relates the change in moles of reactant to the change in the progress variable, and t is time.

Rates for heterogeneous reactions such as catalysis or dissolution are properly referred to per unit of reactive surface area, or preferably, per unit active site (Boudart, 1975). The number of surface sites is generally not known with as much certainty as is the unit surface area and most recent investigators report rates per unit surface area of solid. In some cases rates are reported per unit mass of solid, with specific surface area also given.

For a process involving a sequence of reversible reactions, the rates of which can be formulated from transition-state theory, the overall rate can be expressed as a function of the free energy change of the system (Boudart, 1976):

$$r = \vec{r}(1 - e^{-A/\sigma RT}) \tag{2.18}$$

$\vec{r}$ is the overall rate of the forward reaction, A is the total affinity of the overall reaction:

$$A = \Sigma_k \sigma_k A_k \tag{2.19}$$

and σ is the overall stoichiometric number of the reaction. A_k is the affinity of step k in the forward direction, equal to the negative of the free energy change for the reaction. σ_k is the stoichiometric number of the kth reaction step and is equal to the rate of the kth step relative to the rate of the overall reaction; it is conveniently defined

as $d\xi_k/d\xi$, where ξ_k is the progress variable for step k (Aagaard & Helgeson, 1982). σ is defined by the quantity $\sigma_k A_k/\Sigma_k A_k$.

Figure 2.5 shows schematically the concept of a reaction barrier for a single elementary step corresponding to the formation of an activated complex for going from reactants to products (Gardiner, 1969; Hammes, 1978).

For a single step, j, within the sequence being rate determining, $\vec{r} = \vec{r}_j/\sigma_j$ and $A_j >> \Sigma_k A_k$ for k = j. Then formulating $\vec{r}_j$ from transition-state theory as the rate of decay of an activated complex (Lasaga, 1981; Dibble & Tiller, 1981; Aagaard & Helgeson, 1982), (2.18) becomes:

$$r = \frac{1}{\sigma_j} \frac{kT}{h} C_j^{\ddagger} (1 - e^{-A_j/\sigma_j RT}) \tag{2.20}$$

where k is Boltzmann's constant, T is temperature, h is Planck's constant, and $C_j^{\ddagger}$ is the concentration of the activated complex (mol/cm^2).

Far from equilibrium A_j is large and the exponential term is small. Writing (2.20) in terms of the activated complex precursors, the species that react to form the activated complex in step j, and far from equilibrium, gives:

$$r = \frac{1}{\sigma_j} \frac{kT}{h} \frac{K_j^{\ddagger}}{\gamma_j^{\ddagger}} \prod_i a_i^{-\nu_{ij}} \tag{2.21}$$

Here $K_j^{\ddagger}$ is the equilibrium constant for the reaction leading to formation of the activated complex, $\gamma_j^{\ddagger}$ is the activity coefficient for the activated complex, a_i are the activities of components in
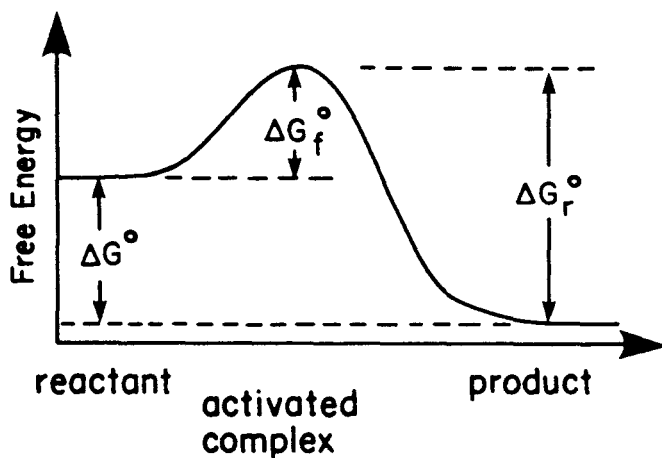
Fig. 2.5. Free energy change ($\Delta G°$) for single, reversible step in dissolution involving activation barrier that corresponds to formation of activated complex in the forward (ΔG^{a}_{f}) and reverse ($\Delta G°_{r}$) directions; $A_{f} \equiv \Delta G^{0}_{f}$ (see text).

equilibrium with the activated complex, and ν_{ij} are the stoichiometric coefficients in the equilibrium reaction.

2.2.3.2. Kinetic Model for Chrysotile Dissolution

Possible activated-complex precursors for pH-dependent dissolution of magnesium hydroxide can be formulated in terms of the degree of surface protonation, or extent of proton adsorption at surface >Mg-OH sites. If adsorption of a single proton is sufficient to bring about release of one magnesium ion into solution, the concentration of activated complex should be proportional to $\{>Mg-OH_2^+\}$, and (2.21) would be:

$$r = k_1 \{>Mg-OH_2^+\} \qquad (2.22)$$

where $k_1 = \dfrac{1}{\sigma_j} \dfrac{kT}{h} \dfrac{K_j^{\ddagger}}{\gamma_j^{\ddagger}} \gamma_+$. γ_+ is the activity coefficient for the

surface species $>Mg-OH_2^+$. If more than one adsorbed proton is involved in forming the activated complex, then the probability that adsorbed protons will occupy adjacent sites must be considered. The formulation is analogous to that for reactions involving surface catalysis (Boudart, 1975; Hill, 1977). Figures 2.6 and 2.7 illustrate possible physical pictures for adsorption of two protons at adjacent sites on a hydroxide surface. As noted above, each surface hydroxide is a potential proton adsorption site, each underlying magnesium is coordinated to three surface hydroxides and each surface hydroxide is coordinated to three underlying magnesiums. Figure 2.6 is a plan view, showing an edge, or
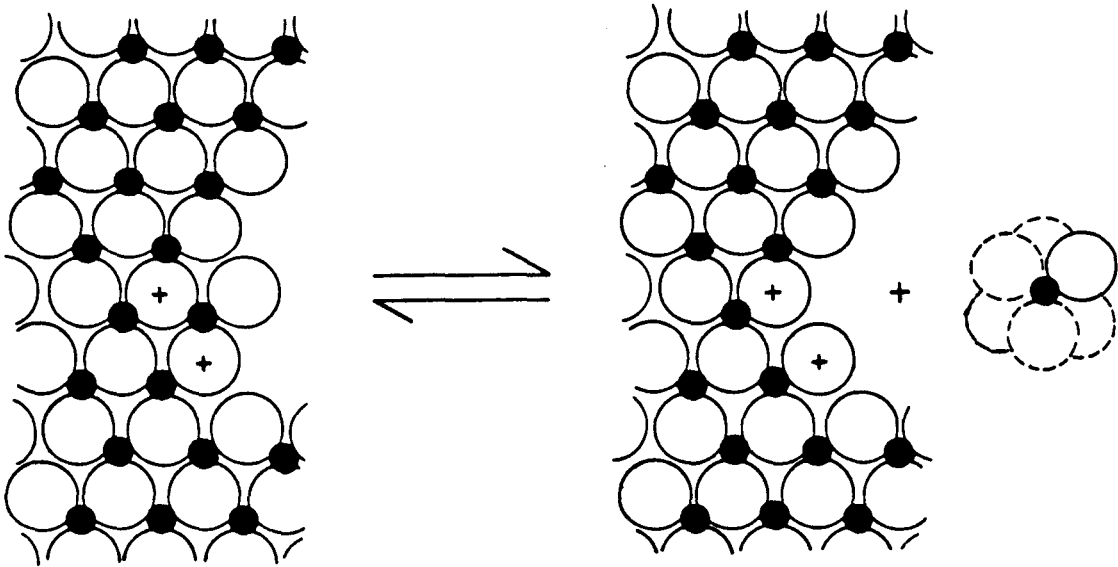
Fig. 2.6. Plan view of magnesium hydroxide surface illustrating release of magnesium resulting from adsorption of protons at adjacent sites; magnesium ● , hydroxide ○ , adsorbed proton + , ○ water molecules.
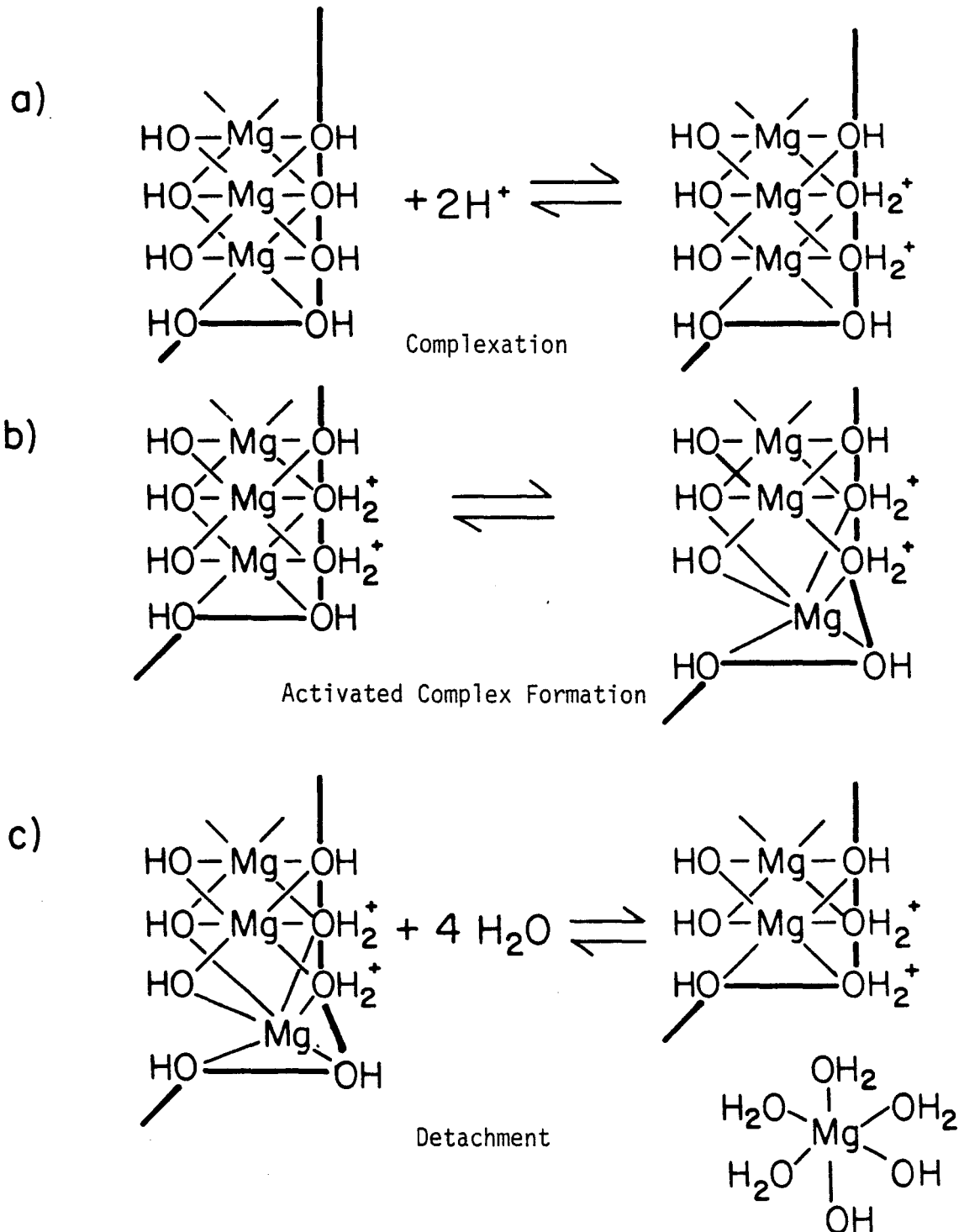
Fig. 2.7. Schematic of chemical steps for release of one magnesium from chrysotile surface; a) complexation of protons at adjacent surface sites, b) formation of activated complex involving lengthening of bonds between magnesium ion and structural oxides, and c) detachment of magnesium from surface and coordination with water molecules.

hole in the surface where dissolution will preferentially occur. Coordination at adjacent surface hydroxides is illustrated. Concentration of positive charge near a single magnesium ion results in a change in the position or bonding of that cation in the solid lattice and eventually in release of a Mg^{2+} ion into solution. This is depicted in the schematic of Figure 2.7. An analogous picture could be developed for adsorption of three protons on adjacent sites.

Following Boudart (1975) and Hill (1977), the probability of two adjacent sites being occupied is proportional to the square of the probability that one site is occupied, where the probability of occupying any one site is independent of the probability of occupying any other site. In the present case, the probability that any one surface >Mg-OH site is ocupied by a proton is $\{>Mg-OH_2^+\} S_m^{-1}$, the fraction of surface sites that are protonated. The total concentration (mol/cm^2) of pairs of sites on the surface is $1/2(z_1 S_m)$, where z_1 is the number of nearest neighbors to any given site, a constant. The factor 1/2 accounts for each pair being counted twice. For the concentration of pairs of protonated sites being C_2, the fraction of pairs of sites that are protonated is $C_2(1/2(z_1 S_m))^{-1}$. This is equal to the square of the fraction of sites that are protonated, $\{>Mg-OH_2^+\}^2 S_m^{-2}$. This gives

$$C_2 = \frac{z_1}{2} \frac{1}{S_m} \{>Mg-OH_2^+\}^2 \tag{2.23}$$

An analogous argument for three adjacent sites would give:

$$C_3 = \frac{z_1 z_2}{6} \frac{1}{S_m^2} \{>Mg-OH_2^+\}^3 \qquad (2.24)$$

where z_2 is the number of nearest neighbors to each pair of sites. Substituting (2.23) into (2.21) for the case of the activated complex involving two adjacent protonated sites gives:

$$r = k_2 \frac{1}{S_m} \{>Mg-OH_2^+\}^2 \qquad (2.25)$$

where $\qquad k_2 = \frac{z_1}{2} \frac{1}{\sigma_j} \frac{kT}{h} \frac{K_j^{\ddagger}}{\gamma_j^{\ddagger}} \gamma_+^2 .$

Analogous expressions for the influence of adsorbed protons and anions in the dissolution of aluminum oxide have been presented (Stumm et al., 1983). Substitution of (2.1) and (2.2) into (2.22) gives an expression in terms of hydrogen ion concentration:

$$r = k_1 S_m \left(\frac{[H^+]e^{-e\psi/kT}}{[H^+]e^{-e\psi/kT} + K_{a1}^s + K_{a1}^s K_{a2}^s/[H^+]e^{-e\psi/kT}} \right) \qquad (2.26)$$

Similar expressions would result for the cases of two (2.25) or three proton adsorption. Over a limited pH range an approximation of the following form can be used (Stumm et al., 1983):

$$\{>Mg-OH_2^+\} \simeq S_m K'[H^+]^a \qquad (2.27)$$

K' and a are empirical constants, with $0 < a \leq 1$. In general, an approximate expression for dissolution rate based on equilibrium adsorption of protons is:

$$r = k_1'[H^+]^{an} \qquad (2.28)$$

n is an integer, likely one, two or three and k_1' incorporates k_1, K', S_m and other constants, depending on n.

Figure 2.8 shows the expected dissolution rate for values of n of 1 (2.22), 2 (2.25), and 3, using the same equilibrium constants as on Figure 2.3. The curves are normalized to zero at pH 9 to permit comparing the expected slopes for these three cases. The slopes (an values) are 0.3, 0.6, and 1.0 for n = 1, 2, and 3, respectively.

2.2.3.3. Observated Kinetic Behavior of Other Minerals

Two sets of data are reported in the literature in the framework outlined above. For dissolution of δ-Al_2O_3, Stumm et al. (1983) reported a rate expression of the form of (2.28) with an = 0.4 and n = 3 over the pH range 3.5-6. Pulfer et al. (1983) reported an = 1 for dissolution of bayerite (γ-$Al(OH)_3$) over the pH range 3-4. Interpretation in the same manner implies n > 3, which seems unlikely based on surface geometry.

Wirth & Gieskes (1979) investigated dissolution of vitreous silica from pH 6-10, with an = -0.5 observed. An evaluation in terms of surface charge, with >Si-O$^-$ being the species of interest, suggests that n = 2, or two OH$^-$ involved in the rate-determining step.
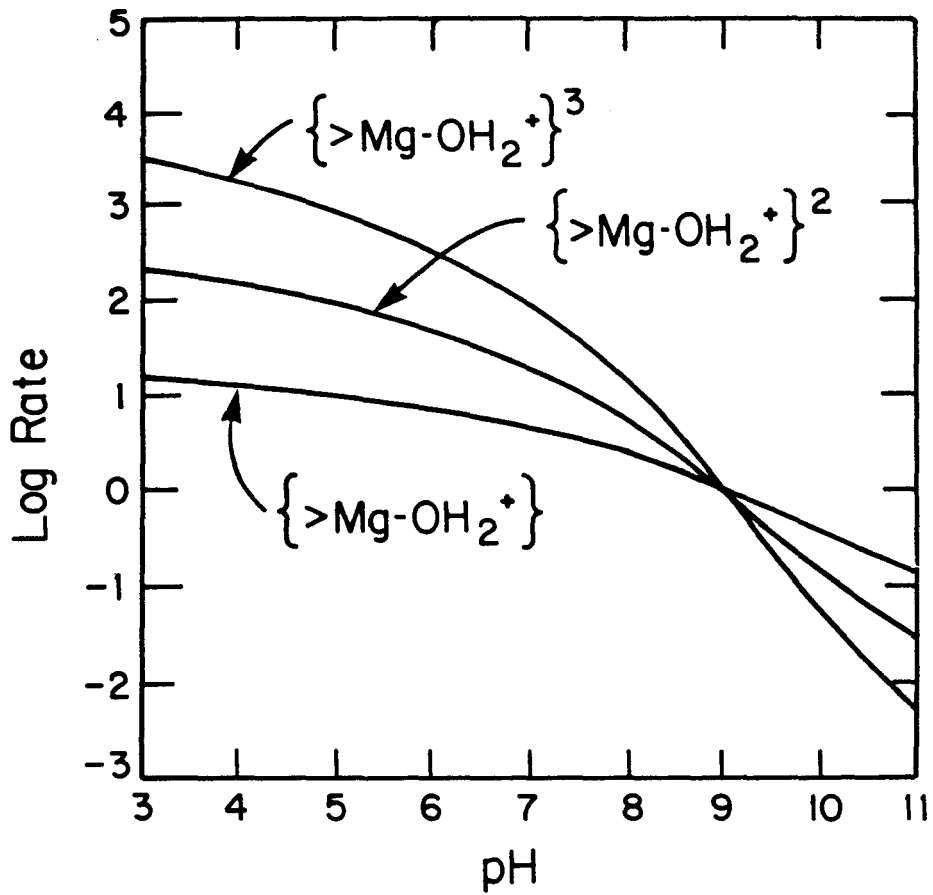
Fig. 2.8. Expected dissolution rates for brucite
outer layer for adsorption of 1, 2, or
3 protons per Mg^{2+} released; rates
normalized to zero at pH 9.

2.3. PARTICLE-PARTICLE INTERACTIONS

2.3.1. Coagulation in Natural Waters

2.3.1.1. Existing Models

Both deterministic (O'Melia, 1980; Lawler et al., 1980; Hunt, 1980) and stochastic (Valioulis, 1983) models of coagulation have been applied to predict particle removal and particle-size distributions in dilute suspensions. The former method uses an empirical coagulation-efficiency factor (α) to account for particle interaction and non-ideal behavior. The latter incorporates functions to describe hydrodynamic interactions and uses linear approximations to describe electrostatic forces between interacting double layers. Both methods treat spherical particles. In principle, either could be modified to describe behavior of non-spherical particles and could express coagulation efficiency in terms of fundamental chemical properties of a system.

For a deterministic model, the rate of disappearance ($L^{-1} s^{-1}$) for a given size and type of particle (indicated by 1) is given by:

$$R_1 = -\alpha n_1 \sum_i k_i n_i \qquad (2.29)$$

where k_i is the coagulation rate constant (L/s) and n_i is the concentration (L^{-1}) of size i particles. n_1 is the concentration of size 1 particles. This is a simplification of the general equation used to predict size distributions (Friedlander, 1977) that considers formation of size 1 particles from aggregation of smaller particles as well.

α should be a function of particle type and size, but in practice is generally observed only for a suspension of different particle sizes and assumed to be constant for given chemical conditions (Lawler, et al., 1983). For a fully destabilized particle, $\alpha = 1$. Stumm (1977) suggests that α may be from 0.1-1.0 in seawater, but that lower values characterize estuaries (0.01-0.1), rivers (10^{-4}-10^{-3}) and lakes (10^{-5}-10^{-4}). The highest α values measured in laboratory experiments are on the order of 0.5 (Birkner & Morgan, 1968), but values on the order of 0.01-0.1 are more commonly reported (Edzwald et al., 1974; Hahn & Stumm, 1968; Eppler, 1975; Gibbs, 1983). Many of the higher values are for estuarine waters and seawater.

Calculated values for k_i for three coagulation mechanisms -- Brownian diffusion, fluid shear and differential sedimentation -- are shown on Figure 2.9.[a] From these calculations it is clear that in the

---

(a) Equations used to calculate k_i are as follows: for Brownian

diffusion, $k_i = 2\pi kT(d_1 + d_i) \dfrac{1}{f_1} \dfrac{1}{f_i}$, where $f_i = 3\pi\mu d$; (sphere)

and $f_1 = f_\parallel /3 + 2f_\perp/3$; $f_\parallel = \dfrac{4\pi\mu a_1}{\ln 2p - 0.72}$ and $f_\perp = \dfrac{8\pi\mu a_1}{\ln 2p + 0.5}$, the Stokes

friction factors for flow parallel and perpendicular to a cylinder axis (Happel & Brenner, 1973; the average friction factor ($f_\parallel /3 + 2f_\perp/3$) applies to random orientation and was derived by Fuchs (1964) for a

prolate ellipsoid. For fluid shear, $k_i = \dfrac{(d_1 + d_i)^3 G}{6}$; for

differential sedimentation, $k_i = \dfrac{\pi g(\rho_p - \rho)(d_1 + d_i)^2 (d_i^2 - d_1^2)}{72\mu}$.
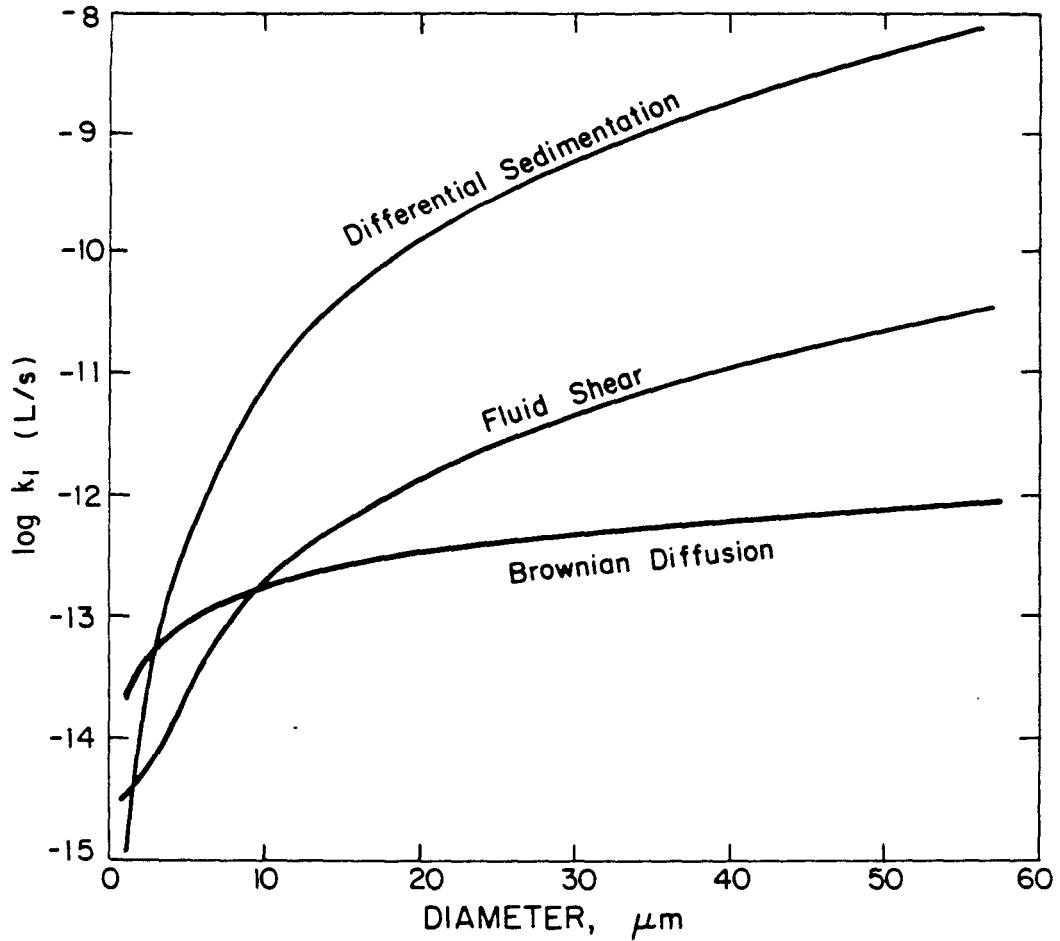
Fig. 2.9. Rate constants for coagulation of chrysotile
fibers (0.05 μm dia. by 0.5 μm long) with larger spherical
particles in water at 20 C with low fluid shear (G = 1 s^{-1})
and high density (ρ_p = 2.6 g/cm^3); adapted from Hunt (1980)
and O'Melia (1980).

presence of larger particles, removal of submicron fibers by differential sedimentation dominates.

In this first-order estimate, the collision radius is assumed to be fiber length rather than diameter. This assumption is valid if fiber rotation is fast relative to translation; otherwise collision radius should be based on the preferred orientation or distribution of particle orientations. The orientation of axisymmetric particles is determined by the combined effects of shear-induced rotation and rotary Brownian motion, which in turn affects translational movement (Cerda & van de Ven, 1983). For a spherical particle, the distance a point on the surface moves by translational and rotational diffusion are approximately equal (Lyklema, 1976). In the absence of shear flow and for long times, Brownian rotation results in equal probability for any given orientation of a non-spherical particle, i.e. random orientation (Fuchs, 1964). The preferred orientation of a rod-shaped particle under weak Brownian motion and in the presence of a simple shear is along the flow (Leal & Hinch, 1971).

$k = 1.4 \times 10^{-16}$ $g \cdot cm^2 s^{-1}$, Boltzmann's constant; $T = 293$ K; $\mu = 0.01$ $g \cdot cm^{-2} s^{-1}$, viscosity; $G = 1$ s^{-1}, fluid shear rate; $g = 980$ $cm \cdot s^{-2}$; $\rho_p = 2.6$ $g \cdot cm^{-3}$, particle density; $\rho = 1.0$ $g \cdot cm^{-3}$, water density; $a_1 = 2.5 \times 10^{-6}$ cm, fiber radius; $d_1 = 5 \times 10^{-5}$ cm, fiber length; $p = d/2a_i = 10$; d_i = size of type i particle.

An analysis of the fiber orientation was not accounted for in the calculated rate constants of Figure 2.9. Orientation was assumed to be random and rotational diffusion was assumed to be fast relative to translation. The effect of having fibers aligned in a flow would be to reduce the collision radius and thus the rate constant. The magnitude of this uncertainty in rate constant is unimportant (small) in the current context (southern California surface waters) for two reasons. First, coagulation rates are greater at d_i large, in which range $d_i \simeq d_i + d_1$ whether one uses fiber length or diameter for d_1. Second, the approximation of other particles as spheres of diameter d_i introduces a similar uncertainty into the collision-radius forms.

2.3.1.2. Model Applied to Fiber Removal

Removal of asbestos fibers in natural waters occurs by coagulation with larger particles that subsequently settle out. Particles with a settling velocity greater than the overflow rate of a reservoir should be removed to a large extent. The Stokes settling velocity for 0.5 µm by 0.05 µm fibers is on the order of 30 cm/yr.[b] To be removed in source-water reservoirs of The Metropolitan Water District of Southern California, fibers should coagulate with particles larger than about 2-5 m in size.

(b) Calculated from Stokes law for a cylinder; average for settling

parallel: $u = \dfrac{2g(\rho_p - \rho)a^2}{9\mu} \cdot \dfrac{9}{4} (\ell n\ 2p - 0.72)$, and perpendicular:

$u = \dfrac{2g(\rho_p - \rho)a^2}{9\mu} \cdot \dfrac{9}{8} (\ell n\ 2p + 0.5)$ to the fiber axis; a is the fiber radius and p is the fiber aspect ratio -- half length divided by radius (Lerman, 1979).

From the rate constant for differential sedimentation as graphed on Figure 2.9:

$$k_i = \frac{\pi g(\rho_p - \rho)(d_1 + d_i)^2(d_i^2 - d_1^2)}{72 \times 10^3 \mu} \qquad (2.30)$$

it is apparent that k_i does not depend on d_1 for $d_1 \ll d_i$. That is, removal of submicron-sized asbestos fibers is not a function of fiber size.

Integration of (2.29) from $t = 0$ to t gives:

$$n_1/n_1^0 = \exp(-\alpha t \sum_i n_i k_i) \qquad (2.31)$$

where n_1^0 is the initial concentration of type 1 particles. The relative concentration of type 1 particles at any time is then calculated from the size distribution of type i particles and the corresponding k_i's.

2.3.2. Deposition in Sand Filters

2.3.2.1. Model Predictions

Deposition of submicron-sized particles onto millimeter-sized sand grains in deep-bed filtration occurs primarily by Brownian diffusion. Interaction due to fluid shear and particle settling are important for larger particle sizes (Yao et al., 1971). Following the development of O'Melia and coworkers (O'Melia, 1980), deposition is given by:

$$\frac{dn_1}{dL} = -\frac{3}{2} \frac{(1-f)}{d_2} \alpha \eta_1 n_1 \qquad (2.32)$$

where L is depth in the bed, d_2 is grain (collector) diameter, f is bed porosity, n_1 is the number concentration of type 1 particles and

is collection efficiency. η_1 is the single-collector contact

efficiency, given for Brownian diffusion by:

$$\eta_1 = 4 \ Pe^{-2/3} \tag{2.33}$$

where Pe is the Peclet number.

Figure 2.10 shows calculated contact efficiencies for the three

deposition mechanisms -- Brownian diffusion, interception and particle

settling for different-sized particles.[c] Calculations are presented

for spherical particles and for fibers of 0.05 μm diameter.

Chrysotile fibers, falling in the 0.1-1 μm size range (length), should

be removed primarily by Brownian diffusion; settling becomes important

only above 1 μm. The contact efficiency is in the range of 10^{-3} for

0.5 μm fibers and decreases at larger sizes. Incorporation of

submicron-sized fibers into 10-30 μm sized spherical flocs with a

density of 1.05 g/cm^3 by coagulation would result in a contact

efficiency (by settling) of up to 10-fold higher. An even higher

value would result for a more dense floc.

(c) η_1 is given for Brownian diffusion by:

$\eta_1 = 6.4 \ \left(\dfrac{kT}{V_o d_2 f_1}\right)^{2/3}$, adapted from Yao, et al. (1971) and Levich

(1962); f_1 is given in footnote (a). For spherical particles, Yao et

al.(1971) give: for Brownian diffusion $\eta_1 = 4 \ Pe^{-2/3} = 0.9 \left(\dfrac{kT}{\mu d_1 d_2 V_o}\right)^{2/3}$;

for fluid shear $\eta_1 = \dfrac{3}{2} \left(\dfrac{d_1}{d_2}\right)^2$; and for sedimentation

$\eta_1 = \dfrac{g(\rho_p - \rho)d_1^2}{18 \, \mu V_o}$; d_2 = 0.05 cm, V_o = 0.34 cm·s^{-1} (5 gpm·ft^{-2}), the

approach velocity of the fluid; other values are in footnote (a).
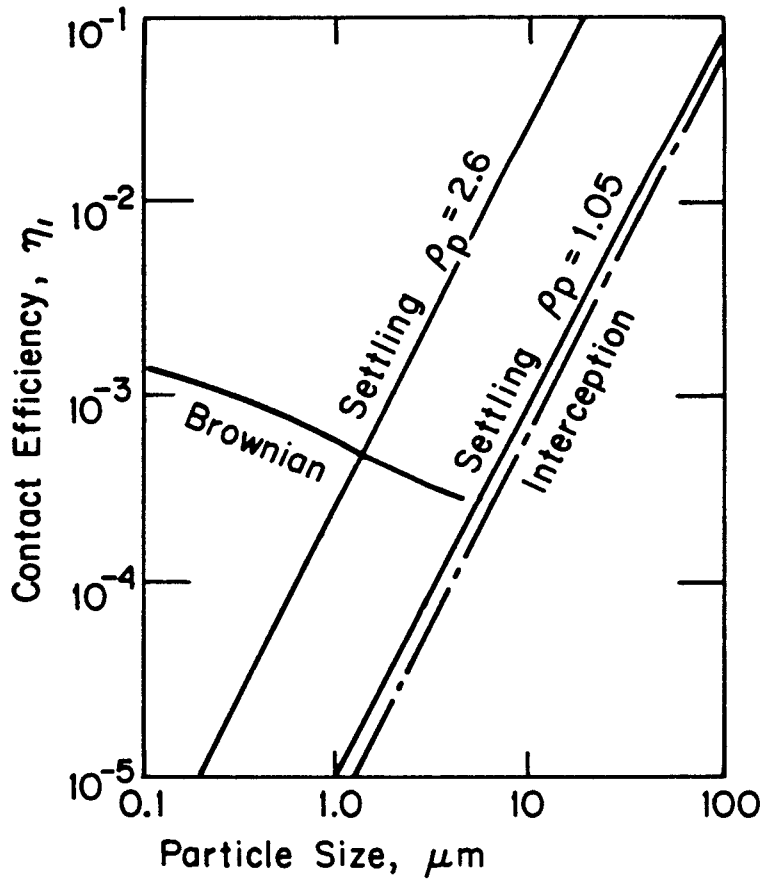
Fig. 2.10. Contact efficiency for deposition
of chrysotile fibers at a stated
length by Brownian diffusion and
deposition at spherical particles
by settling and interception onto
spherical collectors in water at
20°C; adapted from Yao et al. (1971).

Total particle removal in a filter is given by the integrated form of (2.31):

$$n_1/n_1{}^0 = \exp\left(-\frac{3}{2}\;\frac{(1-f)L}{d_2}\;\alpha n_1\right) \qquad (2.34)$$

Optimum removal occurs when particles are fully destabilized ($\alpha=1$) by chemical addition. Water filters at Metropolitan contain 50 cm of anthracite ($d_2 = 0.1$ cm) underlain by 20 cm of sand ($d_2 = 0.05$ cm). Predicted values for $n_1/n_1{}^0$ using these parameters and $f = 0.4$ are given in Table 2.3. Three cases are illustrated: fiber removal without coagulation prior to filtration; removal following coagulation of fibers into loose, low density flocs; and removal following coagulation into dense flocs. These calculations illustrate that significant fiber removal in sand filters is expected only if fibers are first coagulated into larger, loose flocs of 20 μm or greater in size or into dense flocs of 5 μm or greater in size.

2.3.2.2. Reported Removals in Water Filtration Studies

Results of pilot-plant studies on asbestos fiber removal are reported for three different waters: Duluth, Minnesota, on Lake Superior water containing amphibole fibers (Logsdon, 1979); Seattle and Everett, Washington, on water originating in the Cascade mountains containing chrysotile fibers (Kirmeyer, 1979); and Quebec surface waters containing chrysotile fibers (Hunsinger et al., 1980). Fiber removal has also been monitored in full-scale plants in Minnesota (Logsdon et al., 1983), Washington (Logsdon et al., 1981) and Southern California (McGuire et al., 1983).

Table 2.3. Predicted Fiber Removal in Water Filtration[a]

Particle size, μm	η_1	η_1/η_1^o	Mechanism[b]
no coagulation			
0.1	1.4×10^{-3}	0.3	B
0.5	8.3×10^{-4}	0.5	B
1.0	6.0×10^{-4}	0.6	B
coagulation ($\rho_p = 1.05$)			
1.0	1.6×10^{-4}	0.9	B
10	1.4×10^{-3}	0.3	B, I, S
20	5.6×10^{-3}	0.01	I, S
25	8.8×10^{-3}	0.0008	I, S
coagulation ($\rho_p = 2.6$)			
1.0	4.2×10^{-4}	0.5	B, S
3.0	2.3×10^{-3}	0.15	S
5.0	6.5×10^{-3}	0.005	S

[a]From Figure 2.8 and equation (2.32).
[b]B = Brownian, I - interception, S = settling.

These studies were designed to identify the operating conditions that achieved maximum fiber removal, generally by varying the dose of inorganic salt and organic polymer added prior to filtration. the mechanism of fiber removal and the important chemical variables in that mechanism were not addressed.

Sand filtration preceded by coagulation with alum (30-50 mg/L) was shown to reduce fiber concentrations in a raw water from Quebec from 1.3×10^9 fibers/L to below 10^5 fibers/L (Lawrence & Zimmerman, 1976). Fibers were incorporated into the aluminum hydroxide floc formed in coagulation. Polymer addition (0.5-1.0 mg/L) was required to achieve high removal of the resulting turbidity. Further pilot tests of a Canadian surface water spiked with chrysotile asbestos fibers to 10^6-10^7/L achieved approximately a one order-of-magnitude fiber removal; coagulant additions were 30 mg/L alum and 5 mg/L activated silica (Hunsinger et al., 1980).

Reductions in chrysotile fiber levels by 10-1000 fold were achieved in a direct-filtration pilot study on Tolt river water, Washington (Kirmeyer, 1979). Influent concentrations were 10^6-10^7 fibers/L. Alum (3-10 mg/L) was the primary coagulent; in some cases lime (1-4 mg/L) or cationic polymer (2-3 mg/L) was added. A non-ionic or anionic polymer (0.02-0.3 mg/L) was added as filter aid.

From these studies it is apparent that fiber removal can vary from near zero to over 99.99 percent in a given treatment plant, depending on the operating conditions. Mean removals of about 99 percent are typically observed in Metropolitan's plants (Bales et al., 1984).

CHAPTER 3

MATERIALS AND METHODS

3.1. PARTICLES

Most particles used in this experimental work were from natural

ore, have heterogenous surfaces, are of non-uniform size and contain

variable amounts of impurities. The objective in using natural

material rather than model particles is to relate this work more

closely to the weathering behavior of natural silicate minerals,

particularly chrysotile asbestos, in freshwaters. Chrysotile

characterization work reported in this section is aimed toward

defining the range of its physical and chemical properties, both in

the laboratory and in natural-water systems.

3.1.1. Chrysotile

The starting material is raw chrysotile (Calidria) ore

from the Union Carbide Corporation mine near Coalinga, California. As

received, the material is moist and includes particles from about five

millimeters down to one micron in size. Components of the ore include

magnetite, lizardite, brucite and trace impurities, along with

short-fiber chrysotile (Mumpton & Thompson, 1975). Laboratory methods

used to purify particle samples are generally harsher and of shorter

duration than natural weathering, where physical impacts are of low

intensity and chemical attacks are by weaker acids. Chrysotile

purification procedures were designed to minimize both structural

damage to fibers and changes in particle surface.

3.1.1.1. Chrysotile Preparation Procedure

The method used to separate fibers from the raw ore is illustrated on Figure 3.1. The raw ore was hand sorted by texture and color to remove obvious impurities such as massive serpentine or large magnetite fragments, suspended in deionized water and sonicated to release fibers. Separation involved diluting, stirring with a magnetic bar to collect magnetite and decanting to remove larger, heavier material. It was assumed that impurity brucite would dissolve away; the dissolution rate for brucite is about 1000-fold faster than that for chrysotile. The lack of excess magnesium in the processed ore was taken as evidence that impurity brucite was not present. Separation of magnetite from chrysotile by sonication and stirring in water occurred within minutes. Simple grinding fails to separate the two minerals (Allen & Smith, 1975).

After gravity settling, suspensions were centrifuged to separate solids from supernatant. Resulting solids were washed with deionized water and recentrifuged until the centrate reached a constant conductivity. The paste was then dried in an oven at 70 C. The dried cake was placed in an alumina dish with a movable puck and crushed by oscillating for 30 seconds in a Spex Shatterbox. By this procedure about 50 grams of raw ore can be processed in one day, yielding about 30 grams of fibers.

Some initial consideration was given to making synthetic chrysotile, but physical characteristics of the resulting fibers (Yang, 1961) do not resemble those of the natural material found in California. Further, synthetic fibers may contain relatively high

1. hand sort   2. suspend & sonicate   3. magnetic stir & decant

4. settle, centrifuge,   5. dry   6. crush
   wash & recentrifuge
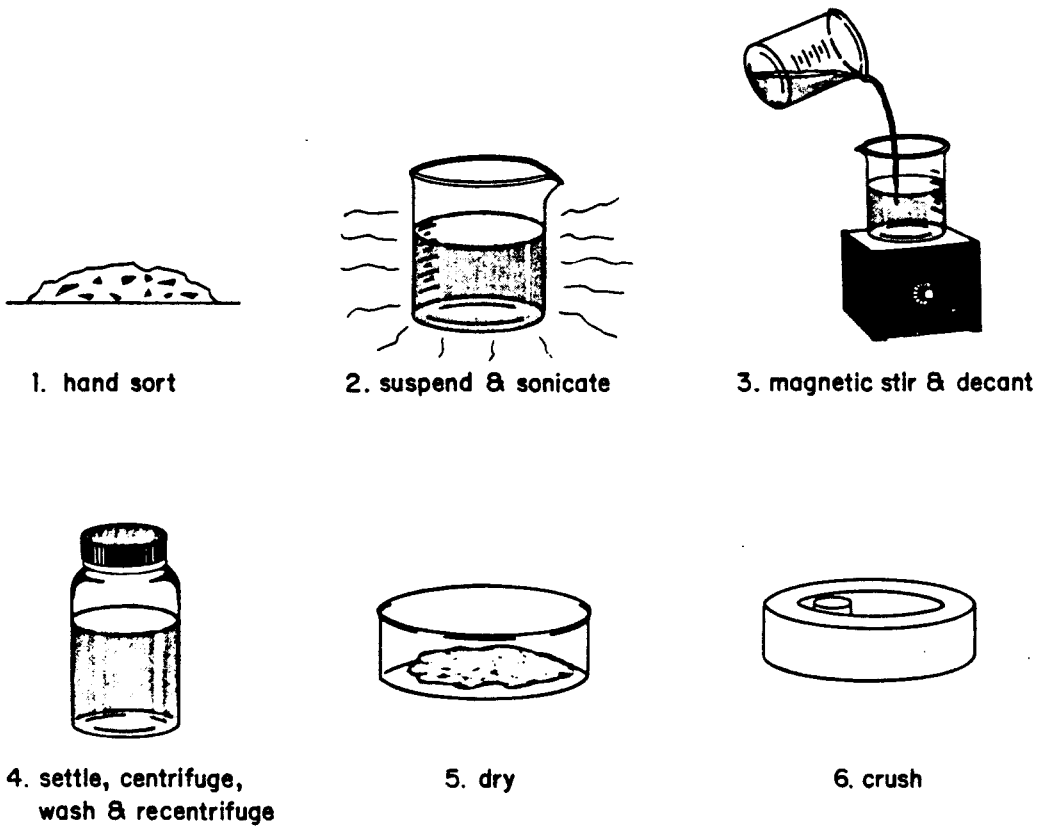
Fig. 3.1. Chrysotile ore purification procedure.

fractions of impurity brucite or silica (Hostetler & Christ, 1968), the two starting materials for synthesis.

3.1.1.2. Chrysotile Chemical Characteristics

Chemical composition of the purified ore was determined by digestion in HF and aqua regia in a teflon bomb (Bernas, 1967) using the molybdate-blue method of Strickland and Parsons for silica (Fanning & Pilson, 1973) and atomic absorption spectrophotometry (AAS) for cations. Na_2SiF_6 was used as a silica standard and Baker analytical standard (1 mg/ml in HNO_3) for magnesium. Results are listed in Table 3.1. Iron accounts for about 3.4 percent of the cation in the octahedral layer. A similar level is reported in a typical analysis by Union Carbide, also listed in Table 3.1. The more extensive analyses of Mumpton and Thompson (1975) are shown as well. In addition, the purified ore contains about 0.5 percent magnetite, determined from the amount of residue collected on the magnetic spin bar in one five-day, constant-pH experiment.

The resulting chemical formula for the analyses done as part of this work is $(Mg,Fe)_3Si_{2.2}O_{5.1}(OH)_4$, versus $Mg_3Si_2O_5(OH)_4$ for pure serpentine. The magnesium to silica ratio in this work is lower than for the other reported analyses. Apparent molar ratios of magnesium plus iron to silica are 1.36 in the current work, 1.54 for the Union Carbide analysis and 1.57 for Mumpton and Thompson's analyses. Analysis of centrate from ore purification showed dissolved magnesium concentrations near 2 mg/L; this is much lower than the nearly 100 mg/L needed to account for the reported differences. Rather, the differences are assumed to be due to different purification and cleaning procedures, as well as raw-material differences.

Table 3.1 Calidria Ore Composition

Component	Weight Percent		
	This Work	Union Carbide[a]	Mumpton & Thompson[b]
MgO	39.70	41.9	42.41
SiO_2	45.44	42.8	41.40
Al_2O_3	≤ 1	0.5	0.13
Fe_2O_3	4.62	4.0	5.02
CaO	0.18	0.11	0.26
NiO	0.03	0.33	0.03
MnO_2	0.09	-	-
K_2O	0.15	-	-
Na_2O	ND[c]	-	-
H_2O & CO_2	9.8[d]	13.5	13.47

[a]Analysis supplied by Union Carbide Corp., with ore.

[b]Average of three reported analyses; reference: Mumpton and Thompson, 1975.

[c]None detected.

[d]Estimated by subtracting sum of other components from 100.

Trace metals associated with chrysotile are generally found in impurity minerals rather than as substitution products in chrysotile (Reimschussel, 1975). The organic content of a hand-sorted, milled Quebec chrysotile was determined by extraction with benzene and cyclohexane to be from 0-50 ppm (Gibbs, 1971). The extract contained a peak at C_2, with a unimodal distribution about that point. It is not known if the organics are part of the crystal or are adsorbed on the surface. The organic material is thought to have its origin either: 1) from circulating groundwater, 2) of magmatic origin, 3) of sedimentary origin, or 4) from distillation of pre-existing oil pools. Percolation of surface water and sample contamination during processing were considered unlikely. Speil and Leinweber (1969) also note that chrysotile contains natural organic impurities. They report that cyclohexane extraction of 11 U.S. and Canadian milled samples yielded from 40-500 ppm organics.

3.1.1.3. Chrysotile Physical Characteristics

The surface area of the purified fibers, measured by single-point BET nitrogen adsorption using a Quantasorb system (Quantachrome Corporation), ranged from 46.3 to 57.7 m^2/g. A representative value is 48.5 m^2/g; this is used in subsequent calculations.

Figure 3.2 shows the distribution of fiber lengths in the purified ore; also shown are the overall distributions for samples taken from the Feather river and from Metropolitan's source-water reservoirs (McGuire et al., 1982; Bales et al., 1984). The natural-water samples have a flatter distribution, reflecting breakup of the larger fibers and disappearance of the smallest size particles. Techniques for
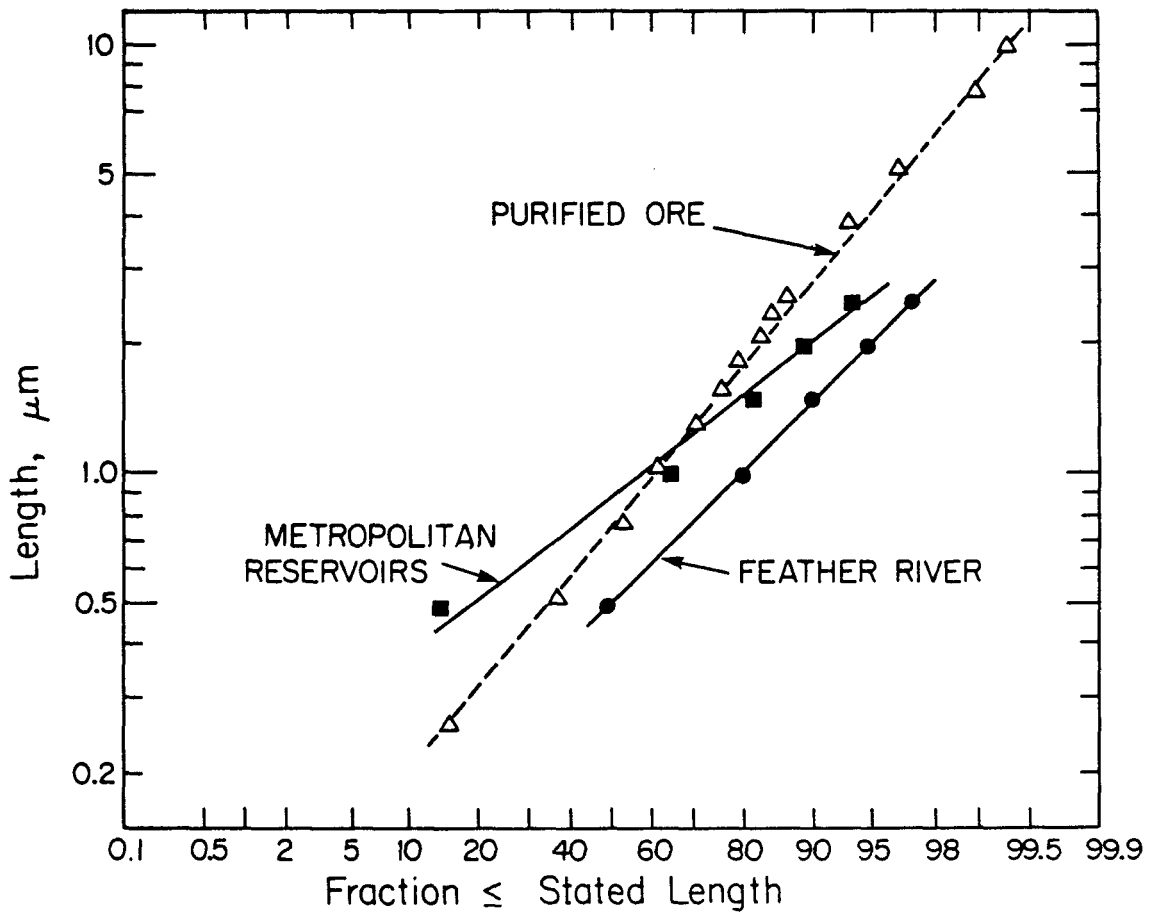
Fig. 3.2. Chrysotile size distribution; values for purified ore from transmission electron microscopy analysis of 500 fibers; includes both single fibers and fiber bundles.

further separating fibers by length (Spurney et al., 1979) were not applicable here.

The size distribution for the purified Calidria ore was obtained from raw ore without intense grinding. Langer et al. (1978) report nearly the same size distribution for Calidria ore dispersed in one percent amyl acetate. Following milling for one minute, their size distribution was shifted down and to the right, with a slope nearer that of the natural-water samples on Figure 3.2. Longer milling shifted the size distribution further down and to the right.

Spurney at al. (1979) note that although use of wetting agents or organic solvents such as methyl alcohol, ethyl alcohol, isobutyl alcohol, etc. facilitates preparing chrysotile suspensions, these organics may adsorb and change surface physical-chemical properties, making the resulting fibers unsuitable for representative biological experiments. These investigators used only double-distilled water to suspend fibers during the sample preparation. They state that surface properties in an aqueous suspension remained practically unchanged during fiber size-separation experiments.

Langer et al. (1974) noted that grinding Quebec chrysotile in a Waring blender for 30 minutes produced irregular rather than straight fiber edges; some fibers exhibited a deformed and collapsed central capillary. Spex milling produced some crushed fibers, but no irregular edges were noted. Speil and Leinweber (1969) show an electron micrograph of Spex-milled chrysotile in which none of the original structure is evident. X-ray diffraction confirmed that the fiber structure was destroyed. They suggest that structural changes were caused by momentary localized temperature surges in a fiber as it

absorbed the impact energy. They confirmed this by comparing fibers that were ball milled wet versus dry. Wet milling precludes high localized temperatures. Langer et al. (1978) also note physical structural and surface damage as well as decreased hemolytic activity for fibers as milling time is increased.

The above considerations indicate that the short milling time (30 seconds) used in the present work had little effect on the size distribution of fibers originally present in the ore. Also, sonication produces fibers with a size distribution similar to that achieved with an organic dispersing agent -- amyl acetate in the work by Langer et al. (1978). The purified ore exhibited electron-diffraction patterns characteristic of chrysotile and revealed no damage due to processing. Figure 3.3 shows typical transmission electron micrographs of the purified ore and of fibers separated from natural waters.

3.1.2. Brucite

Three different $Mg(OH)_2$ materials were used. Initial potentiometic surface-charge experiments were done with $Mg(OH)_2$ powder reagent (MC/B Manufacturing Chemists), which is $\geq$ 95 percent magnesium hydroxide. BET surface area, measured by single-point nitrogen adsorption, is 45 m^2/g. The second and third were natural brucite ($Mg(OH)_2$) from a mining area in Nevada and are termed Lodi brucite and Gabb brucite, respectively. Both were obtained as rocks, through Wards Natural Science Establishment, Rochester, New York. The raw ore was broken and hand sorted to remove obvious impurities, then crushed with a mortar and pestle. Analyses by the same method as above for chrysotile indicated that the first material was about 48 percent
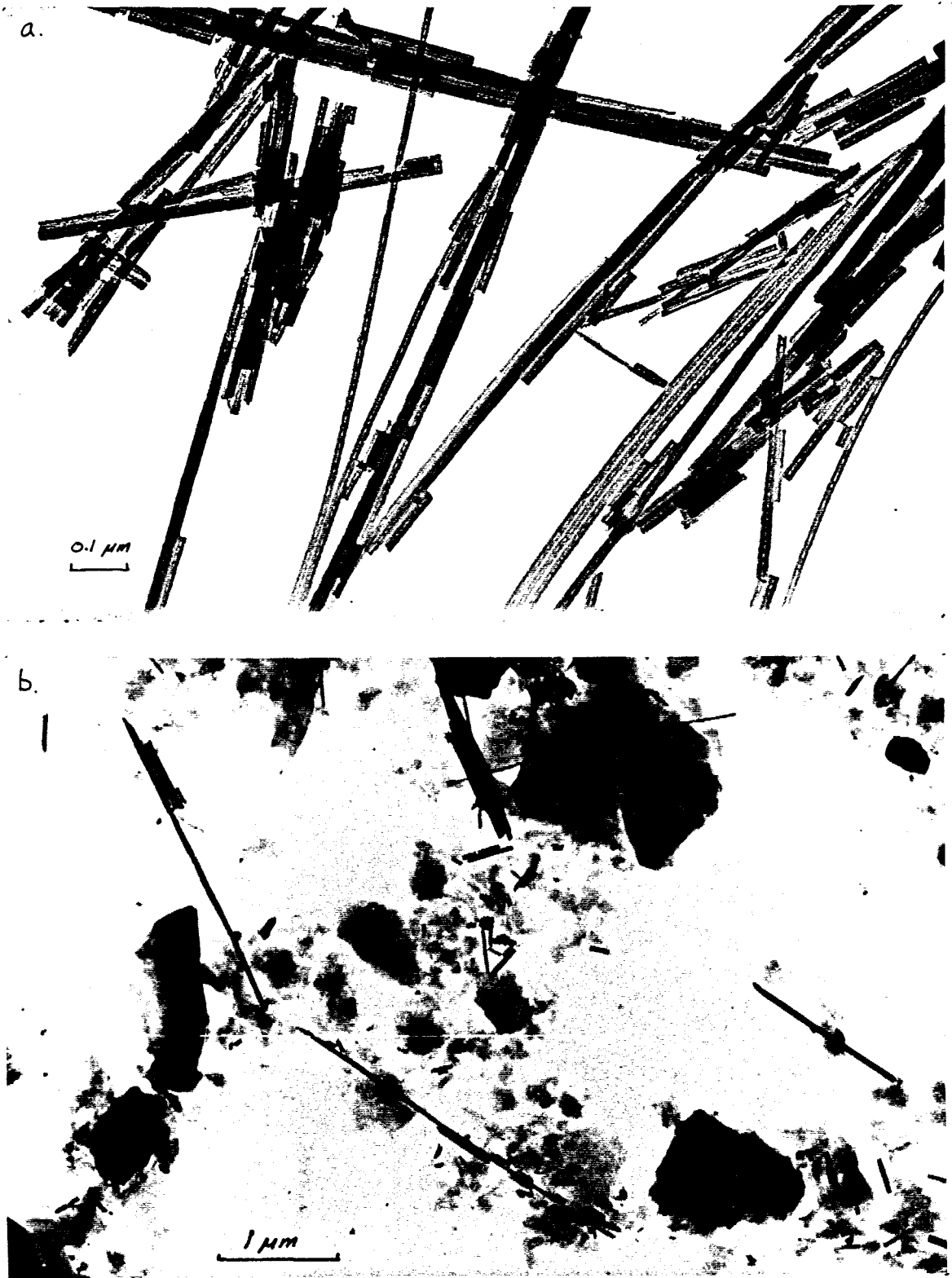
Fig. 3.3. Electron micrographs of chrysotile fibers; a) from chrysotile ore, b) in California aqueduct sediment.

$Mg(OH)_2$ and the second material was 100 percent $Mg(OH)_2$. Surface areas were measured to be 0.67 and 1.96 m^2/g respectively.

3.1.3. Aluminum Oxide

Adsorption experiments were carried out using "Aluminum Oxide C" (Alox), which is manufactured in Germany and was obtained from Degussa Corporation, Teterboro, New Jersey. It is reported to consist predomonantly of γ-Al_2O_3 (Kummert & Stumm, 1980). Prior to its use, the alumina was washed once with 0.1 M NaOH and seven times with double-distilled water (Hohl & Stumm, 1976). The suspension was then centrifuged between washings, with some loss of fine material in the centrate. The washed material was stored in distilled water for approximately one year prior to use. Stock suspensions for experiments were made by drying a portion of the washed alumina at 110 C, grinding lightly with a mortar and pestle to break large aggregates, and transferring the required amount to 0.01 M NaCl solutions. Surface area of the washed material, measured by single-point BET nitrogen adsorption, is 82 m^2/g. This is lower than the 100 m^2/g reported for the untreated colloid and the 130 m^2/g reported for the washed colloid by others (Kummert & Stumm, 1980). The lower value may reflect both the removal of fines during washing and failure to break aggregates before making surface-area measurements.

3.1.4. Silica

Silica (SiO_2) was Min-U-Sil 30 obtained from Pennsylvania Glass Sand Corporation, Berkeley Springs, West Virginia. The manufacturer reports a silica content of 90.7 percent, a specific

gravity of 2.65, a surface area of 0.54 m^2/g and a mean particle size of 8.8 μm. This is a non-porous material.

The cleaning procedure was less rigorous than that used by Vuceta (1976) and Young (1981); the latter noted little difference in adsorption characteristics of cleaned versus uncleaned material. Silica was heated at 500 C for 24 hours to remove organic impurities. It was then washed successively with 4 M HNO_3 and 4 M NaOH. Following each wash, silica was rinsed with double-distilled water until the pH of the supernatant was the same as the pH of the double-distilled water. Washed silica was dried overnight at 130 C. It was planned that many of the fines would be removed in the supernatants. The resulting particle size distribution (Figure 3.4) suggests that coarse material was lost, however.

3.2. OTHER MATERIALS AND CHEMICALS

Acid and base used for the constant-pH experiments was made from Dilut-it analytical concentrate (J.T. Baker). Other chemicals were reagent grade; solutions were filtered through 0.22 μm Millipore filters prior to use. Nitrogen gas was "Matheson-grade," containing less than 0.5 ppm CO_2. Gas was further cleaned and humidified by bubbling successively through 5 M KOH and 0.5 M KOH and two vessels containing distilled water. Nitrogen-carbon dioxide mixtures were from Matheson, certified to be within one percent of the stated CO_2 content.

3.3. EXPERIMENTAL DESIGN

Insofar as possible, experiments were designed to model conditions in water delivered to Southern California through the east
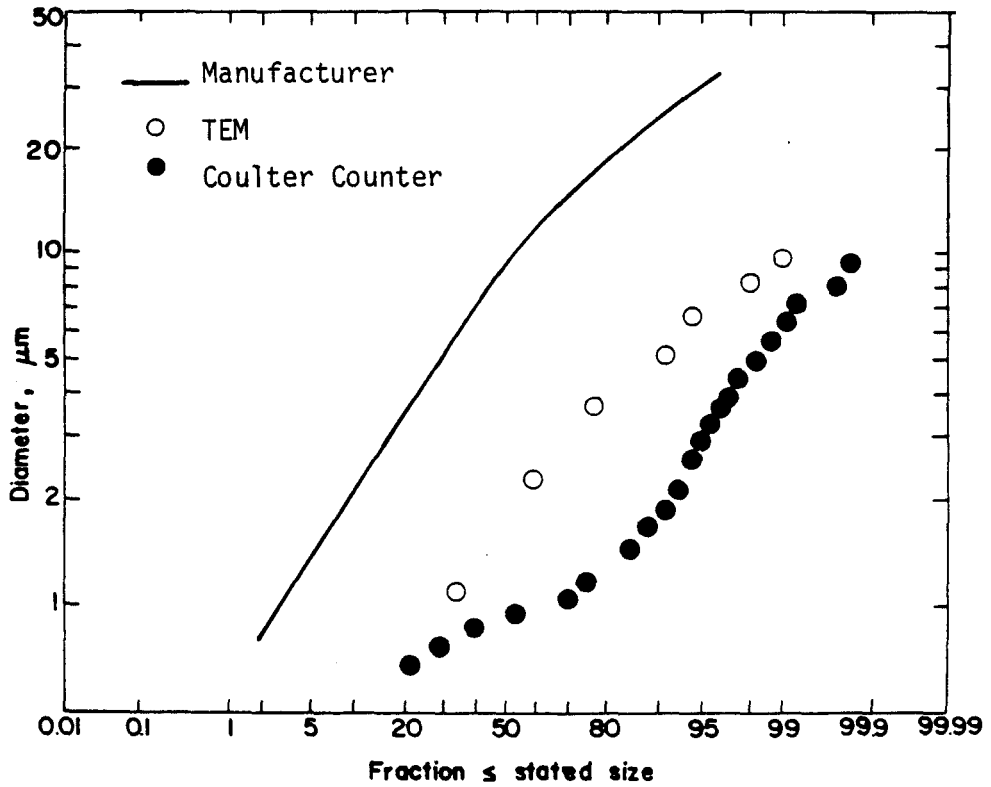
Fig. 3.4. Size distribution of Min-U-Sil 30; comparison of distribution reported by manufacturer versus distributions measured on washed material by TEM counting and by Coulter Counter.

and west branches of the California aqueduct. Major ions are Na^+, HCO_3^- and SO_4^{2-}; ionic strengths are 0.009 M and 0.013 M in the east and west branches respectively. Table 3.2 lists characteristics of the water entering Metropolitan's treatment plants. Adsorption and mobility experiments were carried out in ~ 0.01 M $NaCl/NaHCO_3$ solutions. Dissolution rates were generally measured in 0.1 M solutions; using 0.1 M electrolyte assured that ionic strength remained nearly constant despite addition of millimolar amounts of magnesium to solution.

3.3.1. Potentiometric Experiments

Dissolution and surface-charge behavior were monitored in constant-pH, constant-temperature suspensions of two grams of chrysotile per 200 ml of 0.01-0.1 M electrolyte (KNO_3, $NaNO_3$, NaCl or Na_2SO_4). Some experiments were done with either catechol (1,2-dihydroxybenzoic acid, $C_6H_4(OH)_2$) or oxalic acid ($C_2H_2O_4$) present. Duration was from three to five days, chosen as sufficient to establish a linear dissolution rate after the initial one-day non-linear dissolution start-up period. A constant-pressure nitrogen or nitrogen-carbon dioxide (350 ppm) atmosphere was maintained by bubbling gas through the suspensions. Fifty such experiments were carried out; experimental parameters are listed in Table 1 of Appendix II.

Surface charge density, as defined by equation (2.4) was inferred from the amount of acid or base added in excess of that needed to dissolve the mineral:

$$\sigma = \frac{F}{sa} \ (C_A - C_B - 2[Mg^{2+}] - [MgOH^+] + [OH^-] + [H_3SiO_4^-]) \qquad (3.1)$$

Table 3.2 Characteristics of Metropolitan Surface Waters for 1981-82
Water Year

Property	Units	West Branch[a]		East Branch[b]	
		Average	Range	Average	Range
Silica, SiO_2	mg/L	14.1	13.0-15.4	13.3	11.8-16.0
Calcium	mg/L	44	36-55	22	19-27
Magnesium	mg/L	18.1	16.0-20.5	12.9	9.5-15.5
Sodium	mg/L	51	44-58	50	34-65
Potassium	mg/L	2.8	2.5-3.2	2.6	1.5-3.4
Bicarbonate	mg/L	126	118-140	87	72-105
Sulfate	mg/L	106	85-133	46	34-73
Chloride	mg/L	58	43-66	67	40-96
Nitrate	mg/L	1.7	0.6-2.7	3.1	1.0-6.1
pH	--	7.8	7.4-8.1	8.0	7.8-8.3
Total dissolved solids	mg/L	359	334-385	260	201-309
Total hardness	mg/L	183	162-218	107	92-129
Specific conductance	mho/cm	617	604-635	477	377-565
Turbidity	ntu	1.3	1.0-2.2	2.0	0.9-5.4
Temperature	deg.C	14.0	12.1-19.0	14.9	9.0-24.0

[a]Castaic L. effluent, sampled at Jensen water treatment plant.

[b]Silverwood L. effluent, sampled at Devils Canyon afterbay.

s is the specific surface area of the particles used in the experiments and a is the particle concentration. No measure of surface charge density was available from experiments with bicarbonate, catechol or oxalate present as uncertainties in speciation and complex formation were large relative to other terms in equation (3.1). The amount of catechol or oxalate adsorbed to the solid surface was determined throughout the experiment by measuring changes in solution concentration.

At intervals from approximately 12 to 24 hours samples were withdrawn with a 10 ml Plastipak syringe and passed through a 0.1 μm Nucleopore filter for analysis of dissolved magnesium silica and organics.

To verify that particle concentration did not affect results, experiments at pH 8 were run using 0.18, 1.0 and 2.0 grams of chrysotile per 200 ml; the dissolution rate per gram of solid added was the same in each case, as shown on Figure 3.5. To verify that the glass components were not contributing significant concentrations of silica, parallel experiments were run using brucite (magnesium hydroxide) as the starting material. Above pH 9.5, dissolved silica in the brucite experiments was approximately 5 percent of that in the chrysotile experiments. This amount was from the beaker, pH electrode or glass tube used to bubble in nitrogen gas.

Experimental conditions were designed such that both magnesium and silica were far from solubility equilibrium (Figure 3.6). In suspensions without carbon dioxide, $Mg(OH)_2(s)$ controls magnesium solubility, whereas $MgCO_3(s)$ is controlling for $PCO_2 = 10^{-3.5}$. In nearly all cases experimental conditions were set up to operate to the
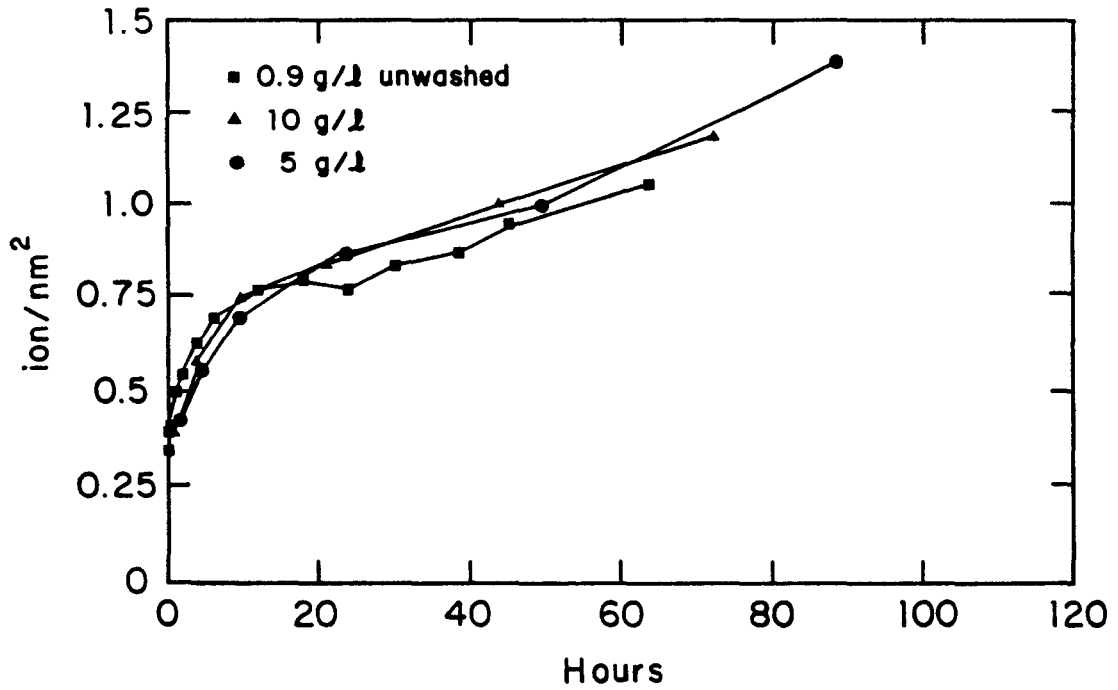
Fig. 3.5. Magnesium release rate at different solids
concentrations; chrysotile at pH 8, 0.1 M KNO_3, N_2 atm.,
25 C.

left of the brucite curve of Figure 3.6. By excluding CO_2 from the dissolution experiments, magnesite could not form.

Chrysotile activity products have been determined experimentally for periods from three months (Hostetler & Christ, 1968) to two years (Luce, 1969). These reflect steady-state dissolution and are not true equilibrium constants. Solid-aqueous solution equilibrium diagrams for the $MgO-SiO_2-H_2O$ system (Hemley et al., 1977) suggest that at 25 C talc is the stable phase in waters with the composition like that of California aqueduct water. Slow reactions apparently prevent its formation over the short times (months) that fibers are suspended in rivers and reservoirs of the state. Formation of minerals other than those shown on Figure 3.6 was not considered, either in dissolution experiments or in modelling dissolution in natural waters.

3.3.2. Electrophoretic Experiments

Electrophoretic mobility of chrysotile was measured on 5-10 mg/L suspensions, again at constant pH. Conditions were chosen to parallel those of the potentiometric experiments, but with solids concentration approximately 1000-fold lower. Electrolyte concentrations were generally 0.01 M.

Mobility measurements were made on chrysotile suspensions aging up to 820 hours in 0.01 M NaCl. Duration of most experiments was from 40 to 100 hours. In many cases more than one experiment was performed under the same conditions to determine the reproducibility of results. The mobility of chrysotile in the presence of three low-molecular-weight organic anions -- phthalate, oxalate, and catechol -- was determined. In a typical experiment, the mobility of chrysotile at constant pH in 0.01 M NaCl was monitored for 24 to 48 hours, a known
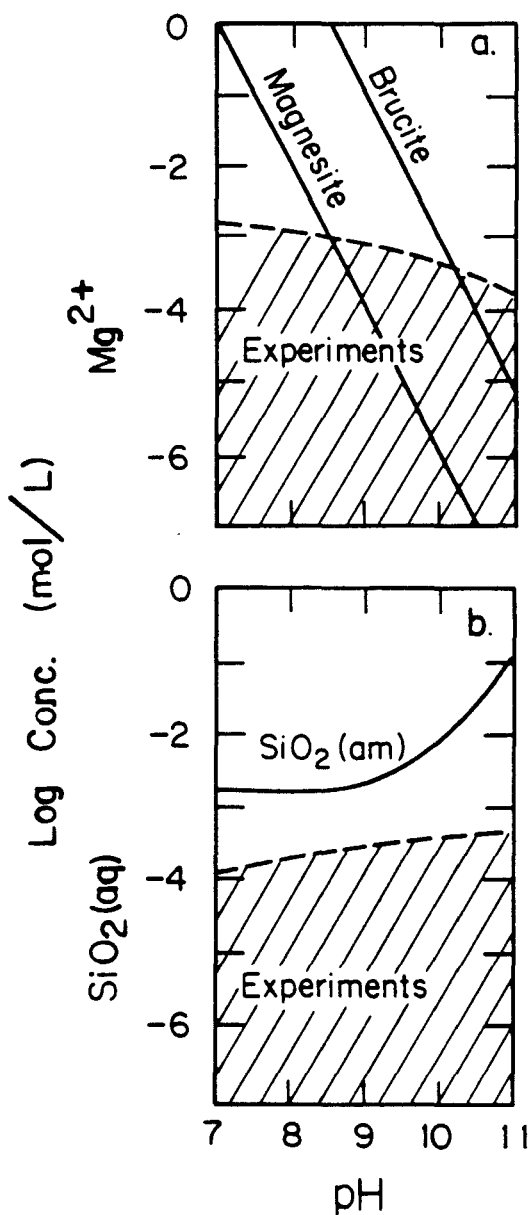
Fig. 3.6. Concentration ranges observed in experiments compared to a) magnesium and b) silica solubility; broken line in each graph is the maximum concentration observed in the dissolution experiments; in most cases the experimental concentrations fell below the line, in the hatched area; solid lines show solution concentrations in equilibrium with appropriate solid phases; adapted from Stumm & Morgan (1981); magnesite plotted for P_{CO_2} = 10-3.5.

concentration of organic acid was added, and mobility was monitored for 24 to 48 hours longer. The mobility of chrysotile in the presence of NOM was determined in a series of experiments at pH 8.

To distinguish the effects of dissolution and adsorption on chrysotile mobility, a series of experiments was carried out using aluminum oxide (Alox). In the absence of organic matter and at constant pH, the mobility of Alox is constant. Mobility changes upon addition of organic matter are due to adsorption, versus a combination of adsorption and dissolution on chrysotile. Two organics, catechol and NOM were used in experiments with Alox. Stock aluminum oxide suspensions for mobility experiments were from 10 to 40 mg/L.

3.3.3. Adsorption Experiments

Adsorption of catechol, oxalate and NOM were measured in parallel with electrophoretic experiments. Conditions were like those of the potentiometric experiments. As with the electrophoretic experiments, electrolyte concentrations were generally 0.01 M. Ionic strength changes in the range 0.002-0.1 M were observed to not strongly influence NOM adsorption onto aluminum oxide (Davis, 1980). Stock chrysotile and alumina suspensions were 100 mg/L and 800 mg/L respectively. Organic concentrations were higher in the adsorption experiments, to maintain the same solid-to-organic ratio as in the mobility experiments. Batch adsorption experiments lasting up to 36 hours were also carried out. These were at room temperature ($\sim$25 C) and open to the atmosphere; pH was held constant.

Some initial batch experiments were done with two other organic acids -- salicylic and phthalic. Both adsorbed to a smaller extent

onto chrysotile than did either catechol or oxalic acid. Further, magnesium interfered with UV absorbance measurements of salicylic and phthalic acids even at acid pH's.

3.4. APPARATUS

3.4.1. Constant-pH Setup

Two constant-pH experiments were run concurrently. Each suspension was in a constant-temperature (25 C) jacketed glass beaker under either a nitrogen or nitrogen-carbon dioxide atmosphere. Each beaker was equipped with either a Radiometer or Orion Ross combination electrode. These were connected to an Orion 801A pH meter via an automatic switching box. In many cases the switching box was not used and the electrodes were connected to separate Orion 801A pH meters. In most cases, radiometer ABU11 autoburettes were used to add acid or base. For some experiments a Gilmont 2.5 ml micrometer syringe driven by a stepping motor was used. An Apple II+ computer system recorded pH and controlled autoburettes. Figure 3.7 is a schematic of a typical setup.

The Apple II+ computer was equipped with a real-time clock and an Interactive Structures, Inc. AI13 data acquisition system, which is a 16-channel, 12-bit, analog-to-digital converter. The recorder output of each pH meter was amplified and connected to a channel of the AI13. Both the AI13's and the pH meter's digital outputs were calibrated with standard pH buffers at the outset of each experiment. A basic program was used to convert the AI13 signal to millivolts, compare it to a predefined set point, and actuate a relay that toggled the Radiometer autoburettes. The latter were set to deliver a constant volume, 0.1 ml, each time. The stepping motors on the micrometer
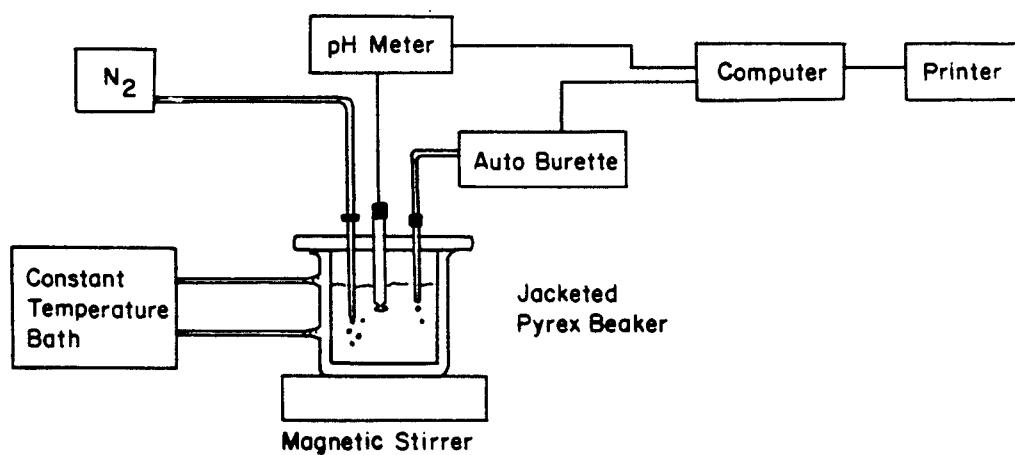
Fig. 3.7. Typical constant-pH reactor setup; two experiments were run concurrently by addition of a second beaker and autoburette.

syringes were controlled by an STM103 Slo-Syn translator module, which was activated by a signal of predetermined duration from the computer.

A machine-language subroutine was used to activate and sample the AI13 outputs, average 5000 conversions, and store the result. Both pH meters could be sampled in less than one second. Sampling of the signals was done at about ten-second intervals. When a single pH meter was used with two electrodes via the switching box, each electrode was sampled for about one minute before switching. Each time one of the autoburettes was activated, the time of day and burette number were printed out. The AI13 signal was printed out at ten-minute intervals to enable later verifying that pH remained constant. In some cases one-minute intervals were used.

Schematic diagrams of the control circuits and listings of the computer programs are in Appendix V.

3.4.2. Electrophoresis

Electrophoretic mobility was measured using a Rank Brothers (Cambridge, England) particle micro-electrophoresis apparatus, Mark II, equipped with a cylindrical cell and 3 mw He/Ne laser illuminator. The greater illumination provided by the laser enabled viewing chrysotile particles in the 0.1 μm size range; many of these are not visible with the Rank II's white light. The rectangular cell and white light were used for aluminum oxide particles.

From 20 to 40 particles were timed in each sample, half at each stationary level. Voltage gradients ranged from 4 to 12 $V \cdot cm^{-1}$ with the cylindrical cell and from 8 to 16 $V \cdot cm^{-1}$ with the rectangular cell. Mobility did not depend on field strength for the cylindrical

particles; a dependence at higher voltage gradients has been noted (van der Drift et al., 1979). For chrysotile, the uncertainty (standard deviation) for a single sample was typically less than 0.25 $\mu m \cdot s^{-1} V \cdot cm^{-1}$ and was typically less than 0.1 $\mu m \cdot s^{-1} V \cdot cm^{-1}$ for Alox.

Results are reported as electrophoretic mobility rather than zeta potential. The ratio of particle radius to double-layer thickness for these experiments is from 10 to 15; Smoluchowski's equation should thus apply at the smaller observed mobilities (Hunter, 1981).

3.5. NATURAL ORGANIC MATTER

Dissolved natural organic matter (NOM) was concentrated from a 190-liter surface-water sample taken on December 5, 1983 from Castaic reservoir. Chemical analyses of water from the reservoir are listed in Table 3.2 (west branch). The long-term average detention time for Castaic and Pyramid reservoirs combined is three years. The range of detention times resulting from demand variations and short circuiting have not been computed. Water from the California aqueduct flows by gravity through Pyramid and then through Castaic. At times water is pumped from Castaic back into Pyramid. The capacity of Castaic is 0.4 km^3, area is 9.0 km^2 and maximum depth is 100 m. Pyramid is about one-half of the size of Castaic.

Water was collected in 20-liter plastic carbouys that had been rinsed successively with 0.1 M NaOH, 0.1 M HCl and double-distilled water. The sampling location was the California Department of Water Resources station 2, near the reservoir's outlet structure. Care was taken to avoid collecting water contaminated by the sampling boat's engine. Samples were acidified to pH 2 with HCl within two hours of

sampling and stored at 4 C. Extraction onto XAD-8 was begun the same day and was completed within 48 hours.

The extraction column was 5.4 cm I.D. and 50 cm long. 500 cm^3 of XAD-8 that had been previously extracted in a Soxhlet apparatus and stored in methanol was packed. Cleanup after packing followed that used by Dempsey (1981). Glass wool was used as a support. The column, support and tubing were rinsed by recirculating 0.01 M HCl for 2 hours, 0.01 M NaOH for 2 hours and 0.01 M HCl for 2 hours. This was followed by soaking overnight in methanol before packing the resin.

All 190 liters of lake water were pumped through the column in a downflow mode at the rate of 6 L/hr. A Minarex variable-speed peristalic pump with silicon-rubber tubing was used. Other connecting tubing was glass. Total organic carbon (TOC) and ultraviolet (UV)absorbance over the range 240-300 nm in the column effluent were periodically monitored.

The column was eluted by first lowering the liquid level to just above the resin, then pumping in an upflow mode one liter of a sodium hydroxide solution maintained at pH 10 with a Radiometer autoburette. This solution was recirculated at 5.4 L/hr until obvious color was removed from the resin. Double-distilled water was used to displace the final volume of eluent. 1.5 liters of 90 mg/L TOC eluent was recovered. It was filtered through a 0.45 μm Millipore filter and stored in a brown glass bottle in the dark at 4 C until used.

A titration curve for the stock NOM solution is shown on Figure 3.8. The plotted points were determined from the amount of base needed to titrate the NOM solution less that needed to titrate 0.01 M
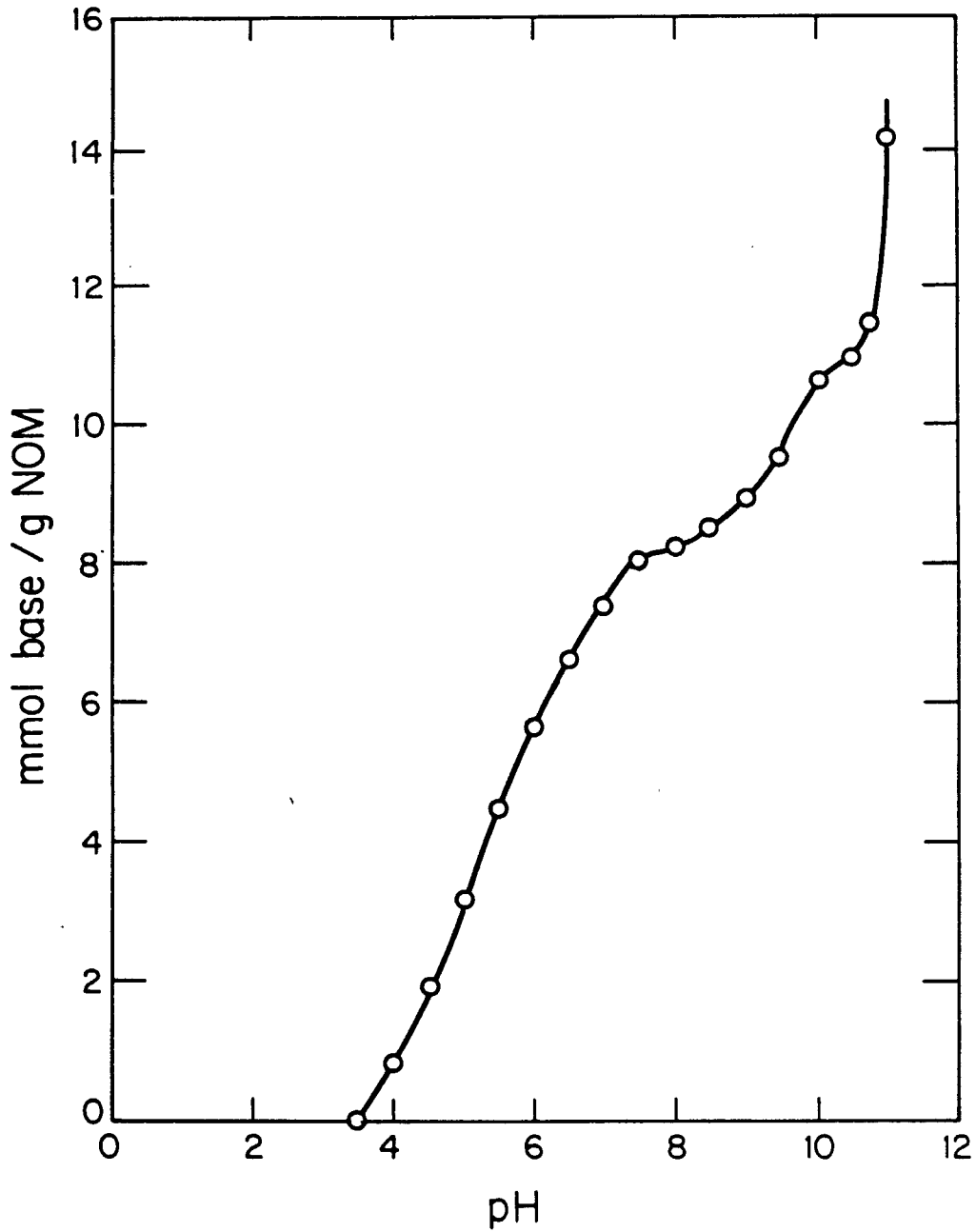
Fig. 3.8. Titration curve of stock solution of dissolved natural organic matter (NOM) from Castaic reservoir; 0.01 M NaCl used as blank.

NaCl under like conditions. Both solutions were adjusted to pH 2 with 0.1 M HCl at the outset. Titration of carboxyl groups appears to be complete at about pH 7.5. This contrasts with the titration curves published by Tipping (1981a) for NOM from three British lakes, where the inflection occurred in the pH range 6-6.5. A second, smaller inflection appears at pH 10.5.

3.6 CHEMICAL AND ANALYTICAL TECHNIQUES

Ultraviolet (UV) and visible absorbance measurements were made using a Beckman Acta CIII. Figure 3.9 shows UV scans for various dilutions of the NOM stock, acidified to pH 2. Absorbance is linearly proportional to concentration in the range 240-280 nm. Scans for filtered samples from the adsorption experiments, acidified to pH 2, were parallel to these curves. Concentrations were determined from three points on the scan -- 240, 260 and 280 nm. A Dohrmann DC50 series with manual injection was used for TOC analyses. Reproducibility was generally $\leq$ 0.5 mg/L. A Dionex ion analyzer was also used for oxalate analyses, however agreement with TOC was poor and standards calibration non-linear. A Varian AA6 atomic absorption spectrophotometer was used for magnesium and other cations.

Transmission electron microscopy was done on a Phillips 201 equipped with selected area electron diffraction (SAED). Two different sample preparation methods were used. For qualitative analyses a 0.01 ml drop of suspension was placed on a carbon-coated 300-mesh copper grid and allowed to dry. For quantitative analyses, 50-100 ml of suspension was filtered through a 0.1 μm Nucleopore filter, the fiber was carbon coated, a portion of the filter was
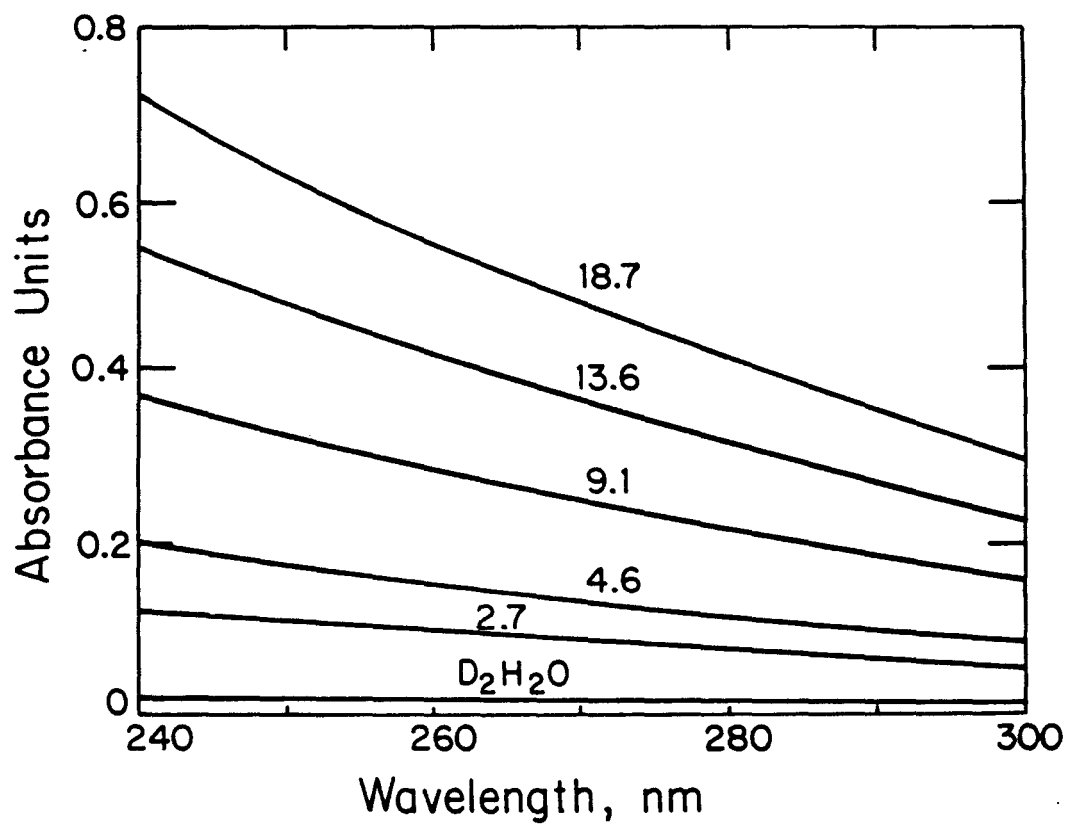
Fig. 3.9. UV scans of Castaic NOM; values on each curve are concentration in mg C/L.

placed carbon-side down on a copper grid in a Jaffe wick washer, and the filter was allowed to evaporate. This is a modification of the U.S. Environmental Protection Agency's recommended procedure for determining the concentration of asbestos fibers in water (Anderson and Long, 1980).

3.7. COAGULATION

Coagulation experiments were designed to determine the approximate rate at which chrysotile fibers coagulate with larger silica particles in a dilute suspension. Two different reactors were used -- a one-liter pyrex beaker and a 0.9-liter pyrex settling column. The column was 53 cm long by 4.6 cm in diameter and was mounted on teflon ends. Holes were drilled in the teflon to enable filling and withdrawing samples.

Two stock suspensions were prepared in 0.01 M NaCl -- 61 mg/l of Min-U-Sil 30 silica and 49 μg/L chrysotile. A 350 ppm CO_2 atmosphere was maintained over both. The chrysotile suspension was made from dilution of an initially-prepared 3.7 mg/L solution that was subsequently diluted to 191 μg/L. Size distributions of the chrysotile and silica are shown on Figures 3.2 and 3.4 respectively. The number concentration of silica particles was determined to be 10^9/L by Coulter counter and 2×10^8/L by counting on the TEM [a]. The lower TEM number and the TEM size distribution used in subsequent calculations because the Coulter counter showed a high background

_____

[a] The average count was 18 particles on a section of each of six squares of a 200-mesh copper grid; standard deviation was two per square.

count in the sample blank, suggesting that the number of silica particles in the smaller size ranges was overestimated due to contamination.

Electrophoretic mobility of the silica in the stock suspension was -1.8 $\mu m \cdot s^{-1} V \cdot cm^{-1}$. An initial mobility measurement made on the chrysotile suspension showed a mobility of +0.7 $\mu m \cdot s^{-1} V \cdot cm^{-1}$. Because of the opposite mobilities it was assumed that there would be no electrostatic barrier to aggregation of chrysotile with silica.

Preliminary experiments showed qualitatively that silica particles did not coagulate with each other. Chrysotile fibers were difficult to disperse, but once dispersed did not appreciably coagulate with each other. Fibers were dispersed by simultaneously sonicating and stirring the stock suspensions. The 49 $\mu g/L$ suspension was prepared by dilution from the 191 $\mu g/L$ suspension after it was verified by TEM analysis that fibers were dispersed. The 49 $\mu g/L$ stock suspension was sonicated for 8-10 hours each day for four days and stirred continuously before being added to the coagulation reactors.

On the four days preceding the coagulation experiment, 50 ml samples of the 49 $\mu g/L$ chrysotile suspension were analyzed by TEM for total fiber count. At least 50 fibers were counted in each of six different grid sections. Results were very reproducible, as indicated in Table 3.3. The number counted was also in the range of the number estimated from the average particle size and specific gravity, lending further confidence to the TEM analytical technique.

The 49 $\mu g/L$ chrysotile suspension was split into two portions and diluted to 4.9 $\mu g/L$. Silica stock was added to one portion, with a

Table 3.3. Total fiber count of 49 µg/L
chrysotile stock suspension.[a]

Date	Hours	10^9 Fibers/L	
		Ave.	S. dev.
5-7-84	1	2.9	0.3
5-8-84	24	2.8	0.5
5-9-84	48	2.3	0.3
5-10-84	72	2.7	0.3
Predicted[b]	-	5	-

[a]Numbers reported were determined from six photographs taken in six different grid squares of the 300-mesh copper grid; from 40-70 fibers were counted on each photograph, the area of which corresponded to approximately $4x10^{-4}$ mm^2 on the original filter.

[b]Based on 10^{11} fibers/mg, the value calculated for average yield of uniform, 0.05 µm dia. by 0.5 µm long fibers.

resulting silica concentration of 11.1 mg/L (3.6×10^7 particles/L). The mixed silica-chrysotile suspension was then split between the two reactors. The pyrex beaker was stirred continuously at a rate just sufficiently fast to keep particles in suspension. The column reactor was inverted twice daily to allow the silica to settle through the chrysotile suspension. Samples were analyzed by TEM after five days to determine the change in fiber concentration in suspension. A three-day sample of the column reactor was also analyzed. Samples of the 4.9 μg/L chrysotile suspension with no silica present were analyzed daily by TEM.

CHAPTER 4

RESULTS AND INTERPRETATION OF EXPERIMENTAL WORK

4.1 WEATHERING BY DISSOLUTION

Three related processes were followed in the constant-pH chrysotile experiments -- dissolution, adsorption and surface charge development. Interpretation of the latter two was augmented by other constant-pH adsorption and electrophoretic experiments.

4.1.1. Surface Coordination of Inorganic Ions

4.1.1.1. Development of Surface Charge on Chrysotile

Results of a typical constant-pH dissolution, surface-charge experiment are shown on Figure 4.1. Concentrations are expressed per unit surface area of solids present and do account for dilution by the acid or base that was added to hold pH constant and for removal of samples.

Figure 4.2 shows the surface-charge development for representative experiments done at different pH's in 0.1 M KNO_3 and NaCl. The initial 24-48 hour rise could be due to slow achievement of steady-state proton adsorption or to slow breakup of fiber bundles into individual fibers. Although chrysotile is crushed to break up the solid cake that forms during sample preparation (section 3.1.1), many clumps of particles are visible in a fresh suspension. After the first day, a suspension looks more uniform with no large clumps visible. Breakup of larger particles to expose more surface area should result in a greater total proton uptake, which would give a greater calculated surface charge. The decrease at longer times is likely due to removal of positively-charged $>Mg-OH_2^+$ sites in the
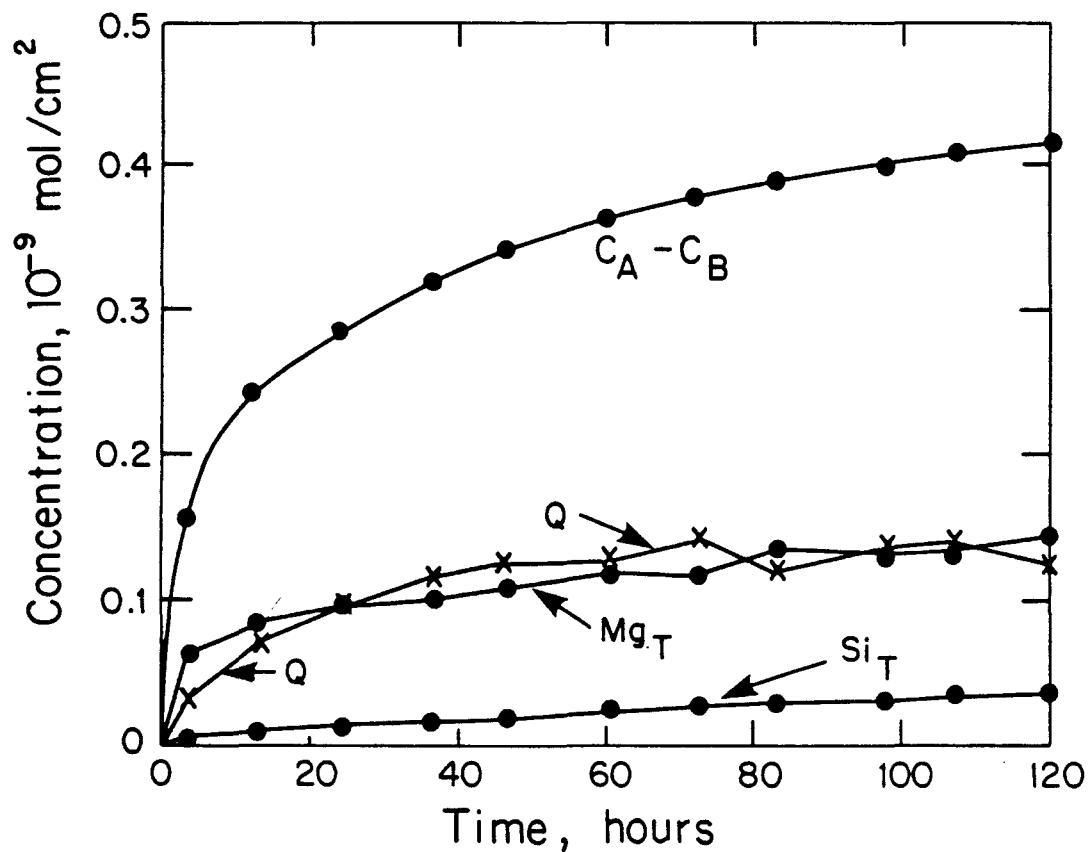
Fig. 4.1. Results of typical constant-pH dissolution experiment; pH 8, 10 g/L chrysotile, 0.1 M NaCl, N_2 atm., 25C; primary data and calculations are shown in Appendix II; data for other experiments in Appendix III; Q is surface charge.
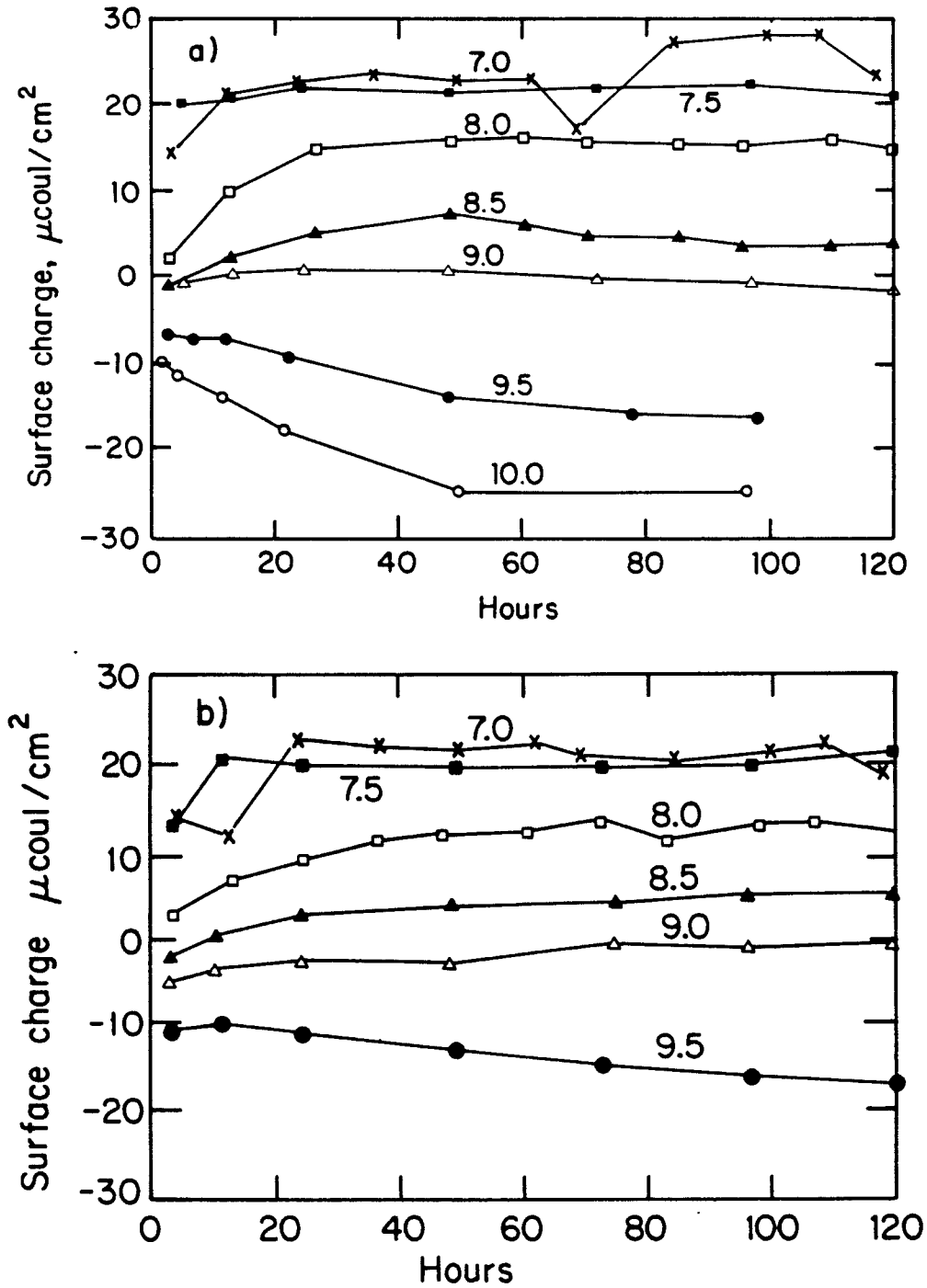
Fig. 4.2. Surface charge in constant-pH, dissolution
experiments; 10 g/L chrysotile, N_2 atm., 25 C, 0.1 M
a) KNO_3, b) NaCl; pH values from 7 to 10.

outer brucite sheet and accompanying exposure of underlying $>SiO^-$ sites on the surface.

The average surface charge at longer times (72-120 hours), shown on Figure 4.3, is zero at pH 8.9. Differences in the observed surface charge in KNO_3, NaCl and Na_2SO_4 media are small, suggesting that either the ions present interact similarly with the surface or the interaction is too weak to be observed at these concentrations. Different ions are expected to complex more or less strongly with the surface, as discussed in section 2.1.3. For example, the constants in Table 2.2 suggest that for 0.1 M SO_4^{2-} at pH 8, most magnesium should be present as a $MgSO_4$ complex; whereas $MgCl^+$ accounts for less than half of the magnesium at pH 8 in 0.1 M Cl^-. As noted in Table 2.2, the equilibrium constant for $MgSO_4$ is 20 times that for $MgCl^+$ (log K of 2.28 vs. 0.91) and there is no evidence of a $MgNO_3^+$ complex. The lack of observed difference plus the lack of difference in surface charge for a 0.01 M versus 0.1 M SO_4^{2-} solution suggests that inorganic anion-surface interactions are weak. In the absence of adsorption of ions other than H^+ and OH^- the species contributing to surface charge are given by (2.4) and the pH_{iep} is equivalent to the pH_{zpc}.

4.1.1.2. Estimation of Surface Equilibrium Constants

From a least-squares fit to the data and for the initial surface assumed to be entirely magnesium hydroxide, pK_{a1}^s is estimated to be near 7.7, with no systematic differences apparent between the three electrolytes NaCl, Na_2SO_4 and KNO_3 (Figure 4.4). The corresponding constant capacitance from this fit is 4.8 C/V cm^2). Considering the surface speciation and charge relationships (2.1)-
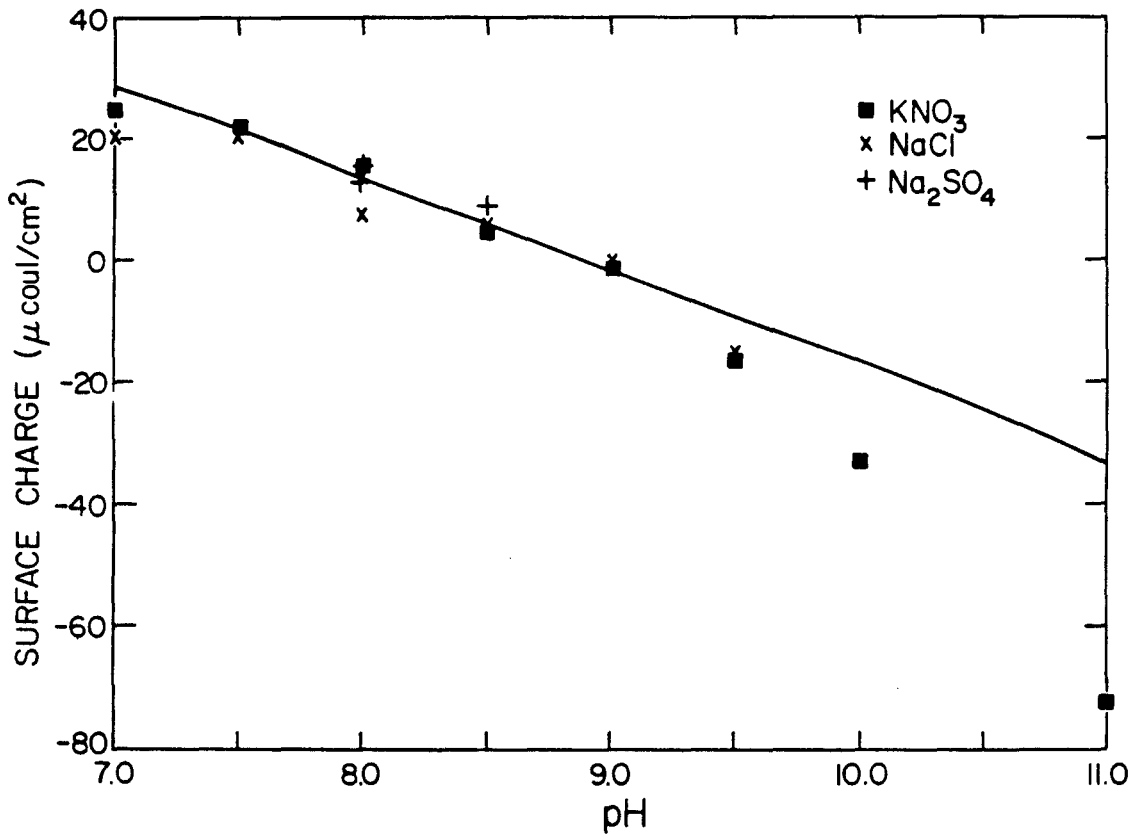
Fig. 4.3. Surface-charge at longer times (72-120 hrs.) in constant-pH, dissolution experiments as a function of pH; points for NaCl and KNO_3 are taken from Fig. 4.2.
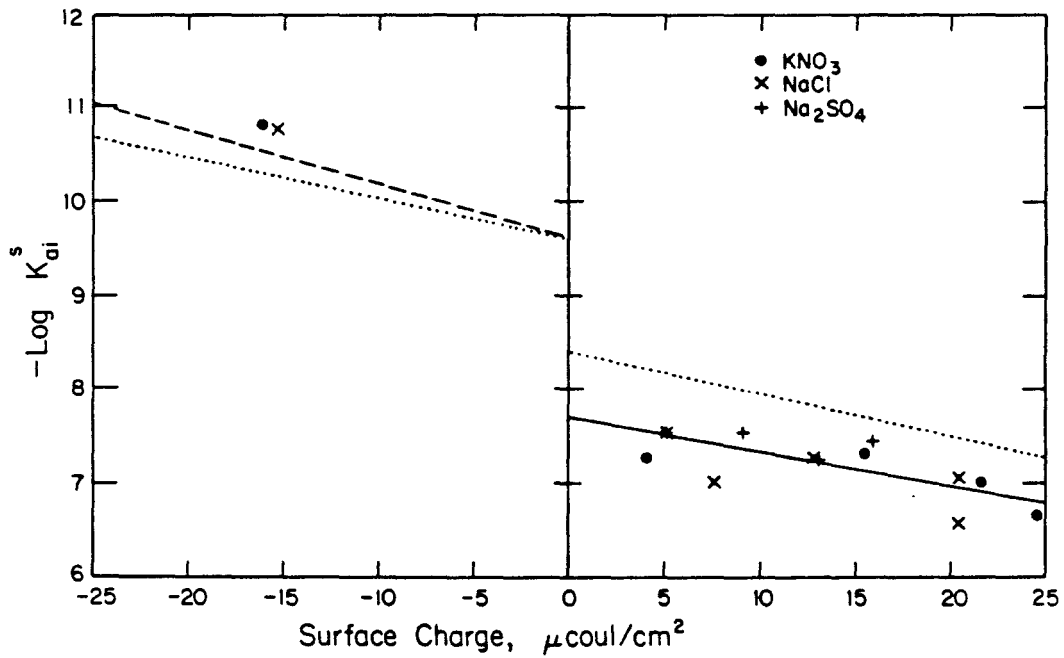
Fig. 4.4. Determination of surface equilibrium constants; points are from experimental data, assuming $S_m = S_T$ at outset of experiment; ———— best fit to points, ······ best overall model fit assuming $S_m = 0.9\ S_T$ at outset, - - - - best fit to brucite data (Appendix IV).

(2.4) together, taking the initial surface to be 10 percent silica (90 percent magnesium hydroxide), and given a pH_{zpc} of 8.9, a better fit to the data is obtained using $pK_{a1}^S = 8.0$, $pK_{a2}^S = 10.0$, $pK_{as}^S = 7.5$ and $C = 4.0$ C/V cm^2. These values were arrived at by iteration and are used in the interpretations of dissolution rate data that follow. Lines with the same slope as these best-fit lines for pK_{a1}^S and pK_{a2}^S are also plotted on Figure 4.4. These lines are not directly comparable to the plotted points, as the points are based on an initial magnesium hydroxide surface and the lines are based on a mixed magnesium hydroxide-silica initial surface. The relation derived in preliminary experiments for brucite, which suggests a capacitance of 3.1 C/V cm^2 and a lower pK_{a2}^S (9.6), is also shown. The latter experiments were "fast" titrations and are described in Appendix IV. The calculated relation of pH vs based on the above constants is shown on Figure 4.3. The model describes observations best near the pH_{zpc} and deviates most at high pH. The fit could be made better by using different capacitances above and below the pH_{zpc}, which would add one more fitting parameter to the model. As is apparent from the data of others, the charge-potential relations on metal-oxide amphoteric surfaces may be quite different above and below the pH_{zpc} (Hohl & Stumm, 1976; Kummert & Stumm, 1980; Sigg & Stumm, 1981).

4.1.2. Dissolution of Chrysotile

4.1.2.1. Dissolution Stoichiometry

The different extents of magnesium and silica released into solution in the presence of the four inorganic anions studied are shown on Figure 4.5. Results for the two organic anions
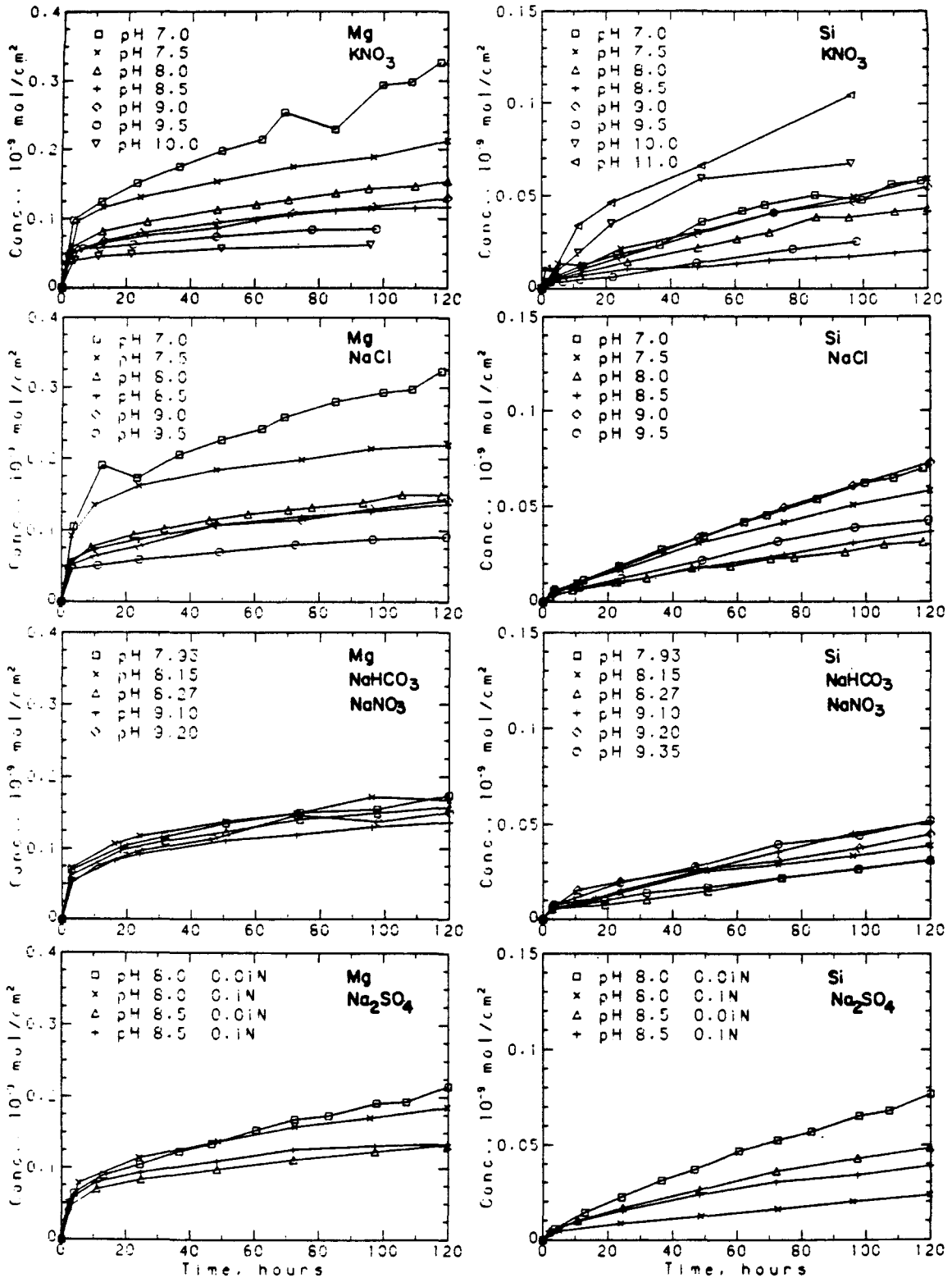
Fig. 4.5.   Extent of magnesium (Mg) and silica (Si) release from
chrysotile in various electrolytes; KNO$_3$ and NaCl were 0.1 M,
NaHCO$_3$/NaNO$_3$ was at fixed PCO$_2$ = 350 ppm; 10 g/L chrysotile, N$_2$ atm.,
25 C.

studied are shown on Figure 4.6. The more rapid magnesium release during the first few hours of each constant-pH experiment has two possible explanations. First, it could be due to preferential dissolution of fine-grained impurities and dissolution at surface discontinuities. These discontinuities result in part from the grinding done during sample preparation causing dislocations in the crystal structure; these dislocations yield "higher-energy" surface sites, more accessible to proton attack. Discontinuities may also be present in the parent material, before sample preparation. For feldspars and pyroxenes, it has been shown that a steady-state dissolution rate occurs essentially from the outset of dissolution in pre-weathered (washed, HF-etched) material. That is, removal of higher-energy surface sites in a prior step yields a more homogeneous starting material. Using freshly-ground material, feldspar and pyroxene dissolution rates are initially high and decline to steady-state after about five and 20 days respectively (Holdren & Berner, 1979; Schott et al., 1981). The same effect has been observed on -Al_2O_3 (Stumm et al., 1983).

Second, the initial release could reflect rapid dissolution of a portion of a uniform outer brucite layer. The initial rate is approximately 1000-fold faster than the constant magnesium release rate that occurs after the first day. Silica dissolution occurs at a constant rate essentially from the outset. This initial rate for magnesium release from chrysotile is of the same order of magnitude as that for brucite dissolution (Figure 4.7). The gradual decline in rate could in part reflect a decrease in the total number of surface
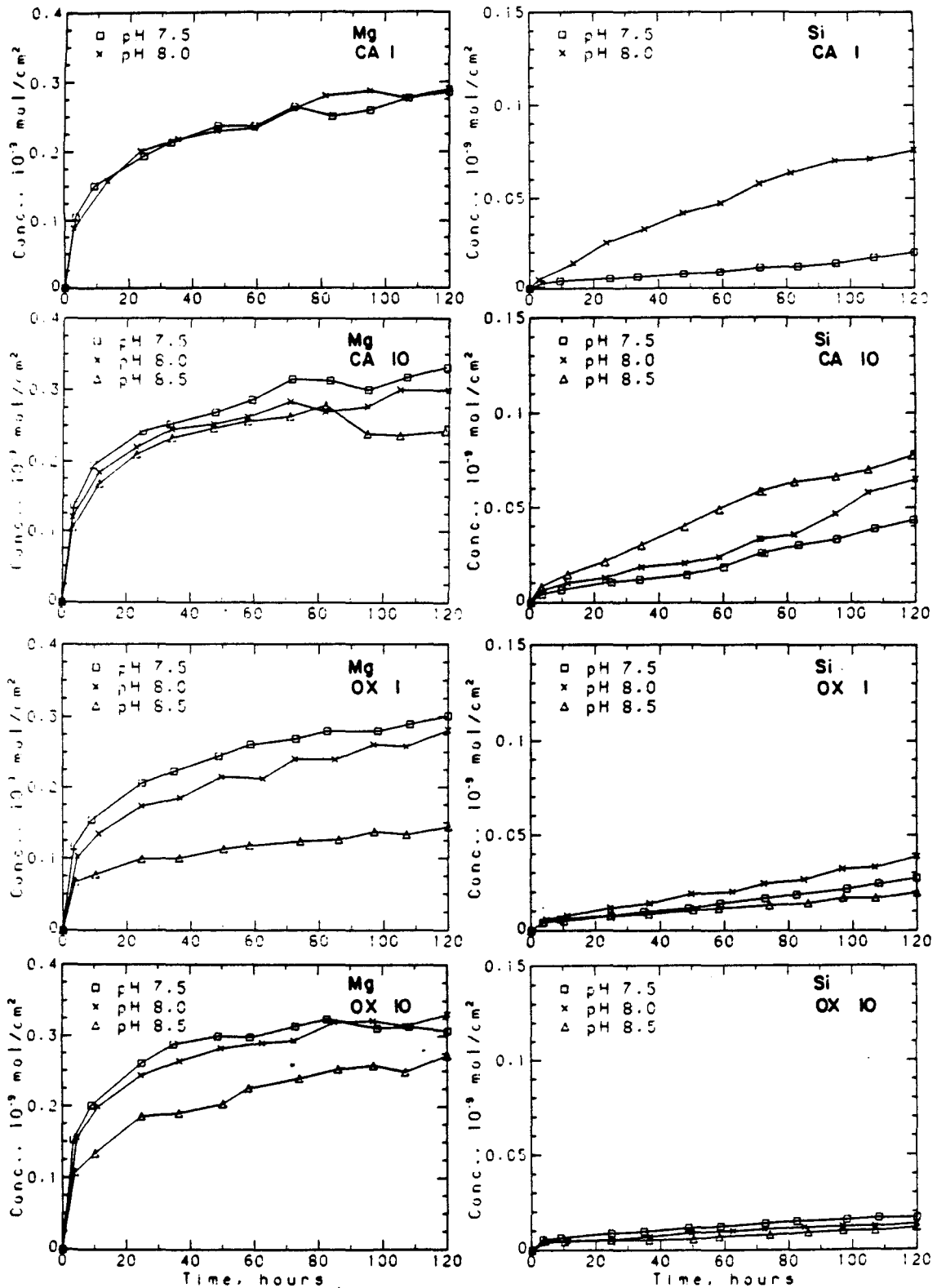
Fig. 4.6.   Extent of magnesium (Mg) and silica (Si) release from chrysotile in the presence of 1 and 10 mmol/L catechol (CA) and oxalate (OX); 0.1 M NaCl, 10 g/L chrysotile, N_2 atm., 25 C.
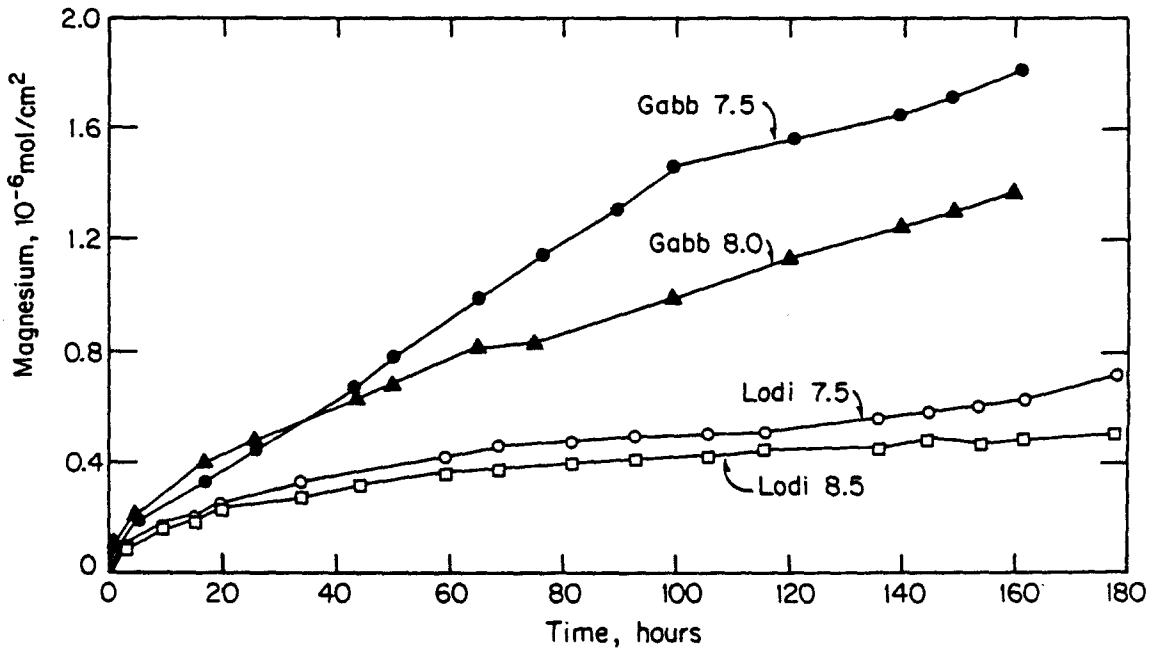
Fig. 4.7. Extent of magnesium release from brucite at
constant pH; 0.1 M NaCl, 20 mg/L (Gabb) and 80 mg/L (Lodi),
N$_2$ atm., 25 C; pH values 7.5, 8.0 and 8.5.

magnesium sites as well as a decrease in the number of higher-energy sites. Extrapolating the linear portion of each magnesium curve to the initial time gives an estimate of the number of magnesium surface sites initially removed. Intercepts range from 0.05 to 0.35×10^{-9} mol/cm^2, or approximately 5-15 percent of the total number of surface sites.

Although the actual composition of the outer surface (fraction S_m vs. S_s) was not known at the outset, the magnitude of the surface charge observed and the small amount of Mg^{2+} dissolved during sample preparation (section 3.1.1) suggest that $S_m > S_s$ initially. Thus the apparent small shift in surface composition could not account for a 1000-fold decline in dissolution rate. The decline must then be due to removal of higher-energy sites created during sample grinding. The fact that silica release is linear from the outset supports this conclusion.

Chowdhury and Kitchener (1975) observed preferential release of magnesium from chrysotile at broken fiber ends or places where fiber bundles were damaged. This direct, although qualitative, observation further suggests that the more rapid initial dissolution is due to surface discontinuities.

On the average, the ratio of molar magnesium to silica release rates is about 2.0 over the pH range 7-9, versus the 1.5 molar ratio in the solid. This suggests that the outer surface, initially magnesium hydroxide, becomes more silica-like with aging time in water. In contrast, dissolution behavior reflecting magnesium, iron and silica molar ratios in the solid was observed for other silicate

minerals, including olivine (Grandstaff, 1980), fayalite and bronzite (Schott & Berner, 1983) and diopside and tremolite (Schott et al., 1981) Dissolution of three other layer silicates -- antigorite, talc and phlogophite -- over several weeks also showed magnesium being released at a faster rate than silica (Lin & Clemency, 1981).

The shift from a magnesium hydroxide to silica surface should result in a gradual decrease in the rate of magnesium release from chrysotile and an increase in the rate of silica release. Eventually the dissolution rates for the two components should converge to a steady-state ratio of 3:2 for Mg:Si and the surface composition should remain constant. This was not observed in any of the five-day dissolution experiments.

4.1.2.2. Comparison with Brucite Dissolution

Magnesium is released from brucite at a rate that is linear from the outset (Figure 4.7). Results from two different natural samples are plotted. There is little pH effect over the range 7.5 to 8.5, but the Gabb brucite dissolved about 5-fold faster than did the Lodi brucite. This difference is though to be due to using different reactors and different stirring rates in the two sets of experiments, as brucite dissolution is thought to be diffusion limited in this pH range (Vermilyea, 1969). The strong dependence on reactor design for diffusion-limited dissolution has been noted by others (Sjöberg & Rickard, 1983).

The observed brucite dissolution rates are about 1000-fold greater than the rates for magnesium release from chrysotile, very likely due to the stronger binding of Mg^{2+} to the silica tetrahedra in chrysotile.

4.1.2.3. pH Dependence of Chrysotile Dissolution Rate

The rate of release of magnesium from chrysotile decreases at higher pH. At pH 10 the solution is near saturation with respect to magnesium hydroxide, resulting in a low driving force, or affinity for dissolution. At pH 11 it is above saturation. At pH 9.5 the solution is 10 percent of saturation, at pH 9 it is about 3 percent and at pH 8 about 0.04 percent (Figure 3.6). At the lower pH's the solution is far from equilibrium and the affinity of the dissolution reaction is large. Far from equilibrium the rate of a chemically-controlled dissolution reaction is assumed to be independent of the magnitude of the affinity (Dibble & Tiller, 1981). Rather, the rate is a function of the concentration of a distinct reactive surface species (eqn. 2.20-2.21).

The apparent rates from Figure 4.5 are shown as a function of pH on Figure 4.8. Following (2.28), the resulting rate law for release of magnesium into solution is:

$$r = k_1'[H^+]^{0.24} \tag{4.1}$$

The constant k_1' depends on the dissolution mechanism, the specific surface area of the solid and the charge-potential relation at the surface. These three factors are assumed to not vary significantly over the pH range 7-10 of the experiments.

Figure 2.3 shows that below the pH_{zpc}, the dominant charged species on a magnesium-hydroxide surface is $>Mg-OH_2^+$. Equation 2.27 gives an approximation for the concentration of this species in terms of $[H^+]$. For the observed change in σ with pH (Figure 4.3), the exponent a in (2.27) is calculated to be 0.32, implying that n = 0.75,
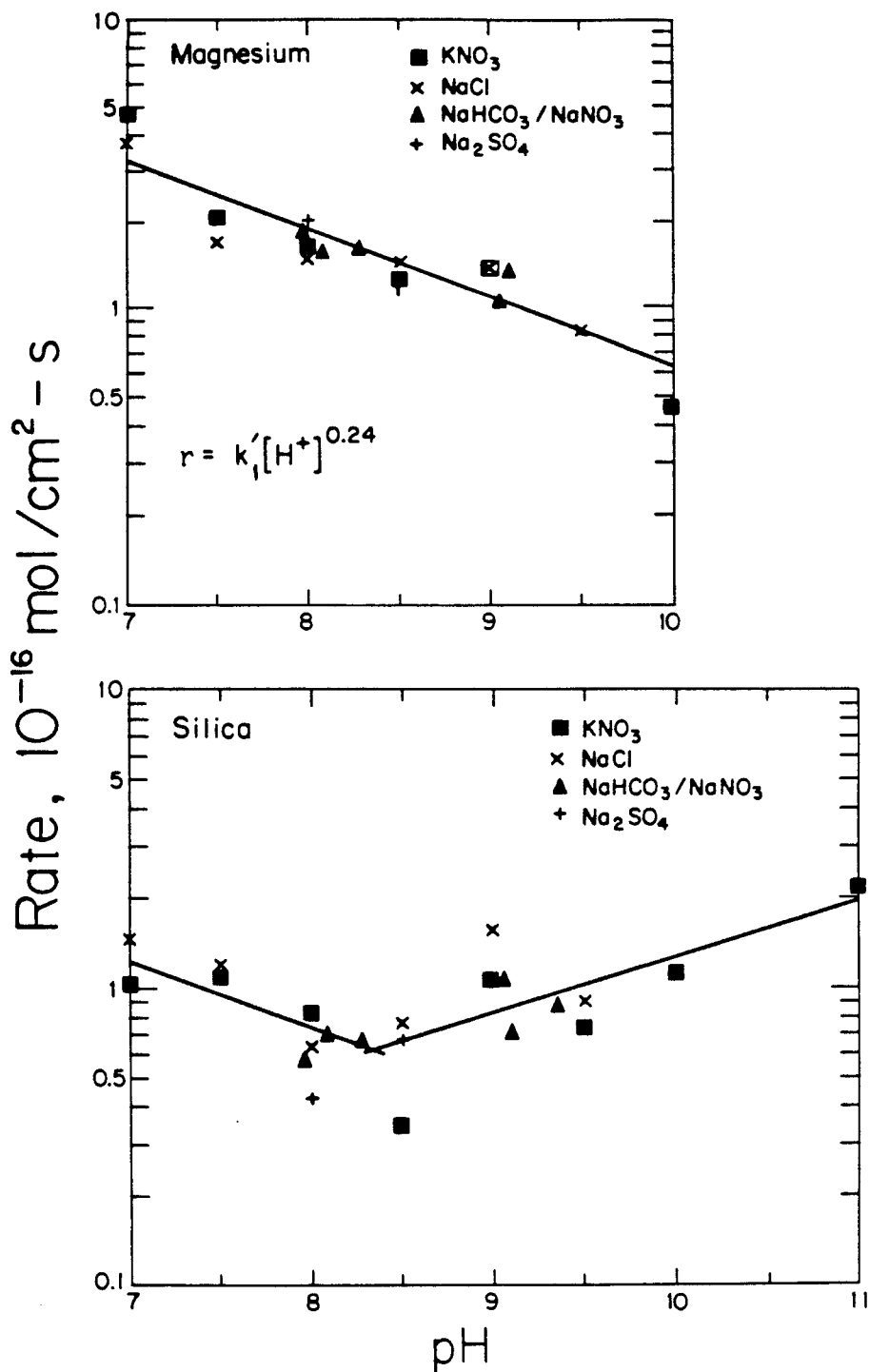
Fig. 4.8. Chrysotile dissolution rate as a function of
pH; points represent slopes of best fit to
data of Fig. 4.5 for times greater than one
day.

or less than one surface $>MgOH_2^+$ group is formed to release one Mg^{2+} ion into solution.

Data for silica release during chrysotile dissolution in 0.1 M KNO_3 are also shown on Figures 4.5, 4.6 and 4.8. The rate increases from pH 8.5-11, but also increases below pH 8.5. For dissolution of vitrous silica, the rate decreases from pH 10 down to pH 6 (Wirth and Gieskes, 1979). At the lower pH (7.0-8.5) in the chrysotile system, silica release follows more closely the magnesium release rate. This is consistent with Mg^{2+}-catalyzed dissolution of silica; however no such enhancement has been observed in previous silica experiments (Wirth & Gieskes, 1979). Taken as a whole, the silica data show no significant pH dependence.

4.1.2.4. pH Dependence of Initial Magnesium Release

A second observed pH effect was on the initial extent of magnesium release into solution, or the "intercept" referred to in section 4.1.2.1. In going to lower pH's, the Mg-release curves of Figure 4.5 have both a greater slope and and a greater initial rise during the first day of each five-day experiment. Figure 4.9 illustrates this increase, characterized by the zero-time intercept of the straight-line portion of the curves.

Considering that hydrogen-ion concentration changes by 1000-fold in going from pH 10 to pH 7, the change in intercept is small -- about a factor of three. The change is systematic, however, and may reflect an initial diffusion limitation on dissolution at certain higher-energy surface sites. This suggestion is consistent with the slow ($\sim$20 hrs.) achievement of a steady-state charge due to proton adsorption apparent on Figure 4.2. Surface charge may reach a
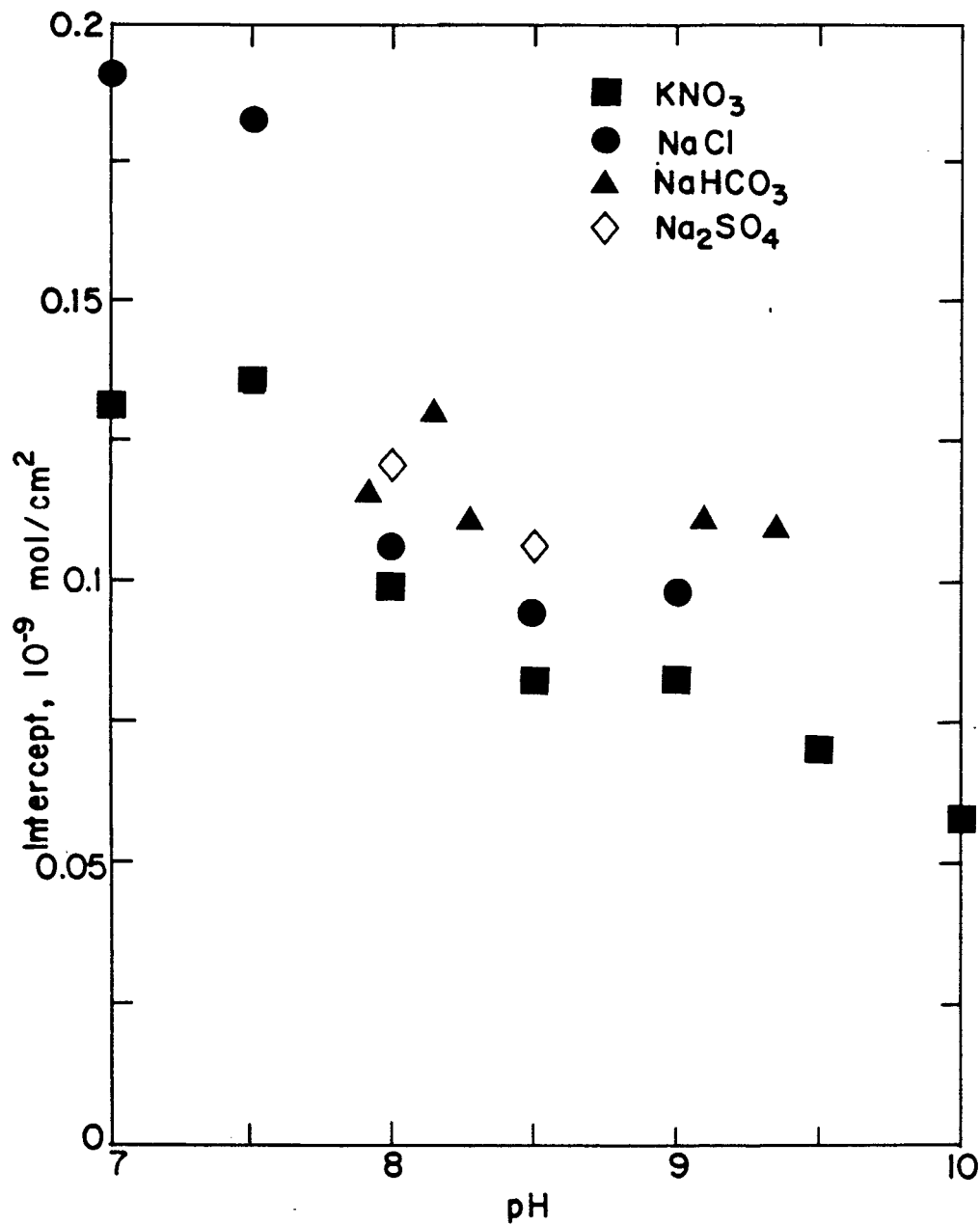
Fig. 4.9. Effect of pH on initial extent of magnesium release from chrysotile; intercepts calculated from Fig. 4.5 data, with slopes given by Fig. 4.8.

steady-state value only after higher-energy sites have been dissolved away by proton attack.

The increase in intercept and initial slope at lower pH suggests that dissolution at the higher-energy surface sites is more pH dependent than dissolution at the more-predominant, lower-energy sites. The higher-energy sites at edges or dislocations are less-tightly bound in the crystal and may adsorb protons to a greater extent and dissolve via an activated complex involving a single proton. Lower-energy sites may involve either coordination of a single proton or attack by H_2O dipoles to form an activated complex. The latter has been suggested as a mechanism for feldspar dissolution at neutral to alkaline pH (Aagaard & Helgeson, 1982).

These considerations suggest that a single-term rate expression of the form of (2.21), where a single type of surface complex controls the overall reaction rate, is a greatly simplified view. These experimental data for the hetrogeneous chrysotile surface do not yield information concerning the nature of the activated complex, but do suggest that a proton is involved. The rate expression (2.25) is a further simplification of the species involved.

4.1.2.5. Effect of Inorganic Ions

The effect of solution electyrolyte on dissolution at pH values from 7-9 is illustrated on Figure 4.10. The differences in magnesium release rates in all four media are small. There is a small apparent enhancement in initial extent of dissolution in going from NO_3^- to Cl^- to SO_4^{2-} as supporting anion. This is consistent with the relative tendency of these ligands to form solution complexes with magnesium (Table 2.2), suggesting that inorganic electrolyte ions
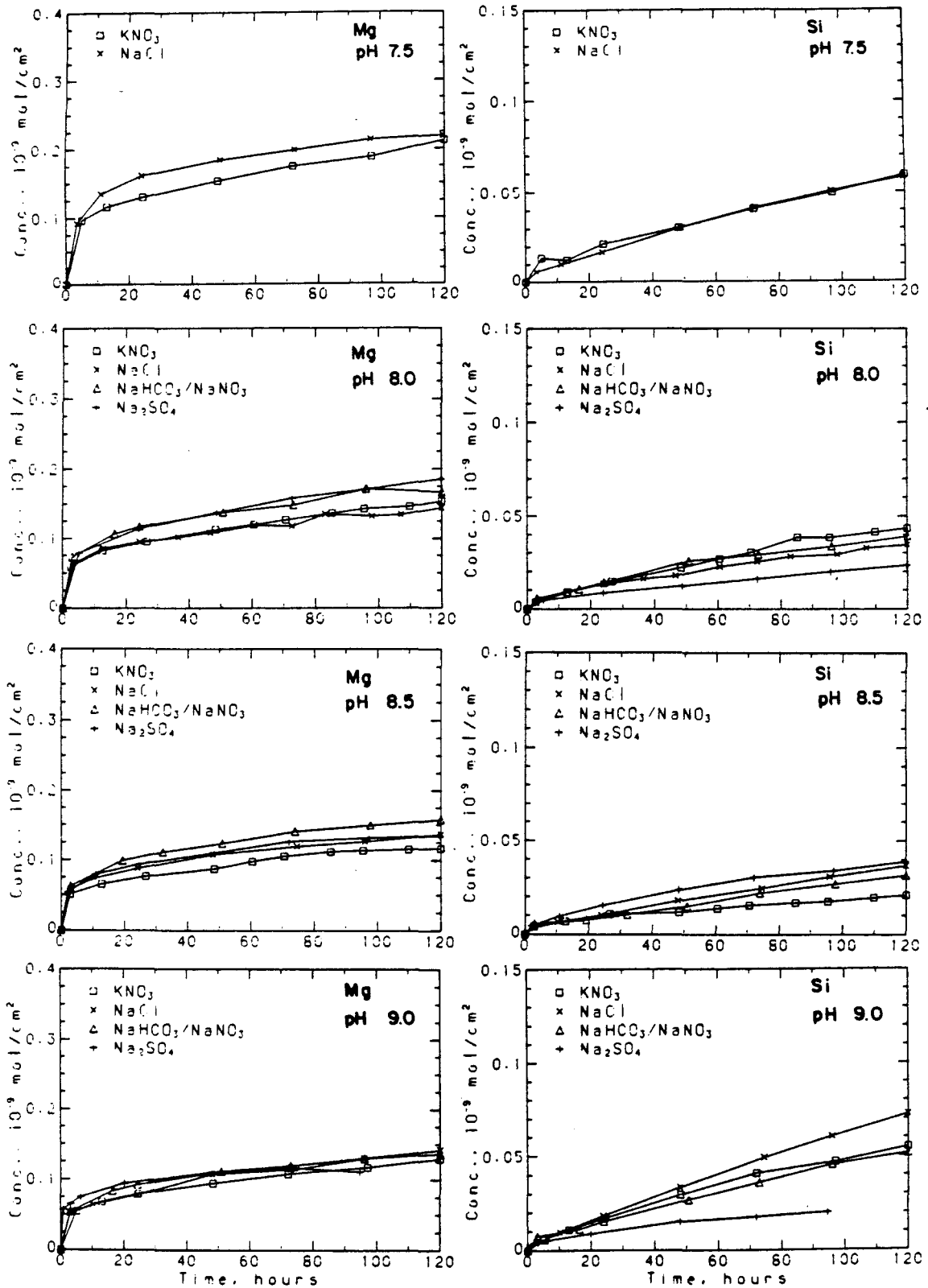
Fig. 4.10.   Extent of chrysotile dissolution in different inorganic electrolytes; these same results are shown on Fig. IV.5 by electrolyte rather than by pH.

have a small but perceptible tendency to form complexes at the magnesium hydroxide surface.

Figure 4.9 also illustrates the slight enhancement in initial magnesium release in going from NO_3^- to Cl^- to SO_4^{2-}. The presence of an effect only early in the dissolution suggests that ligand attack is more important at the higher-energy surface sites. The oversimplified nature of (2.21) is further reinforced by the small but perceptible anion effect. Two ions not studied in this work, F^- and PO_4^{3-}, were shown previously to enhance the initial (60 min.) dissolution of magnesium from chrysotile to a greater extent at pH 7.0 than did SO_4^{2-}, Cl^- or NO_3^- (Gupta & Smith, 1975). The effects of HCO_3^- are mixed (Figure 4.9), but generally are greater than for NO_3^- and Cl^-.

The effect of anions on silica release is ambiguous, there being an SO_4^{2-} inhibition at pH's 8.0 and 9.0, but a possible enhancement at pH 8.5. As noted above, parallel reaction pathways for silica release in the presence of complexing cations as well as possible interfering anions preclude postulating a rate law or mechanism.

Changing the SO_4^{2-} or NO_3^- concentration from 0.01 to 0.1 M at pH 8-8.5 had no significant effect on release of either magnesium or silica in these experiments. This is consistent with observations by others. The effect of ionic strength (0.01-0.3 M KCl) on the rate of release of silica from diopside and enstatite was negligible (Schott et al., 1981). Ionic strength effects (0.1-3.5 M NaCl) for dissolution of vitreous silica (pH 6-10) were apparently due to changes in surface charge, or OH^- adsorption, brought about by the higher electrolyte concentrations (Wirth & Gieskes, 1979).

4.1.2.6. Effect of Low Molecular Weight Organic Ions

As the data on Figure 4.6 suggest, catechol and oxalate have no strong systematic effect on the release rate of magnesium from chrysotile. This is further seen on Figure 4.11 where rates are plotted as a function of pH. There is a small but systematic increase in the initial extent of dissolution in the presence of increasing concentrations of these organics at constant pH (Figures 4.12 and 4.13); the effects of oxalate and catechol are comparable. Because oxalate forms a stronger solution complex with magnesium than does catechol in this pH range (Table 2.2), it was predicted that oxalate would enhance dissolution to a greater extent.

Using photoelectron spectroscopy (XPS), Thomassin, et al. (1977) observed no difference in chrysotile dissolution rates in 0.01 N versus 0.1 N oxalic acid. This led them to conclude that diffusion of oxalate ions to the particle surface did not control reaction rate. Subsequent experiments showed a difference in initial dissolution rates, involving complete dissolution of the surface layer, for 0.1 N versus 10^{-4} N oxalic acid (Thomassin et al., 1980). This difference may simply reflect the changes in pH. It is concluded that in general, the presence of oxalate at the surface has no effect on chrysotile's dissolution rate. Similiarly, phthalate had no effect on the dissolution rate of enstatite, diopside or tremolite in the pH range 1-6 (Schott et al., 1981).

In contrast to the observed lack of effect for magnesium release from chrysotile, dissolution of δ-Al_2O_3 was reported to follow a general rate law (Furrer & Stumm, 1983):
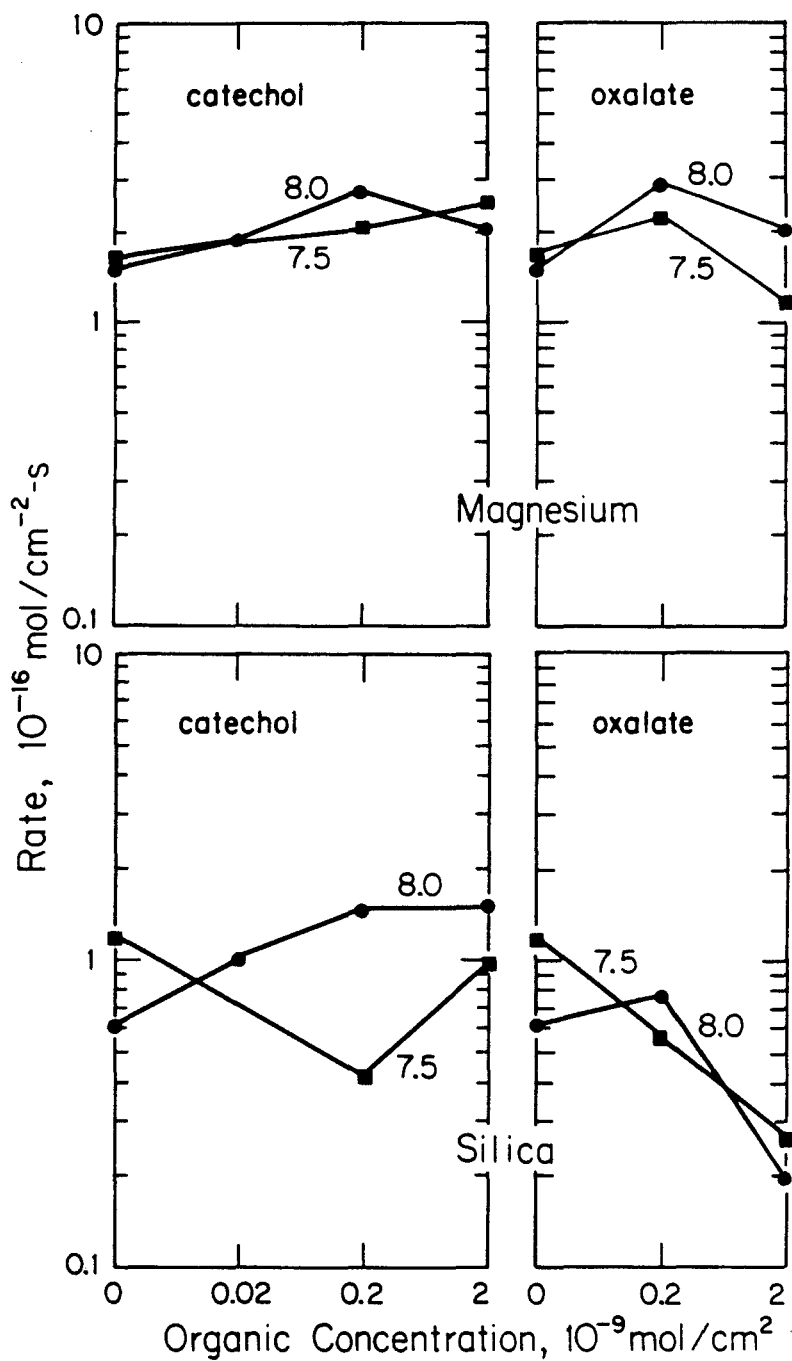
Fig. 4.11. Chrysotile dissolution rate as a function of organic concentration in suspension, at pH 7.5 and 8; points represent best fit to data of Fig. 4.6 for times greater than one day.
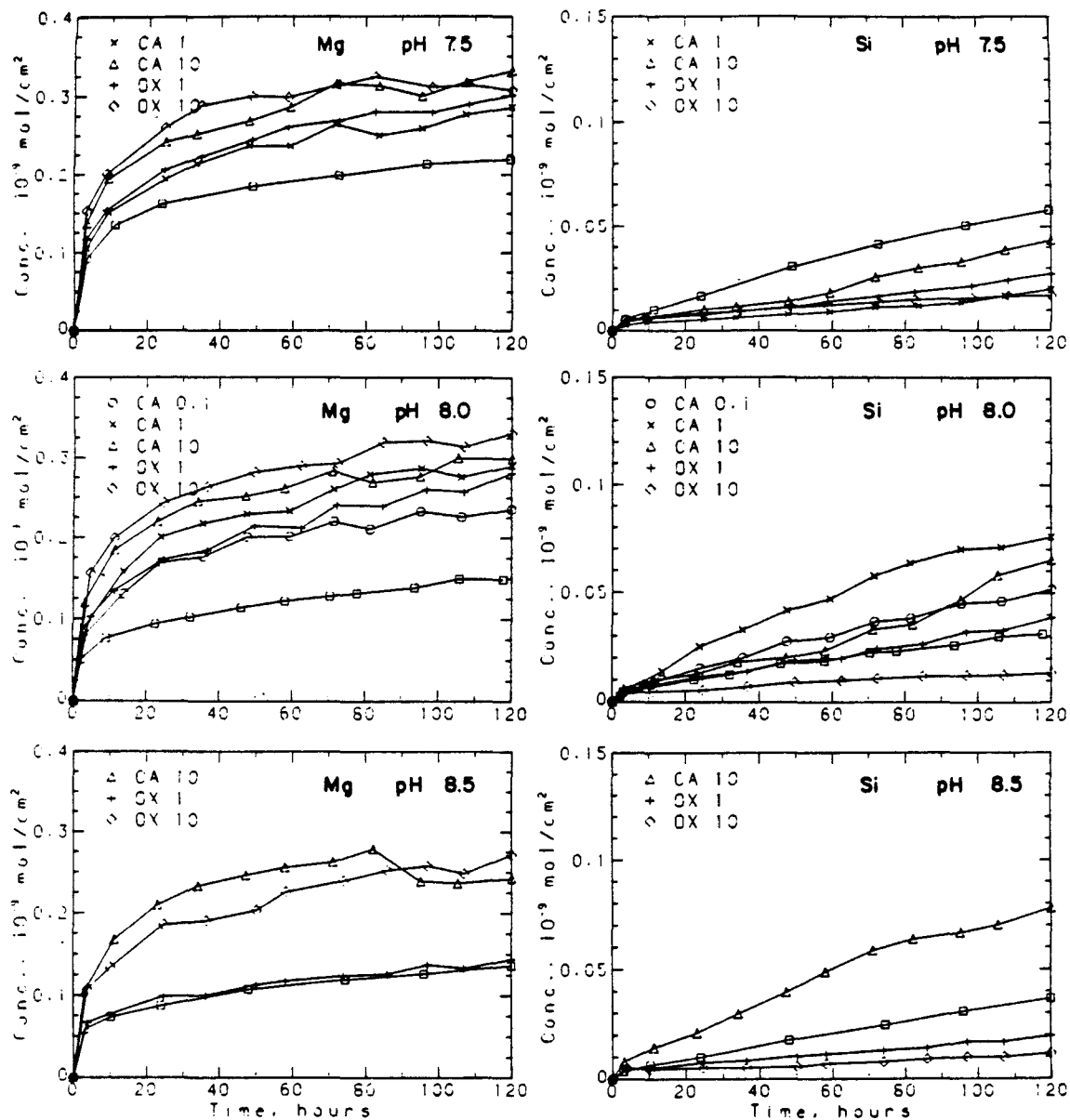
Fig. 4.12. Extent of chrysotile dissolution in the presence of
organic anions;   □ symbols are for experiments in the absence of
organics; conditions are noted on Fig. 4.5. CA 1 refers to 1 mmol/L
catechol added (0.2 x 10^{-9} mol/cm^2), CA 10 refers to 10 mmol/L, etc.;
these same results are shown on Figs. 4.5 and 4.6 by electrolyte
rather than by pH.
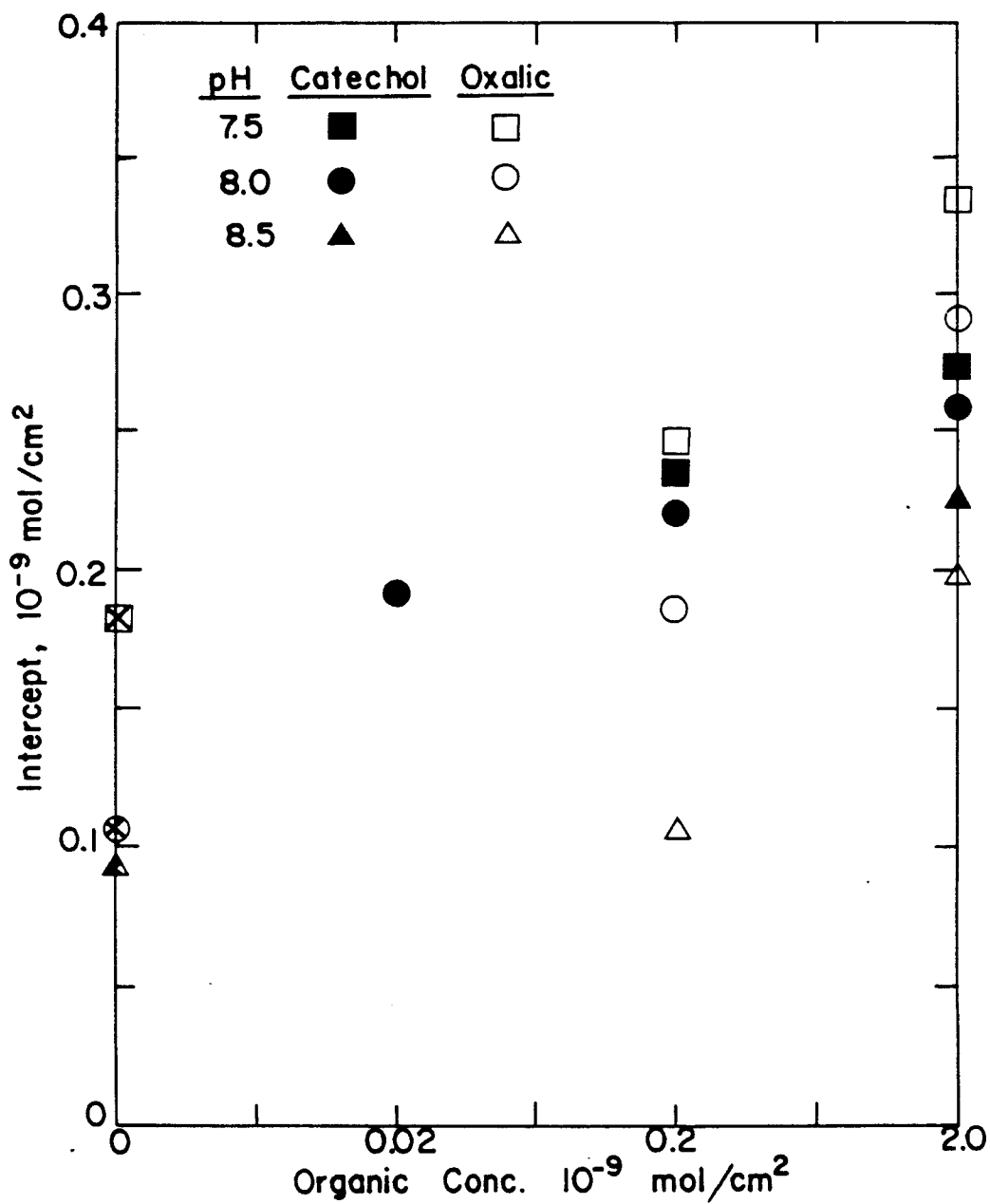
Fig. 4.13. Effect of catechol and oxalate on initial
release of magnesium from chrysotile;
intercepts calculated from Figs. 4.5 and
4.6 data; with slopes given by Fig. 4.11.

$$r = k_H \{>Al-OH_2^+\}^3 + k'_L \{>Al-L\} + k''_L \{>Al-LH\} + \cdots \qquad (4.2)$$

This rate law was applied in the pH range 2.5-6 in the presence of oxalate, salicylate, citrate and benzoate. Grandstaff (1977) measured olivine dissolution rates over 8 days in the presence of varying concentrations of phthalate and EDTA and fit data to the general expression:

$$r = k_1 [H^+] + k_2[H^+]^{0.5}[L]^{0.5} \qquad (4.3)$$

In the presence of 0.001 M ligand and at pH 4.5, the relative ligand effect on dissolution rate decreased in the order:

    EDTA $\sim$ citrate > oxalate > tannic >> succinate > phthalate >

    acetate $\sim$ Cl$^-$

Dissolution was strongly dependent on the organic anion concentration and in the absence of organics was strongly pH dependent over the range studied (3-5).

These two expressions -- (4.2) written in terms of surface species and (4.3) written in terms of the observable solution concentrations -- are compatible descriptions of hydrogen-ion and ligand catalyzed dissolution.

Catechol had a slight enhancing effect on silica release at pH's 8 and 8.5, but the effect is mixed at pH 7.5. Catechol can complex both silica and cations and is known to enhance silica dissolution in neutral to slightly-alkaline solutions but inhibit dissolution in more-alkaline solutions (Iler, 1979). The nature of the catalytic effect is uncertain. Oxalate inhibits silica release with increasing

pH over the range 7.5-8.5. Oxalate should adsorb to >Mg-OH rather than >Si-OH surface sites and thus not directly affect silica release. The inhibiting effect may be due to the more negative surface charge resulting from oxalate adsorption with an accompanying decrease in OH$^-$ concentration near the surface.

4.2. RELATION BETWEEN ADSORPTION OF ORGANIC MATTER, DISSOLUTION AND SURFACE CHARGE

It is generally assumed that simple anions adsorb to oxide surfaces by ligand exchange with surface >M-OH and >M-OH$_2^+$ groups (Schindler, 1981). At constant pH a Langmuir isotherm is typically used to describe anion-adsorption data. As part of a more general surface model (eqn 2.1, 2.2, 2.4 and 2.8), a pH-independent relation of the form:

$$*K_a^S = \frac{\{>M-HA\}}{\{>M-OH\} \ [H_2A]} \tag{4.4}$$

is typically used (Stumm & Morgan, 1981).

Chrysotile was dissolving throughout the experiments and did not reach solubility or adsorption equilibrium over the times studied. Adsorption data are therefore interpreted in terms of a simple Langmuir adsorption equation and are not incorporated into the general surface model that relates extent of adsorption to surface charge. The quasi-equilibrium interpretations that follow enable making relative comparisons between extents of adsorption and magnitudes of surface charge for different organics and at different pH's and organic-to-surface ratios.

4.2.1. Adsorption

4.2.1.1. Catechol Adsorption Density

The amount of catechol adsorbed to both chrysotile and γ-Al_2O_3 was observed to increase during the first 15-36 hours of constant-pH adsorption and dissolution experiments (Figure 4.14). For comparison, the observed relations at 21 hours are used. These data can be fit to a Langmuir adsorption equation of the general form:

$$\Gamma = \frac{CK \ \Gamma_m}{1 + CK} \tag{4.5}$$

giving the results shown on Figure 4.15 for catechol on chrysotile. Γ is the extent of adsorption or adsorption density and can be expressed in both mass (mg/cm^2) and molar (mol/cm^2) units; Γ_m is the maximum adsorption density, expressed in the same units. C is the solution concentration of adsorbate, expressed in the corresponding mass (mg/L) or molar (mol/L) units; K is the adsorption equilibrium constant, or affinity for adsorption, and has units of reciprocal concentration.

It should be recognized that the chrysotile-organic systems are not in equilibrium and thus the Figure 4.15 plots are not equilibrium isotherms; rather the fitted curves provide a convenient means of comparing the extents of adsorption under different conditions. As can be seen from the full set of data on Figure 4.14, different fitted
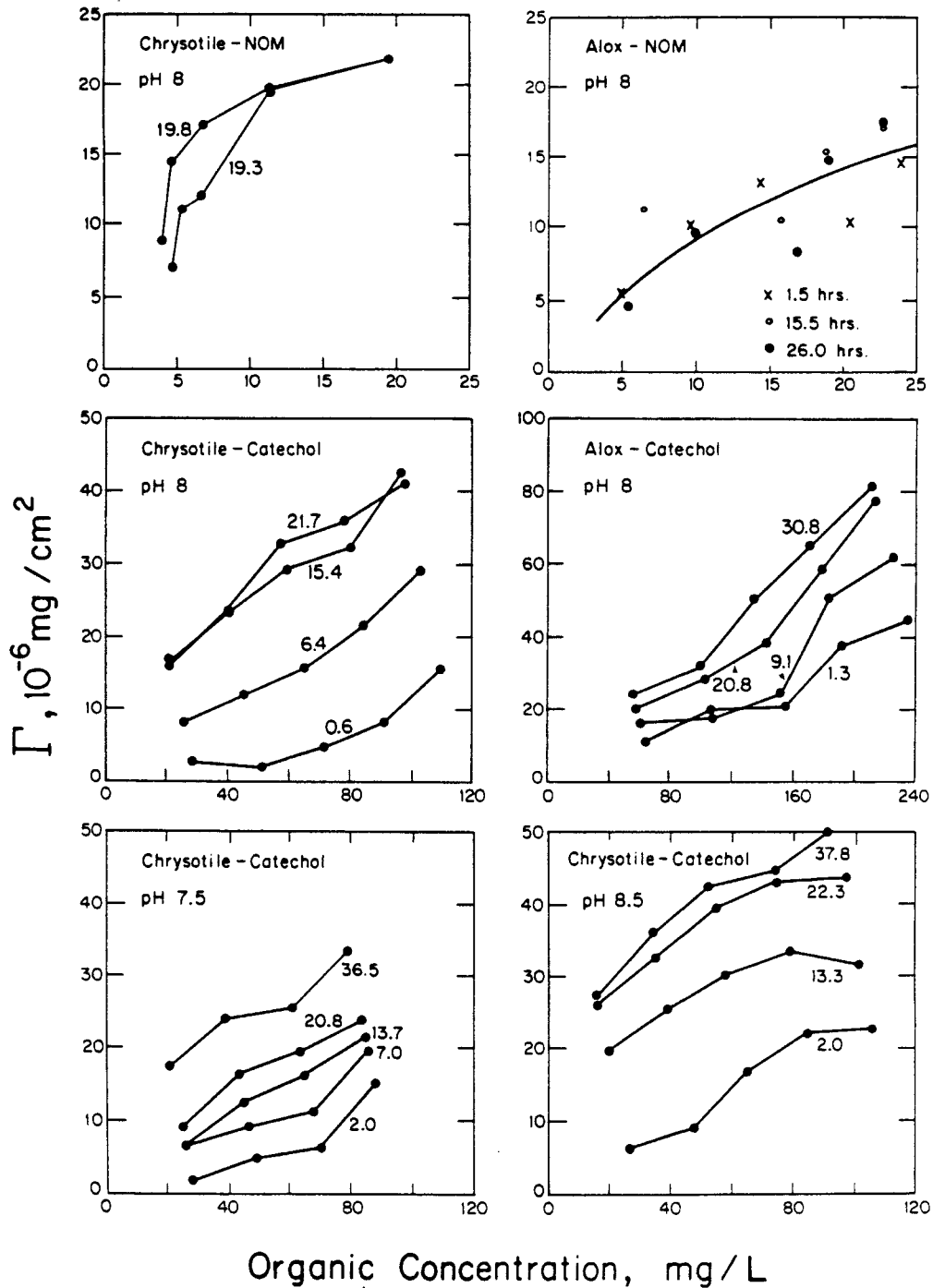
Fig. 4.14. Batch adsorption experimental results for catechol
and NOM; 0.01 M NaCl, room temp., open to atm.; chrysotile
1.02 g/L, Alox 0.81 g/L; times from 0.6 to 37.8 hrs.
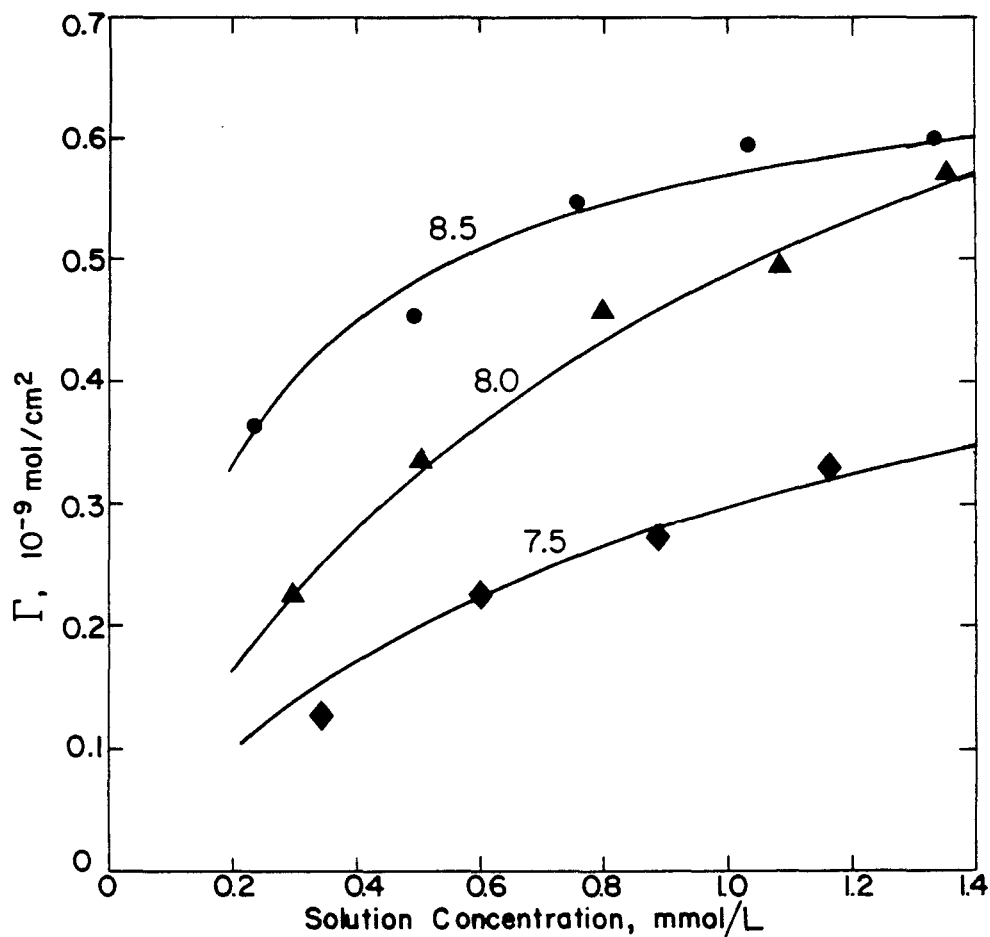
Fig. 4.15.   Adsorption isotherms for adsorption of catechol onto chrysotile after 21 hours equilibration at constant pH; data from Fig. 4.14; curves from Fig. 4.16 (0.1×10^{-9} mol/cm^2 = 0.6 ion/nm^2 = 7.2×10^{-6} mg/cm^2); pH values, 7.5, 8.0 and 8.5.

curves would result from using the 13-hour versus 22-hour versus 36-hour results. The constants Γ_m and K were determined as shown on Figure 4.16. The average intercept of the plots for chrysotile (Figure 4.16) yields a Γ_m value of 0.73×10^{-9} mol/cm^2, which corresponds to 4.4 ion/nm^2, or about one third that of S_T, the estimated surface hydroxide site density. This is in the same range as the estimated maximum density of H_2O or OH^- exchangeable groups of 0.5×10^{-9} mol/cm^2 on the similiarly-shaped geothite particles (Tipping, 1981). The curves shown on Figure 4.15 use the individual values of Γ_m. However, there would be little difference in their shape using the average Γ_m along with corresponding fitted K's. Given the limited range of data, no attempt is made to fit a pH-independent relation of the form of equation (4.4).

The increase in affinity for catechol at higher pH is consistent with the predicted increase in magnesium-catechol complexation in solution at high pH's (Figure 4.17). For stronger acids such as oxalic acid (Figure 4.17), no change in solution complexation over the pH range 6-9 is predicted. The greater catechol adsorption in going from pH 7.5-8.5 could be due to adsorption on >Si-OH as well as >Mg-OH surface sites. As noted above, the catechol enhancement of silica dissolution at neutral to slightly-alkaline pH is consistent with the greater observed catechol adsorption in this pH range. In terms of a Langmuir relation, the affinity (K) for anion adsorption should decrease at higher pH due to greater electrostatic repulsion from the lower surface charge, and the maximum adsorption density should decrease due to fewer >M-OH and >M-OH$_2^+$ sites (Tipping, 1981). The
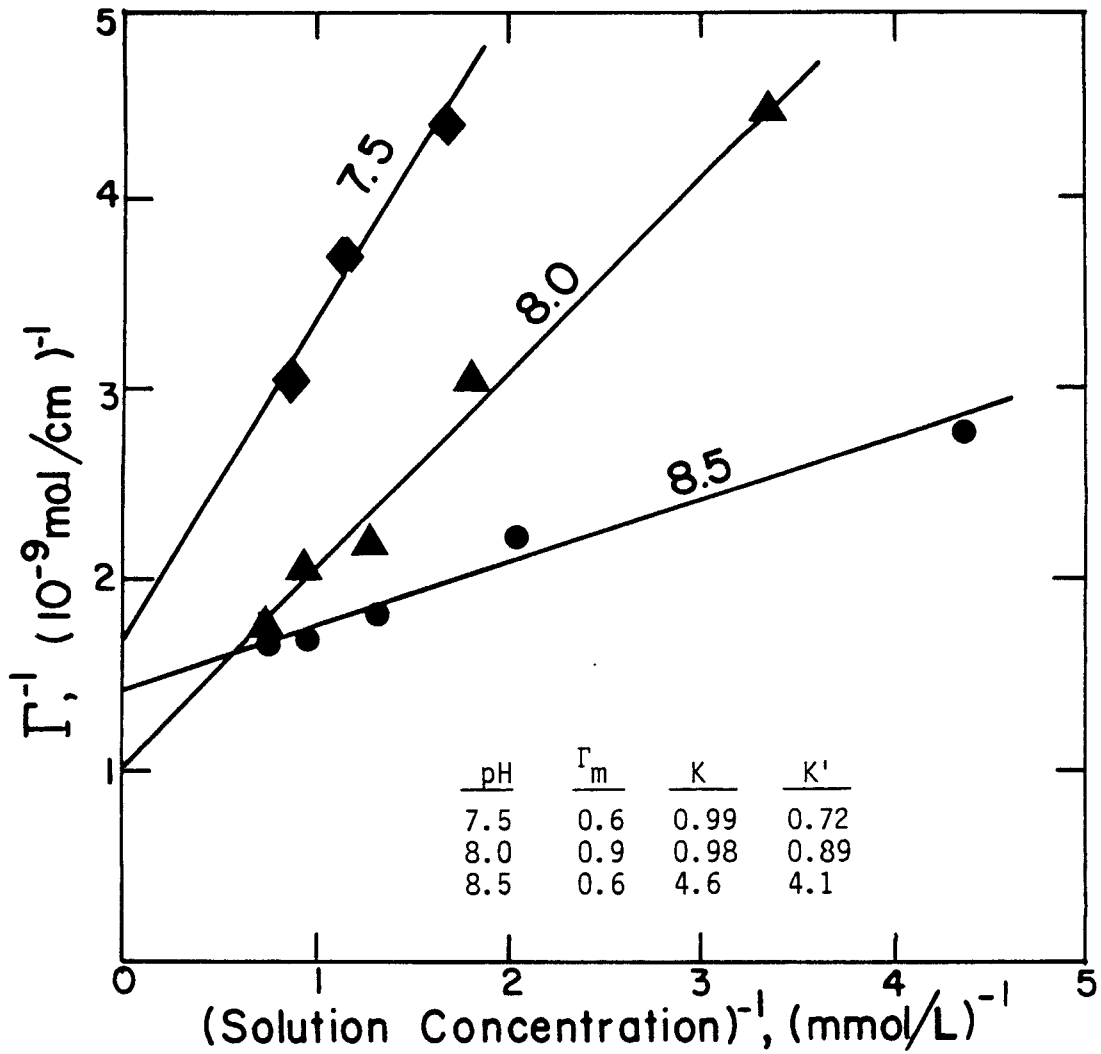
Fig. 4.16. Langmuir plot of catechol adsorption onto chrysotile; constants refer to eqn. (4.3); K' based on Γ_m =0.73, average for three pH values; data from Fig. 4.15.
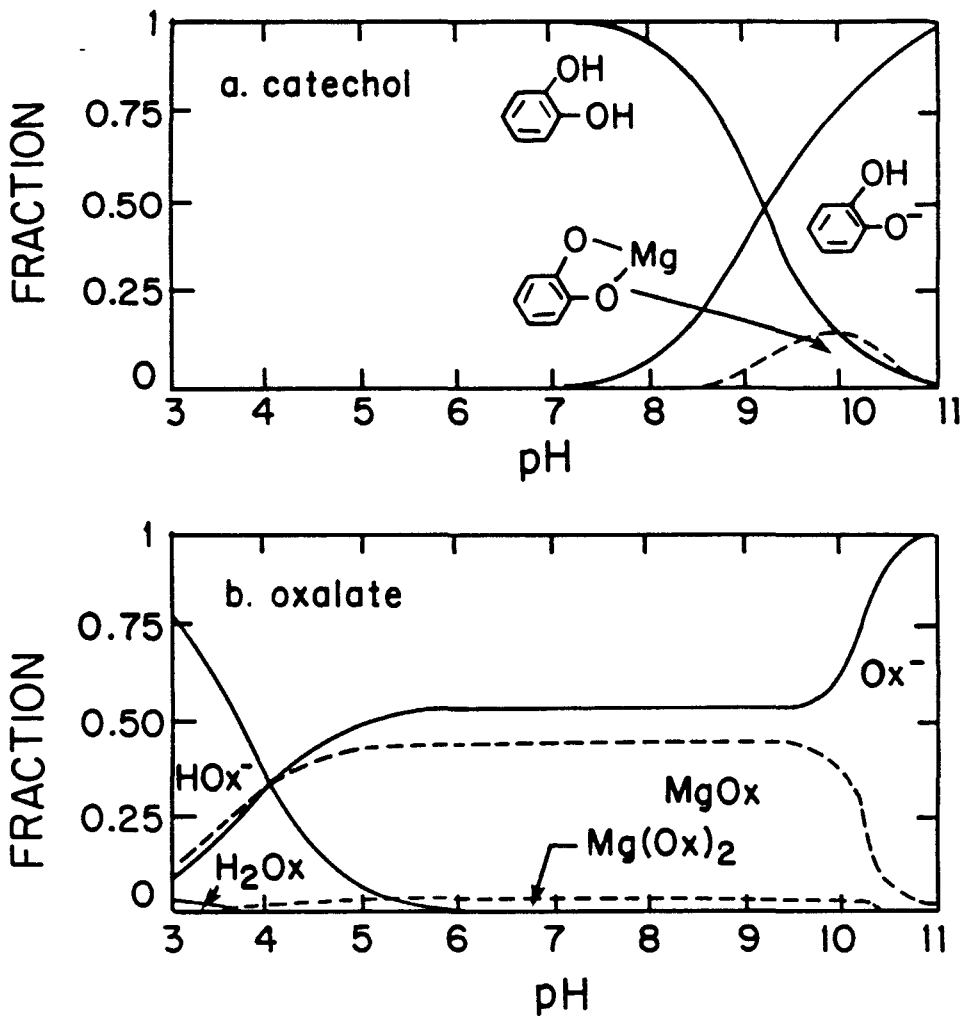
Fig. 4.17. Speciation of catechol and oxalate
with magnesium in solution; equilibrium constants
given in Table 2.2.

binding of catechol to both >Mg-OH and >Si-OH sites could explain why the results on Figure 4.17 are counter to this.

Effects of catechol and oxalate adsorption were also measured in the dissolution experiments described in section 4.1.2.6. The amounts of each adsorbed showed a general increase with time over the five days of each experiment (Figure 4.18). At the lower catechol concentration (0.001 M), adsorption density falls at the lower end of the Figure 4.15 isotherm. For the higher concentration (0.01 M), adsorption density and solution concentration are above that reported on Figure 4.15. The observed adsorption densities in the dissolution experiments are consistent with the Figure 4.15 curves, however.

4.2.1.2. Adsorption of Oxidized Polymers of Catechol

At longer times the UV absorbance peak for catechol was observed to broaden as well as become smaller in magnitude (Figure 4.19). This was accompanied by a darkening in color of the suspensions. The initially-clear catechol-chrysotile suspensions became darker in color with aging time and became very black after several days. Catechol solutions aged without chrysotile present remained much clearer when kept at pH 2 but became colored, although more slowly, when allowed to age at near neutral or higher pH. No attempt was made to exclude trace amounts of oxygen from the nitrogen-carbon dioxide gas mixture used in these experiments. It is known that reaction of oxygen with mono- and polyhydric phenols, especially in alkaline media, gives rise to dark-colored, very complex mixtures of poorly defined products (Mihailovic & Cekovic, 1971). In experiments with catechol present, it was necessary to add base to the
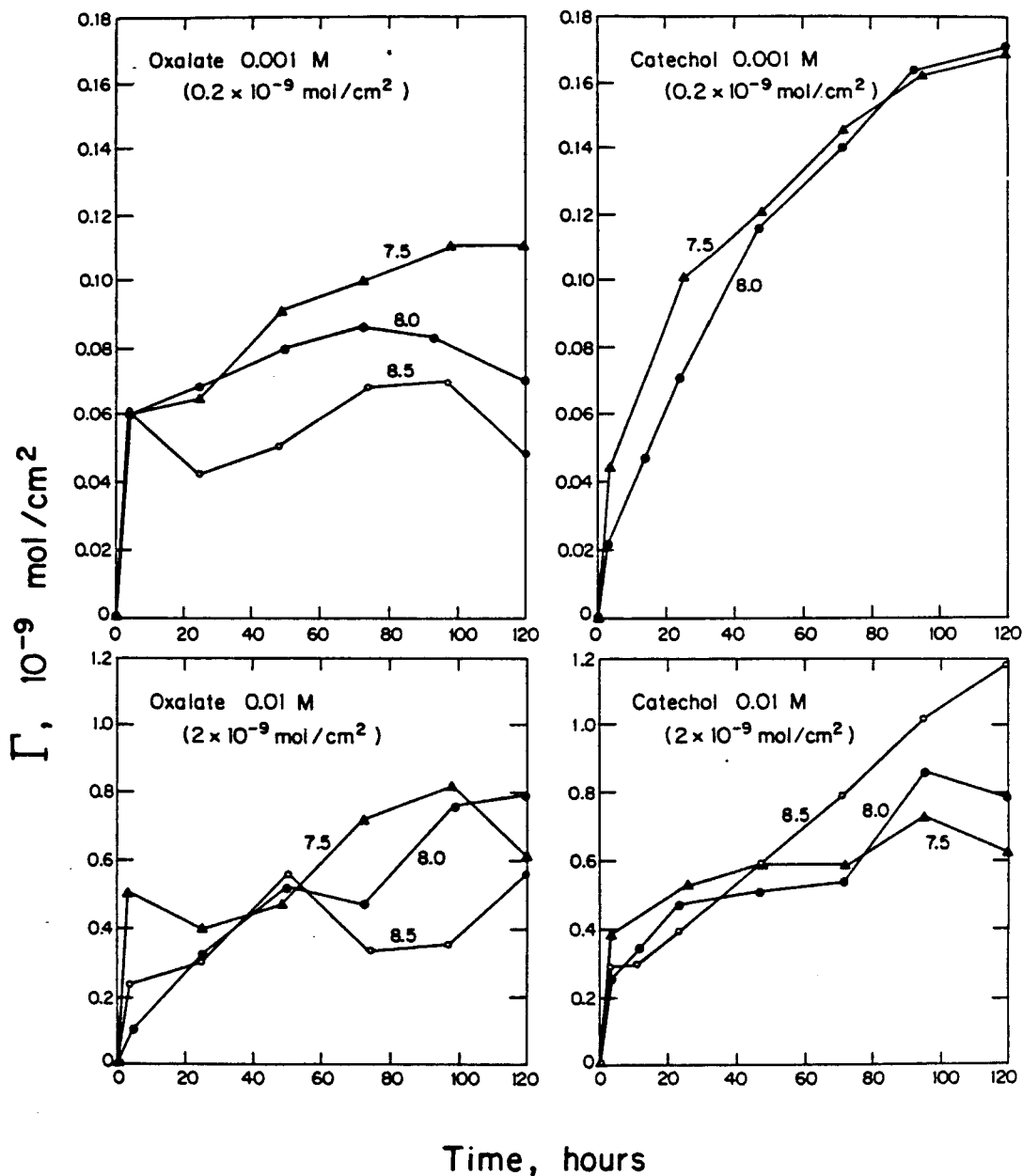
Fig. 4.18. Adsorbed amount as a function of time in the dissolution experiments; conditions noted on Figure 4.6; estimated surface site density of adsorbable surface sites is 2 x 10^{-9} mol/cm^2. Catechol measured by UV and oxalate by IC; pH values 7.5, 8.0 and 8.5.
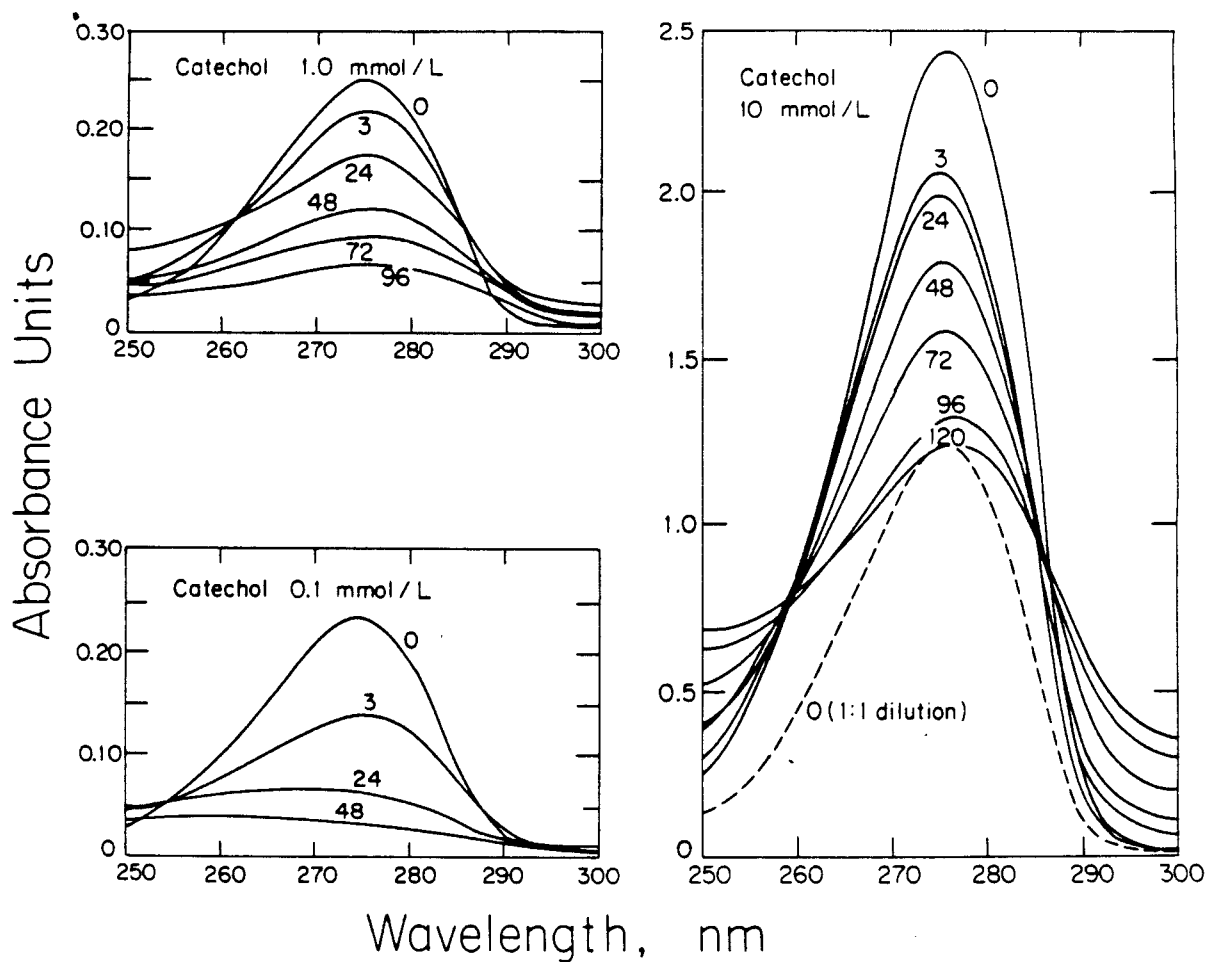
Fig. 4.19. UV scans for catechol remaining in solution in dissolution experiments; conditions noted on Fig. 4.6; times from 0 to 120 hours.

reactor to maintain a constant pH. This is consistent with a reaction of the form:

$$\text{(catechol)} \xrightarrow{-2e^-} \text{(o-quinone)} + 2H^+ \tag{4.6}$$
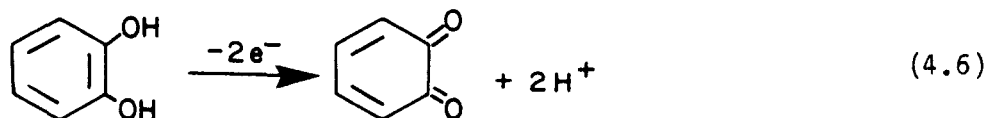
The o-quinone products may then react further to form complex humic-acid type polymers as the main products (Musso, 1963). The broadening of the peak for catechol in the presence of manganese oxide was cited by Stone (1983) as evidence for oxidative polymerization of catechol.

The darkening of the suspension and broadening of the UV absorbance peak is enhanced in the presence of the chrysotile surface. This effect could reflect reduction of Fe(III) impurities in the chrysotile. No attempt was made to confirm this, but it is known that Fe(III) does oxidize phenols (Mihailovic & Cekovic, 1971). Alternately, adsorption of catechol at $>$Si-OH or $>$Si-O$^-$ sites, with the accompanying higher local OH$^-$ concentration, could enhance the oxidation by either iron or molecular oxygen.

The apparent increased adsorption of catechol at longer times, evident on both Figures 4.14 and 4.18, is then the result of two effects. First, adsorption of polymerized species, of higher molecular weight than catechol, at constant molar adsorption density results in a greater removal of organic material from solution. Second, adsorption density was inferred from the reduction in UV absorbance peak at $\lambda = 256$ nm. A portion, though not all, of the

reduction in peak magnitude was associated with polymerization in solution -- polymerized species cause a broadening of the peak.

Two measurements of the amount of catechol that could be desorbed from the chrysotile at pH 12 showed recoveries of at least 50 percent of that missing from solution. Concentrations were too low to confirm by TOC and there was a substantial broadening of the absorbance peak of the desorbed catechol, probably due to increased oxidative polymerization at the high OH^- concentration in the desorption suspension.

4.2.1.3. Oxalate Adsorption Density

Oxalate adsorption also exhibited a gradual increase with time in the dissolution experiments. The adsorption densities, up to approximately 0.6×10^{-9} mol/cm^2 are slightly less than those for catechol. In studying the adsorption of oxalate and benzoate onto goethite, Parfitt et al. (1977) observed equilibrium within two hours and one week, respectively. Oxalate adsorption was near zero at pH 8 and increased to 110 µmol/g ($\sim 0.1 \times 10^{-9}$ mol/cm^2) at pH 4.2. Oxalic acid is a common plant acid and is found to persist in soils. Similarly, oxalate adsorption on gibbsite dropped off from 20-30 µmol/g ($\sim 0.05 \times 10^{-9}$ mol/cm^2) at pH 5 to near zero above pH 7 (Parfitt et al., 1977a). At low solution concentrations, oxalate adsorbed as a bidentate ligand, but only to edge sites of the gibbsite. Relative concentrations of edge and face $>Al(OH)(OH_2)$ sites were estimated to be 60 and 2000 µmol/g respectively. Oxalate appears to adsorb more strongly onto chrysotile than onto either gibbsite or goethite.

4.2.1.4. Adsorption of Other Organics

The ability of chrysotile to adsorb a variety of other organics has been studied in connection with manufacturing asbestos products (Novak, 1953a; Hodgson, 1965; Pundsack & Reimschussel, 1967) and health-related studies (Schnitzer, 1974; Morgan et al., 1977; Desai & Richards, 1978; Valerio et al., 1979). For example, adsorption of Aerosol OT (dioctyl ester of sodium sulfo succinate) to chrysotile freshly suspended in water involves chemisorption of its polar head to the surface, making the fiber organophilic. Surface coverage is 0.3×10^{-9} mol/cm^2 for one monolayer (Otouma & Take, 1975). In general, it has been observed that organic anions with hydroxyl and carboxyl groups readily adsorb to the positively-charged chrysotile surface and disperse fibers. Long-chain organics with multiple functional groups adsorb to the greatest extent. In health-related studies, it has been observed that positively charged (uncoated) fibers react to a much greater extent with body cells and membranes than do negatively charged (organic coated) chrysotile fibers (Light & Wei, 1977).

4.2.1.5. Adsorption of Natural Organic Matter

The amount of natural organic matter (NOM) adsorbed to chrysotile at pH 8 reached a steady value after about 20 hours; adsorption of NOM on γ-Al$_2$O$_3$ showed no systematic difference from 1.5 to 26 hours (Figure 4.14). The latter is consistent with results of Davis (1980), who reported that in a 72-hour experiment, adsorption of NOM extracted from Lake Urnersee sediment onto γ-Al$_2$O$_3$ at pH 5 reached a constant value after about one hour. For adsorption of aquatic humus onto iron oxide, Tipping (1981) observed constant values

within 116 hours. Figure 4.14 shows the extent of NOM adsorption as measured by UV absorbance. The NOM data can also be fit to a Langmuir equation, as shown on Figure 4.20. The maximum adsorption density of 26×10^{-6} mg C/cm^2 on chrysotile is approximately 50 percent of the equivalent mass value for catechol (53×10^{-6} mg C/cm^2).

At most ~ 60 percent of the NOM was removed from solution in the chrysotile-NOM experiments and ~ 40 percent in the Alox-NOM experiments, versus the ~ 33 percent removal for comparable surface loadings in the system studied by Davis (1982). The apparent amounts adsorbed in these three cases are approximately 8×10^{-6}, 5×10^{-6}, and 3×10^{-6} mg C/cm^2 respectively. At ten-fold lower surface loadings ($\sim 0.5 \times 10^{-6}$ mg C/cm^2 adsorbed) Davis observed over 50 percent NOM removal at pH 8 and a maximum removal of ~ 66 percent at pH 5. Tipping (1981) observed from 10 to 30 percent removal of aquatic humus in the presence of goethite at pH 8 and from 50 to 90 percent removal at pH 5. The amounts adsorbed were in the range of 3-9 mg humics/g ($\sim 20\text{-}60 \times 10^{-6}$ mg/cm^2) at pH 8. The humic material was 50-60 percent carbon. In estuarine studies, Hunter found that a relatively constant and significant fraction of terresterial NOM is surface active -- defined in this case as being adsorbable at the mercury-solution interface (Hunter, 1983; Hunter & Liss, 1982).

The fraction of NOM removed from solution (adsorbed) in the current experiments is at least as much as that observed by those noted above. In a source-water reservoir such as Castaic with $10^2\text{-}10^3$ cm^2/L of suspended and colloidal particle surface area and 2-3 mg C/L the available loading is $10^3\text{-}10^4$ greater than in the conditions of these experiments.
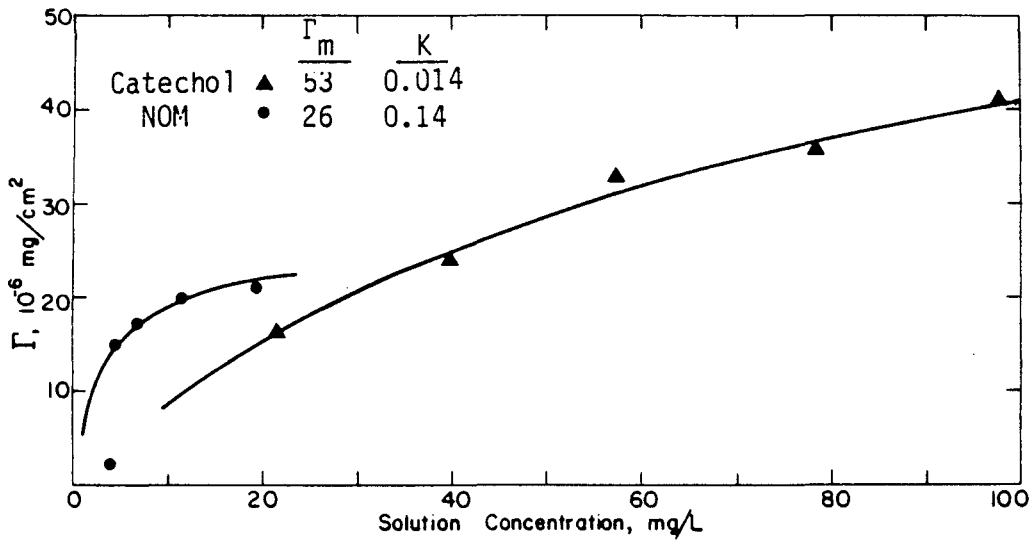
Fig. 4.20. Adsorption isotherms for adsorption of catechol and NOM onto chrysotile at pH 8 after 20-21 hours equilibration; catechol curve from Fig. 4.15, conditions noted on Fig. 4.14.

Results of these adsorption experiments are consistent with three points that have been recently suggested by other studies. First, because of the high surface loadings, changes in suspended particle concentration over at least one to two orders of magnitude will have little effect on the amount of NOM in a water. For example, it is observed that dissolved NOM is conservative in the mixing of rivers into estuaries, a situation where certain inorganic colloids such as iron that are stabilized by NOM are removed by coagulation and sedimentation (Hunter, 1983).

Second, the surfaces of suspended and colloidal material in natural waters are almost completely covered with NOM (Hunter, 1980; Davis, 1982; Baccini et al., 1982). This is expected, as a high fraction ($\sim$30-60 percent) is adsorbable and molar adsorption densities for model organics are high. On some solids, only a fraction of the surface offers strong adsorption sites. For example, only the edge sites of gibbsite adsorb fulvics at pH $\geq$ 7, with face sites contributing to adsorption at lower pH; soil fulvic acid is adsorbed onto gibbsite and goethite by a ligand-exchange process (Parfitt et al., 1977b). The adsorption densities in the current work are sufficiently high to suggest that NOM adsorption occurs over most of the chrysotile surface. It was noted above that the Γ_m for catechol corresponds to one molecule per three surface >Mg-OH groups, and that at pH 8, Γ_m for NOM is about 50 percent that for catechol.

Third, material actually adsorbed may be only the most active or most-strongly complexing. Perdue and Lytle (1983) showed that proton and copper binding by aquatic humus can be modelled by a Gaussian distribution of binding sites. Preferential binding of the most

reactive NOM may selectively concentrate other species such as dissolved cations at the particle surface.

The pH dependence of NOM adsorption was not measured in these experiments. Adsorption is reported to increase with decreases in pH in the range 5-9 for goethite (Tipping, 1981a; Parfitt et al., 1977b), gibbsite (Parfitt et al., 1977b) and γ-aluminum oxide (Davis, 1982). This is consistent with carboxyl or hydroxyl acid groups in the NOM binding to the oxide surface.

4.2.2. Adsorption and Surface Charge

Natural particles in both freshwater and seawater are observed to have a fairly uniform, negative mobility due to adsorption of NOM. In seawater, the magnitude of the mobility decreases with increasing ionic strength due to compression of the electrical double layer (Hunter, 1980). In California freshwaters ionic strengths are too low to have an appreciable effect on mobility. The primary variables are pH and concentration of complexing cations.

4.2.2.1. Chrysotile Surface Charge in Inorganic Electrolytes

The positive to negative shift in mobility of chrysotile particles aging in a non-binding electrolyte at constant pH is illustrated on Figure 4.21. This shift occurs as the surface becomes more silica-like and less brucite-like due to preferential release of magnesium during dissolution. Qualitatively similiar behavior was observed for chrysotile suspended in a pH 4 acetic acid solution, with the mobility going from +2.3 to -0.4 in 80 hours (Chowdhury & Kitchener, 1975). At pH 6.8, the change was from +2.3 to +2.0 in 48 hours. Acetic acid forms only weak complexes with
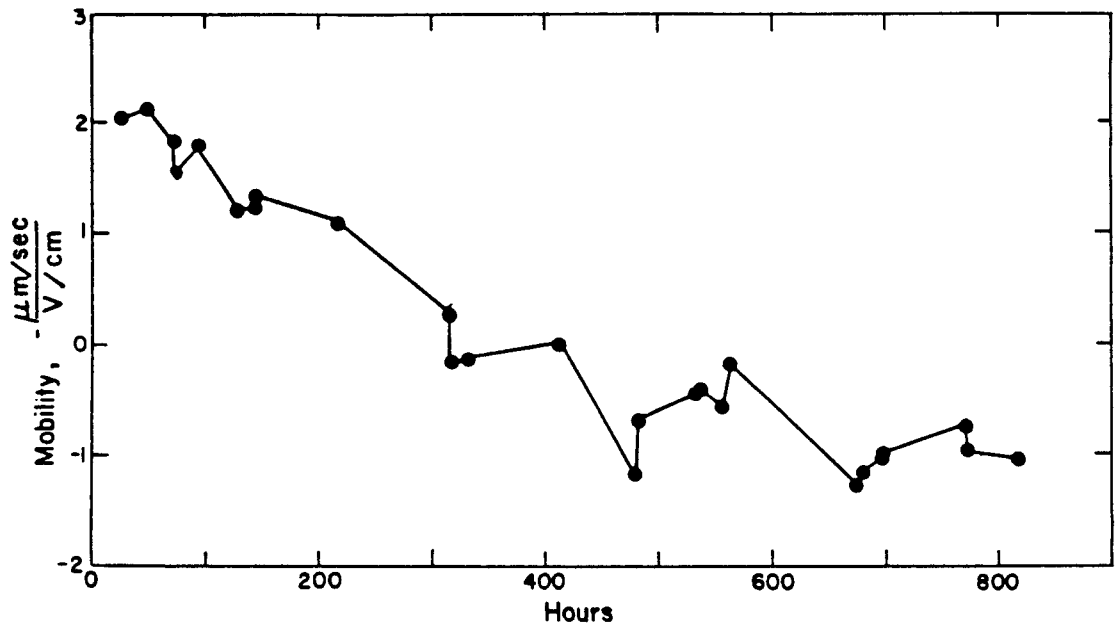
Fig. 4.21. Mobility of stock chrysotile suspension; solids conc. 10.0 mg/L, 25 C, 0.01 M NaCl, 350 ppm CO_2 in N_2 atm., pH 8.0.

magnesium, so the charge reversal was apparently due to dissolution rather than adsorption. In other experiments where pH was not held constant but allowed to change as the particle dissolved, the pH_{iep} in water dropped from 11 to 9 over 70 days (Smith & Trivedi, 1974). Freshly-suspended, natural-chrysotile samples from different sources also frequently exhibit widely-varying mobilities, reflecting differing ratios of outer brucite to outer silica area (Erkova et al., 1981).

Part of the negative charge observed during aging could be due to readsorption of dissolved $H_3SiO_4^-$ ions at >Mg-OH surface sites. However, the data of Ahmed (1981) suggest that silicate concentrations below those needed to precipitate silica from solution ($10^{-3.5}$) have little effect on chrysotile mobility. The silicate to chrysotile ratio in his work was not reported. Dissolved silica concentrations in the current experiments are on the order of 10^{-6} M, based on the above-reported dissolution results. This suggests that the surface charge will not be appreciably affected by dissolved silica.

Dissolved silica in the east branch of the California aqueduct averages about 13 mg/L and is about 14 mg/L in the west branch (Table 3.2), or about $10^{-3.65}$ mol/L. Two observations suggest that this concentration is below the level needed to affect the surface charge. First, the mobilities reported by Ahmed for up to two hours aging indicate charge reversal (Above pH 6) in going from $10^{-3.3}$ to $10^{-3.0}$ M silica; only a one-unit change in mobility (+3 to +2) was reported in going from $10^{-5.0}$ to $10^{-3.3}$ M silica at pH 8. Second, at 10^{-3} M total silica and total magnesium in solution, the extent of magnesium-to-silica complexation at pH 8 is small. The ratio of

complexed to not complexed magnesium was calculated to be $10^{-3.7}$ (Table 2.2).

The general shift toward a lower pH_{iep} has been observed for other oxide minerals, and was assumed to be due to loss of soluble cations (Smith & Trivedi, 1974). Later shifts to higher values were assumed to be due to readsorption of cations as the solid dissolved and the solution neared saturation. As suggested in section 2.1.2, readsorption of dissolved Mg^{2+} is unimportant in determining the charge on chrysotile in these experiments. There is no experimental evidence to contradict this supposition.

In the absence of specific adsorption, the pH_{iep}, measured by electrophoretic mobility, should equal the pH_{zpc}, inferred from potentiometric experiments. The data on Figure 4.22 are consistent with this equality. The pH_{zpc} for chrysotile was found to be 8.9 (Figure 4.3). Initial mobilities of suspensions in the pH range 5-8 are positive. Similar behavior was observed in experiments by others (Ahmed, 1981; Smith & Trivedi, 1974); these are shown on Figure 4.22 for reference. In their experiments, pH was not held constant, but was determined at the beginning of each mobility measurement.

4.2.2.2. Consistency of Surface Charge and Dissolution Results

One check on the consistency of the dissolution, surface-charge and mobility data is to compare the extent of charge reversal due to dissolution, predicted from the surface-chemical model, with the extent of charge reversal observed in the mobility experiments. From Figure 4.8, the magnesium and silica components dissolve (pH 8) at 1.90×10^{-16} and 0.73×10^{-16} $mol/cm^2 \cdot s$ respectively.
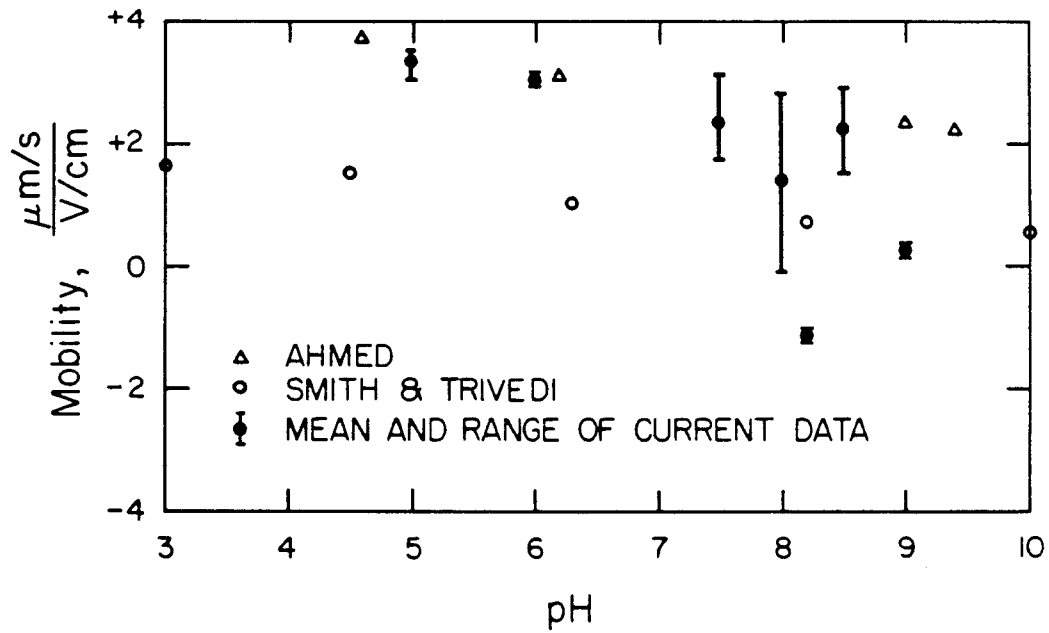
Fig. 4.22. Initial mobility of chrysotile; results of Ahmed (1981) and Smith & Trivedi (1974) shown for reference; current data are taken from mobility vs. time results of Appendix III.

Assuming that these rates hold as the surface becomes more silica-like, the fraction of silica on the surface of a chrysotile fiber is directly proportional to time. Using the surface-equilibrium constants derived in section 4.1.1, the surface charge can then be computed as a function of time (Figure 4.23). This calculation suggests that the surface charge at pH 8 should be zero after about ten weeks, which is about five-fold longer than the two-week observed time for mobility reversal (Figure 4.21).

This lack of close agreement between the two sets of data reflects the oversimplified nature of the surface-chemical model used to describe the compound, heterogeneous chrysotile surface. The charge-potential relation and surface acidity constants were determined for a limited set of conditions and are not expected to fit data taken under greatly different experimental conditions. For example, the surface-acidity constants were determined during five-day experiments, during which time the surface was made up of a large fraction of >Mg-OH sites and a smaller fraction of >Si-OH sites. Adsorption of protons at the >Mg-OH sites was responsible for the positive surface charge below pH 8.9 and the charge-potential relation was determined largely by the nature of the more abundant >Mg-OH sites rather than by the >Si-OH sites. The same charge-potential relation would not necessarily apply to a surface with a greater fraction of >Si-OH sites. Further, the acidity constant for the >Si-OH sites, K_{as}^{s} (2.3), was assumed, based on previous studies on a silica surface with no >Mg-OH sites present. Because of the initially small relative abundance of >Si-OH sites on chrysotile, varying the value of K_{as}^{s} over an order of magnitude had little effect on the model fit to the
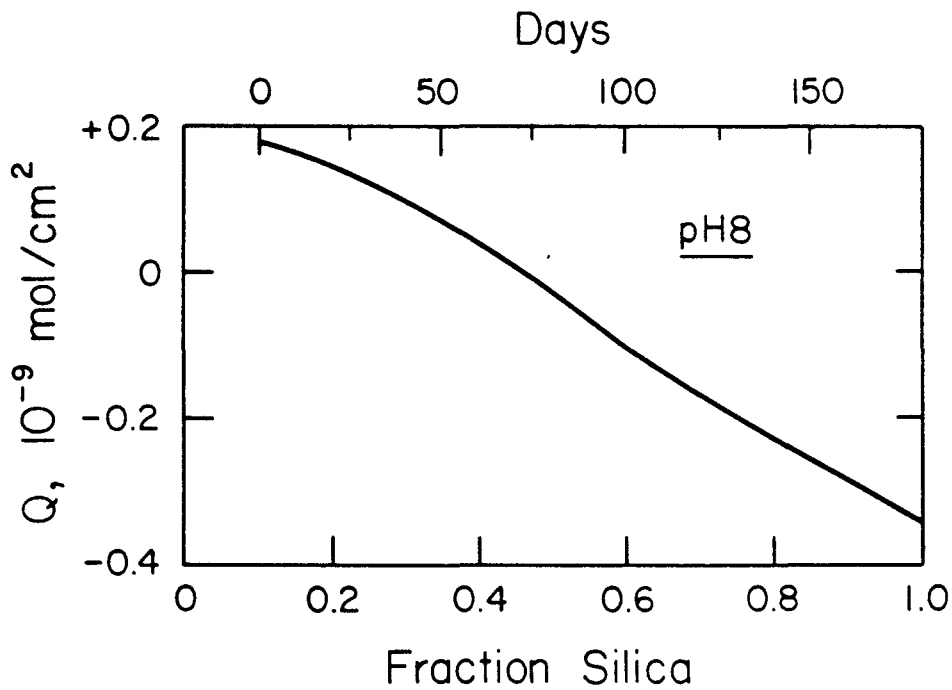
Fig. 4.23. Predicted chrysotile surface charge during dissolution; fraction of surface that is silica vs. magnesium increases with time; time scale based on surface being 10 percent silica at the outset.

surface charge results in the five-day experiments. The magnitude of $K_{as}{}^S$ has a greater effect on the calculated charge for a surface with a greater fraction of >Si-OH sites, corresponding to the larger times on Figure 4.23.

4.2.2.3. Effect of Model Organic Anions

The addition of organic anions makes the surface charge and mobility of chrysotile negative in two ways -- by adsorption of negatively charged species to the surface and by enhancing release of magnesium from the surface. Results of a ten-day mobility and adsorption experiment are shown on Figure 4.24. The effect of adsorbed catechol in giving chrysotile a negative mobility is apparent during the first 24 hours after adding the organic. During that time, only about 15 percent of the catechol is adsorbed, which corresponds to 40 percent of the maximum adsorption density.

The UV-absorbance peaks for catechol showed a progressive broadening in this experiment (Figure 4.25), like that noted above in the dissolution experiments (Figure 4.19). Along with this broadening, or apparent oxidative polymerization, is a decrease in the magnitude of the negative mobility. This is consistent with oxidation of adsorbed organics to form uncharged, polymeric species. That the decrease in absorbance at $\lambda = 256$ nm is associated with catechol removal from solution was confirmed by the TOC analyses shown on Figure 4.24. Other mechanisms for reduction of the magnitude of the mobility, such as shifting the plane of shear due to polymer adsorption (Kavanagh et al., 1975), charge neutralization by counterions, or changes in the double-layer parameters seem less likely.
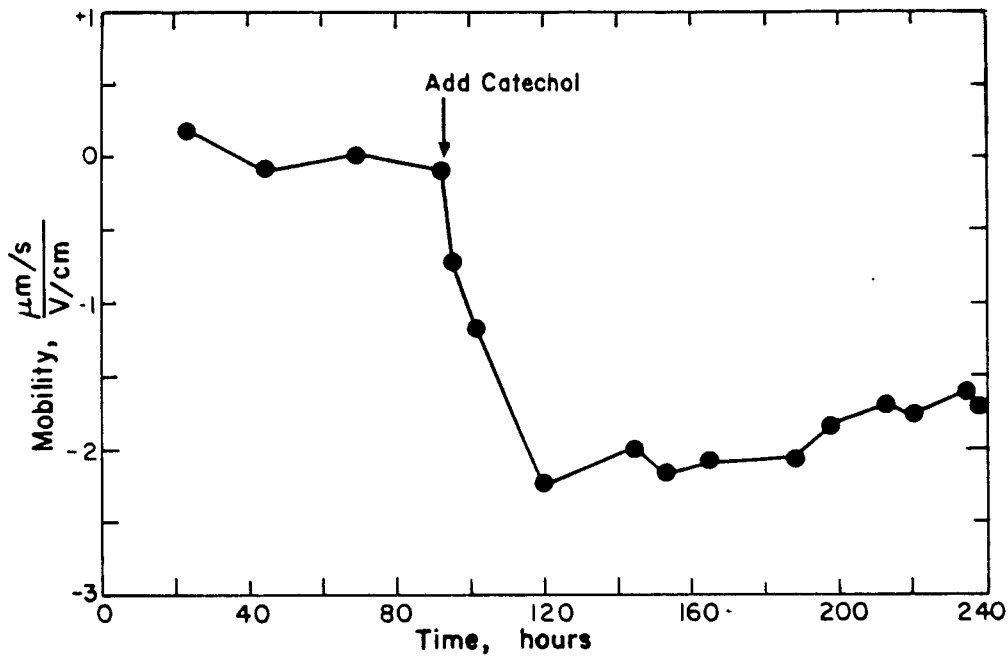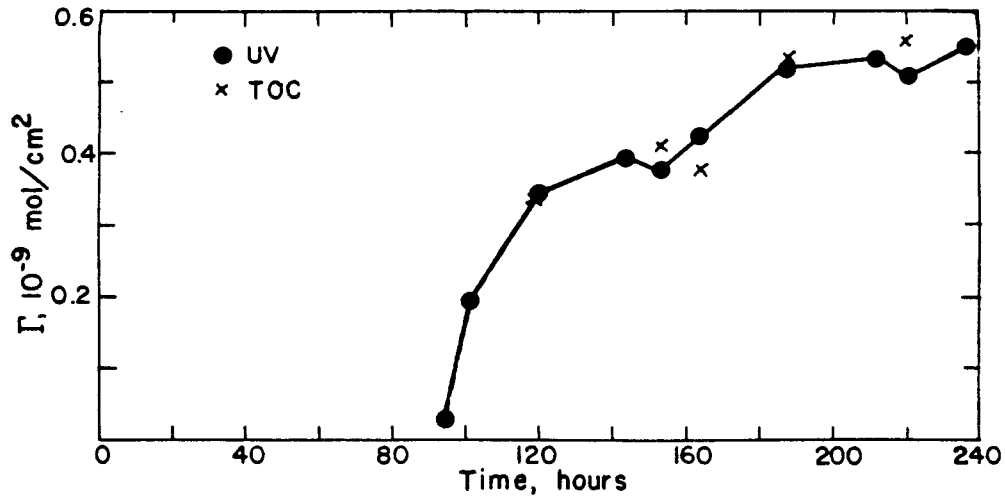
Fig. 4.24. Chrysotile surface charge and mobility resulting from catechol adsorption; pH 8, 0.01 M NaCl, 25 C, N_2-CO_2 (350 ppm) atm., solids 10.9 mg/L (mobility) and 1.02 g/L (adsorption); 1.9 x 10^{-9} mol/cm^2 catechol added.
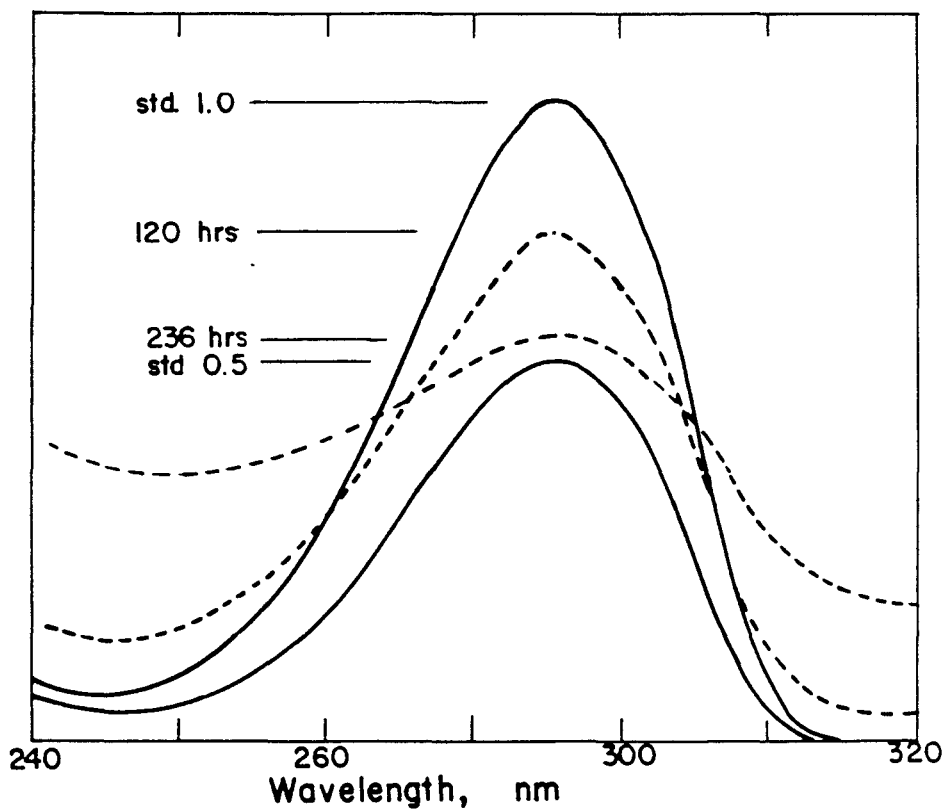
Fig. 4.25. UV scans of catechol in the presence of chrysotile; experimental results on Fig. 4.15.

A series of subsequent experiments examined the charge reversal apparent on the middle portion of Figure 4.24, from one day prior to organic addition to several days after organic addition. Aliquots were withdrawn from the stock suspension whose mobility is shown on Figure 4.21, catechol or oxalic added, and the effect noted. Parallel adsorption experiments were run. All mobility curves showed qualitatively the same behavior, as did those for preliminary experiments done with phthalic acid (Appendix III). Within 24 hours after adding the organic, a new, lower steady-state mobility value was reached. Figure 4.26 summarizes these latter steady-state values for the range of conditions studied. If charge reversal was due only to anion adsorption at the maximum densities suggested by Figures 4.15 and 4.18 there should be little charge enhancement beyond an organic to surface molar ratio of one. The presence of an enhancement at higher ratios suggests either multi-layer adsorption, increased magnesium removal like that observed on Figure 4.13, or both.

The effect of different initial mobilities, prior to organics addition, was small; this was evidenced by the similar post-addition mobilities for pH 8, equimolar catechol and surface, for initial mobilities of from +1 to 0 (Figures 4.26 and Appendix III). Oxalate has less of an effect on chrysotile mobility than does catechol, consistent with the above-noted lower adsorption of oxalate on the surface. The mixed effect of catechol and oxalate on dissolution of the magnesium-hydroxide layer was noted on Figure 4.11 and 4.13. However the lesser adsorption of oxalate is counter to the stronger magnesium-oxalate solution complexation equilibria noted in Table 2.2
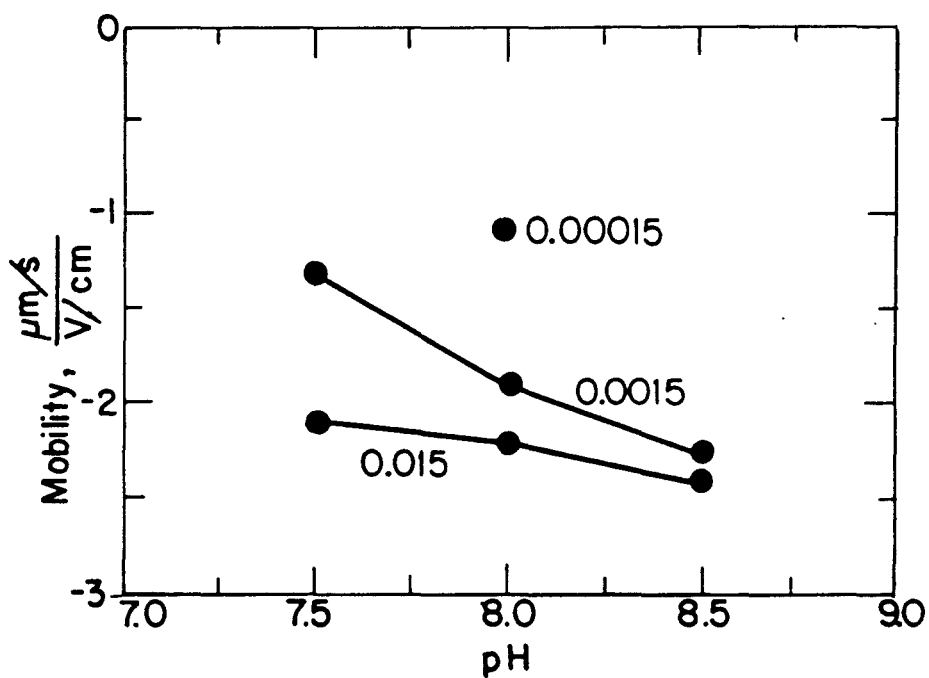
Fig. 4.26. Mobility of chrysotile in the presence of various catechol concentrations (mg C/cm^2), where 0.015 mg C/cm^2 = 200 10^{-9} mol catechol/cm^2, or 100-fold excess organic relative to surface site density.

and on Figure 4.17. These mobility data provide additional evidence that catechol adsorbs to both >Si-OH and >Mg-OH surface sites.

That the negative charge on chrysotile is due to a combination of anion adsorption and enhanced magnesium hydroxide dissolution can also be seen by comparing the Alox and chrysotile mobilities of Figures 4.26-4.28. The pH_{iep} of Alox in the absence of organic matter is seen from Figure 4.28 to be about 9.4, which is near the pH_{zpc} of 8.9 for chrysotile. From 10^{-3} to 10^{-2} mg C/cm^2 (catechol) causes a small charge reversal of Alox at pH 8 (Figure 4.27) due to adsorption. The same concentrations cause a greater charge reversal on chrysotile. Concentrations on the order of 10^{-4} mg C/cm^2 at pH 8 cause a charge reversal on chrysotile but not on Alox. From Figure 4.14 it is seen that catechol adsorbs more strongly onto Alox than onto chrysotile. The greater magnitude mobility on chrysotile in the presence of catechol (Figure 4.27) is then due largely to enhanced dissolution rather than greater adsorption.

4.2.2.4. Effect of Natural Organic Matter

Adsorption of NOM in the range 10^{-5}-10^{-3} mg C/cm^2 caused greater charge reversal on chrysotile than did either oxalic acid or catechol. NOM is composed of a distribution of carboxyl and hydroxyl acidic functional groups that are available to bind to the surface and give a negative charge to the surface. The greater magnitude mobility at lower organic adsorption densities suggests that NOM contains a greater abundance of acidic groups that are deprotonated at this pH.
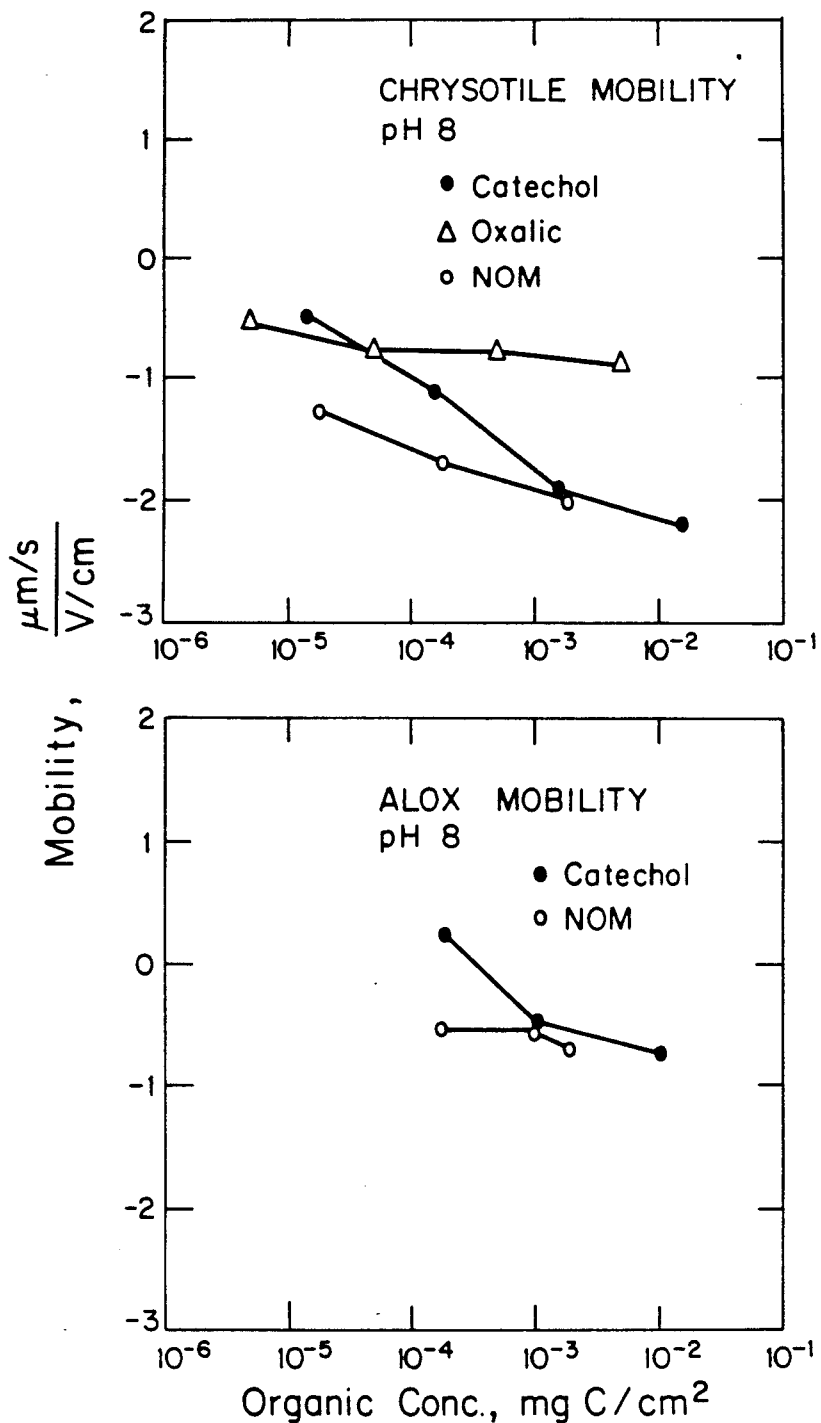
Fig. 4.27. Mobility of chrysotile and Alox in
the presence of increasing organic concentrations
(amt. organic added); conditions of each experiment
are noted on mobility vs. time results of
Appendices II and III.
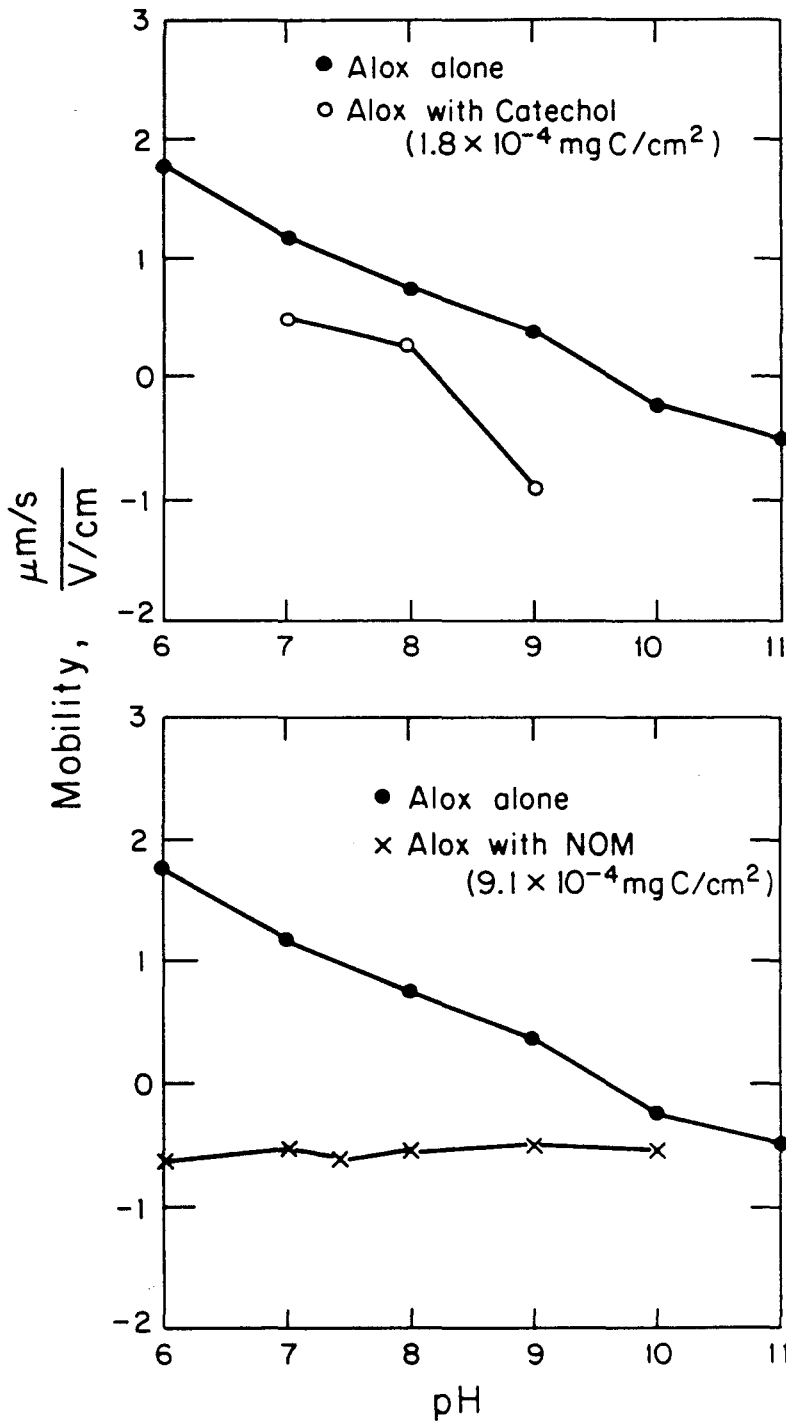
Fig. 4.28. Alox mobility as a function of pH in the presence of organic matter; conditions of each experiment as noted on mobility vs. time plots of Appendix III.

Mobility was also lower on Alox in the presence of NOM than in the presence of catechol. Little change in mobility was observed in going from 10^{-4} to 10^{-3} mg C/cm^2. Charge reversal at low organic concentrations is consistent with the findings of Tipping and Cooke (1982), who observed reversal of mobility with adsorption of as little aquatic humus as 10 mg/g ($\sim 60 \times 10^{-6}$ mg/cm^2) onto goethite at pH 7. Less negative charge was conferred per unit mass of humics adsorbed as adsorption density was increased by a factor of three. In the presence of Ca^{2+} and Mg^{2+}, little change was observed in going from 20 to 60 mg/g adsorbed. These same divalent cations are known to interact strongly with humics in solution (Dempsey, 1981) and adsorbed on the surface of goethite particles (Tipping & Cooke, 1982). In the latter case, mobility decreased with increasing cation concentration.

The mobility of Alox in the presence of NOM was not pH dependent (Figure 4.28) in the pH range 4-10. This is in contrast to the results of Davis (1982), where at least a one-unit mobility change was observed over a similiar pH range for organic concentrations about 20-fold lower.

Particles in samples taken from the Feather river in May, 1983 all showed mobilities of -1.1 $\pm$0.5 μm·s^{-1}V·cm^{-1}. The chrysotile fiber concentration in these samples was on the order of 10^8/L and the concentration of larger (2-100 μm) particles was about 10^7/L. This suggests that even far upstream in natural waters, chrysotile fibers, as well as other particles present, have a negative charge due to adsorption of NOM. The magnitude of that charge is equal to or lower than that observed in the laboratory, with little variation in

individual mobilities despite the wide range of particle sizes and presumably particle identities in the river-water samples. This is consistent with observations by others. For example, after several successive exposures to seawater, mobilities of three model particles -- Al_2O_3, a cationic polymer and a hydrophobic organic polymer -- converged to a negative value like that observed for natural particles (Hunter, 1980). Initial mobilities were positive.

The mobility of two samples taken from Castaic reservoir in August, 1983 had the same mobility as the earlier Feather river samples -- $-1.1 \pm 0.3 \ \mu m \cdot s^{-1} V \cdot cm^{-1}$. Chrysotile added to filtered Castaic water (pH 8.5) acquired a negative mobility (-1.5) within a few hours; the mobility remained constant overnight.

4.3. COAGULATION

From 5 to 50 fold reduction in fiber concentration was observed in the two five-day coagulation experiments. Results are shown in Table 4.1. This reduction is apparently due to coagulation of fibers with silica particles. The experimental blank -- a 4.9 g/L chrysotile suspension with no silica present -- showed a relatively constant fiber concentration.

Following equation (2.31), up to a 600-fold reduction in chrysotile fiber concentration is expected over the five-day period [a]. It is assumed that differential sedimentation is primarily

---

[a] $n_1/n_1^0 = \exp(-\alpha t \Sigma n_i k_i)$; from Table II.10, $n_i k_i = 14.8 \times 10^{-6} \ s^{-1}$ for the silica suspension used in this experiment; for $\alpha = 1$ and $t = 0.43 \times 10^6$ s, $n_1/n_i^0 = e^{-6.38} = 0.0017$.

Table 4.1. Total fiber count in coagulation experiments.

Date	Hours	10^8 Fibers/L	
		Ave.	S. dev.
4.9 µg/L blank[a]	2	4.0	1.6
5-10-84	24	2.0	0.8
5-11-84	28	2.8	0.4
5-12-84	48	1.8	0.4
5-16-84[b]	144	0.7	0.6
Stirred beaker[c]			
5-16-84	120	0.05	0.08
Settling column			
5-14-84[d]	68	1.7	0.6
5-16-84[a]	120	0.5	0.2

[a]Numbers reported were determined from six photographs taken in six different grid squares of the 300-mesh copper grid; an average of 8-18 fibers were counted on each photograph, the area of which corresponded to approximately 4×10^{-4} mm^2 on the original filter.

[b]Lower value due in part to problems with sample preparation.

[c]Three fibers were counted in an area corresponding to approximately 10^{-3} mm^2 on the original filter.

[d]Eighteen fibers were counted in an area corresponding to approximately 10^{-3} mm^2 on the original filter.

responsible for particle contact. Fluid shear may be important in the stirred beaker; although the shear rate was not determined, the analysis of section 2.3.1.2 suggests that the rate constant for fluidshear is about 10-fold lower than the constant for differential sedimentation for the particle size range of interest. Results of the experiments, however, showed ten-fold greater fiber removal in the stirred reactor than in the settling column, suggesting that fluid shear is important.

There is qualitative agreement between the removals predicted from coagulation theory and observed in the experiment. Freshly suspended, positively-charged chrysotile fibers coagulate with larger, negatively-charged silica particles with a high efficiency. An α value in the range 0.01-0.1 characterizes the process. In California surface waters it is observed that weathered, negatively-charged chrysotile fibers coagulate with the larger particles present at a slower rate -- α is on the order of 0.001 (Bales et al., 1984). The lower rate, or efficiency, in natural waters is apparently due to the more uniform negative surface charge on all particles, brought on by adsorption of NOM.

Other explanations are possible for the effect of NOM. For example, Tipping and Higgins (1982) observed that adsorbed humics enhance stability of hematite particles; the mechanism is thought to be steric stabilization, as electrophoretic mobilities changed little with changes in humic concentration from 1-20 mg/L. Estuarine particles in general have highly uniform surface properties in spite of their potentially variable and mixed composition (Hunter, 1983).

CHAPTER 5

CONCLUSIONS

The research work described in this thesis provides insight into the chemical behavior and the influence of surface chemistry on the physical behavior of chrysotile asbestos particles in natural waters and in water treatment processes. Chrysotile fibers are present in surface waters of central and northern California at concentrations from 10^7 to 10^{11} fibers/L as a result of natural, physical weathering in the Sierra Nevada and coastal mountains. Two important chemical processes that occur on the surface of chrysotile particles suspended in natural waters are adsorption of organic matter and dissolution, or chemical weathering. Both processes cause a reversal of chrysotile's surface charge and affect the rate at which fibers coagulate with other suspended matter. In water treatment, the surface identity of the fibers influences the rate and extent to which they adsorb or serve as nucleation sites for added coagulant chemicals, coagulate with other particles, and deposit onto sand filter grains.

5.1. CHRYSOTILE DISSOLUTION

5.1.1. pH Dependence of Chrysotile Dissolution

Over the pH range 7-10 chrysotile suspended in 0.1 M inorganic electrolyte for up to five days dissolves with magnesium being released into solution in excess of the 3:2 magnesium to silica molar ratio in the solid. The rate of magnesium release (mol/cm^2·s) exhibits a fractional pH dependence:

$$r = k_1' [H^+]^{0.24} \qquad (5.1)$$

where $[H^+]$ is the hydrogen ion concentration in solution (mol/L). k_1' is the observed dissolution rate constant and depends on the dissolution mechanism, the specific surface area of the solid and the charge-potential relation at the surface. Interpreted in terms of a site-binding model for adsorption and desorption of protons on the surface, this fractional dependence implies that the dissolution rate is limited by a chemical reaction involving an average of less than one adsorbed proton per magnesium ion released into solution. Silica release from chrysotile shows a weaker pH dependence and the rate cannot be characterized by a simple equation like (5.1). The rate at which chrysotile dissolves ($10^{-15.7}$ mol/cm^2·s at pH 8) is consistent with the rates observed for other magnesium silicate minerals and for magnesium hydroxide; the magnitude of the rate further confirms that a chemical reaction rather than diffusion of reactants (protons) to the surface is rate limiting.

Chrysotile suspended in inorganic electrolytes exhibits a rapid but declining rate of release of Mg^{2+} into solution for 12-24 hours, followed by a slower, constant rate of release for the following four to five days. The rate of silica release is linear from the outset. Up to 15 percent of the outer magnesium hydroxide surface is released into solution (based on a 100 percent magnesium-surface initially) during the initial 12-24 hour period. After the first day magnesium release follows equation (5.1), which is a smaller pH dependence than observed on other silicate and oxide minerals (Figure 5.1). For example, the following are reported: bronzite, $[H^+]^{0.5}$; diopside, $[H^+]^{0.7}$; enstatite, $[H^+]^{0.8}$; forsterite, $[H^+]^{1.0}$; δ-aluminum oxide, $[H^+]^{1.0}$; and bayerite, $[H^+]^{1.0}$, all at acidic pH's. Although data are
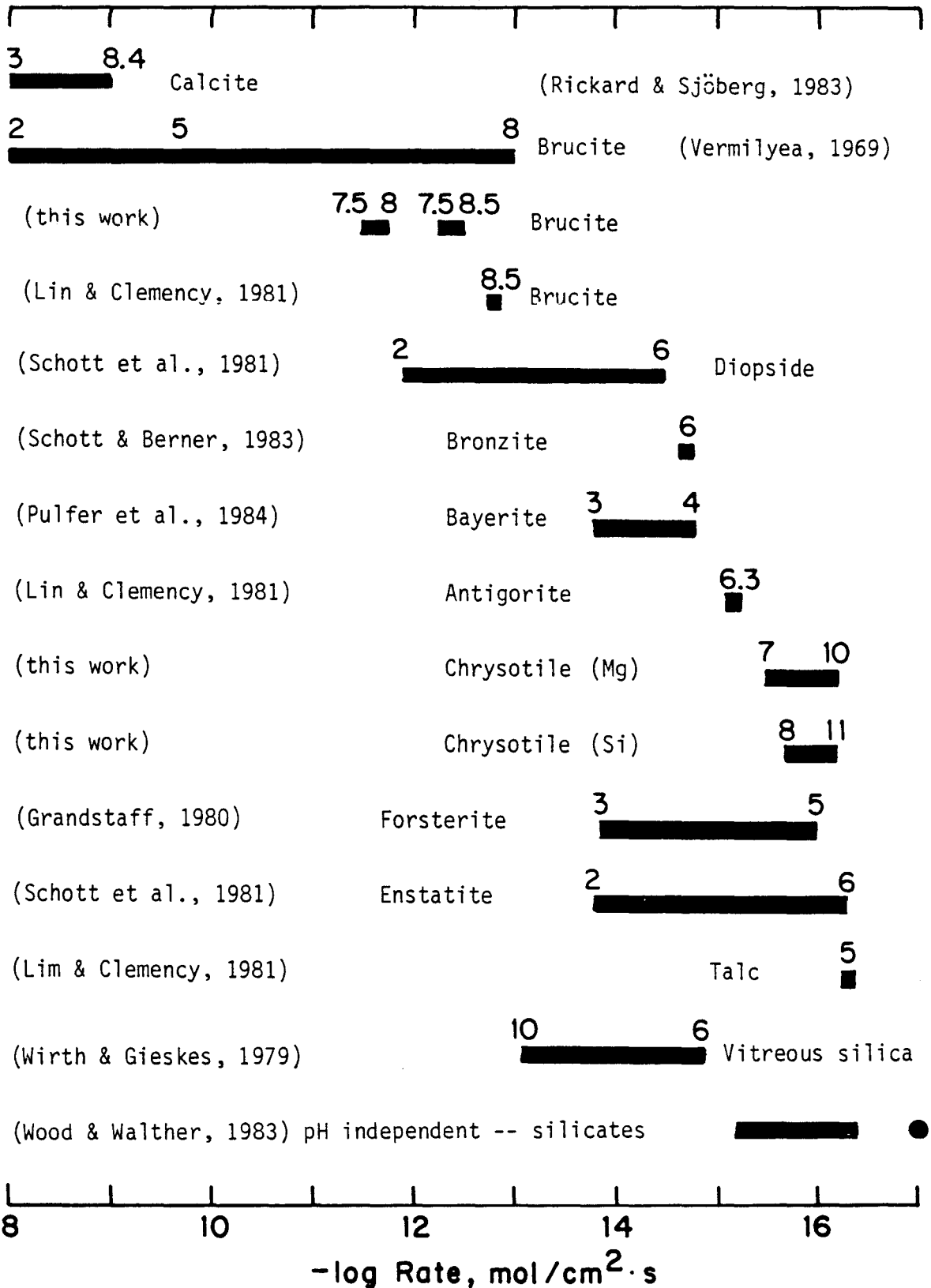
Fig. 5.1. Dissolution rates for a variety of minerals at 25 C; length of bar indicates range at rates observed; numbers above each bar indicate pH over which rate was measured.

not directly comparable because different pH ranges were studied, the lower pH dependence for magnesium release from chrysotile suggests that magnesium hydroxide is more easily dissolved than minerals such as aluminum oxide, and that attack by H_2O rather than H_3O^+ may be more important in chrysotile dissolution.

5.1.2. Effect of Anions on Chrysotile Dissolution

The inorganic anions NO_3^-, Cl^-, HCO_3^- and SO_4^{2-} and the organics catechol and oxalate affect the rate of magnesium release only during the initial 12-24 hours of each experiment. After that period, rates with and without organics present were the same. Oxalate inhibited silica release. The nature of this inhibition is unclear, as oxalate is not known to interact directly with a silica surface. If Mg^{2+} plays a role in the release of silica, the oxalate inhibition could be due to formation of magnesium-oxalate complexes. There is no independent evidence for Mg^{2+} being involved in silica dissolution, however. Catechol had a slight enhancing effect on the release of silica from chrysotile, which is consistent with the enhancement reported for dissolution of silica in the presence of catechol.

5.1.3. Attainment of Steady-State Dissolution

Chrysotile dissolves with the ratio of magnesium to silica released being near 2.0 in the pH range 7-9, which is greater than the 1.5 molar ratio in chrysotile. If dissolution occurs only, or primarily, at the surface, the rate of magnesium release should diminish as the fraction of surface that is magnesium hydroxide diminishes and the rate of silica release increase as the fraction of surface that is silica increases. Eventually a surface of constant

composition should result and the ratio of the dissolution rates should reflect the molar ratio in the material. This did not occur during the five-day experiments; several days to weeks may be required to reach this steady state.

5.1.4. Consistency of Chrysotile Dissolution with Rates for Other Minerals

The dissolution rate for chrysotile is compared with rates reported for other silicates and oxides on Figure 5.1. These rates span nearly nine orders of magnitude, from the diffusion-limited dissolution of calcite at pH 3 (10^{-8} mol/cm^{2}s) to the reaction-limited dissolution of silicates (10^{-17} mol/cm^{2}s).

The minerals containing magnesium hydroxide layers exhibit decreasing dissolution rates with increasing structure, from brucite to antigorite and chrysotile to talc. All four minerals involve the stacking of semi-infinite brucite sheets composed of magnesium in octahedral coordination with oxide and hydroxide. In antigorite and chrysotile each octahedrally-coordinated brucite sheet is bonded to a sheet composed of silica tetrahedra (t-o structure), with the result that magnesium is less easily removed than in the absence of the tetrahedral sheet. In talc each octahedral sheet is sandwiched between two silica sheets (t-o-t structure) and the dissolution rate for the magnesium component is lowest. There are no data available concerning the pH dependence of talc dissolution, but the rate at pH 5 is near the 10^{-17} mol/cm^{2}s value (based on SiO_2) estimated by Wood and Walther (1983) for the pH-independent dissolution of feldspars and micas; it is expected that the rate for talc would decline only slightly above pH 5.

It has been suggested that both solubility and dissolution rates for silicates should decrease with increasing structure -- increasing sharing of oxides by silica tetrahedra -- in the order: neso $\sim$ soro > ino > tecto $\geq$ phyllo (Hurd et al., 1979). In comparing the more rapid dissolution of fayalite (Fe_2SiO_4), an olivine (nesosilicate), to the slower dissolution of bronzite ($Fe_{0.3}Mg_{1.7}Si_2O_6$), a pyroxene (inosilicate), it was suggested that dissolution of an olivine is easier and faster because it involves no breaking of strong Si-O bonds (Schott & Berner, 1983). In olivines, silica tetrahedra are linked by other cations (Mg^{2+}, Fe^{2+}, etc.) and do not share oxides, whereas in pyroxenes adjacent silica tetrahedra share two corner oxides. Comparing the dissolution rates of Figure 5.1 for magnesium silicates with differing degrees of structure (sharing of oxygens in silica tetrahedra) fails to give the same consistent pattern. Forsterite (Mg_2SiO_4), an olivine, dissolves at about the same rate as enstatite ($Mg_2Si_2O_6$), a pyroxene. Dissolution of about the same or faster rate is observed in chrysotile and antigorite, serpentines (phyllosilicates), where silica tetrahedra share three corner oxygens. Apparently the nature of the octahedral sites strongly influences the release of silica from these chemically similar minerals.

5.2. ADSORPTION AND SURFACE CHARGE

An ideal, unweathered fiber has a magnesium-hydroxide outer surface and fibers freshly suspended in water of pH below 8.9 have a positive surface charge. Particles aging in natural waters acquire a negative surface charge by rapid (within hours) adsorption of natural organic matter and by slower (within days) dissolution of the outer

magnesium-hydroxide sheet and accompanying exposure on the surface of the underlying silica sheet.

5.2.1. Adsorption of Organics onto Chrysotile and Aluminum Oxide

The amount of catechol that is lost from solution (adsorbs) in the presence of chrysotile or aluminum oxide in the pH range 7.5-8.5 does not reach equilibrium but increases over five days. After one day the maximum adsorption density on chrysotile, estimated using a Langmuir adsorption equation, is 0.7×10^{-9} mol/cm^2 (50 mg C/cm^2). This is approximately one-third of the estimated number of surface sites available for proton exchange, 2×10^{-9} mol/cm^2. The corresponding maximum density for adsorption of natural organic matter was 26×10^{-6} mg C/cm^2 on chrysotile and 32×10^{-6} mg C/cm^2 on aluminum oxide. These densities suggest that in California surface waters, the surfaces of chrysotile fibers and clay particles should be essentially completely covered with NOM.

The steady increase in amount adsorbed with time in each experiment is apparently due to further adsorption of oxidized polymers of catechol. Oxidation and polymerization of catechol is enhanced in the presence of both chrysotile and aluminum oxide surfaces. The oxidant in these experiments was either molecular oxygen, present in trace amounts in the N_2 gas used to exclude CO_2 from the reactor, or Fe(III), present as an impurity in the chrysotile.

The adsorption densities and charges resulting from adsorption of catechol and oxalate onto chrysotile were comparable. Oxalic acid is a stronger acid, should bind to >Mg-OH sites to a greater extent than

catechol, and should be present as an anion, whereas catechol should be an uncharged species, in the pH range 7-9. Binding of catechol onto both >Mg-OH and >Si-OH sites could account for its adsorption and surface-charge behavior. Some charge reversal upon adsorption of catechol occurred within one hour and a near-constant charge was reached within 24 hours.

5.2.2. Chrysotile Surface Charge

At pH values below the pH_{zpc} (8.9), chrysotile's surface charge is initially positive, but becomes negative due to both dissolution and adsorption. For example, at pH 8 in 0.01 M NaCl, chrysotile's surface charge (electrophoretic mobility) is initially positive but becomes zero after about two weeks and is negative thereafter. The positive-to-negative shift is due to the faster dissolution of the positively-charged brucite sheet relative to the negatively-charged silica sheet in chrysotile's outer layer. Chrysotile adsorbs sufficient catechol, oxalate, phthalate or natural organic matter within one day to reverse its surface charge.

The surface charge of freshly suspended chrysotile fibers changes more rapidly during the first day as proton uptake and the rate of magnesium release reach steady-state values. Particle breakup may be partly responsible for the initial change. Surface charge then changes more slowly, reflecting the relative rates of magnesium and silica release. After four weeks, further changes in surface charge, (electrophoretic mobility) are slow, possibly reflecting a new steady state in dissolution wherein magnesium and silica release rates are in a ratio that more closely reflects the Mg:Si molar ratio in the solid.

Chrysotile's surface charge was the same in the presence of the different inorganic anions NO_3^-, Cl^-, HCO_3^- and SO_4^{2-}, suggesting that adsorption of these anions is weak.

In the pH range 7.5-8.5, adsorption of catechol and NOM on aluminum oxide (at the same or higher adsorption densities) causes a smaller charge reversal than on chrysotile. Aluminum oxide has a pH_{iep} of 9.4, near that of chrysotile aged for less than one week. The larger charge reversal on chrysotile reflects an enhanced removal of the surface brucite layer accompanying the rapid (order of hours) adsorption.

5.2.3. Surface Chemical Model

A constant-capacitance model can be used to relate surface charge to adsorption and desorption of protons over a limited, 1.5-2 pH-unit, range. The best-fit model parameters are $pK_{a1}^S = 8.0$, $pK_{a2}^S = 10.0$ for >Mg-OH and $pK_{as}^S = 7.5$ for >Si-OH, and a capacitance of 4 C/V·cm^2. Poorest fit for any of the combinations of constants tried is at higher pH values, 10-11. Best fit is below the pH_{zpc}.

5.3. FIBER REMOVAL IN NATURAL WATERS AND WATER TREATMENT

In reservoirs, submicron-sized chrysotile particles coagulate with larger (> 2 μm) particles that subsequently settle out. In four of The Metropolitan Water District of Southern California's source-water reservoirs, approximately one-log removal occurs for each year of detention time. This is based on long-term averages; no annual or seasonal variations are accounted for.

Coagulation efficiency for freshly-suspended, positively-charged chrysotile fibers with larger, negatively-charged silica particles is in the range 0.01-0.1. Electrostatic barriers should be absent, as

the silica and chrysotile are oppositely charged. In natural waters, chrysotile fibers are coated with NOM, are negatively charged, and coagulate more slowly. Efficiency is near 0.001.

The observed chrysotile dissolution rates at pH 8 suggest that complete dissolution of a fiber would require at least 5-10 years. As the residence time for suspended particles in California surface waters is shorter, up to three years, dissolution is not directly responsible for fiber removal.

Removal of chrysotile particles in water treatment occurs by deposition of coagulated fibers onto sand grains in filtration. Capture efficiency for single fibers is low; removal is enhanced from 10- to 100-fold by incorporating fibers into larger flocs that have a greater capture efficiency.

CHAPTER 6

RECOMMENDATIONS

The surface-chemical studies of chrysotile described in chapters 1-5 have motivated additional questions regarding the chemical weathering of natural minerals, the aggregation of colloids in natural waters and the deposition of submicron sized particles in water treatment by filtration.

6.1. CHEMICAL WEATHERING

The technique used in the potentiometric experiments could be applied to other minerals. It enables determining both dissolution rate and surface charge in the same constant-pH experiment. Measuring both enables interpreting the dissolution rate in terms of the number of hydrogen ions adsorbed on the surface, or the number involved in the rate-limiting step in dissolution. Holding pH constant during dissolution of a heterogeneous material such as chrysotile is necessary if the pH dependence of the rate is to be determined, because the time to reach a steady-state rate after changing pH may be long -- from hours to days. It is recommended that the methods employed in the dissolution experiments be applied to other oxides and silicates that dissolve at comparable rates.

Insight into the importance of silicate structure on dissolution rate of phyllosilicates could be determined by studying the dissolution of talc under conditions like those used for chrysotile. Talc has two tetrahedral silica sheets for each octahedral magnesium-hydroxide sheet versus the one-to-one ratio in chrysotile. It is recommended that the pH and temperature dependence of talc dissolution be studied over the pH range 6-9.

Additional experimental determinations of dissolution rates are needed to confirm the importance of crystal structure on dissolution rates across the broad class of silicate minerals. Speculation that silicate hydrolysis at low temperatures (∿25 C) is independent of or only weakly dependent on structure and pH is not well documented. It is recommended that experiments with well-characterized magnesium silicates be carried out as a first step in the investigation of these dependences.

Determination of an activation energy for dissolution of weathered chrysotile in the pH range 7-9 could further clarify the dissolution mechanism. Past determinations of activation energies have considered only one component -- magnesium -- and have not been done at constant pH (e.g., Choi and Smith, 1972). It is recommended that chrysotile dissolution experiments be carried out over the temperature range 10-40 C at pH 8 and at one or more additional pH values in the range 7-9.

It was projected that at longer times -- from two to seven weeks -- the ratio of the rates of magnesium and silica release from chrysotile should equal the 3:2 ratio of magnesium and silica in the solid. It is recommended that one or more long-term dissolution experiments on a well-characterized chrysotile be carried out to confirm this projection.

It is not known if chrysotile dissolving at neutral pH over long times (months) in a solution near saturation with regard to silica solubility builds up a surface layer of different composition than the original solid. Indirect evidence indicates that this may be the case for dissolution at acidic pH's. It is recommended that surface characterization accompany long-term dissolution experiments to determine surface versus bulk solid magnesium-to-silica molar ratios and to determine if a new solid phase forms on the surface.

Brucite dissolution is apparently transport limited, as evidenced by its linear dependence as hydrogen ioh concentration and by its dependence on suspension stirring rate. It is recommended that the pH and transport dependences of brucite dissolution be determined in a system with well-defined transport, such as a rotating disk electrode.

6.2. PARTICLE AGGREGATION AND DEPOSITION

Results of the coagulation experiments carried out as part of this work suggest that submicron-sized chrysotile fibers readily coagulate with oppositely charged particles from 1 to 10 μm in size. It is recommended that coagulation experiments be continued in three areas. First is a quantitative measurement of coagulation rate for chrysotile with oppositely-charged, model particles over a several-day period. Second is measurement of the same rate for fibers with particles of like charge; charge of fibers could be reversed by adsorption of natural organic matter. Third is carrying out of the same experiments with a monodisperse suspension of model particles rather than the heterodisperse chrysotile particles; this should give a more confident measure of coagulation efficiency for submicron-sized particles.

Removal of fibers in water filtration depends on the degree of aggregation that occurs prior to passage of fibers through the filter media. A primary area for study is the nucleation of coagulant solids -- $Al(OH)_3$, $Fe(OH)_3$, etc. -- onto chrysotile fibers and the ensuing coagulation. It is recommended that as a first step the rate and extent of coagulant deposition onto chrysotile be determined under well-controlled conditions and that the resulting aggregates be

characterized by size and identity. This should be done in parallel with work on model particles.

6.3. PILOT FILTRATION STUDIES

It is recommended that pilot filtration studies focus on the importance of operating variables specific to removal of chrysotile fibers. From three to six well-characterized pilot runs should be carried out on water to which a known concentration of weathered fibers is added. Initial variables to be addressed are coagulation time, coagulant dose and pH. Order-of-magnitude variations in coagulant dose and coagulation time should be used. Characterization by particle counting, turbidity measurement, transmission electron microscopy, and mobility measurement should be done at three points in the pilot setup -- before rapid mixing, after coagulation and after filtration.

APPENDIX I

REFERENCES

Aagaard, P. and Helgeson, H. C. Thermodynamic and Kinetic Constants on
    Reaction Rates among minerals and Aqueous Solution. I. Theoretical
    Considerations. Amer. Jour. Sci. 282:237-285 (1982).

Ahmed, S. M. Surface Chemistry and Adsorption Properties of Milled
    Chrysotile Asbestos Fibers. in Adsorption from Aqueous Solutions.
    P. H. Tewari, ed. Plenum, New YORK (1981).

Albers, J. P. Economic Deposits of the Klamath Mountains in Geology of
    Northern California. E. H. Bailey, ed. Bull. Calif. Div. Mines
    Geology. 190:51 (1966).

Allen, M. P. and Smith, R. W. Dissolution of Asbestos Minerals in Acid
    and Buffered Salt Solutions. Proc. 3rd Intl. Conf. Phys. Chem.
    Miner. Asbestos. Univ. Laval, Quebec. Sect. 4.16 (1975).

Anderson, C. H. and Long, J. M. Interim Method for Determining Asbestos
    in Water. U. S. EPA, Envir. Res. Lab., Athens, GA. Report EPA
    600/4-80-005 (1980).

Baccini, P.; Grieder, E.; Stierli, R. and Goldberg, S. The Influence of
    Natural Organic Matter on the Adsorption Properties of Mineral
    Particles in Lake Water. Schweiz. Z. Hydrol. 44:1:99-116 (1982).

Bales, R. C.; Newkirk, D. D. and Hayward, S. B. Chrysotile Asbestos in
    California Surface Waters: From Upstream Rivers through Water
    Treatment. J. AWWA 76:66-74 (1984).

Bernas, B. A New Method for Decomposition and Comprehensive Analysis of
    Silicates by Atomic Absorption Spectrometry. Anal. Chem.
    39:1210:1682-1686 (1967).

Berner, R. A. Early Diagenesis. Princeton Univ. Press. (1978).

Berner, R. A. Kinetics of Weathering and Diagenesis. in Kinetics of
    Geochemical Processes. A. C. Lasaga and R. J. Kirkpatrick, eds.
    Mineral. Soc. Amer. (1981).

Berner, R. A. and Holdren, G. R. Jr. Mechanism of Feldspar Weathering
    -- II. Observations of Feldspars from Soils. Geoch. Cosmoch. Acta
    43:1173-1186 (1979).

Berner, R. A. and Schott, J. Mechanism of Pyroxene and Amphibole
    Weathering. II. Observations of Soil Grains. Amer. Jour. Sci.
    282:1214-1231 (1982).

Birkner, F. B. and Morgan, J. J. Polymer Flocculation Kinetics of Dilute Colloidal Suspensions. J. AWWA, 60:175-191 (1968).

Boudart, M. Consistency Between Kinetics and Thermodynamics. Jour. Phys. Chem. 80:26:2869-2890. (1976).

Boudart, M. Heterogeneous Catalysis. in Physical Chemistry, an Advanced Treatise, v. 7. H. Eyring, ed. Academic Press, NY (1975).

Cerda, C. M. and van de Ven, T. G. M. Translation of Axisymmetrical Particles in Shear Flow. Jour. Coll. Interface Sci. 93:54-62 (1983).

Choi, I. and Smith, R. W. Kinetic Study of Dissolution of Asbestos Fibers in Water. Jour. Coll. Interface Sci. 40:253-262 (1972).

Chowdhury, S. Kinetics of Leaching of Asbestos Minerals at Body Temperature. J. Appl. Chem. Biotechnol. 25:347-353 (1975).

Chowdhury, S. and Kitchener, J. A. The Zeta Potentials of Natural and Synthetic Chrysotiles. Internat. Jour. of Min. Proc. 2:277-285 (1975).

Clark, L. D. Foothills Fault System, Western Sierra Nevada, California. Bull. Geological Soc. Amer. 71:483 (1960).

Coleman, R. G. Petrologic and Geophysical Nature of Serpentinites. Bull. Geological Soc. 82:897-918 (1971).

Cooper, R. C.; Kanarek, M.; Murchio, J.; Conforti, P.; Jackson, L.; Collard, R. and Lysmer, D. Asbestos in Domestic Water Supplies in Five California Counties. Parts I, II. Rept. 78-1, 78-2. School of Public Health, Univ. of Calif., Berkeley (1978, 1979).

Davis, J. A. Adsorption of Natural Organic Matter from Freshwater Environments by Aluminum Oxide. in Contaminants and Sediments, vol. 2. R. A. Baker, ed. Ann Arbor Science, Ann Arbor, MI 272-304 (1980).

Davis, J. A. Adsorption of Natural Organic Matter at the Oxide/Water Interface. Geoch. Cosmoch. Acta. 46:2381-2393 (1982).

Deer, W. A.; Howie, R. A. and Zussman, J. j An Introduction to the Rock-Forming Minerals. Longman, London (1966).

Dempsey, B. A. The Protonation, Calcium Complexation, and Adsorption of a Fractionated Aquatic Fulvic Acid. Ph.D. Thesis, University of North Carolina, Chapel Hill, NC (1981).

Desai, R. and Richards, R. J. The Adsorption of Biological Macromolecules by Mineral Dusts. Envir. Res. 16:449-464 (1978).

Dibble, W. E., Jr. and Tiller, W. A. Non-Equilibrium Water/Rock Interactions - I. Model for Interface-Controlled Reactions. Geoch. Cosmoch. Acta. 45:79-92 (1981).

Edzwald, J. K.; Upchurch, J. B.; and O'Melia, C. R. Coagulation in Estuaries. Envir. Sci. Technol. 8:58-63 (1974).

Eppler, B.; Neis, U. and Hahn, H. H. Engineering Aspects of the Coagulation of Colloidal Particles in Natural Waters. Prog. Water Technol. 7:2:207-216 (1975).

Erkova, L. N.; Skvortsova, T. A.; Lazareu, S. Ya. and Grachev, O. I. Electrosurface Phenomena in Aqueous Suspensions of Chrysotile Asbestos during Adsorption of Surfactants. Zhurnal Prikladnoi Khimii. 54:9:1986-1990 (1981).

Evans, B. W. Metamorphism of Alpine Peridotite and Serpentinite. Annual Review Earth Planetary Sci. 5:397 (1977).

Fanning, R. A. and Pilson, M. E. Q. On the Spectrophotometric Determination of Dissolved Silica in Natural Waters. Anal. Chem. 45:1:136-140 (1973).

Farrell, C. and Qualley, G. Evaluation of Sediment-Removal Project. California Dept. of Water Resources Internal Report, December (1982).

Fuchs, N. A. The Mechanics of Aerosols. Macmillan, NY (1964).

Friedlander, S. K. Smoke, Dust and Haze. Wiley, NY (1977).

Furrer, G. and Stumm, W. The Role of Surface Coordination in the Dissolution of $-Al_2O_3$ in Dilute Acids. Chimia 37:9:338-341 (1983).

Gardiner, W. C., Jr. Rates and Mechanisms of Chemical Reactions. W. A. Benjamin, Menlo Park, CA (1969).

Gibbs, G. W. The Organic Geochemistry of Chrysotile Asbestos from the Eastern Townships, Quebec. Geoch. Cosmoch. Acta 35:485-502 (1971).

Gibbs, R. J. Effect of Natural Organic Coatings on the Coagulation of Particles. Environ. Sci. Technol. 17:237-240 (1983).

Grandstaff, D. E. Some Kinetics of Bronzite Orthopyroxene Dissolution. Geoch. Cosmoch. Acta 91:1097-1103 (1977).

Grandstaff, D. E. The Dissolution Rate of Forsteritic Olivine from Hawaiian Beach Sand. Proc. 3rd Intl. Symp. Water-Rock Interaction. Edmondton, Canada (1980).

Grauer, R. and Stumm, W. Die Koordinationschemie Oxidischer
    Grenzflächen und Ihre Auswirkung auf die Auflösungskinetik
    Oxidischer Festphasen in Wäbrigen Lösungen. Coll. & Polymer Sci.
    260:959-970 (1982).

Gupta, A. K. and Smith, R. W. Kinetic Study of the Reaction of Acids
    with Asbestos Minerals. Proc. Inter. Symp. Rock-Water Inter.
    Czechoslovakia 417-424 (1975).

Hahn, H. H. and Stumm W. Kinetics of Coagulation with Hydrolyzed
    Al(III). J. Coll. Interface Sci. 28:134-144 (1968).

Hammes, G. G. Principles of Chemical Kinetics. Academic, NY. (1978).

Happel, J. and Brenner, H.   Low Reynolds Number Hydrodynamics, 2nd rev.
    ed. Noordhoff, Leydon, The Netherlands (1973).

Hayward, S. B. Field Monitoring for Chrysotile Asbestos in California
    Waters. J. AWWA 76:66-73 (1984).

Hemley, J. J.; Montoya, J. W.; Christ, C. L. and Hostetler, P. B.
    Mineral Equilibria in the MgO-SiO$_2$-H$_2$O System: I. Talc - Chrysotile
    - Forsterite - Brucite Stability Relations. Amer. Jour. Sci.
    277:322-351 (1977).

Hill, C. G., Jr. An Introduction to Chemical Kinetics and Reactor
    Design. Wiley, NY (1977).

Hodgson, A. A. Fibrous Silicates. Royal Institute of Chemistry
    (London) Lecture Series No. 4 (1965).

Hohl, H. and Stumm W. Interaction of Pb^{2+} With Hydrous γ-Al$_2$O$_3$. Jour.
    Coll. Interface Sci. 55:281-288 (1976).

Holdren, G. R. and Berner, R. A. Mechanism of Feldspar Weathering -- I.
    Experimental Studies. Geoch. Cosmoch. Acta 43:1161-1171 (1979).

Hostetler, P. B. and Christ, C. L. Studies in the System
    MgO-SiO$_2$-CO$_2$-H$_2$O(I): The Activity-Product Constant of Chrysotile.
    Geoch. Cosmoch. Acta 32:485-497 (1968).

Huang, C. P. The Surface Acidity of Hydrous Solids. in Adsorption of
    Inorganics at Solid-Liquid Interface. M. A. Anderson and A. J.
    Rubin, eds. Ann Arbor Sci., Ann Arbor, MI (1981).

Hunsinger, R. B.; Roberts, K. J. and Lawrence, J. Chrysotile Asbestos
    Fiber Removal During Potable Water Treatment. Pilot Plant Studies.
    Envir. Sci. Technol. 14:333-336 (1980).

Hunt, J. R. Coagulation in Continuous Particle Size Distributions;
    Theory and Experimental Verification. W. M. Keck Lab. Envir. Eng.
    Sci. Report AC-5-80. California Institute of Technology, Pasadena,
    CA (1980).

Hunter, K. A. Microelectrophoretic Properties of Natural Surface-Active Organic Matter in Coastal Seawater. Limnol. Oceanog. 25:807-822 (1980).

Hunter, K. A. On the Estuarine Mixing of Dissolved Substances in Relation to Colloid Stability and Surface Properties. Geoch. Cosmoch. Acta 47:467-473 (1983).

Hunter, K. A. and Liss, P. S. Organic Matter and the Surface Charge on Suspended Particles in Estuarine and Coastal Waters. Limnol. Oceanogr. 27:322-335 (1982).

Hunter, R. J. Zeta Potential in Colloid Science. Academic Press, London (1981).

Hurd, D. C.; Fraley, C. and Fugate, J. K. Silica Apparent Solubilities and Rates of Dissolution and Precipitation. in Chemical Modeling in Aqueous Systems. E. A. Jenne, ed. Amer. Chemical Soc. Symp. Ser. 93 (1979).

Hurlbut, C. S., Jr. and Klein, C. Manual of Mineralogy, 19th ed. Wiley, NY (1977).

Iler, R. K. The Chemistry of Silica. Wiley, New York (1979).

International Agency for Research on Cancer. Asbestos. IARC Monographs on the Evaluation of Carcinogenic Risk to Man: Vol. 14 International Agency for Research on Cancer, Lyon, France (1977).

James, R. O. and Parks, G. A. Characterization of Aqueous Colloids by Their Electrical Double-Layer and Intrinsic Surface-Chemical Properties. E. Matijevic, ed. Surf. & Coll. SCI. 12:119-216 (1982).

Jones, P. and Hockey, J. A. Infra-red Studies of Rutile Surfaces. Part 2. - Hydroxylation, Hydration and Structure of Rutile Surfaces. Trans. Faraday SOC. 67:2679-2685 (1971).

Kavanagh, B. V.; Posner, A. M. and Quirk, J. P. Effect of Polymer Adsorption on the Properties of the Electrical Double Layer. Chem. Soc. Faraday Discuss. 59:242-249 (1975).

Kirmeyer, G. J. Seattle Tolt Water Supply Mixed Asbestiform Removal Study. U.S. EPA, Municipal Envir. Res. Labor., Cinn., OH. Report EPA-600/2-79-125 (1979).

Kummert, R. and Stumm, W. The Surface Complexation of Organic Acids on Hydrous γ-Al$_2$O$_3$. Jour. Colloid Interface Sci. 75:373-385 (1980).

Langer, A. M., Mackler, A. D. and Pooley, F. D. Electron Microscopal Investigation of Asbestos Fibers. Envir. Heal. Perspect. 9:63-80 (1974).

Langer, A. M. et al. Variation of Properties of Chrysotile Asbestos Subjected to Milling. Jour. Toxic & Envir. Health 4:173-188 (1978).

Lasaga, A. C. Transition State Theory. in Kinetics of Geochemical Processes. A. C. Lasaga and R. J. Kirkpatrick, eds. Mineral. Soc. Amer. (1981).

Lawler, D. F.; Izurieta, E. and Kao, C. P. Changes in Particle Size Distributions in Batch Flocculations. J. AWWA. 75:604-612 (1983).

Lawler, D. F.; O'Melia, C. R. and Tobiason, J. E. Integral Water Treatment Plant Design; From Particle Size to Plant Performance. in Particles in Water; Characterization, Fate, Effects, and Removal, M. C. Kavanaugh and J. O. Leckie, eds. Amer. Chem. Soc., Adv. in Chem. Ser. 189. Washington, D.C. (1980).

Lawrence, J. and Zimmermann, H. W. Potable Water Treatment for Some Asbestiform Minerals: Optimization and Turbidity Data. Water Research. 10:195-198 (1976).

Leal, L. G. and Hinch, E. J. The Effect of Weak Brownian Rotations on Particles in Shear Flow. J. Fluid Mech. 46:685-703 (1971).

Lemen, R. A.; Dement, J. M. and Wagoner, J. K. Epidemiology of Asbestos-Related Diseases. Envir. Heal. Persp. 34:1-11 (1980).

Lerman, A. Geochemical Processes Water and Sediment Environments. Wiley-Interscience, NY (1979).

Levich, V. G. Physiochemical Hydrodynamics. Prentice-Hall, Inc. Englewood Cliffs, NJ (1962).

Lin, F. and Clemency, C. V. The Dissolution Kinetics of Brucite, Antigorite, Talc and Phlogopite at Room Temperature and Pressure. Amer. Mineralogist. 66:801-806 (1981).

Light, W. G. and Wei, E. T. Surface Charge and Asbestos Toxicity. Nature 265:537-539 (1977).

Logsdon, G. S. Water Filtration for Asbestos Fiber Removal. U. S. EPA, Municipal Envir. Res. Labor., Cinn., OH. Report EPA-600/2-79-206 (1979).

Logsdon, G. S. et al. Filter Plant Design for Asbestos Fiber Removal. Jour. Envir. Engr. 109:900-914 (1983).

Logsdon, G. S.; Symons, J. M. and Sorg, T. J. Monitoring Water Filters for Asbestos Removal. Jour. Envir. Engr. Div., Amer. Soc. Civil Engr. 107:1297-1315 (1981).

Luce, R. W. Dissolution of Magnesium Silicates. Ph.D. Thesis, Stanford University, Stanford, CA (1969).

Luce, R. W.; Bartlett, R. W. and Parks, G. A. Dissolution of Magnesium Silicates. Geoch. Cosmoch. Acta 36:35-50 (1972).

Lykelma, H. Lyphobic Stability in Mixed Media. Pure & Appl. Chem. 48:449-455 (1976).

Martel, A. E. and Smith, R. M. Critical Stability Constants, Vol. 3: Other Organic Ligands. Plenum, NY (1976).

Martinez, E. and Zucker, G. L. Asbestos Ore Body Minerals Studied by Zeta Potential Measurements. Jour. Phys. Chem. 64:924-926 (1960).

McDonald, J. C. and Liddell, F. D. K. Mortality in Canadian Miners and Millers Exposed to Chrysotile. Ann. N.Y. Acad. Sci. 330:1-9 (1979).

McGee, K. A. and Hostetler, P. B. Studies in the System $MgO-SiO_2-CO_2-H_2O$ (IV): The Stability of $MgOH^+$ from 10° to 90^oC. Amer. Jour. Sci. 275:304-317 (1975).

McGuire, M. G.; Bowers, A. E. and Bowers, D. A. Asbestos Analysis Case History: Surface-Water Supplies in Southern California. J. AWWA 74:471-478 (1982).

McGuire, M. G.; Bowers, A. E. and Bowers, D. A. Optimization of Large-Scale Water-Treatment Planats for Asbestos Fiber Removals. J. AWWA 75:364-370 (1983).

Michaels, L. and Chissick, S. S. Asbestos: Properties, Applications and Hazards, Vol. I. Wiley-Interscience (1979).

Mihailovic, M. L. and Cekovic, Z. Oxidation and Reduction of Phenols. in The Chemistry of the Hydroxyl Group Part 1. S. Pati, ed. Interscience, London (1971).

Miller, L. G.; Sparrow, D. and Ginns, L. C. Asbestos Exposure Correlates with Alterations in Circulating T Cell Subsets. Clin. Exp. Immunol. 51:110-116 (1983).

Millette, J. R.; Clark, P. J. and Pansing, M. F. Exposure to Asbestos from Drinking Water in the United States. USEPA Rept. EPA-600/1-79-028. HERL, Exposure Eval. Branch, Cincinnati, OH (1979).

Millette, J. R.; Clark, P. J.; Pansing, M. F. and Twyman, J. D. Concentration and Size of Asbestos in Water Supplies. Envir. Health Perspectives. 34:13-25 (1980).

Moody, J. B. Serpentinization: A Review. Lithos 9:125 (1976).

Morel, F. M. M. Principles of Aquatic Chemistry. Wiley-Interscience, NY (1983).

Morel, F. M. M.; Westhall, J. C. and Yeasted, J. G. Adsorption Models: A Mathematical Analysis in the Framework of General Equilibrium Calculations. in Adsorption of Inorganics at Solid-Liquid Interfaces. M. A. Anderson and A. J. Rubin, eds. Ann Arbor Science, Ann Arbor, MI (1981).

Morgan, A. et al. The Biological Effects of Magnesium-Leached Chrysotile Asbestos. Br. Jour. Exp. Path. 58:465-473 (1977).

Morgan, A.; Lally, A. E. and Holmes, A. Some Observations on the Distribution of Trace Metals in Chrysotile Asbestos. Ann. Occup. Hyg. 16:231-240 (1973).

Mumpton, F. A. and Thompson, C. S. Mineralogy and Origin of the Coalinga Asbestos Deposit. Clays & Clay Minerals 23:131-143 (1975).

Musso, H. Phenolic Coupling. in Oxidative Coupling of Phenols. W. I. Taylor and A. R. Battersby, eds. Marcel Dekkor, NY (1967).

National Research Council, Safe Drinking Water Committee. Drinking Water and Health. National Academy of Sciences, Washington, D.C. (1977).

National Research Council, Safe Drinking Water Committee. Drinking Water and Health, v. 5 National Acad. Press, Washington, D.C. (1983).

Newhouse, M. L. and Berry, G. Patterns of Mortality in Asbestos Factory Workers in London. Ann. N.Y. Acad. Sci. 330:53-60 (1979).

Novak, I. J. Asbestos Dispersions and Method of Forming Same. U. S. Patent 2626213 (1953).

Novak, I. J. Asbestos Dispersions. U. S. Patent 2652325 (1953a).

O'Melia, C. R. Aquasols: The Behavior of Small Particles in Aquatic Systems. Envir. Sci. Technol. 14:1052-1060 (1980).

Olmsted, F. A. Pre-Cenozic Geology of the Southern Half of the Auburn 15-Minute Quadrangle, California. Bull. U.S. Geol. Surv. 1341 (1971).

Otouma, T. and Take, S. Adsorption of Anionic Surface Active Agents on Chrysotile Asbestos. Nippon Kagaku Kaishi (Japan) 10:1897-1902 (1974) in Chem. Abstracts 83:65953w (1975).

Parfitt, R. L.; Farmer, V. C. and Russell, J. D. Adsorption on Hydrous Oxides I. Oxalate and Benzoate on Geothite. Jour. Soil Sci. 28:29-39 (1977).

Parfitt, R. L; Fraser, A. R.; Russell, J. D. and Farmer, V. C. Adsorption on Hydrous Oxides II. Oxalate, Benzoate and Phosphate on Gibbsite. Jour. Soil Sci. 28:40-47 (1977a).

Parfitt, R. L.; Fraser, A. R. and Farmer, V. C. Adsorption on Hydrous Oxides III. Fulvic Acid and Humic Acid on Geothite, Gibbsite and Imogolite. Jour. Soil Sci. 28:289-296 (1977b).

Parks, G. A. Aqueous Surface Chemistry of Oxides and Complex Oxide Minerals. Isoelectronic Point and Zero Point of Charge. in Equilibrium Concepts in Natural Water Systems. R. F. Gould, ed. American Chemical Society, Washington, D.C. (1967).

Perdue, E. M. and Lytle, C. R. Distribution Model for Binding of Protons and Metal Ions by Humic Substances. Envir. Sci. Technol. 17:654-660 (1983).

Petrovíc, R. Rate Control in Feldspar Dissolution -- II. The Protective Effect of Precipitates. Geoch. Cosmoch. Acta 40:1509-1521 (1976).

Polissar, L.; Severson, R. K.; Boatman, E. S. & Thomas, D. B. Cancer Incidence in Drinking Water in the Puget Sound Area Region. Jour. Epidemiol. 116:314-328 (1982).

Pulfer, K.; Schindler, P. W.; Westhall, J. C. and Grauer, R. Kinetics and Mechanisms of Dissolution of Bayerite (γ-Al(OH)$_3$) in HNO$_3$-HF-Solution at 298.2 K. submitted to Jour. Coll. Interface Sci. (1984).

Pundsack, F. L. The Properties of Asbestos. I. The Colloidal and Surface Chemistry of Chrysotile. J. Phys. Chem. 59:892-895 (1955).

Pundsack, F. L. and Reimschussel, G. P. Composition Characterized by Uniformly Distributed Inorganic Additives. U. S. Patent 3304197 (1967).

Reimschussel, G. Association of Trace Metals with Chrysotile Asbestos. CIM Bulletin. 68:760:76-83 (1975).

Rice, S. J. Asbestos. in Mineral Commodities of California. Bull. Calif. Div. Min. 176:49-58 (1957).

Rickard, D. and Sjöberg, J. Mixed Kinetic Control of Calcite Dissolution Rates. Amer. Jour. Sci. 283:815-830 (1983).

Schindler, P. W. Surface Complexes at Oxide-Water Interfaces. in Adsorption of Inorganics at Solid-Liquid Interfaces. M. A. Anderson and A. J. Rubin, eds. Ann Arbor Sci., Ann Arbor, MI (1981).

Schnitzer, R. J. Modification of Biological Surface Activity of Particles. Envir. Heal. Perspectives 9:260-266 (1974).

Schott, J. and Berner, R. A. X-ray Photoelectron Studies of the Mechanism of Iron Silicate Dissolution During Weathering. Geoch. Cosmoch. Acta 47:2233-2240 (1983).

Schott, J.; Berner, R. A. and Sjöberg, E. L. Mechanisms of Pyroxene and Amphibole Weathering -- I. Experimental Studies of Iron-Free Minerals. Geoch. Cosmoch. Acta 45:2123-2135 (1981).

Selikoff, I. J.; Hammond, E. L. and Seidman, H. Mortality Experience of Insulation Workers in the United States and Canada, 1943-1976. Ann. N.Y. Acad. Sci. 330:91-116 (1979).

Sherwood, T. K.; Pigford, R. L. and Wilke, C. R. Mass Transfer. McGraw Hill, NY (1975).

Sigg, L. and Stumm, W. The Interaction of Anions and Weak Acids with the Hydrous Geothite (γ-FeOOH) Surface. Colloids and Surfaces. 2:101-117 (1981).

Sjöberg, E. L. and Rickard, D. The Influence of Experimental Design on the Rate of Calcite Dissolution. Geoch. Cosmoch. Acta 47:2281-2285 (1983).

Smith, R. W. and Trivedi, N. Variation of Point of Zero Charge of Oxide Minerals as a Function of Aging Time in Water. Trans. Soc. Mining Engr., AIME. 255:69-74 (1974).

Speil, S. and Leinweber, J. P. Asbestos Minerals in Modern Technology. Envir. Res. 2:166-208 (1969).

Springer, R. K. Contact Metamorphosed Ultramafic Rocks in the Western Sierra Nevada Foothills, California. J. Petrology. 15:160-195 (1974).

Spurney, K. R.; Stober, W.; Opiela, H. & Weiss, G. Size-Selective Preparation of Inorganic Fibers for Biological Experiments. Jour. Am. Ind. Hyg. Assn. 40:20-38 (1979).

Stone, A. T. The Reduction and Dissolution of Mn(III) and MN(IV) Oxides by Organics. W. M. Keck Envir. Eng. Sci. Report AC-1-83. California Institute of Technology, Pasadena, CA (1983).

Stumm, W. Chemical Interaction in Particle Separation. Envir. Sci. Technol. 11:1066-1069 (1977).

Stumm, W.; Furrer, G. and Kunz, B. The Role of Surface Coordination in Precipitation and Dissolution of Mineral Phases. 5th International Summer Conference on Solid/Liquid Interfaces, Cavat (1982); Croat. Chem. Acta 58:585. (1983).

Stumm, W.; Kummert, R. and Sigg, L. A Ligand Exchange Model for the Adsorption of Inorganic and Organic Ligands at Hydrous Oxide Interfaces. Croata Chemica Acta 52:291-312 (1980).

Stumm, W. and Morgan, J. J. Aquatic Chemistry. Wiley, New York (1981).

Thomassin, J. H.; Goni, J; Baillif, P.; Touray, J. C. and Jaurand, M. C.
    An XPS Study of the Dissolution Kinetics of Chrysotile in 0.1 N
    Oxalic Acid at Different Temperatures. Phys. Chem. Minerals.
    1:385-398 (1977).

Thomassin, J. H.; Touray, J. C.; Baillif, P.; Jaurand, M. C.; Magne, L.
    and Goni, J. Surface Interaction Between Chrysotile and Solutions
    (Dissolution and Adsorption): Systematic X-Ray Photoelectron
    Spectroscopy Studies. in Biol. Effects of Mineral Fibers. J. C.
    Wagner, ed. IARC Sci. Publ. 30, Lyon (1980).

Tipping, E. The Adsorption of Aquatic Humic Substances by Iron Oxides.
    Geoch. Cosmoch. Acta 45:191-199 (1981).

Tipping, E. Adsorption by Geothite (α-FeOOH) of Humic Substances from
    Three Different Lakes. Chemical Geol. 33:81-89 (1981a).

Tipping, E. and Cooke, D. The Effects of Adsorbed Humic Substances on
    the Surface Charge of Geothite (α-FeOOH) in Freshwaters. Geoch.
    Cosmoch. Acta 46:75-80 (1982).

Tipping, E. and Higgins, D. C. The Effect of Adsorbed Humic Substances
    on the Colloid Stability of Haematite Particles. Colloids &
    Surfaces. 5:85-92 (1982).

Toft, F.; Wigle, D.; Meranger, J. C. and Mao, Y. Asbestos and Drinking
    Water in Canada. Sci. of the Total Envir. 18:77-89 (1981).

Van Der Drift, W. P. J. T.; De Keizer, A. and Overbeek, J. T. G.
    Electrophoretic Mobility of a Cylinder with High Surface Charge
    Density. J. Coll. Interface. Sci. 71:67-78 (1979).

Valerio, F.; Puntoni, R. and Santi, L. Adsorption Properties of UICC
    Rhodesian Chrysotile and Crocidolite in Aqueous Solution -- Effects
    of Cation Depletion. Jour. Am. Indust. Hyg. Assn. 40:9:781-788
    (1979).

Valioulis, I: A. Particle Collisions and Coalescence in Fluids. W. M.
    Keck Lab. Hyd. & Wat. Res. Report KH-R-44, California Institute of
    Technology, Pasadena, CA (1983).

Valverde, N. and Wagner, C. Considerations on the Kinetics and the
    Mechanism of the Dissolution of Metal Oxides in Acidic Solutions.
    Ber. Bunsenges Phys. Chem. 80:330-333 (1976).

Vermilyea, D. A. The Dissolution of MgO and $Mg(OH)_2$ in Aqueous
    Solutions. J. Electrochem. Soc. 116:1179-1183 (1969).

Vuceta, J. Adsorption of Pb(II) and Cu(II) on α-Quartz from Aqueous Solutions: Influence of pH, Ionic Strength and Complexing Ligands. Ph.D. Thesis, California Institute of Technology, Pasadena, CA (1976).

Wadsworth, M. E. Reactions at Surfaces. in Physical Chemistry, an Advanced Treatise. H. Eyring, ed. Academic Press, NY (1975).

Walton, W. H. The Nature, Hazards and Assessment of Occupational Exposure to Airborne Asbestos Dust: A Review. Ann. Occup. Hyg. 25:117-247 (1982).

Whittaker, E. J. W. The Structure Chrysotile. II. Clino-Chrysotile. Acta Cryst. 9:855-862 (1956).

Wicks, F. J. Mineralogy, Chemistry and Crystallography of Chrysotile Asbestos. in Short Course in Mineralogical Techniques of Asbestos Determination. R. L. Ledoux, ed. Mineral. Assoc. Can. Short Course, Sect. 1, Part B, 4:35-78 (1979).

Wicks, F. J. Introduction: Serpentine Mineralogy, Petrology and Paragenesis Symposium. Canadian Mineralogist. 17:673-677 (1979a).

Wicks, F. J. and Whittaker, E. J. W. A Reappraisal of the Structures of the Serpentine Minerals. Canadian Minerologist 13:227-243 (1975).

Wiebelt, F. J. and Smith, C. M. A Reconnaissance of Asbestos Deposits in the Serpentine Belt of Northern California. U. S. Bur. Min. Info. Circu. 7860 (1959).

Wirth, G. S. and Gieskes, J. M. The Initial Kinetics of the Dissolution of Vitreous Silica in Aqueous Media. Jour. Coll. & Interface Sci. 68:492-500 (1979).

Wood, B. J. and Walther, J. V. Rates of Hydrothermal Reactions. Science. 222:413-415 (1983).

Yada, K. Microstructures of Chrysotile and Antigorite by High-Resolution Electron Microscopy. Canadian Mineralogist. 17:679-691 (1979).

Yada, K. Study of Microstructure of Chrysotile Asbestos by High Resolution Electron Microscopy. Acta Cryst. A27:659-664 (1971).

Yang, J. C. The Growth of Synthetic Chrysotile Fiber. Amer. Mineral. 46:748-752 (1961).

Yao, K; Habibian, M. T. and O'Melia, C. R. Water and Waste Water Filtration: Concepts and Applications. Envir. Sci. Technol. 5:1105-1112 (1971).

Yates, D. E.; James, R. O. and Healy, T. W.   Titanium
    Dioxide-Electrolyte Interface.   Part 1. - Gas Adsorption and Tritium
    Exchange Studies.   Jour. Chem. Soc. Faraday I.   76:1-8 (1980).

Young, J. R.   A Study of the Adsorption of Ni(II) onto an Amorphous
    Silica Surface by Chemical and NMR Methods.   Report AC-8-81,
    California Institute of Technology, Pasadena, CA (1981).

Zutić, V. and Stumm, W.   On the Role of Surface Complexation in
    Weathering Reactions; Dissolution Kinetics of Hydrous Alummina in
    the Presence of Organic Acids.   Developments in Sedimentology, v.
    35, Proc. Inter. Clay Conf. Elsevier, pp. 613-622 (1982).

APPENDIX II

SUMMARY OF EXPERIMENTS
AND SAMPLE CALCULATIONS

Tables in this appendix provide clarification for the results

presented in Chapter 4. Table II.1 lists conditions for other dis-

solution experiments. Tables II.2 - II.5 illustrate the calculation of

results from the set of dissolution data corresponding to Figure 4.1.

Table II.6 is data from one adsorption experiment. Tables II.7 - II.9

list conditions for the mobility experiments. Table II.10 gives the

values used to estimate coagulation efficiency in Section 4.3.

Table II.1. Parameters for Chrysotile Constant pH Dissolution Experiments.

Date	pH[a]	Electrolyte	Solids conc. g/ℓ	Duration hrs.	Ore[b]	Acid or Base[c]	Comments[d]
10-30-82	8	0.1 M KNO_3	10	22	V	0.01 M HNO_3	N_2 flowmeter problems
10-30-82	9	0.1 M KNO_3	10	22	V	0.01 M HNO_3	stirrer failure; excess acid added
11-4-82	8	0.1 M KNO_3	5	88	V	0.01 M HNO_3	autoburette & N_2 flowmeter problems
11-4-82	9	0.1 M KNO_3	5	88	V	0.01 M HNO_3	excess acid added; autoburette problems
11-13-82	10	0.1 M KNO_3	5	94	V	0.1 M KOH	--
11-13-82	11	0.1 M KNO_3	5	94	V	0.1 M KOH	--
11-19-82	8	0.1 M KNO_3	10	72	V	0.01 M HNO_3	--
11-19-82	9	0.1 M KNO_3	10	72	V	0.01 M HNO_3	--
11-24-82	10	0.1 M KNO_3	10	95	V	0.1 M KOH	--
11-24-82	11	0.1 M KNO_3	10	95	V	0.1 M KOH	--
12-6-82	8.5	0.1 M KNO_3	10	98	V	0.01 M HNO_3	--
12-6-82	9.5	0.1 M KNO_3	10	98	V	0.1 M KOH	0.01 M HNO_3, t $\geq$ 48
1-2-83	8.5	0.1 M Na_2SO_4	10	95	V	0.1 M HNO_3	--
1-2-83	9.5	0.1 M Na_2SO_4	10	95	V	0.1 M KOH	0.01 M HNO_3, t $\geq$ 48
1-16-83	8	0.1 M NaCl	10	120	V	0.01 M HNO_3	--
1-16-83	8.5	0.1 M NaCl	10	120	V	0.01 M HNO_3	--
1-22-83	8.5A	0.1 M NaCl	10	120	VI	0.01 M HNO_3	AA problems
1-22-83	9	0.1 M NaCl	10	120	VI	0.01 M HNO_3	AA problems
1-30-83	7.5	0.1 M NaCl	10	120	VI	0.1 M HNO_3	0.01 M HNO_3, t $\geq$ 24
1-30-83	9.5	0.1 M NaCl	10	120	VI	0.01 M HNO_3	0.1 M NaOH also
2-6-83	7.5	0.1 M KNO_3	10	120	VI	0.1 M HNO_3	0.01 M HNO_3, t $\geq$ 24
2-6-83	9A	0.1 M KNO_3	10	120	VI	0.01 M HNO_3	--
2-13-83	7.93	$NaNO_3$	10	120	VI	0.2 M HNO_3	350 ppm CO_2 atm.
2-13-83	8.27	$NaNO_3$	10	120	VI	0.2 M HNO_3	350 ppm CO_2 atm.
2-21-83	9.35	$NaNO_3$	10	120	VI	0.02 M HNO_3	350 ppm CO_2 atm.
2-21-83	9.2	$NaNO_3$	10	120	VI	0.02 M HNO_3	350 ppm CO_2 atm.
2-28-83	9.1	$NaNO_3$	7.5	120	VI	0.1 M HNO_3	350 ppm CO_2 atm.
2-28-83	8.15	$NaNO_3$	7.5	120	VI	0.1 M HNO_3	350 ppm CO_2 atm.
3-7-83	8	0.01 M KNO_3	10	120	VII	0.01 M HNO_3	AA problems
3-7-83	8	0.05 M Na_2SO_4	10	120	VII	0.01 M HNO_3	AA problems

174

Table II.1. (Continued)   -2-

Date	pH[a]	Electrolyte	Solids conc. g/ℓ	Duration hrs.	Ore[b]	Acid or Base[c]	Comments
3-13-83	8.5	0.005 M Na$_2$SO$_4$	10	120	VII	0.01 M HNO$_3$	AA problems
3-13-84	8.5	0.05 M Na$_2$SO$_4$	10	120	VII	0.01 M HNO$_3$	AA problems
4-2-83	8A	0.1 M KNO$_3$	10	120	VII	0.02 M HNO$_3$	--
4-2-83	8.5A	0.1 M KNO$_3$	10	120	VII	0.02 M HNO$_3$	--
4-10-83	8A	0.1 M NaCl	10	120	VII	0.01 M HNO$_3$	--
4-10-83	8	0.005 M Na$_2$SO$_4$	10	120	VII	0.01 M HNO$_3$	--
6-16-83	8B	0.1 M NaCl	10	120	VIII	0.02 M HCl	--
6-16-83	8C	0.1 M NaCl	10	120	VIII	0.02 M HCl	--
6-30-83	7	0.1 M NaCl	10	120	VIII	0.1 M HCl	--
6-30-83	7	0.1 M KNO$_3$	10	120	VIII	0.1 M HNO$_3$	--
7-18-83	8	0.1 M NaCl	10	120	VIII	0.02 M HCl	0.0001 M catechol
7-18-83	8	0.1 M NaCl	10	120	VIII	0.02 M HCl	0.001 M catechol
7-24-83	8	0.1 M NaCl	10	120	VIII	0.02 M HCl	0.01 M catechol; 0.05 M NaOH
7-24-83	8.5	0.1 M NaCl	10	120	VIII	0.02 M HCl	0.01 M catechol; 0.05 M NaOH
7-30-83	7.5	0.1 M NaCl	10	120	VIII	0.02 M HCl	0.001 M catechol
7-30-83	7.5	0.1 M NaCl	10	120	VIII	0.02 M HCl	0.01 M catechol; 0.01 M NaOH
8-5-83	8	0.1 M NaCl	10	120	IX	0.02 M HCl	0.001 M oxalate
8-5-83	8	0.1 M NaCl	10	120	IX	0.02 M HCl	0.01 M oxalate
8-11-83	8.5	0.1 M NaCl	10	120	IX	0.02 M HCl	0.001 M oxalate
8-11-83	8.5	0.1 M NaCl	10	120	IX	0.02 M HCl	0.01 M oxalate
8-17-83	7.5	0.1 M NaCl	10	120	IX	0.02 M HCl	0.001 M oxalate
8-17-83	7.5	0.1 M NaCl	10	120	IX	0.02 M HCl	0.01 M oxalate

[a]Subsequent experiments done at same conditions as a previous experiment are noted by a letter: A, B, C, etc.

[b]Batches of 20-30 grams were prepared as needed for these experiments; small variations between batches were apparent.

[c]Used to maintain constant pH; if both acid and base were needed, the second is noted under comments.

[d]N$_2$ atmosphere used unless otherwise noted; last 12 experiments were done with organics present as noted.

Table II.2. Typical data for chrysotile dissolution; experiment pH 8A, 0.1 M NaCl.

Time,[a] hr	Acid added,[a] ml	Volume,[a] L	pH[b]	Solids conc.,[c] g/L	Concentration, μmol/L				
					Mg_T[d]	Si_T[e]	OH[f]	C_A-C_B[a]	Q[g]
0	0	.2000	8.306	10.000	0	0	2.609	0	
3.667	15.4	.2074	8.003	9.285	287.34	23.34	1.296	715.0	141.9
12.830	23.1	.2071	7.981	8.953	371.50	40.53	1.232	1047.0	306.2
24.250	27.0	.2030	7.982	8.787	404.60	56.28	1.237	1213.0	405.8
36.500	30.0	.1980	8.018	8.659	427.50	67.37	1.342	1341.0	488.3
46.670	31.8	.1918	8.018	8.581	450.40	73.82	1.342	1419.0	520.6
60.500	33.7	.1857	7.998	8.497	491.10	92.79	1.281	1503.0	523.7
72.500	34.6	.1786	8.021	8.456	483.00	103.50	1.353	1544.0	581.1
83.000	35.4	.1714	7.994	8.418	552.30	116.10	1.271	1582.0	480.3
97.830	36.3	.1643	7.943	8.374	537.00	120.40	1.131	1626.0	554.8
107.100	36.8	.1568	8.003	8.349	544.60	132.50	1.296	1651.0	565.4
120.000	37.1	.1491	7.992	8.333	582.80	139.30	1.266	1667.0	505.1

[a]From Table II.4.

[b]Calculated from Table III.5 data: pH = a + mv/b; where a $\simeq$ 7.0 and b $\simeq$ 59 mv; actual values used were determined by calibration with standard pH buffers.

[c]Calculated from: (prev. conc. x prev. vol.)/(curr. vol. + sample vol.).

[d]From atomic absorption results.

[e]From spectrophotometric results.

[f]Calculated by $[OH^-]$ = exp(2.303 x (pH - 14 + 0.1101)) where 0.1101 is the activity coefficient for OH^- for I = 0.1 M, calculated by the Davies eqn. and 14 is pK_w.

[g]Surface charge: $Q = C_A-C_B - 2[Mg^{2+}]-[MgOH^+]+[H_3SiO_4^-]+[OH^-]$; where $[Mg^{2+}]$ = 0.9997 Mg_T, $[MgOH_2^+]$ = $Mg_T - [Mg^{2+}]$, and $[H_3SiO_4]$ = 0.0175 Si_T; the speciation coefficient for Mg^{2+} is calculated using p^*K_1 = 11.2; the speciation coefficient for $H_3SiO_4^-$ is calculated using p^*K_1 = 9.86; both coefficients are pH dependent.

Table II.3. Typical results for chrysotile dissolution;
experiment pH 8A, 0.1 M NaCl.

Time,[a] hr	Concentration, 10^{-9} mol/cm^2 [b]				$pK_{a1}{}^s$ (c)
	Mg_T	Si_T	C_A-C_B	Q	
0					
3.666	.0638	.0052	.1588	.0315	
12.83	.0856	.0093	.2412	.0705	
24.25	.0949	.0132	.2846	.0952	
36.50	.1018	.0160	.3193	.1163	
46.67	.1082	.0177	.3409	.1251	
60.50	.1192	.0225	.3647	.1271	
72.50	.1178	.0252	.3765	.1417	7.259
83.00	.1353	.0284	.3874	.1176	7.237
97.83	.1322	.0296	.4002	.1366	7.271
107.10	.1345	.0327	.4077	.1396	7.275
120.00	.1442	.0345	.4125	.1250	7.261

[a] From Table II.2.

[b] Calculated from Table II.2 quantities by: (soln. conc./solids cons.)/ S_A; where S_A is the specific surface area of chrysotile in these experiments, 485,000 cm^2/g.

[c] Apparent equilibrium constant, of the form of eqn. 2.1; calculated by: $\log(Q_D)-\log(S_M-Q_D)$ + pH - 0.1101; where S_M is the number of magnesium-type sites, given by Q-[>SiO$^-$], where >Si-O$^-$ is defined by eqns. 2.3, 2.5, 2.8, and 2.9. The quantity 0.1101 is the activity coefficient for H$^+$. For Q<0, $pK_{a2}{}^s$ is calculated similarly.

Table II.4 Typical data for chrysotile dissolution;
experiment pH 8A, 0.1 M NaCl.

Time hour	Acid added,[a] ml	Sample withdrawn, L	Volume,[b] L	$C_A - C_B$ [c] μmol/L
0	0	0	.2000	0
1.000	8.3	0	.2083	398.46
2.500	12.9	0	.2129	605.92
3.666	15.4	.008	.2074	714.95
5.000	17.2	.008	.2092	794.84
7.000	19.3	.008	.2113	886.32
10.000	21.5	.008	.2135	980.24
12.833	23.1	.016	.2071	1047.30
16.000	24.4	.016	.2084	1103.20
20.000	25.8	.016	.2098	1162.50
24.250	27.0	.024	.2030	1212.80
30.000	28.7	.024	.2047	1285.80
36.500	30.0	.032	.1980	1340.80
42.000	31.1	.032	.1991	1388.60
46.666	31.8	.040	.1918	1418.80
54.000	33.0	.040	.1930	1472.10
60.500	33.7	.048	.1857	1503.00
66.000	34.1	.048	.1861	1521.20
72.500	34.6	.056	.1786	1543.90
78.000	35.0	.056	.1790	1562.80
83.000	35.4	.064	.1714	1581.60
90.000	35.8	.064	.1718	1601.20
97.833	36.3	.072	.1643	1625.60
102.000	36.4	.072	.1644	1630.70
107.170	36.8	.080	.1568	1651.00
114.000	36.9	.080	.1569	1656.30
120.000	37.1	.088	.1491	1667.00

[a] Volume of acid or base added, calculated from Table II.5.

[b] Volume of suspension, calculated from (prev. vol. + vol. acid added - vol. sample withdrawn).

[c] Calculated by: (prev. vol. x prev. $C_A C_B$ + (amt. added since prev. x molarity))/(cur. vol.).

Table II.5 Typical autoburette use and pH record;
experiment pH 8A, 0.1 M NaCl.

```
2 04/12/83 15:30:00    1475    -68.9             1767    -33.3
2 04/12/83 15:36:32    ABU11 #1        333
2 04/12/83 15:40:00    1503    -64.6             1775    -31.9
2 04/12/83 15:50:00    1490    -66.6             1761    -34.3
2 04/12/83 15:55:55    ABU11 #2        358
2 04/12/83 16:00:00    1480    -68.1             1799    -27.9
2 04/12/83 16:10:00    1477    -68.5             1784    -30.4
2 04/12/83 16:20:00    1473    -69.1             1787    -29.9
2 04/12/83 16:30:00    1472    -69.4             1791    -29.3
2 04/12/83 16:36:55    ABU11 #1        334
2 04/12/83 16:40:00    1504    -64.5             1773    -31.4
2 04/12/83 16:50:00    1494    -66        1784    -30.4
2 04/12/83 17:00:00    1487    -67        1775    -31.9
2 04/12/83 17:10:00    1483    -67.6             1777    -31.7
2 04/12/83 17:20:00    1479    -68.5             1767    -33.3
2 04/12/83 17:30:00    1474    -69        1773    -32.3
2 04/12/83 17:40:00    1474    -69        1762    -34.1
2 04/12/83 17:48:06    ABU11 #1        335
2 04/12/83 17:50:00    1500    -65.1             1770    -32.8
2 04/12/83 18:00:00    1491    -66.5             1759    -34.6
2 04/12/83 18:10:00    1486    -67.2             1766    -33.5
2 04/12/83 18:20:00    1480    -68.1             1773    -32.3
2 04/12/83 18:30:00    1475    -68.9             1761    -34.3
2 04/12/83 18:40:00    1472    -69.4             1767    -33.3
2 04/12/83 18:49:38    ABU11 #1        336
2 04/12/83 18:50:00    1489    -66.7             1759    -34.6
2 04/12/83 19:00:00    1496    -65.7             1762    -34.1
2 04/12/83 19:05:47    ABU11 #2        359
2 04/12/83 19:10:00    1489    -66.7             1803    -27.3
2 04/12/83 19:20:00    1484    -67.5             1787    -29.9
2 04/12/83 19:30:00    1478    -68.5             1787    -29.9
2 04/12/83 19:40:00    1475    -68.9             1778    -31.4
2 04/12/83 19:50:00    1472    -69.4             1783    -30.7
2 04/12/83 19:55:20    ABU11 #1        337
2 04/12/83 20:00:00    1504    -64.5             1773    -32.3
2 04/12/83 20:10:00    1496    -65.7             1779    -31.3
2 04/12/83 20:20:00    1487    -67        1767    -33.3
2 04/12/83 20:30:00    1479    -68.2             1773    -32.3
2 04/12/83 20:40:00    1475    -68.9             1767    -33.3
2 04/12/83 20:50:00    1474    -69        1773    -32.3
2 04/12/83 21:00:00    1468    -70        1766    -33.5
2 04/12/83 21:00:02    ABU11 #1        338  ←─────┐
2 04/12/83 21:10:00    1499    -65.2             1772    -32.5
2 04/12/83 21:20:00    1488    -67        1763    -34
2 04/12/83 21:30:00    1480    -68.1             1771    -32.5
```

| day | date | time | AI13 & mv signal for #1 | | AI13 & mv signal for #2 | |

which autoburette and
number of consecutive
additions

Table II.6 Typical data for catechol adsorption onto chrysotile; pH 8,
0.01 M NaCl, 1.021 g/L chrysotile, room temperature and atm.

Concentration, mmol/L		Catechol Adsorbed[a]	
catechol added	catechol remaining	10^{-9} mol/cm^2	10^{-6} mg C/cm^2
Sample at 0.6 hrs.			
0.408	0.389	0.038	2.8
0.715	0.703	0.028	2.0
1.021	1.000	0.064	4.6
1.327	1.272	0.115	8.3
1.634	1.522	0.218	15.7
Sample at 6.4 hrs.			
0.408	0.353	0.111	8.0
0.715	0.633	0.166	11.9
1.021	0.912	0.220	15.8
1.327	1.179	0.299	21.5
1.634	1.433	0.406	29.2
Sample at 15.4 hrs.			
0.408	0.293	0.232	16.7
0.715	0.556	0.321	23.2
1.021	0.819	0.408	29.3
1.327	1.107	0.444	32.0
1.634	1.343	0.588	42.3
Sample at 21.7 hrs.			
0.408	0.297	0.224	16.2
0.715	0.551	0.331	23.9
1.021	0.795	0.456	32.8
1.327	1.083	0.493	35.5
1.634	1.351	0.572	41.1

[a]Calculated using S_A = 485000 cm^2/g for chrysotile.

Table II.7 Chrysotile mobility experiments reported

Date	pH	Conditions			Prior to organic addition		After organic addition		Organic lowering, $10^{-9}/cm^2$
		atm[a]	elec[b]	org[c]	Mobility, $\mu m \cdot s^{-1} V \cdot cm^{-1}$	Duration hours	Mobility, $\mu m \cdot s^{-1} V \cdot cm^{-1}$	Duration hours	
5-16-83	5.0	N	K	-	+3.1	25	-	-	-
5-18-83	6.0	N	K	P	+3	24	+2	24	0.006
5-20-83	7.5	N	K	P	+2.1	41	0	21	13
5-23-83	8.0	N	K	P	+3 → 0	46	-0.5 → -2	7	ND
5-26-83	7.5	N	K	P	+2	32	-0.5	19	ND
5-28-83	8.5	N	K	-	+3.0 → +0.5	46	-	-	-
9-21-83	8.0	N	N	C	0	19	-2.1	72	2
9-28-83	8.2	C	N	C	-1	21	-2	76	2
10-2-83	8.0	C	N	C	+2	22	-1.3	75	2
10-7-83	7.5	C	N	C	+3	23	$\geq$ -0.9	77	2
10-13-83	8.0	C	N	C	+1.5 → -1	190	-1.4	50	2

[a] N = N_2 atm ; C = 350 ppm CO_2 in N_2.

[b] K = 0.01 M KNO_3; N = 0.01 M NaCl media.

[c] P = phthalate; C = catechol.

Table II.8   Chrysotile mobility experiments using aged stock suspension.

Date	pH	Cond.[a]	Prior to organics addition		After organics addition		Organic loading	
			Mobility $\mu m \cdot s^{-1} V \cdot cm^{-1}$	Duration, hours[b]	Mobility, $\mu m \cdot s^{-1} V \cdot cm^{-1}$	Duration hours	10^{-9} mol/cm^2	10^{-6} mgC/cm^2
11-11-83[c]	8.0	-	+2 → -1	820	-	-	-	-
11-15-83	8.0	C	+1.2	145	-1.1	53	2	144
11-20-83	8.0	C	+1.1	216	-0.6	52	0.2	14
11-22-83	8.0	C	-	-	-1.1	39	2	140
11-25-83	8.0	C	-0.1	336	-1.9	52	20	1400
11-25-83	8.0	C	-0.1	336	-2.2	52	200	14000
11-28-83	8.0	O	0.0	415	-0.7	42	20	480
11-28-83	8.0	O	0.0	415	-0.9	42	200	4800
12-01-83	8.0	O	-	483	-0.6	19	2	48
12-01-83	8.0	O	-	483	-0.8	19	0.2	4.8
12-04-83	7.5	C	-0.5	557	-1.8	68	20	1400
12-04-83	7.5	C	-0.5	557	-2.1	68	200	14000
12-10-83	8.5	C	-1.1	698	-2.2	58	20	1400
12-10-83	8.5	C	-1.1	698	-2.4	58	200	14000
12-13-83	8.0	NOM	-1.0	771	-1.7	31	-	180
12-13-83	8.0	NOM	-1.0	771	-2.0	31	-	1800
12-15-83	8.0	NOM	-1.0	820	-	46	-	18

[a]0.01 M NaCl, 350 ppm CI_2 in N_2 atm. for all experiments; organics: C = catechol, O = oxalate, NOM = natural organic matter.

[b]Duration stock aged before adding organics to this aliquot.

[c]Stock suspension; for plot of mobility, see Fig. 4.21.

Table II.9 Alox mobility experiments reported.

Date	pH	Cond.[a]	Mobility prior to organics addition, $\mu m \cdot s^{-1} V \cdot cm^{-1}$	After organics addition		Organic loading	
				Mobility $\mu m \cdot s^{-1} V \cdot cm^{-1}$	Duration hours	$10^{-9} mol/cm^2$	$10^{-6} mg/cm^2$
2-29-84	7.0	C	+0.8	+0.5	70	25	180
2-29-84	8.0	C	+0.4	+0.2	70	25	180
3-05-84	8.0	C	-0.2	-1.0	26	25	1800
3-05-84	9.0	C	-0.4	-0.9	26	2.5	180
3-07-84	8.0	NOM	+0.6	-0.7	22	-	1800
3-07-84	8.0	NOM	+0.5	-0.6	22	-	180
3-11-84	8.0	C	+0.5	-0.4	39	14	1000
3-11-84	8.0	C	+0.5	-0.8	39	140	10000

[a] 0.01 M NaCl, 350 ppm CO_2 in N_2 atm for all experiments; organics: C = catechol, NOM = natural organic matter.

Table II.10. Coagulation Rate Constant for Chrysotile-Silica Suspension

d_i (a) μm	cum. fraction[a]	n_i 10^6 L^{-1}	k_1 (b) $10^{-1} L \cdot s^{-1}$	$k_i n_i$ $10^{-6} s^{-1}$
1.1	0.34	12.2	0.00	0.00
2.3	0.59	9.0	0.02	0.18
3.7	0.77	6.5	0.13	0.85
5.2	0.91	5.0	0.50	2.50
6.7	0.94	1.1	1.38	1.52
8.2	0.98	1.4	3.09	4.33
9.7	0.99	0.4	6.06	2.42
10.2	1.00	0.4	7.41	2.96
Total	-	36	-	14.76

[a]From Figure 3.4.

[b]From eqn. (2.30).

APPENDIX III

EXPERIMENTAL DATA

Tables III.1 - III.28 give data from the dissolution experiments carried out in NaCl or KNO_3 electrolyte that were used in the results and interpretation of Chapter 4. Data for experiments in $NaHCO_3$ and H_2SO_4 are available upon request. Figure III.1 - III.23 are mobility results for the chrysotile and alox experiments.

TABLE III.1.   PH 7, 0.1 M NACL

TIME HR.	ACID ADDED ML	VOL. L	PH	SOLIDS CONC. G/L	MG-T	SI-T	(OH-)	CA-CB	Q
0	0	.2	7	10	0	0		0	
3.667	7	.199	7	9.662	493	27.13	.1289	1643.	656.6
12.5	14	.198	7	9.334	864.1	52.69	.1289	2266.	538.2
23.5	17.2	.1932	7	9.185	768.4	83.88	.1289	2548.	1012.
36.5	19.8	.1878	7	9.063	902.4	120.4	.1289	2780.	975.4
49.67	23	.183	7	8.911	976.4	147.4	.1289	2901.	948.4
62.17	26	.178	7	8.768	1027.	176.9	.1289	3016.	962.3
69.17	27.3	.1713	7	8.704	1088.	190.6	.1289	3066.	890.1
84.83	30.2	.1662	7	8.559	1162.	222.0	.1289	3182.	857.3
99.67	32.7	.1607	7	8.432	1197.	253.5	.1289	3283.	888.4
108.7	33.8	.1538	7	8.375	1207.	262.2	.1289	3328.	914.2
117.8	35	.147	7	8.310	1301.	280.6	.1289	3380	778.5

TABLE III.1A.   PH 7, 0.1 M NACL

TIME HR.	ACID ADDED ML	SAMPLE WITHDR L	VOLUME L	CA-CB UMOL/L
0	0		.2	0
1.6667	2.5		.2025	1234.6
3.6667	7	.008	.199	1642.5
6	10	.008	.202	1915.1
8	11.6	.008	.2036	2057.3
10	12.8	.008	.2048	2162.4
12.5	14	.016	.198	2266.3
16	15.3	.016	.1993	2382.0
20	16.3	.016	.2003	2469.9
23.5	17.2	.024	.1932	2548.4
30	18.7	.024	.1947	2682.8
36.5	19.8	.032	.1878	2780.1
38.733	20.2	.032	.1882	2795.4
42	21	.032	.189	2825.9
49.667	23	.04	.183	2901.1
56	24.6	.04	.1846	2962.6
62.167	26	.048	.178	3015.6
69.167	27.3	.056	.1713	3066.2
76	28.6	.056	.1726	3118.4
84.833	30.2	.064	.1662	3181.6
92	31.4	.064	.1674	3230.5
99.667	32.7	.072	.1607	3282.7
108.67	33.8	.08	.1538	3328.3
117.83	35	.088	.147	3380.0

TABLE III.2. PH 7.5, 0.1 M NACL

TIME HR.	ACID ADDED ML	VOL. L	PH	SOLIDS CONC. G/L	MG-T	SI-T	(OH-)	CA-CB	Q
0	0	.2	6.143	10	0	0	.0179	.72	
3.42	3.1	.1931	7.526	9.847	441.3	27.15	.4324	1527.	644.7
11.25	4.7	.1847	6.765	9.766	640.4	48.67	.0750	2286.	1006.
24.15	5.1	.1751	7.452	9.745	764.8	79.85	.3650	2497.	968.2
49	8.3	.161	7.507	9.979	850.7	142.0	.4142	2632.	931.5
72.58	11	.1534	7.406	9.832	907.3	189.2	.3285	2749.	935.0
96.58	13.4	.1453	7.487	9.712	961.6	227.1	.3951	2855.	933.2
119.4	15.3	.1586	7.444	8.370	974.8	257.4	.3582	2943.	994.3

TABLE III.2A. PH 7.5, 0.1 M NACL

TIME HR.	ACID ADDED ML	SAMPLE WITHDR L	VOLUME L	CA-CB UMOL/L
0	0		.2	.72
1	1.93		.20193	956.49
2	2.6		.2026	1284.0
3.42	3.1	.01	.1931	1527.1
4.5	3.43	.01	.19343	1695.0
6	3.7	.01	.1937	1832.1
8.5	4	.01	.194	1983.9
11.25	4.6	.02	.1846	2286.1
16	4.7	.02	.1847	2339.0
20	4.9	.02	.1849	2444.6
24.15	5	.03	.175	2497.4
30	5.6	.03	.1756	2523.0
36	6.4	.03	.1764	2556.9
42	7.2	.03	.1772	2590.5
49	8.2	.04	.1682	2632.1
54	8.8	.04	.1688	2658.3
60	9.5	.04	.1695	2688.6
66	10.2	.04	.1702	2718.7
72.58	10.9	.05	.1609	2748.5
78	11.5	.05	.1615	2775.4
84	12.2	.05	.1622	2806.6
90	12.7	.05	.1627	2828.7
96.58	13.3	.06	.1533	2855.1
102	13.8	.06	.1538	2878.3
108	14.2	.06	.1542	2896.8
114	14.7	.06	.1547	2919.7
119.42	15.2	.07	.1452	2942.5

TABLE III.3.   PH 8B, 0.1 M NACL

TIME HR.	ACID ADDED ML	VOL. L	PH	SOLIDS CONC. G/L	CONCENTRATION, UMOL/L MG-T	SI-T	(OH-)	CA-CB	Q
0	0	.2	7.999	10	0	0		0	
2.167	5.3	.1973	8.019	9.742	267.7	14.18	1.346	516.3	-17.5
9	8.2	.1842	7.935	10.00	376.3	35.54	1.109	798.6	47.68
22.33	10.3	.1783	8.024	9.888	469.4	60.44	1.361	1015	78.62
31.83	11.4	.1714	7.999	9.827	505.9	76.36	1.284	1131.	122.2
45.83	12.8	.1648	8.027	9.747	579.2	97.95	1.372	1284.	129.0
57.83	13.5	.1575	7.985	9.706	615.9	110.3	1.245	1363.	134.8
70.33	14.2	.1502	8.019	9.663	669.2	132.7	1.346	1446.	111.2
77.67	14.6	.1426	8.029	9.638	659.1	134.8	1.377	1495.	180.7
93.5	15.4	.1354	7.962	9.584	687.5	150.3	1.180	1598.	227.2
105.7	16.2	.1282	8.02	9.527	769.2	176.4	1.349	1707.	172.5
117.7	16.9	.1209	7.894	9.476	735.2	180.6	1.010	1806.	339.6

TABLE III.3A. PH 8B, 0.1 M NACL

TIME HR.	ACID ADDED ML	SAMPLE WITHDR L	VOLUME L	CA-CB UMOL/L
0	0		.2	0
1	4.1		.2041	401.76
2.1667	5.3	.008	.1973	516.32
4	6.4	.008	.1984	624.34
6	7.2	.008	.1992	702.16
8	7.9	.008	.1999	769.73
9	8.2	.024	.1842	798.55
12	8.8	.024	.1848	860.89
16	9.5	.024	.1855	933.11
20	10.1	.024	.1861	994.59
22.333	10.3	.032	.1783	1015.0
24	10.5	.032	.1785	1036.3
31.833	11.4	.04	.1714	1131.4
36	11.9	.04	.1719	1186.3
42	12.5	.04	.1725	1251.7
45.833	12.8	.048	.1648	1284.3
54	13.3	.048	.1653	1340.9
57.833	13.5	.056	.1575	1363.4
66	14	.056	.158	1422.4
70.333	14.2	.064	.1502	1445.9
77.667	14.6	.072	.1426	1495.2
84	14.9	.072	.1429	1534.0
93.5	15.4	.08	.1354	1598.4
102	16	.08	.136	1679.6
105.67	16.2	.088	.1282	1706.5
114	16.6	.088	.1286	1763.4
117.67	16.9	.096	.1209	1805.8

TABLE III.4. PH 8C, 0.1 M NACL

TIME HR.	ACID ADDED ML	VOL. L	PH	SOLIDS CONC. G/L	MG-T	SI-T	(OH-)	CA-CB	Q
0	0	.2	8.019	10	0	0		0	
2.167	6.1	.1981	7.982	9.704	266.8	11.6	1.235	592.0	59.79
9	9.5	.1855	7.982	9.935	366.3	17.72	1.235	919.4	188.4
22.33	11.9	.1799	8.027	9.808	431.1	26.81	1.372	1163.	302.7
31.83	13.5	.1735	7.915	9.721	476.7	30.64	1.060	1329.	377.4
45.83	15.3	.1673	7.943	9.622	524.2	40.13	1.129	1521.	474.3
57.83	16	.16	8.027	9.581	552.6	52.18	1.372	1598.	495.0
70.33	16.7	.1527	8.007	9.540	573.7	60.44	1.309	1678.	533.1
77.67	16.9	.1449	8.026	9.527	590.2	65.26	1.367	1702	524.1
93.5	17	.137	8.019	9.521	618.7	76.62	1.346	1715.	479.9
105.7	17.9	.1299	7.832	9.459	679.3	88.66	.8756	1834	477.8
117.7	18.3	.1223	7.973	9.429	656.3	92.79	1.211	1890.	580.0

TABLE III.4A. PH 8C, 0.1 M NACL

TIME HR.	ACID ADDED ML	SAMPLE WITHDR L	VOLUME L	CA-CB UMOL/L
0	0		.2	0
1	4.6		.2046	449.66
2.1667	6.1	.008	.1981	591.95
4	7.5	.008	.1995	728.14
6	8.5	.008	.2005	824.26
8	9.2	.008	.2012	890.98
9	9.5	.024	.1855	919.43
12	10.3	.024	.1863	1001.4
16	11.1	.024	.1871	1082.6
20	11.7	.024	.1877	1143.1
22.333	11.9	.032	.1799	1163.1
24	12.2	.032	.1802	1194.5
31.833	13.5	.04	.1735	1329.2
36	14.1	.04	.1741	1393.5
42	14.9	.04	.1749	1478.6
45.833	15.3	.048	.1673	1520.9
54	15.9	.048	.1679	1586.9
57.833	16	.056	.16	1597.9
66	16.5	.056	.1605	1655.2
70.333	16.7	.064	.1527	1678.1
77.667	16.9	.072	.1449	1702.0
84	16.9	.072	.1449	1702.0
93.5	17	.08	.137	1714.6
102	17.6	.08	.1376	1794.4
105.67	17.9	.088	.1299	1834.0
114	18.2	.088	.1302	1875.8
117.67	18.3	.096	.1223	1889.8

TABLE III.5.   PH 8.5A, 0.1 M NACL

TIME HR.	ACID ADDED ML	VOL. L	PH	SOLIDS CONC. G/L	MG-T	SI-T	(OH-)	CA-CB	Q
0	0	.2	8.682	10	0	0	6.197	-.002	
3	9.5	.1995	8.531	9.547	271.9	16.09	4.373	453.5	-85.1
10.25	14.5	.1945	8.505	9.313	333.4	29.48	4.124	686.9	25.77
24	19	.189	8.512	9.103	387.2	44.65	4.189	897.5	129.6
48	23.1	.1831	8.519	8.909	464	77.38	4.255	1091.	171.1
74.5	25.4	.1754	8.522	8.799	510.1	105.0	4.288	1201.	191.0
96	27.2	.1672	8.495	8.709	533.2	130.2	4.027	1291.	235.2
120	28.6	.1586	8.481	8.637	571.6	153.9	3.903	1363.	231.9

The heading for the concentration columns is: CONCENTRATION, UMOL/L

TABLE III.5A. PH 8.5A, 0.1 M NACL

TIME HRS.	ACID ADDED ML	SAMPLE WITHDR L	VOLUME L	CA-CB UMOL/L
0	0		.2	-.002
1.5	7.3		.2073	352.14
3	9.5	.01	.1995	453.46
6	12.2	.01	.2022	580.93
9	13.9	.01	.2039	659.47
10.25	14.5	.02	.1945	686.87
12	15.2	.02	.1952	720.27
15	16.3	.02	.1963	772.27
18	17.3	.02	.1973	819.04
24	19	.03	.189	897.47
30	20.4	.03	.1904	964.40
36	21.5	.03	.1915	1016.3
42	22.4	.03	.1924	1058.3
48	23.1	.04	.1831	1090.7
54	23.7	.04	.1837	1119.8
60	24	.04	.184	1134.3
66	24.5	.04	.1845	1158.3
74.5	25.4	.05	.1754	1201.3
78	25.8	.05	.1758	1221.3
84	26.2	.05	.1762	1241.2
90	26.6	.05	.1766	1261.1
96	27.2	.06	.1672	1290.6
102	27.5	.06	.1675	1306.2
108	27.7	.06	.1677	1316.6
114	28.1	.06	.1681	1337.3
120	28.6	.07	.1586	1363.0
124	28.9	.07	.1589	1379.3

TABLE III.6.   PH 9, 0.1 M NACL

| | ACID | VOL. | | SOLIDS CONC. | CONCENTRATION, UMOL/L | | | | |
| TIME | ADDED | | | | | | | | |
HR.	ML	L	PH	G/L	MG-T	SI-T	(OH-)	CA-CB	Q
0	0	.2	8.296	10	0	0	2.549	-.002	
3	5	.195	9.026	9.756	245	19.59	13.68	243.9	-229.
10.25	8.5	.1885	9.026	9.584	298.8	44.13	13.68	415.9	-161.
24	11.7	.1817	9.028	9.424	356.4	83.85	13.74	575.9	-110.
48	16.1	.1761	9.016	9.201	479.4	149.2	13.37	798.7	-124.
74.5	18.9	.1689	9.026	9.057	502.4	215.5	13.68	942.7	-15.8
96	20.7	.1607	9.018	8.962	563.9	262.5	13.42	1038.	-36.5
120	22.7	.1527	9.024	8.852	610	311.4	13.63	1148.	-11.0

TABLE III.6A.   PH 9, 0.1 M NACL

| TIME | ACID ADDED | SAMPLE WITHDR | VOLUME | CA-CB |
HR.	ML	L	L	UMOL/L
0	0		.2	-.002
1.5	3.4	.01	.1934	167.16
3	5	.01	.195	247.84
6	6.9	.01	.1969	341.94
9	8.1	.01	.1981	400.44
10.25	8.5	.02	.1885	419.79
12	15.2	.02	.1952	748.62
15	9.6	.02	.1896	475.37
18	10.4	.02	.1904	515.39
24	11.7	.03	.1817	579.71
30	13.2	.03	.1832	656.84
36	14.4	.03	.1844	717.64
42	15.3	.03	.1853	762.73
48	16.1	.04	.1761	802.43
54	16.8	.04	.1768	838.85
60	17.5	.04	.1775	874.98
66	18.2	.04	.1782	910.82
74.5	18.9	.05	.1689	946.39
78	19.2	.05	.1692	962.44
84	19.6	.05	.1696	983.75
90	20.1	.05	.1701	1010.3
96	20.7	.06	.1607	1041.9
102	21.2	.06	.1612	1069.6
108	21.7	.06	.1617	1097.3
114	22.2	.06	.1622	1124.7
120	22.7	.07	.1527	1152.0
124	23.1	.07	.1531	1175.1

TABLE III.7. PH 9.5, 0.1 M NACL

TIME HR.	ACID ADDED ML	VOL. L	PH	SOLIDS CONC. G/L	CONCENTRATION, UMOL/L				
					MG-T	SI-T	(OH-)	CA-CB	Q
0	0	.2	9.286	10	0	0	24.88	-19.3	
3.42	.5	.1905	9.523	9.975	224	33.26	42.91	-124	-517.
11.25	2	.182	9.517	9.897	245.5	35.87	42.41	-44.9	-481.
24.15	2.2	.1722	9.509	9.886	282.9	60.01	41.58	-33.9	-536.
49	2.2	.1622	9.471	9.886	334.9	103.8	38.15	-33.9	-628.
72.58	2.2	.1522	9.432	9.886	383.5	151.2	34.86	-33.9	-712.
96.58	2.2	.1422	9.403	9.886	418.6	185.8	32.61	-33.9	-772.
119.4	2	.1322	9.429	9.886	436.1	204	34.59	-48.0	-812.

TABLE III.7A. PH 9.5, 0.1 M NACL

TIME HR.	ACID ADDED ML	SAMPLE WITHDR L	VOLUME L	CA-CB UMOL/L
0	0		.2	-19.31
1	-.26		.19974	-149.5
2	.4		.2004	-129.1
3.42	.5	.01	.1905	-124.0
4.5	.5	.01	.1905	-124.0
6	.8	.01	.1908	-108.1
8.5	1.7	.01	.1917	-60.63
11.25	2	.02	.182	-44.91
16	2.1	.02	.1821	-39.39
20	2.1	.02	.1821	-39.39
24.15	2.2	.03	.1722	-33.88
30	2.2	.03	.1722	-33.88
36	2.2	.03	.1722	-33.88
42	2.2	.03	.1722	-33.88
49	2.2	.04	.1622	-33.88
54	2.2	.04	.1622	-33.88
60	2.2	.04	.1622	-33.88
66	2.2	.04	.1622	-33.88
72.58	2.2	.05	.1522	-33.88
78	2.2	.05	.1522	-33.88
84	2.2	.05	.1522	-33.88
90	2.2	.05	.1522	-33.88
96.58	2.2	.06	.1422	-33.88
102	2.06	.06	.14206	-43.77
108	2	.06	.142	-48.01
114	2	.06	.142	-48.01
119.42	2	.07	.132	-48.01

TABLE III.8.   PH 7.5, CATECHOL 1 MMOL/L

TIME HR.	ACID ADDED ML	VOL. L	PH	SOLIDS CONC. G/L	CONCENTRATION, UMOL/L					
					MG-T	SI-T	(OH-)	CA-CB	CAT-T	Q
0	0	.2	7.687	10	0	0		0	1000	
3.5	11.4	.2014	7.475	9.461	482.4	11.6	.3843	1079.	791	132.7
9.5	16.9	.1969	7.478	9.209	674.7	17.96	.3873	1582.		
25	21.6	.1916	7.509	8.995	844.7	23.61	.4156	2011.	556	335.1
33.5	22.2	.1822	7.487	8.966	927.1	27.62	.3950	2067.		
47.83	22.9	.1729	7.509	8.932	1025.	34.2	.4156	2136.	472	97.56
59.17	22.9	.1629	7.500	8.932	1022.	39.18	.4076	2136.		
71.67	23	.153	7.504	8.927	1143.	49.51	.4108	2147.	365	-129.
83.5	23.2	.1432	7.478	8.915	1081.	51.98	.3873	2170		
95.33	23.8	.1338	7.398	8.878	1115.	58.96	.3222	2244.	299	21.87
107.3	23.8	.1238	7.521	8.878	1191.	72.48	.4273	2244.		
119.5	23.8	.1138	7.509	8.878	1229.	85.79	.4156	2244.	269	-207.

TABLE III.8A.   PH 7.5, CATECHOL 1 MMOL/L

TIME HR.	ACID ADDED ML	SAMPLE WITHDR L	VOLUME L	CA-CB UMOL/L
0	0		.2	0
1	6		.206	582.52
2	8.6		.2086	824.54
3.5	11.4	.01	.2014	1078.5
6	14.3	.01	.2043	1347.1
8	15.9	.01	.2059	1492.1
9.5	16.9	.02	.1969	1581.5
12	18.1	.02	.1981	1693.1
14	18.9	.02	.1989	1766.7
16	19.6	.02	.1996	1830.7
20	20.7	.02	.2007	1930.2
25	21.6	.03	.1916	2010.9
30	22	.03	.192	2048.4
33.5	22.2	.04	.1822	2067.1
42	22.7	.04	.1827	2116.1
47.833	22.9	.05	.1729	2135.7
54	22.9	.05	.1729	2135.7
59.167	22.9	.06	.1629	2135.7
66	23	.06	.163	2146.7
71.667	23	.07	.153	2146.7
78	23.2	.07	.1532	2170.0
83.5	23.2	.08	.1432	2170.0
90	23.6	.08	.1436	2219.6
95.333	23.8	.09	.1338	2244.4
102	23.8	.09	.1338	2244.4
107.33	23.8	.1	.1238	2244.4
114	23.8	.1	.1238	2244.4
119.5	23.8	.11	.1138	2244.4

TABLE III.9. PH 7.5, CATECHOL 10 MMOL/L

TIME HR.	ACID ADDED ML	VOL. L	PH	SOLIDS CONC. G/L	CONCENTRATION, UMOL/L MG-T	SI-T	(OH-)	CA-CB	CAT-T	Q
0	0	.2	7.498	10	0	0		0	10000	
3.5	12.5	.2025	7.516	9.412	623.2	18.76	.4223	1177.	8190	122.3
9.5	16.8	.1968	7.507	9.216	868.7	29.19	.4141	1568.		
25	19.8	.1898	7.507	9.078	1066.	46.21	.4141	1845.	7660	-108.
33.5	20.3	.1803	7.507	9.054	1106.	52	.4141	1892.		
47.83	.8	.1711	7.490	9.014	1173.	62.44	.3980	1661	7410	-510.
59.17	2.9	.1632	7.498	8.905	1233.	78.73	.4060	1520.		
71.67	3.6	.1539	7.498	8.867	1354.	110.5	.4060	1470.	7459	-1062
83.5	4.7	.145	7.498	8.804	1335.	127.9	.4060	1389		
95.33	4.7	.135	7.618	8.804	1280.	141.0	.5352	1389	6880	-1008
107.3	.6	.1256	7.507	8.765	1350.	164.1	.4141	1471.		
119.5	.7	.1157	7.495	8.758	1409.	184.1	.4028	1486.	7350	-1158

TABLE III.9A. PH 7.5, CATECHOL 10 MMOL/L

TIME HR.	ACID ADDED ML	SAMPLE WITHDR L	VOLUME L	CA-CB UMOL/L
0	0		.2	0
1	7		.207	676.33
2	9.8		.2098	934.22
3.5	12.5	.01	.2025	1176.5
6	15	.01	.205	1406.0
8	16.1	.01	.2061	1505.3
9.5	16.8	.02	.1968	1567.9
12	17.5	.02	.1975	1633.2
14	18.1	.02	.1981	1688.8
16	18.6	.02	.1986	1734.9
20	19.3	.02	.1993	1799.1
25	19.8	.03	.1898	1844.6
30	20.2	.03	.1902	1882.8
33.5	20.3	.04	.1803	1892.3
42	20.3	.04	.1803	1892.3
47.833	.8	.05	.1711	1661.0
54	1.9	.05	.1722	1586.5
59.167	2.9	.06	.1632	1519.6
66	3.5	.06	.1638	1477.4
71.667	3.6	.07	.1539	1470.4
78	4.1	.07	.1544	1433.2
83.5	4.7	.08	.145	1389.0
90	4.7	.08	.145	1389.0
95.333	4.7	.09	.135	1389.0
102	.6	.09	.1356	1471.3
107.33	.6	.1	.1256	1471.3
114	.7	.1	.1257	1486.1
119.5	.7	.11	.1157	1486.1

TABLE III.10. PH 8, CATECHOL 0.1 MMOL/L

TIME HR.	ACID ADDED ML	VOL. L	PH	SOLIDS CONC. G/L	CONCENTRATION, UMOL/L					
					MG-T	SI-T	(OH-)	CA-CB	CAT-T	Q
0	0	.2	7.910	10	0	0		0	100	
2.833	7	.197	7.974	9.662	364.1	19.03	1.214	676.3	60	-46.1
13.67	13.3	.1933	8.026	9.362	593.1	46.46	1.367	1275.	43	94.11
23.92	16.3	.1863	7.981	9.219	756.7	68.97	1.233	1561.	26	52.17
35.5	18.2	.1782	7.986	9.126	780.9	89.02	1.248	1748.		
47.58	19.5	.1695	8.021	9.060	882.2	121.1	1.351	1880.	13	119.7
59.33	20.2	.1602	7.984	9.023	881.4	129.1	1.243	1954.		
71.5	20.6	.1506	7.965	9.000	960.5	160	1.190	1999.	0	82.09
81.42	21	.141	7.972	8.977	917	166.1	1.209	2047.	0	216.9
95.25	21.6	.1316	8.006	8.939	1008.	195.3	1.307	2123.	0	111.8
106.3	21.9	.1219	8.012	8.918	976.3	199.3	1.324	2164.	0	215.7
119.8	22.1	.1121	8.021	8.904	1016.	222.7	1.351	2193.	0	166.4

TABLE III.10A. PH 8, CATECHOL 0.1 MMOL/L

TIME HR.	ACID ADDED ML	SAMPLE WITHDR L	VOLUME L	CA-CB UMOL/L
0	0		.2	0
1	4.2		.2042	411.36
2.8333	7	.01	.197	676.33
4	8.2	.01	.1982	793.32
6	9.7	.01	.1997	937.59
8	10.9	.01	.2009	1051.5
10	11.9	.01	.2019	1145.3
12	12.7	.01	.2027	1219.7
13.667	13.3	.02	.1933	1275.1
16	14.2	.02	.1942	1361.9
20	15.4	.02	.1954	1476.4
23.917	16.3	.03	.1863	1561.3
30	17.4	.03	.1874	1669.5
35.5	18.2	.04	.1782	1747.5
42	19	.04	.179	1829.0
47.583	19.5	.05	.1695	1879.7
54	20	.05	.17	1932.9
59.333	20.2	.06	.1602	1954.2
66	20.5	.06	.1605	1987.9
71.5	20.6	.07	.1506	1999.1
78	20.8	.07	.1508	2023.0
81.417	21	.08	.141	2046.8
90	21.5	.08	.1415	2110.2
95.25	21.6	.09	.1316	2122.9
102	21.8	.09	.1318	2150.0
106.33	21.9	.1	.1219	2163.5
114	22	.1	.122	2178.2
119.83	22.1	.11	.1121	2192.8

TABLE III.11. PH 8, CATECHOL 1 MMOL/L

	ACID	VOL.		SOLIDS CONC.	CONCENTRATION, UMOL/L					
TIME HR.	ADDED ML	L	PH	G/L	MG-T	SI-T	(OH-)	CA-CB	CAT-T	Q
0	0	.2	7.297	10	0	0		0	1000	
2.833	7	.197	7.990	9.662	414.4	22.65	1.260	676.3	900	-87.4
13.67	13.7	.1937	7.989	9.344	714.9	63.25	1.255	1312.	790	-59.8
23.92	16.2	.1862	7.994	9.225	897.6	113.1	1.270	1550	680	-194.
35.5	16.9	.1769	8.014	9.190	970.2	146.6	1.332	1619.		
47.58	17.7	.1677	8.014	9.149	1016.	185.3	1.332	1702.	480	-292.
59.33	18	.158	8.006	9.133	1032.	208.4	1.306	1735.		
71.5	18.2	.1482	7.994	9.121	1154.	255	1.270	1758.	380	-518.
81.42	18.6	.1386	7.947	9.097	1233.	280.1	1.142	1807.		
95.25	19.1	.1291	8.007	9.064	1261.	307.4	1.311	1872.	280	-623.
106.3	19.3	.1193	8.014	9.050	1213.	310.9	1.332	1900.		
119.8	20	.11	7.990	8.997	1265.	330.4	1.260	2006.	250	-499.

TABLE III.11A. PH 8, CATECHOL 1 MMOL/L

TIME HR.	ACID ADDED ML	SAMPLE WITHDR L	VOLUME L	CA-CB UMOL/L
0	0		.2	0
1	4		.204	392.16
2.8333	7	.01	.197	676.33
4	8.3	.01	.1983	803.01
6	9.9	.01	.1999	956.66
8	11.2	.01	.2012	1079.7
10	12.2	.01	.2022	1173.3
12	13	.01	.203	1247.5
13.667	13.7	.02	.1937	1311.9
16	14.5	.02	.1945	1388.8
20	15.6	.02	.1956	1493.4
23.917	16.2	.03	.1862	1550.0
30	16.8	.03	.1868	1609.3
35.5	16.9	.04	.1769	1619.1
42	17.4	.04	.1774	1670.9
47.583	17.7	.05	.1677	1701.9
54	18	.05	.168	1734.6
59.333	18	.06	.158	1734.6
66	18.2	.06	.1582	1757.7
71.5	18.2	.07	.1482	1757.7
78	18.5	.07	.1485	1794.5
81.417	18.6	.08	.1386	1806.8
90	19	.08	.139	1859.1
95.25	19.1	.09	.1291	1872.2
102	19.3	.09	.1293	1900.2
106.33	19.3	.1	.1193	1900.2
114	19.7	.1	.1197	1960.7
119.83	20	.11	.11	2005.8

TABLE III.12.   PH 8, CATECHOL 10 MMOL/L

TIME HR.	ACID ADDED ML	VOL. L	PH	SOLIDS CONC. G/L	CONCENTRATION, UMOL/L					
					MG-T	SI-T	(OH-)	CA-CB	CAT-T	Q
0	0	.2	8	10	0	0		0		
3.083	7.2	.1972	8.116	9.653	561.5	28.1	1.682	695.0	8800	194.6
11.25	10.5	.1905	8.014	9.494	849.7	46.31	1.331	1013.	8400	-92.4
23	-	.183	8.029	9.371	998.7	57.53	1.379	823.5	7840	-619.
34.08	-	.1735	7.997	9.345	1110	82.87	1.280	768		
47.25	.4	.1639	8.014	9.324	1140.	91.83	1.331	651.2	7690	-1083
57.92	1.1	.1546	7.997	9.284	1179.	105.4	1.280	435.8		
71.08	2.7	.1462	8.016	9.189	1263.	147.4	1.336	-80.8	7530	-2072
82.08	4.6	.1381	8.006	9.071	1185.	155.7	1.305	-721.		
95.08	6.4	.1299	7.997	8.954	1202.	202.6	1.280	-1355	6250	-3313
105.3	6.4	.1199	8.026	8.954	1302.	252.1	1.368	-1355		
118.9	6.4	.1099	8.069	8.954	1300.	282.7	1.509	-1355	6560	-3485

TABLE III.12A.   PH 8, CATECHOL 10 MMOL/L

TIME HR.	ACID ADDED ML	SAMPLE WITHDR L	VOLUME L	CA-CB UMOL/L
0	0		.2	0
1	4		.204	392.16
3.0833	7.2	.01	.1972	694.98
4	7.9	.01	.1979	763.27
6	9	.01	.199	869.60
8	9.6	.01	.1996	927.11
10	10.2	.01	.2002	984.27
11.25	10.5	.02	.1905	1012.7
14	10.8	.02	.1908	1042.6
16	10.8	.02	.1908	1042.6
20	10.8	.02	.1908	1042.6
23	0	.03	.183	823.46
30	0	.03	.1834	795.68
34.083	0	.04	.1735	768
42	.1	.04	.1736	738.76
47.25	.4	.05	.1639	651.22
54	.9	.05	.1644	497.18
57.917	1.1	.06	.1546	435.82
66	1.9	.06	.1554	176.17
71.083	2.7	.07	.1462	-80.81
78	3.9	.07	.1474	-487.2
82.083	4.6	.08	.1381	-721.2
90	5.9	.08	.1394	-1181.
95.083	6.4	.09	.1299	-1355.
102	6.4	.09	.1299	-1355.
105.25	6.4	.1	.1199	-1355.
114	6.4	.1	.1199	-1355.
118.92	6.4	.11	.1099	-1355.

TABLE III.13. PH 8.5, CATECHOL 10 MMOL/L

TIME HR.	ACID ADDED ML	VOL. L	PH	SOLIDS CONC. G/L	CONCENTRATION, UMOL/L					
					MG-T	SI-T	(OH-)	CA-CB	CAT-T	Q
0	0	.2	8.447	10	0	0		0		
3.083	1.4	.1914	8.501	9.930	502.6	38.83	4.087	139.0	8600	804.1
11.25	3.7	.1837	8.447	9.813	798.9	68.54	3.602	374.9	8580	444.5
23	0	.1761	8.507	9.686	985.6	98.82	4.136	47.61	8140	-339.
34.08	.8	.1691	8.481	9.524	1076.	137.6	3.898	-444.		
47.25	3.8	.1629	8.493	9.314	1112.	178.9	4.007	-1307	7330	-2098
57.92	6.5	.1556	8.481	9.163	1137.	216.9	3.898	-2100		
71.08	10.7	.1498	8.484	8.922	1136.	253.4	3.929	-3359	6580	-4341
82.08	13.9	.143	8.481	8.735	1180	269.7	3.898	-4335		
95.08	15.7	.1348	8.484	8.627	998.2	278.7	3.929	-4903	5370	-5842
105.3	16.6	.1257	8.527	8.569	981.3	291.7	4.336	-5202		
118.9	17.1	.1162	8.501	8.535	1003.	322.1	4.087	-5379	5100	-6377

TABLE III.13A. PH 8.5, CATECHOL 10 MMOL/L

TIME HR.	ACID ADDED ML	SAMPLE WITHDR L	VOLUME L	CA-CB UMOL/L
0	0		.2	0
1	0		.2	0
3.0833	1.4	.01	.1914	139.03
4	2	.01	.192	201.09
6	3.4	.01	.1934	344.41
8	3.7	.01	.1937	374.86
10	3.7	.01	.1937	374.86
11.25	3.7	.02	.1837	374.86
14	3.7	.02	.1837	374.86
16	3.7	.02	.1837	374.86
20	3.7	.02	.1837	374.86
23	0	.03	.1761	47.61
30	0	.03	.1789	-109.6
34.083	.8	.04	.1691	-444.4
42	2.5	.04	.1716	-937.6
47.25	3.8	.05	.1629	-1307.
54	5.3	.05	.1644	-1751.
57.917	6.5	.06	.1556	-2100.
66	9	.06	.1581	-2858.
71.083	10.7	.07	.1498	-3359.
78	12.7	.07	.1518	-3974.
82.083	13.9	.08	.143	-4335.
90	15.2	.08	.1443	-4746.
95.083	15.7	.09	.1348	-4903.
102	16.3	.09	.1354	-5102.
105.25	16.6	.1	.1257	-5202.
114	16.9	.1	.126	-5308.
118.92	17.1	.11	.1162	-5379.

TABLE III.14. PH 7.5, OXALIC ACID 1 MMOL/L

| | ACID | | | SOLIDS | CONCENTRATION, UMOL/L | | | | | |
| TIME | ADDED | VOL. | | CONC. | | | | | | |
HR.	ML	L	PH	G/L	MG-T	SI-T	(OH-)	CA-CB	OXA-T	Q
0	0	.2	7.5	10	0	0		0	1000	
3.5	14.5	.2045	7.484	9.324	527.6	18.35	.3927	1352	1000	1364.
9	19.7	.1997	7.499	9.093	678.7	26.17	.4069	1814.	930	1450.
24.83	26.8	.1968	7.445	8.781	877	33.28	.3588	2439.	860	1603.
34.83	29	.189	7.552	8.684	938.9	41.1	.4595	2633.		
48.67	30.9	.1809	7.411	8.597	1019	48.21	.3317	2806.	750	1569.
58.67	31.9	.1719	7.479	8.550	1081.	58.17	.3881	2900.		
72.67	33	.163	7.411	8.495	1108.	68.84	.3317	3009	720	1562.
82.5	33.6	.1536	7.547	8.464	1148.	76.66	.4541	3071.		
98.17	34.5	.1445	7.479	8.415	1141.	88.03	.3881	3170.	690	1625.
108.2	35	.135	7.516	8.386	1177.	99.41	.4232	3228		
120.8	35.5	.1255	7.476	8.355	1219.	110.8	.3851	3290.	630	1525.

TABLE III.14A. PH 7.5, OXALIC ACID 1 MMOL/L

| | ACID | SAMPLE | | |
| TIME | ADDED | WITHDR | VOLUME | CA-CB |
HR.	ML	L	L	UMOL/L
0	0		.2	0
1	8.1		.2081	778.47
2	11		.211	1042.7
3.5	14.5	.01	.2045	1352.0
6	17.2	.01	.2072	1595.0
8	18.9	.01	.2089	1744.8
9	19.7	.02	.1997	1814.4
12	21.6	.02	.2016	1985.8
14	22.7	.02	.2027	2083.6
16	23.6	.02	.2036	2162.8
20	25.2	.02	.2052	2301.8
24.833	26.8	.03	.1968	2438.8
30	28.1	.03	.1981	2554.0
34.833	29	.04	.189	2632.9
42	30.1	.04	.1901	2733.4
48.667	30.9	.05	.1809	2805.8
54	31.4	.05	.1814	2853.2
58.667	31.9	.06	.1719	2900.3
66	32.5	.06	.1725	2959.8
72.667	33	.07	.163	3009.0
78	33.4	.07	.1634	3050.6
82.5	33.6	.08	.1536	3071.3
90	34.1	.08	.1541	3126.3
98.167	34.5	.09	.1445	3169.9
102	34.8	.09	.1448	3204.8
108.17	35	.1	.135	3228.0
114	35.3	.1	.1353	3265.2
120.83	35.5	.11	.1255	3289.9

TABLE III.15.   PH 7.5, OXALIC ACID 10 MMOL

TIME HR.	ACID ADDED ML	VOL. L	PH	SOLIDS CONC. G/L	CONCENTRATION, UMOL/L MG-T	SI-T	(OH-)	CA-CB	OXA-T	Q
0	0	.2	7.5	10	0	0		0	10000	
3.5	20	.21	7.479	9.091	673.2	23.95	.3881	1818.	10200	11358
9	26.5	.2065	7.571	8.818	858.8	26.78	.4798	2364.		
24.83	34.3	.2043	7.532	8.497	1074.	35.97	.4384	3006	9900	11425
34.83	36.4	.1964	7.469	8.411	1176.	39.51	.3791	3179.		
48.67	38.2	.1882	7.261	8.334	1210	46.57	.2349	3332.	9300	10837
58.67	38.9	.1789	7.547	8.303	1199.	49.4	.4541	3393.		
72.67	39.8	.1698	7.445	8.262	1257.	55.76	.3588	3477.	9200	10781
82.5	40.2	.1602	7.515	8.242	1296.	60.01	.4215	3515.		
98.17	40.7	.1507	7.539	8.217	1239.	62.83	.4453	3567.	8600	10267
108.2	41	.141	7.470	8.200	1246.	67.08	.3806	3599.		
120.8	41.2	.1312	7.506	8.189	1323.	72.73	.4133	3623.	8900	10476

TABLE III.15A.   PH 7.5, OXALIC ACID 10 MMOL/L

TIME HR.	ACID ADDED ML	SAMPLE WITHDR L	VOL. L	CA-CB UMOL/L
0	0		.2	0
1	11.3		.2113	1069.6
2	15.4		.2154	1429.9
3.5	20	.01	.21	1818.2
6	23.3	.01	.2133	2099.5
8	25.6	.01	.2156	2290.4
9	26.5	.02	.2065	2364.1
12	28.9	.02	.2089	2566.7
14	30.2	.02	.2102	2674.5
16	31.2	.02	.2112	2756.5
20	32.9	.02	.2129	2894.2
24.833	34.3	.03	.2043	3006.0
30	35.5	.03	.2055	3105.2
34.833	36.4	.04	.1964	3178.9
42	37.4	.04	.1974	3264.1
48.667	38.2	.05	.1882	3331.6
54	38.6	.05	.1886	3367.0
58.667	38.9	.06	.1789	3393.4
66	39.4	.06	.1794	3439.7
72.667	39.8	.07	.1698	3476.5
78	40	.07	.17	3496.0
82.5	40.2	.08	.1602	3515.4
90	40.5	.08	.1605	3546.2
98.167	40.7	.09	.1507	3566.6
102	40.8	.09	.1508	3577.5
108.17	41	.1	.141	3599.3
114	41.1	.1	.1411	3610.9
120.83	41.2	.11	.1312	3622.5

TABLE III.16.   PH 8, OXALIC ACID, 1 MMOL/L

TIME HR.	ACID ADDED ML	VOL. L	PH	SOLIDS CONC. G/L	CONCENTRATION, UMOL/L					
					MG-T	SI-T	(OH-)	CA-CB	OXA-T	Q
0	0	.2	9.095	10	0	0		0	1000	
4.667	11.9	.2019	7.946	9.438	469.6	26.68	1.138	1123.		
11.17	16.2	.1962	7.933	9.242	603.2	34.64	1.103	1517.	980	1358.
24.67	21.3	.1913	8.039	9.007	756.5	51.29	1.411	1985.	900	1435.
36.67	23.8	.1838	8.002	8.891	795.8	60.7	1.295	2218.		
49.67	26.2	.1762	8.039	8.777	913.7	80.97	1.411	2447.	940	1625.
62.5	27.5	.1675	7.746	8.712	896	84.59	.7183	2575.		
72.33	28.4	.1584	7.951	8.666	1010	102.3	1.152	2668.	850	1559.
84.83	29	.149	7.980	8.633	1002.	111.0	1.231	2734.		
• 96.83	29.4	.1394	8.039	8.610	1089.	134.2	1.411	2780	860	1525.
107	29.8	.1298	7.975	8.585	1073.	137.1	1.216	2829.		
121.3	30.3	.1203	7.972	8.552	1165.	160.3	1.207	2895.	830	1455.

TABLE III.16A.   PH 8, OXALIC ACID 1 MMOL/L

TIME HR.	ACID ADDED ML	SAMPLE WITHDR L	VOLUME L	CA-CB UMOL/L
0	0		.2	0
1	6		.206	582.52
2	8.3		.2083	796.93
4.6667	11.9	.01	.2019	1123.2
6	12.9	.01	.2029	1216.2
8	14.4	.01	.2044	1354.1
10	15.5	.01	.2055	1453.9
11.167	16.2	.02	.1962	1516.8
14	17.5	.02	.1975	1638.5
16	18.4	.02	.1984	1721.8
20	19.9	.02	.1999	1858.9
24.667	21.3	.03	.1913	1985.1
30	22.8	.03	.1928	2125.3
36.667	23.8	.04	.1838	2217.5
42	25.1	.04	.1851	2342.4
49.667	26.2	.05	.1762	2446.7
54	26.8	.05	.1768	2506.3
62.5	27.5	.06	.1675	2575.3
66	27.9	.06	.1679	2616.8
72.333	28.4	.07	.1584	2668.4
78	28.7	.07	.1587	2701.1
84.833	29	.08	.149	2733.8
90	29.1	.08	.1491	2745.4
96.833	29.4	.09	.1394	2780.0
102	29.6	.09	.1396	2804.7
107	29.8	.1	.1298	2829.3
114	30.1	.1	.1301	2868.9
121.33	30.3	.11	.1203	2895.2

TABLE III.17.   PH 8, OXALIC ACID 10 MMOL/L

TIME HR.	ACID ADDED ML	VOL. L	PH	SOLIDS CONC. G/L	CONCENTRATION, UMOL/L					
					MG-T	SI-T	(OH-)	CA-CB	OXA-T	Q
0	0	.2	9.197	10	0	0			0	10000
4.667	18.9	.2089	7.932	9.137	691.6	17.27	1.102	1727.	10200	11232
11.17	25.3	.2053	8.018	8.865	856.7	20.16	1.343	2270	9700	10912
24.67	31.8	.2018	7.958	8.593	1014.	22.34	1.169	2814.	8900	10288
36.67	34.5	.1945	7.898	8.479	1085.	28.85	1.019	3041		
49.67	37	.187	7.918	8.372	1146.	36.81	1.068	3256.	8500	10040
62.5	38	.178	7.984	8.327	1171.	39.71	1.241	3345.		
72.33	39	.169	7.853	8.281	1177	43.55	.9192	3438.	9100	10799
84.83	40.4	.1604	8.018	8.213	1273.	47.16	1.343	3574.		
96.83	42.3	.1523	7.944	8.117	1265.	48.62	1.133	3767.	8500	10311
107	44.1	.1441	7.984	8.022	1222.	48.62	1.241	3956.		
121.3	45.7	.1357	7.881	7.934	1273.	52.24	.9790	4133.	8800	10981

TABLE III.17A.   PH 8, OXALIC ACID 10 MMOL/L

TIME HR.	ACID ADDED ML	SAMPLE WITHDR L	VOLUME L	CA-CB UMOL/L
0	0		.2	0
1	9.7		.2097	925.13
2	13.4		.2134	1255.9
4.6667	18.9	.01	.2089	1726.8
6	20.5	.01	.2105	1865.7
8	22.7	.01	.2127	2053.3
10	24.5	.01	.2145	2203.9
11.167	25.3	.02	.2053	2270.0
14	27.1	.02	.2071	2424.1
16	28.1	.02	.2081	2508.6
20	30.1	.02	.2101	2675.1
24.667	31.8	.03	.2018	2814.1
30	33.3	.03	.2033	2940.9
36.667	34.5	.04	.1945	3041.0
42	35.9	.04	.1959	3162.2
49.667	37	.05	.187	3256.2
54	37.4	.05	.1874	3292.0
62.5	38	.06	.178	3345.3
66	38.4	.06	.1784	3382.6
72.333	39	.07	.169	3438.4
78	39.5	.07	.1695	3487.2
84.833	40.4	.08	.1604	3574.4
90	41.2	.08	.1612	3655.9
96.833	42.3	.09	.1523	3766.7
102	43.1	.09	.1531	3851.5
107	44.1	.1	.1441	3956.3
114	44.9	.1	.1449	4044.9
121.33	45.7	.11	.1357	4132.5

TABLE III.18. PH 8.5, OXALIC ACID 1 MMOL/L

TIME HR.	ACID ADDED ML.	VOL. L	PH	SOLIDS CONC. G/L	CONCENTRATION, UMOL/L					
					MG-T	SI-T	(OH-)	CA-CB	CAT-T	Q
0	0	.2	8.5	10	0	0		0	1000	
3.833	6.4	.1964	8.548	9.690	316	21.39	4.551	620.2	712	754.1
10.17	8.1	.1881	8.524	9.607	360.9	23.56	4.308	786.5		
24.67	9.8	.1798	8.509	9.521	457.6	35.11	4.159	958.6	809	913.2
36.33	10.3	.1703	8.504	9.494	461	39.45	4.112	1011.		
50.17	10.6	.1606	8.534	9.478	519.7	48.83	4.411	1045.	782	847.4
58.17	10.8	.1508	8.514	9.466	540.4	52.45	4.208	1068.		
74	11.1	.1411	8.524	9.447	568.1	59.84	4.308	1106.	687	710.8
86	11.4	.1314	8.492	9.427	576.7	64.93	4.000	1146		
97	11.6	.1216	8.467	9.413	626.7	77.29	3.772	1175.	681	656.4
107	11.6	.1116	8.524	9.413	607.8	77.29	4.308	1175.		
121.3	11.6	.1016	8.472	9.413	657.8	89.65	3.817	1175.	781	701.6

TABLE III.18A. PH 8.5, OXALIC ACID 1 MMOL/L

TIME HR.	ACID ADDED ML	SAMPLE WITHDR L	VOLUME L	CA-CB UMOL/L
0	0		.2	0
1	4.2		.2042	411.36
2	5.4		.2054	525.80
3.8333	6.4	.01	.1964	620.16
6	7.2	.01	.1972	698.78
8	7.7	.01	.1977	747.59
10.167	8.1	.02	.1881	786.46
12	8.4	.02	.1884	817.06
14	8.7	.02	.1887	847.56
16	9	.02	.189	877.96
20	9.4	.02	.1894	918.34
24.667	9.8	.03	.1798	958.56
30	10.1	.03	.1801	990.27
36.333	10.3	.04	.1703	1011.4
42	10.4	.04	.1704	1022.5
50.167	10.6	.05	.1606	1044.8
54	10.7	.05	.1607	1056.5
58.167	10.8	.06	.1508	1068.3
66	10.9	.06	.1509	1080.9
74	11.1	.07	.1411	1105.9
78	11.2	.07	.1412	1119.3
86	11.4	.08	.1314	1146.0
90	11.5	.08	.1315	1160.3
97	11.6	.09	.1216	1174.7
102	11.6	.09	.1216	1174.7
107	11.6	.1	.1116	1174.7
114	11.6	.1	.1116	1174.7
121.33	11.6	.11	.1016	1174.7

TABLE III.19. PH 8.5, OXALIC ACID 10 MMOL/L

| | ACID | | | SOLIDS | CONCENTRATION, UMOL/L | | | | | |
| TIME | ADDED | VOL. | | CONC. | | | | | | |
HR.	ML	L	PH	G/L	MG-T	SI-T	(OH-)	CA-CB	OXA-T	Q
0	0	.2	8.5	10	0	0		0	10000	
3.833	11.6	.2016	8.537	9.452	492.1	22.84	4.434	1096.	10400	11223
10.17	15.6	.1956	8.468	9.268	600.9	19.95	3.789	1464.		
24.67	19.7	.1897	8.503	9.078	818.4	22.84	4.099	1845.	9800	10678
36.33	21.1	.1811	8.508	9.011	832.2	22.84	4.148	1978.		
50.17	22.2	.1722	8.528	8.957	884	25	4.348	2087.	9100	10041
58.17	23.1	.1631	8.477	8.910	975.5	30.06	3.865	2180.		
74	24.5	.1545	8.477	8.834	1026.	33.66	3.865	2331.	9300	10216
86	25.3	.1453	8.445	8.789	1076.	38.75	3.586	2422.		
97	25.8	.1358	8.383	8.759	1095.	42.39	3.115	2483.	9600	10550
107	26	.126	8.525	8.746	1053.	42.39	4.314	2508.		
121.3	26.3	.1163	8.486	8.725	1150.	49.66	3.941	2550	9400	10294

TABLE III.19A. PH 8.5, OXALIC ACID 10 MMOL/L

| | ACID | SAMPLE | | |
| | ADDED | WITHDR | VOLUME | CA-CB |
TIME	ML	L	L	UMOL/L
0	0		.2	0
1	7		.207	676.33
2	9.3		.2093	888.68
3.8333	11.6	.01	.2016	1096.4
6	13.3	.01	.2033	1254.5
8	14.5	.01	.2045	1364.5
10.167	15.6	.02	.1956	1464.2
12	16.3	.02	.1963	1530.3
14	17	.02	.197	1595.9
16	17.7	.02	.1977	1661.1
20	18.7	.02	.1987	1753.4
24.667	19.7	.03	.1897	1844.7
30	20.5	.03	.1905	1921.0
36.333	21.1	.04	.1811	1977.7
42	21.6	.04	.1816	2027.4
50.167	22.2	.05	.1722	2086.5
54	22.7	.05	.1727	2138.4
58.167	23.1	.06	.1631	2179.7
66	23.9	.06	.1639	2266.7
74	24.5	.07	.1545	2331.3
78	24.8	.07	.1548	2365.6
86	25.3	.08	.1453	2422.4
90	25.5	.08	.1455	2446.5
97	25.8	.09	.1358	2482.6
102	25.9	.09	.1359	2495.5
107	26	.1	.126	2508.4
114	26.2	.1	.1262	2536.1
121.33	26.3	.11	.1163	2550.0

TABLE III.20. PH 7, 0.1 M KNO3

TIME HR.	ACID ADDED ML	VOL. L	PH	SOLIDS CONC. G/L	MG-T	SI-T	(OH-)	CA-CB	Q
0	0	.2	7	10	0	0		0	
3.667	6.6	.1986	7	9.681	460.1	27.84	.1289	1607	686.9
12.5	12.4	.1964	7	9.406	567.5	57.69	.1289	2129.	994.0
23.5	15.4	.1914	7	9.264	677	83	.1289	2398.	1044.
36.5	17.9	.1859	7	9.145	773.5	103.6	.1289	2625.	1078.
49.67	21.1	.1811	7	8.990	862.9	156.3	.1289	2750.	1024.
62.17	23.8	.1758	7	8.858	919.8	179.3	.1289	2856	1017.
69.17	25	.169	7	8.798	1080.	191.8	.1289	2905.	745.2
84.83	29.2	.1652	7	8.585	950.9	209.6	.1289	3077.	1175.
99.67	38.8	.1668	7	8.113	1154.	188.1	.1289	3457.	1149.
108.7	39.3	.1593	7	8.089	1168.	220.5	.1289	3476.	1141.
117.8	39.8	.1518	7	8.064	1278.	227.7	.1289	3497.	941.5

TABLE III.20A. PH 7, 0.1 M KNO3

TIME HR.	ACID ADDED ML	SAMPLE WITHDR L	VOLUME L	CA-CB UMOL/L
0	0		.2	0
1.6667	2.5		.2025	1234.6
3.6667	6.6	.008	.1986	1607.0
6	9.1	.008	.2011	1835.6
8	10.4	.008	.2024	1952.3
10	11.4	.008	.2034	2041.0
12.5	12.4	.016	.1964	2128.9
16	13.6	.016	.1976	2237.4
20	14.6	.016	.1986	2326.9
23.5	15.4	.024	.1914	2397.8
30	16.8	.024	.1928	2525.6
36.5	17.9	.032	.1859	2624.7
38.733	18.2	.032	.1862	2636.6
42	19	.032	.187	2668.1
49.667	21.1	.04	.1811	2749.5
56	22.5	.04	.1825	2805.1
62.167	23.8	.048	.1758	2856.0
69.167	25	.056	.169	2904.5
76	26.1	.056	.1701	2950.3
84.833	29.2	.064	.1652	3076.5
92	36.8	.064	.1728	3381.0
99.667	38.8	.072	.1668	3456.8
108.67	39.3	.08	.1593	3476.3
117.83	39.8	.088	.1518	3496.7

TABLE III.21. PH 7.5, 0.1 M KNO3

| | ACID | | | | SOLID---UMOL/L--- | | | | UMOL/L | | |
| TIME | ADDED | VOL. | | | | | | | | | |
HR.	ML	L	PH	G/L	MG-T	SI-T	SI-	(OH-)	CA-CB	Q
0	0	.2	5.445	10	0	0		.0036	3.59	
5	3.7	.1937	7.084	9.818	461.6	65.27	.3649	.1565	1820.	897.2
13	7.1	.1871	7.490	9.649	544.2	58.56	.3274	.3983	2098	1010.
24.5	10.6	.1806	7.516	9.472	600	99.34	.5553	.4225	2243.	1044.
48.15	14.1	.1741	7.499	9.292	691.5	137.7	.7696	.4062	2391.	1009.
72	17.8	.1678	7.490	9.098	769.6	179.7	1.005	.3983	2549.	1011.
97	20.1	.1601	7.419	8.975	819.7	215.8	1.206	.3378	2650.	1012.
120.2	22.5	.1525	7.507	8.843	910	255.7	1.430	.4143	2758.	940.0

TABLE III.21A. PH 7.5, 0.1 M KNO3

| | ACID | SAMPLE | | |
| TIME | ADDED | WITHDR | VOLUME | CA-CB |
HR.	ML	L	L	UMOL/L
0	0		.2	3.59
1	1.9		.2019	944.62
2	2.6		.2026	1286.9
3.5	3.2		.2032	1578.3
5	3.7	.01	.1937	1819.9
7	4	.01	.194	1971.7
10	5.7	.01	.1957	2041.5
13	7.1	.02	.1871	2098.0
16	8.3	.02	.1883	2148.4
20	9.5	.02	.1895	2198.1
24.5	10.6	.03	.1806	2243.1
30	11.8	.03	.1818	2294.3
36	13	.03	.183	2344.8
42	14	.03	.184	2386.5
48.15	14.1	.04	.1741	2390.6
54	15.7	.04	.1757	2459.9
60	16.5	.04	.1765	2494.1
66	17.2	.04	.1772	2523.7
72	17.8	.05	.1678	2548.9
78	18.4	.05	.1684	2575.5
84	19.1	.05	.1691	2606.2
90	19.4	.05	.1694	2619.3
97	20.1	.06	.1601	2649.7
102	20.6	.06	.1606	2672.6
108	21.2	.06	.1612	2699.8
114	21.9	.06	.1619	2731.4
120.17	22.5	.07	.1525	2758.2
127	23.2	.07	.1532	2791.3

TABLE III.22. PH 8, 0.1 M KNO3

TIME HR.	ACID ADDED ML.	VOL. L.	PH	SOLIDS CONC. G/L	CONCENTRATION, UMOL/L				
					MG-T	SI-T	(OH-)	CA-CB	Q
0	0	.2	7.858	10	0	0	.9292	0	
2.7	2.7	.1947	7.928	9.867	282.1	18.08	1.092	671.3	108.5
12.58	8.6	.1926	7.976	9.577	381.3	40.61	1.219	1240.	479.1
26.58	12.1	.1881	7.920	9.406	435.6	66.52	1.072	1575.	705.7
48.33	14	.182	8.006	9.312	511.1	99.38	1.306	1759.	739.7
60.42	14.8	.1749	7.914	9.271	540.7	120.3	1.057	1839.	760.5
70.5	15.1	.1671	7.987	9.255	570.4	136.2	1.251	1870.	732.7
85.17	15.7	.1597	7.891	9.222	610.8	172.2	1.003	1935.	717.1
95.42	16.1	.1521	7.942	9.199	637.7	171.5	1.127	1980.	708.6
109.8	16.6	.1446	7.996	9.169	651.2	184.5	1.277	2039.	741.0
120	16.7	.1367	8.003	9.162	683.6	193.1	1.297	2051.	688.8

TABLE III.22A. PH 8, 0.1 M KNO3

TIME HR.	ACID ADDED ML	SAMPLE WITHDR L	VOL. L	CA-CB UMOL/L
0	0		.2	0
1	1.3		.2013	408.15
2	1.9		.2019	594.75
2.7	2.7	.008	.1947	671.34
4	4	.008	.196	799.54
7	6.2	.008	.1982	1012.7
10	7.7	.008	.1997	1155.3
12.583	8.6	.016	.1926	1239.8
16	9.7	.016	.1937	1346.4
20	10.8	.016	.1948	1451.7
24	11.6	.016	.1956	1527.6
26.583	12.1	.024	.1881	1574.7
30	12.5	.024	.1885	1613.8
36	13.2	.024	.1892	1681.8
42	13.6	.024	.1896	1720.4
48.833	14	.032	.182	1758.9
54	14.4	.032	.1824	1798.9
60.417	14.8	.04	.1748	1838.7
66	14.9	.04	.1749	1849.1
72.5	15.1	.048	.1671	1869.9
78	15.3	.048	.1673	1891.5
85.167	15.7	.056	.1597	1934.7
90	15.9	.056	.1599	1957.3
95.417	16.1	.064	.1521	1979.9
102	16.4	.064	.1524	2015.3
109.83	16.6	.072	.1446	2038.9
114	16.6	.072	.1446	2038.9
119.75	16.7	.08	.1367	2051.3

TABLE III.23.   PH 8, 0.01 M KNO3

	ACID			SOLIDS	CONCENTRATION, UMOL/L				
	ADDED	VOL.		CONC.					
TIME									
HR.	ML	L	PH	G/L	MG-T	SI-T	(OH-)	CA-CB	Q
0	0	.2		10	0	0		.72	
5.167	15.9	.2059	7.994	9.264	332.3	24.09	1.070	736.5	73.34
24	25.9	.2059	7.968	8.834	454.9	68.18	1.009	1166.	257.9
48.75	31.3	.2013	8.004	8.609	572.1	116.8	1.095	1391.	250.2
72.5	33.5	.1935	7.989	8.516	654.7	163.3	1.057	1484.	178.9
95.75	35	.185	8.011	8.450	717.6	197.7	1.112	1550.	119.3
119.8	36.9	.1769	8.004	8.364	725.5	226.5	1.095	1636.	189.9

TABLE III.23A.   PH 8, 0.01 M KNO3

| | ACID | SAMPLE | | |
| TIME | ADDED | WITHDR | VOLUME | CA-CB |
HR.	ML	L	L	UMOL/L
0	0		.2	0
1	6.9		.2069	333.49
2	9.9		.2099	471.65
3.5	13		.213	610.33
5.167	15.9	.01	.2059	736.45
7	18.5	.01	.2085	851.97
10	22.2	.01	.2122	1011.5
13	23.7	.01	.2137	1074.6
16	23.8	.01	.2138	1078.7
20	24.5	.01	.2145	1107.9
24	25.9	.02	.2059	1165.5
30	26.4	.02	.2064	1186.9
36	26.9	.02	.2069	1208.2
42	28.8	.02	.2088	1288.2
48.75	31.3	.03	.2013	1391.3
54	32.4	.03	.2024	1438.1
60	32.8	.03	.2028	1455.0
66	33.1	.03	.2031	1467.6
72.5	33.5	.04	.1935	1484.4
78	33.6	.04	.1936	1488.8
84	34.2	.04	.1942	1515.1
90	34.6	.04	.1946	1532.5
95.75	35	.05	.185	1549.9
102	35.7	.05	.1857	1581.7
108	36.4	.05	.1864	1613.3
114	36.7	.05	.1867	1626.8
119.75	36.9	.06	.1769	1635.8

TABLE III.24.   PH 8.5, 0.1 M KNO3

| | ACID | | | SOLIDS | CONCENTRATION, UMOL/L | | | | |
| TIME | ADDED | VOL. | | CONC. | | | | | |
HR.	ML.	L.	PH	G/L	MG-T	SI-T	(OH-)	CA-CB	Q
0	0	.2	7.598	10	0	0	.5102	0	
2.7	1.7	.1937	8.506	9.916	244.3	19.77	4.135	425.6	-58.5
12.58	4.7	.1887	8.456	9.765	309	32.59	3.680	724.1	110.4
26.58	7	.183	8.340	9.647	357.5	49.77	2.816	956.2	244.9
48.33	8.9	.1769	8.378	9.547	403.3	54.41	3.080	1152.	349.3
60.42	9.3	.1693	8.351	9.526	451.8	63.43	2.893	1195.	294.9
70.5	9.3	.1613	8.490	9.526	486.8	71.17	3.977	1195.	226.1
85.17	9.5	.1575	8.446	9.285	503	54.54	3.596	1218.	216.3
95.42	9.5	.1455	8.319	9.526	524.6	52.3	2.687	1218.	172.1
109.8	9.8	.1378	8.437	9.507	540.7	91.87	3.526	1256.	180.1
120	9.8	.1298	8.302	9.507	538	96.52	2.585	1256.	184.7

TABLE III.24A.   PH 8.5, 0.1 M KNO3

| | ACID | SAMPLE | | |
| TIME | ADDED | WITHDR | VOL. | CA-CB |
HR.	ML	L	L	UMOL/L
0	0		.2	0
1	.8		.2008	251.79
2	1.2		.2012	376.94
2.7	1.7	.008	.1937	425.58
4	2.5	.008	.1945	506.09
7	3.6	.008	.1956	615.72
10	4.4	.008	.1964	694.68
12.583	4.7	.016	.1887	724.12
16	5.4	.016	.1894	795.37
20	6.1	.016	.1901	866.08
24	6.7	.016	.1907	926.28
26.583	7	.024	.183	956.24
30	7.1	.024	.1831	966.64
36	7.8	.024	.1838	1039.1
42	8.3	.024	.1843	1090.6
48.833	8.9	.032	.1769	1151.9
54	9.1	.032	.1771	1173.2
60.417	9.3	.04	.1693	1194.5
66	9.3	.04	.1693	1194.5
72.5	9.3	.048	.1613	1194.5
78	9.3	.048	.1613	1194.5
85.167	9.5	.056	.1535	1217.7
90	9.5	.056	.1535	1217.7
95.417	9.5	.064	.1455	1217.7
102	9.6	.064	.1456	1230.6
109.83	9.8	.072	.1378	1256.4
114	9.8	.072	.1378	1256.4
119.75	9.8	.08	.1298	1256.4

TABLE III.25. PH 9, 0.1 M KNO3

| | ACID | | | SOLIDS | CONCENTRATION, UMOL/L | | | | |
| TIME | ADDED | VOL. | | CONC. | | | | | |
HR.	ML	L	PH	G/L	MG-T	SI-T	(OH-)	CA-CB	Q
0	0	.2	9.444	10	0	0	35.83	-27.8	
5	6.5	.1965	9.027	9.685	257.6	26.64	13.71	449.8	-42.1
13	9.9	.1899	8.993	9.520	314.5	50.31	12.67	612.2	14.00
24.5	12.1	.1821	9.005	9.411	362.5	77.51	13.03	719.7	35.66
48.15	14.1	.1741	8.996	9.309	426.1	133.3	12.77	820.5	29.08
72	15.1	.1651	9.001	9.256	484.1	183.2	12.92	873.0	-16.4
97	16	.156	8.993	9.206	523.6	209.3	12.67	922.5	-36.7
120.2	16.7	.1467	9.005	9.165	575.5	243.9	13.03	963	-87.2

TABLE III.25A. PH 9, 0.1 M KNO3

| | ACID | SAMPLE | | |
| TIME | ADDED | WITHDR | VOL. | CA-CB |
HR.	ML	L	L	UMOL/L
0	0		.2	-27.8
1	3.3		.2033	134.97
2	5.2		.2052	387.13
3.5	5.6	.01	.1956	405.84
5	6.5	.01	.1965	449.78
7	7.7	.01	.1977	507.75
10	9	.01	.199	569.76
13	9.9	.02	.1899	612.21
16	10.6	.02	.1906	646.69
20	11.4	.02	.1914	685.79
24.5	12.1	.03	.1821	719.73
30	12.8	.03	.1828	755.26
36	13.2	.03	.1832	775.45
42	13.7	.03	.1837	800.56
48.15	14.1	.04	.1741	820.54
54	14.5	.04	.1745	841.59
60	14.8	.04	.1748	857.30
66	14.9	.04	.1749	862.53
72	15.1	.05	.1651	872.97
78	15.2	.05	.1652	878.49
84	15.5	.05	.1655	895.03
90	15.7	.05	.1657	906.02
97	16	.06	.156	922.45
102	16.2	.06	.1562	934.08
108	16.5	.06	.1565	951.45
114	16.5	.06	.1565	951.45
120.17	16.7	.07	.1467	963.00
127	17.1	.07	.1471	987.58

TABLE III.26. PH 9.5, 0.1 M KNO3

TIME HR.	ACID ADDED ML	VOL. L	PH	SOLID G/L	CONCENTRATION, UMOL/L				
					MG-T	SI-T	(OH-)	CA-CB	Q
0	0	.2	7.696	10	0	0	.6400	0	
2.25	1.5	.1915	9.510	9.926	230.8	14.75	41.68	74.44	-340.
6.58	2.8	.1828	9.509	9.859	274.9	16.55	41.57	141.4	-361.
11.92	2.8	.1728	9.503	9.859	279.8	21.96	41.02	141.4	-369.
22.08	1.8	.1629	9.479	9.853	301	28.81	38.81	83.98	-469.
48	-.2	.1531	9.420	9.841	356.5	66.6	33.86	-39.3	-694.
77.83	-.53	.1434	9.487	9.822	402.5	102.2	39.51	-61.0	-790.
97.83	-.83	.1337	9.493	9.801	404.9	121.6	40.11	-82.1	-808.

TABLE III.27. PH 10, 0.1 M KNO3

TIME HR.	BASE ADDED ML	VOL. L	PH	SOLIDS CONC. G/L	CONCENTRATION, UMOL/L				
					MG-T	SI-T	(OH-)	CB-CA	Q
0	0	.2	10.06	10	0	0	146.3	146.3	
1.42	.35	.19	10.08	10	163.4	15.77	153.8	321.3	-479.
4	.33	.18	10.06	10	197.0	41.51	147.1	310.8	-526.
11.3	.41	.17	10.05	10	223.4	93.72	144.3	355.2	-591.
21.55	.59	.161	10.04	10	239.5	168.8	141.6	461.1	-684.
49.55	.91	.151	10.04	10	280.0	285.4	140.7	659.8	-889.
96.05	1.41	.141	10.04	10	303.5	326.9	140.7	991.0	-1239

TABLE III.27A. PH 10, 0.1 M KNO3

TIME HR.	BASE ADDED ML	SAMPLE WITHDR L	VOL. L	CA-CB UMOL/L
0	0		.2	146.29
1.42	.36	.01	.19036	325.70
3	.32	.01	.19032	304.75
4	.32	.02	.18032	304.75
6	.32	.02	.18032	304.75
7.5	.35	.02	.18035	321.34
9	.35	.02	.18035	321.34
11.3	.41	.03	.17041	354.49
15	.44	.03	.17044	372.03
18	.51	.03	.17051	412.93
21.55	.59	.04	.16059	459.63
24	.62	.04	.16062	478.22
30	.71	.04	.16071	533.96
36	.78	.04	.16078	577.26
42	.83	.04	.16083	608.17
49.55	.91	.05	.15091	657.59
54	.93	.05	.15093	670.75
60	.96	.05	.15096	690.49
72	1.04	.05	.15104	743.09
84	1.15	.05	.15115	815.32
96.05	1.41	.06	.14141	985.64

TABLE III.28   PH 11, 0.1 M KNO3

TIME HR.	BASE ADDED ML	VOL. L	PH	SOLIDS CONC. G/L	CONCENTRATION, UMOL/L				
					MG-T	SI-T	(OH-)	CB-CA	Q
0	0	.2	10.97	10	0	0	1208.	1208.	
1.42	1.2	.1912	10.94	9.940	64.24	53.67	1120.	1797.	-740.
4	1.5	.1815	10.95	9.925	60.82	50.01	1160.	1951.	-851.
11.3	1.9	.1719	10.95	9.903	42.27	163.1	1158.	2166.	-929.
21.55	2.6	.1626	10.96	9.863	30.06	221.0	1164.	2563.	-1243
49.55	4.1	.1541	10.95	9.773	22.25	312.6	1157.	3454.	-2040
96.05	6.8	.1468	10.94	9.604	11.02	486.3	1114.	5116.	-3562

TABLE III.28A.   PH 11, 0.1 M KNO3

TIME HR.	BASE ADDED ML	SAMPLE WITHDR L	VOL. L	CA-CB UMOL/L
0	0		.2	1207.8
1.42	1.2	.01	.1912	1797.0
3	1.4	.01	.1914	1899.6
4	1.5	.02	.1815	1950.9
6	1.6	.02	.1816	2004.9
7.5	1.7	.02	.1817	2058.8
9	1.8	.02	.1818	2112.7
11.3	1.9	.03	.1719	2166.5
15	2.1	.03	.1721	2280.2
18	2.3	.03	.1723	2393.6
21.55	2.6	.04	.1626	2563.2
24	2.7	.04	.1627	2623.1
30	3.1	.04	.1631	2861.9
36	3.4	.04	.1634	3040.3
42	3.7	.04	.1637	3218.0
49.55	4.1	.05	.1541	3453.9
54	4.3	.05	.1543	3579.0
60	4.6	.05	.1546	3766.1
72	5	.05	.155	4014.5
84	5.7	.05	.1557	4446.0
96.05	6.8	.06	.1468	5116.4
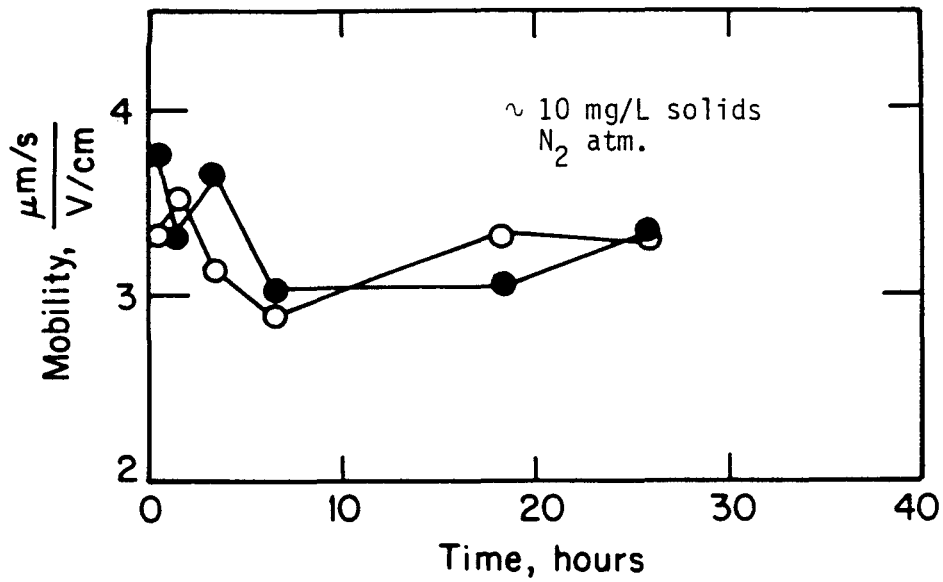
Fig. III.1.   Chrysotile mobility at pH 5 in
             0.01 M KNO$_3$.
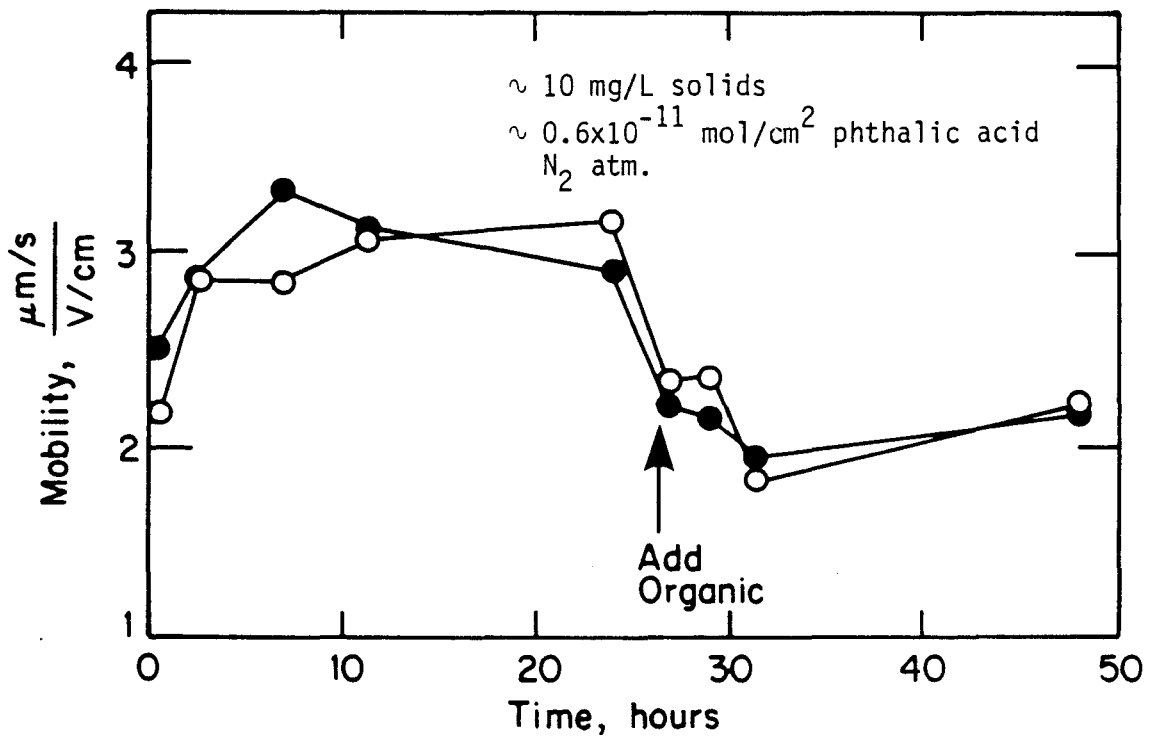
Fig. III.2.   Chrysotile mobility at pH 6 in 0.01 M KNO$_3$.
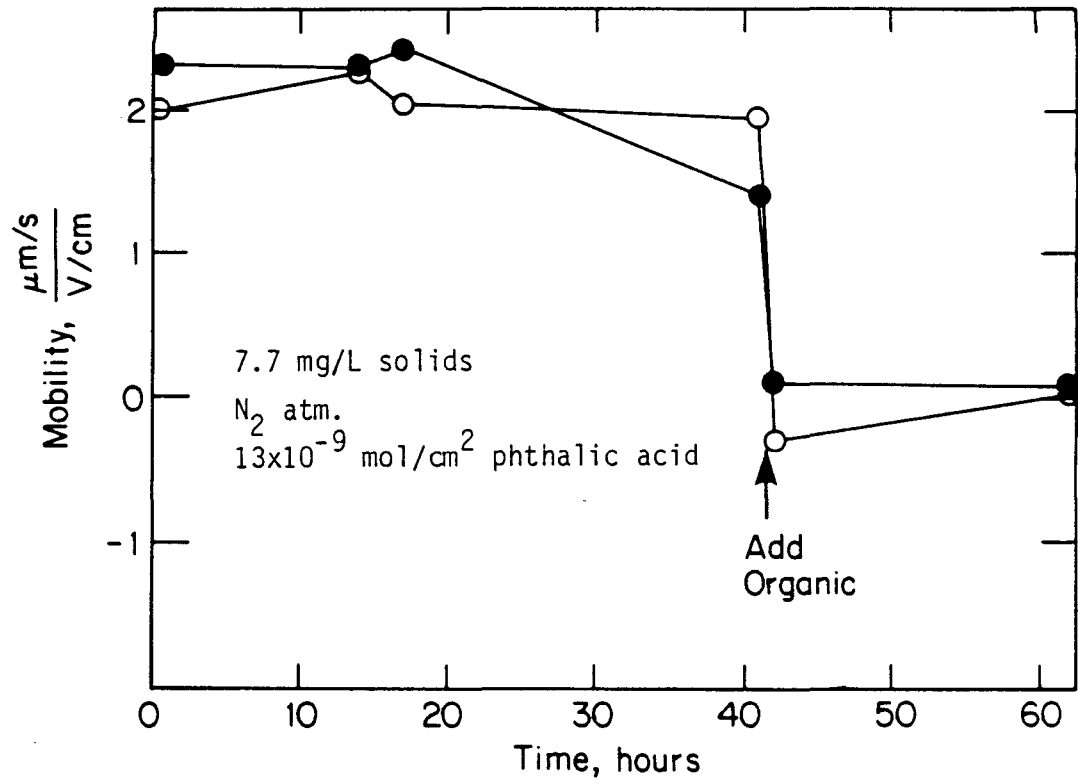
Fig. III.3.   Chrysotile mobility at pH 7.5 in 0.01 M KNO_3.
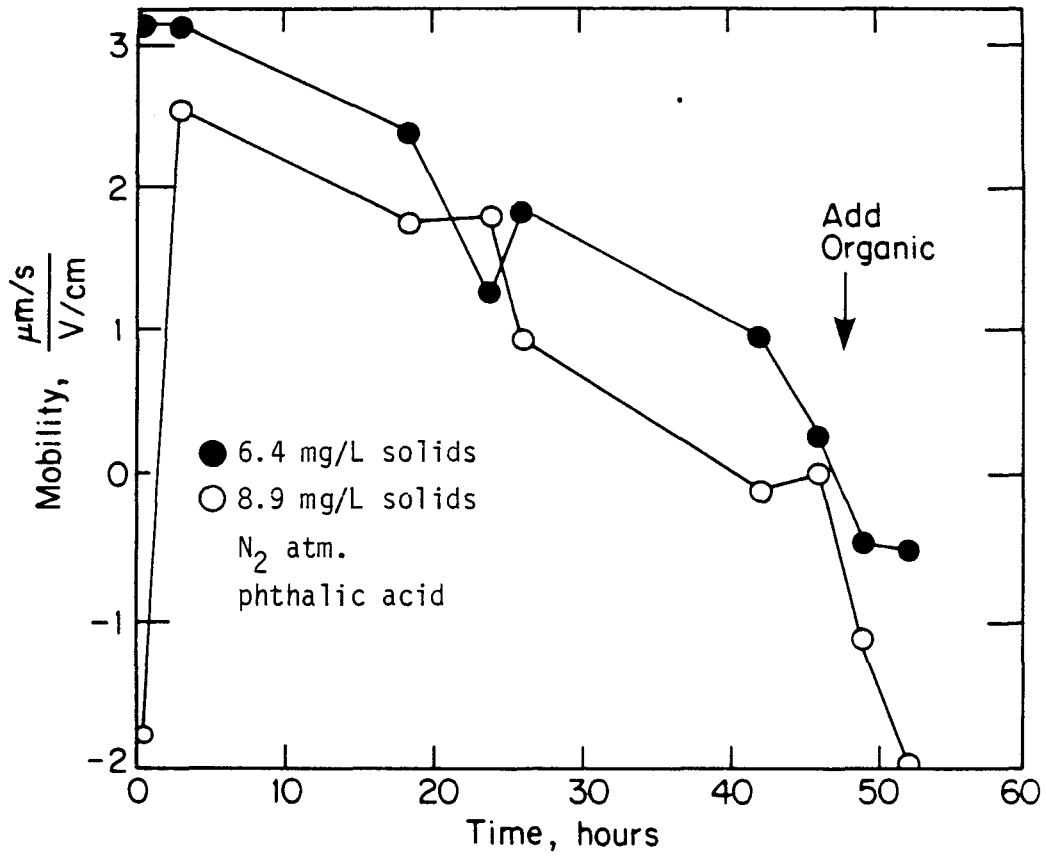
Fig. III.4. Chrysotile mobility at pH 8 in 0.01 M KNO$_3$.
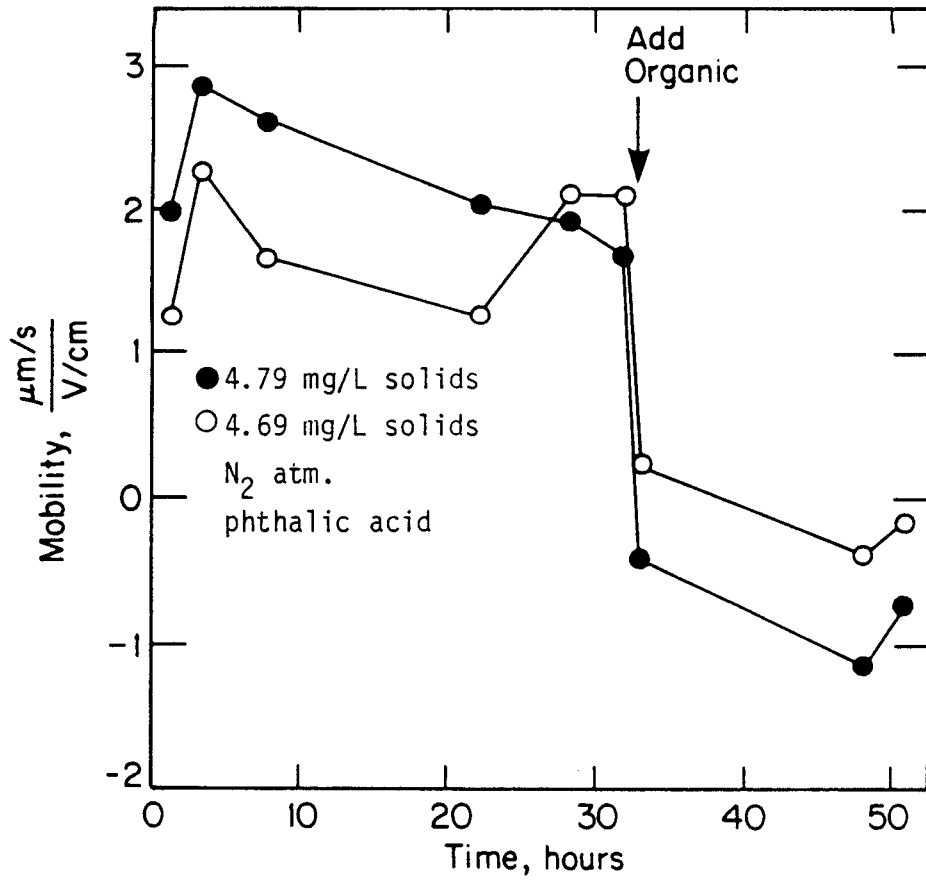
Fig. III.5. Chrysotile mobility at pH 7.5 in
0.01 M KNO₃.
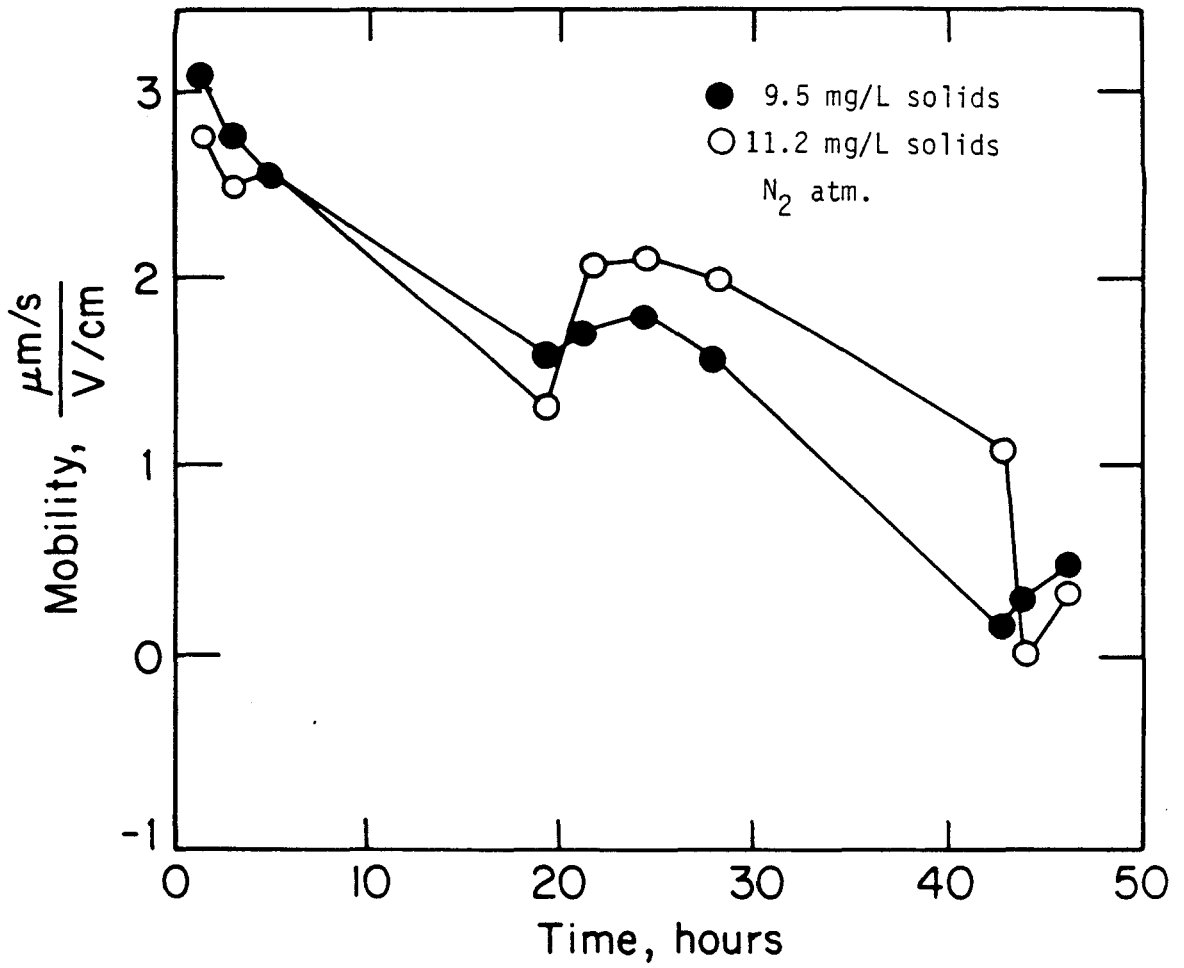
Fig. III.6.   Chrysotile mobility at pH 8.5 in 0.01 M KNO_3.
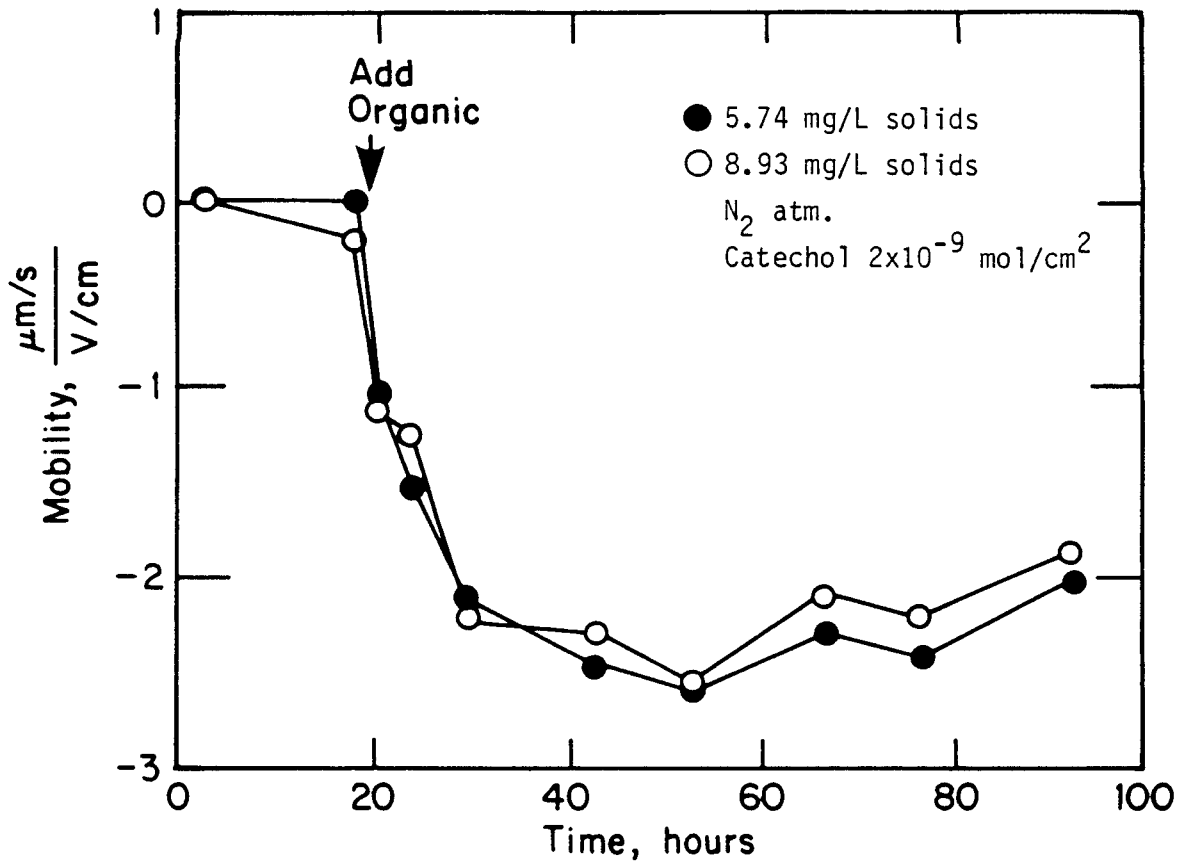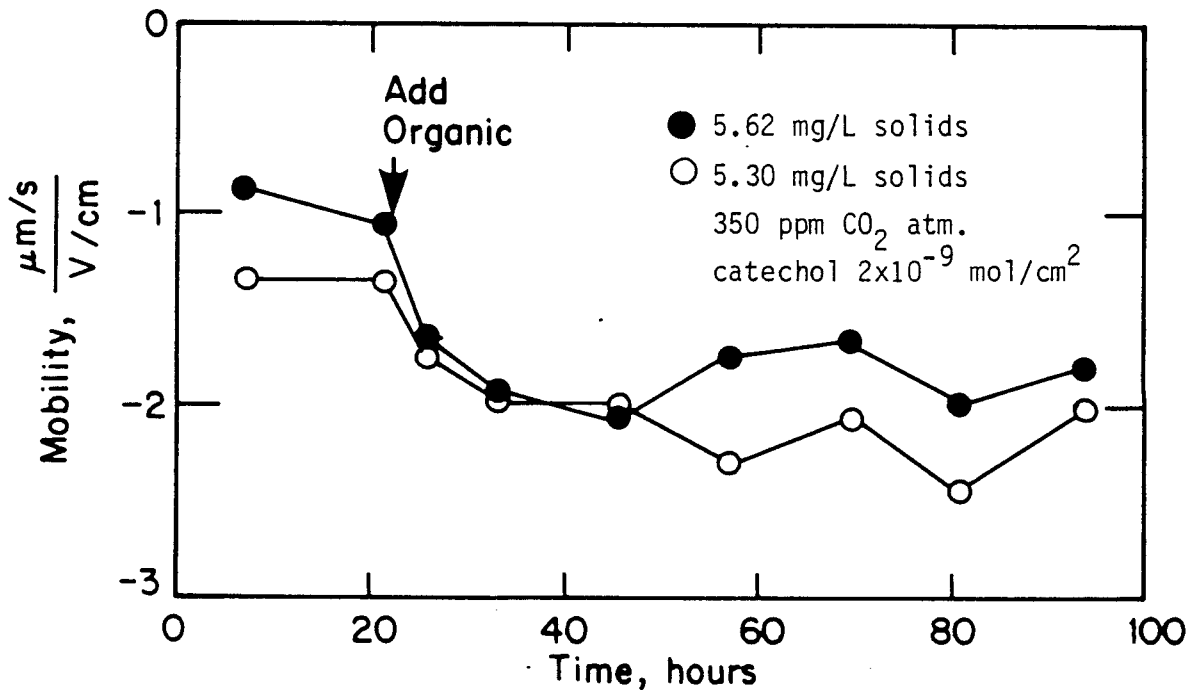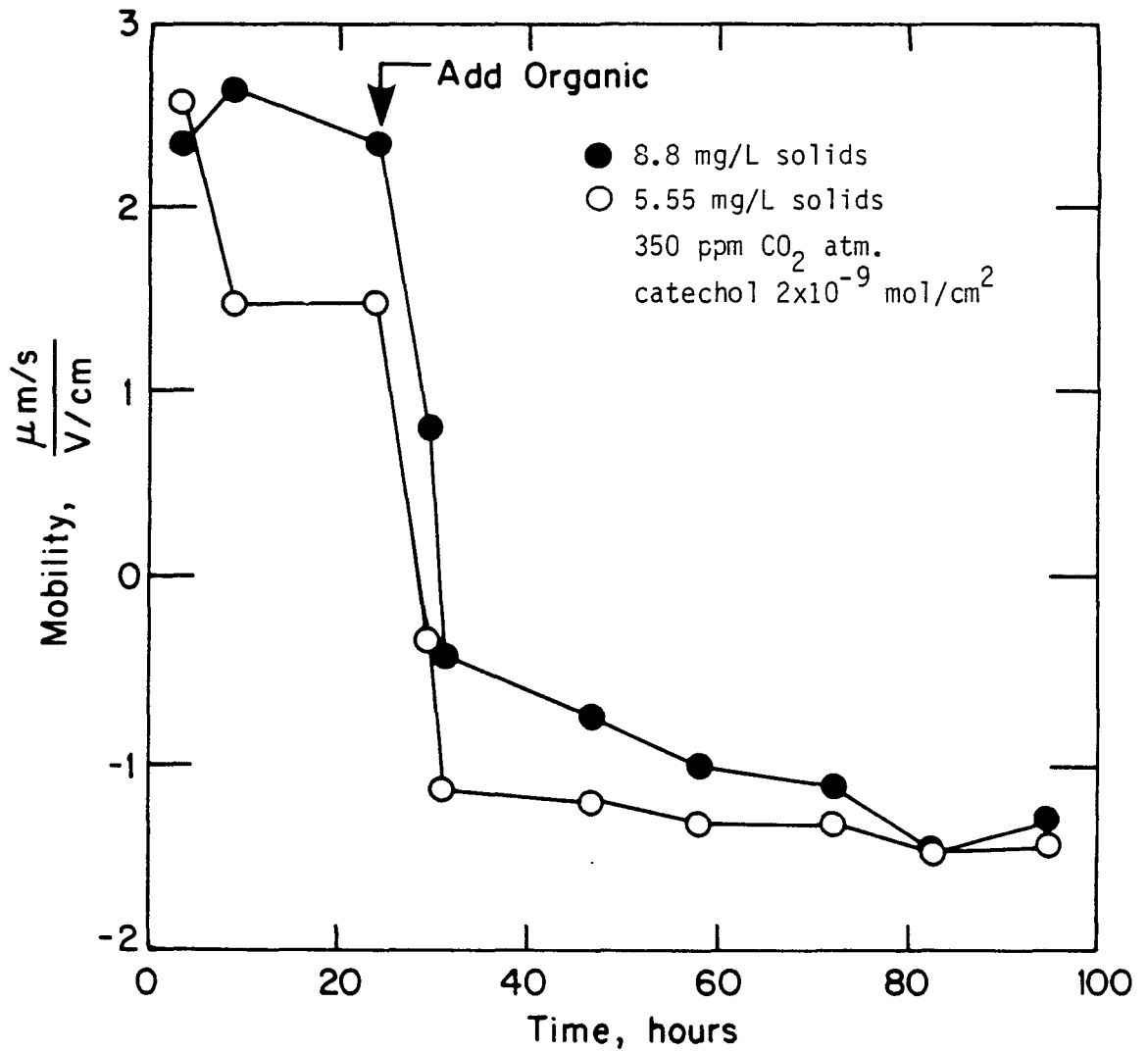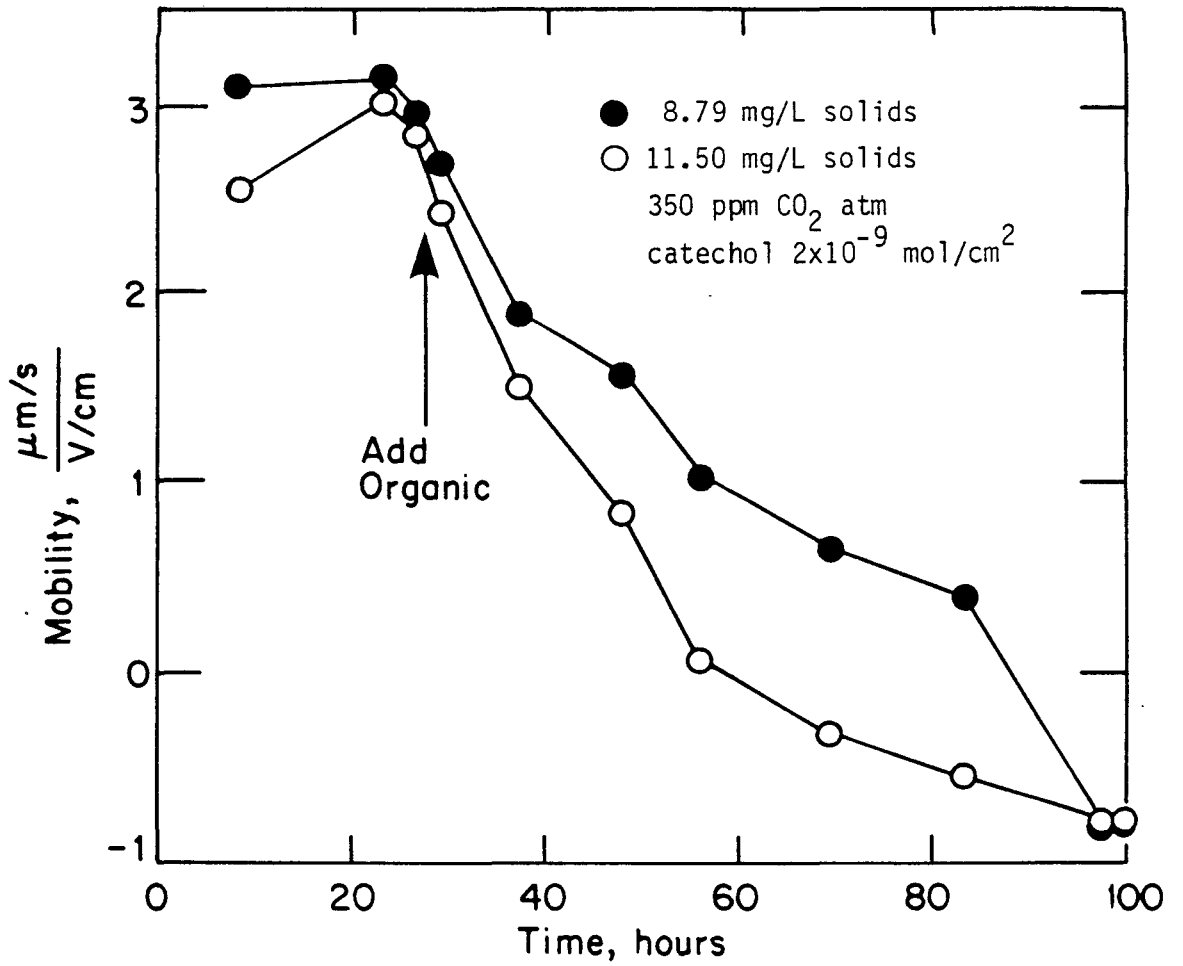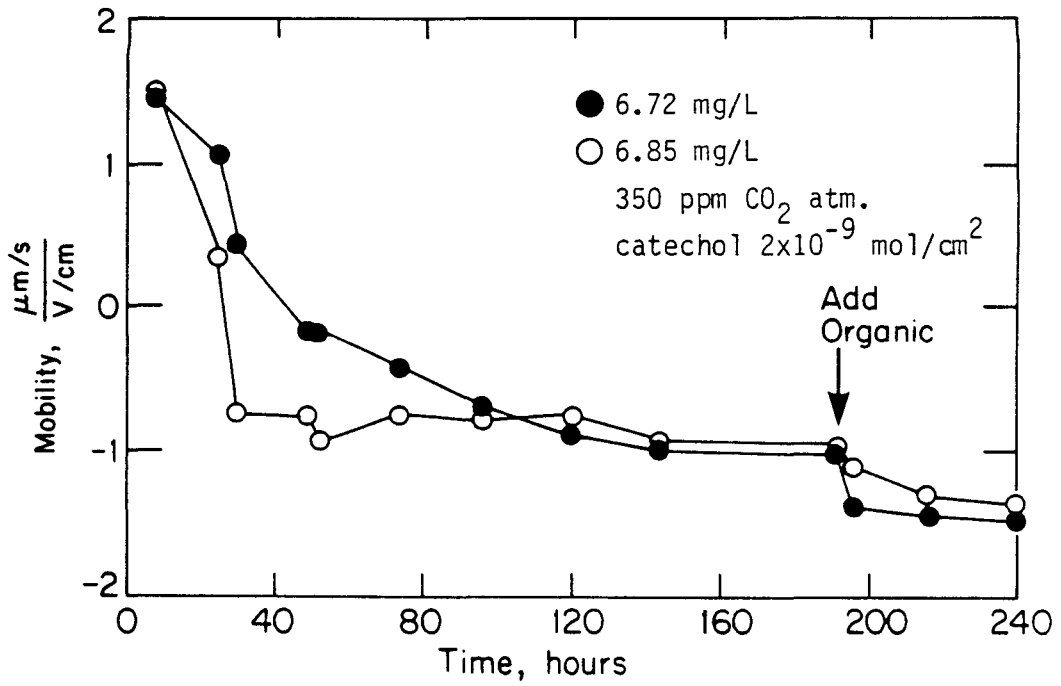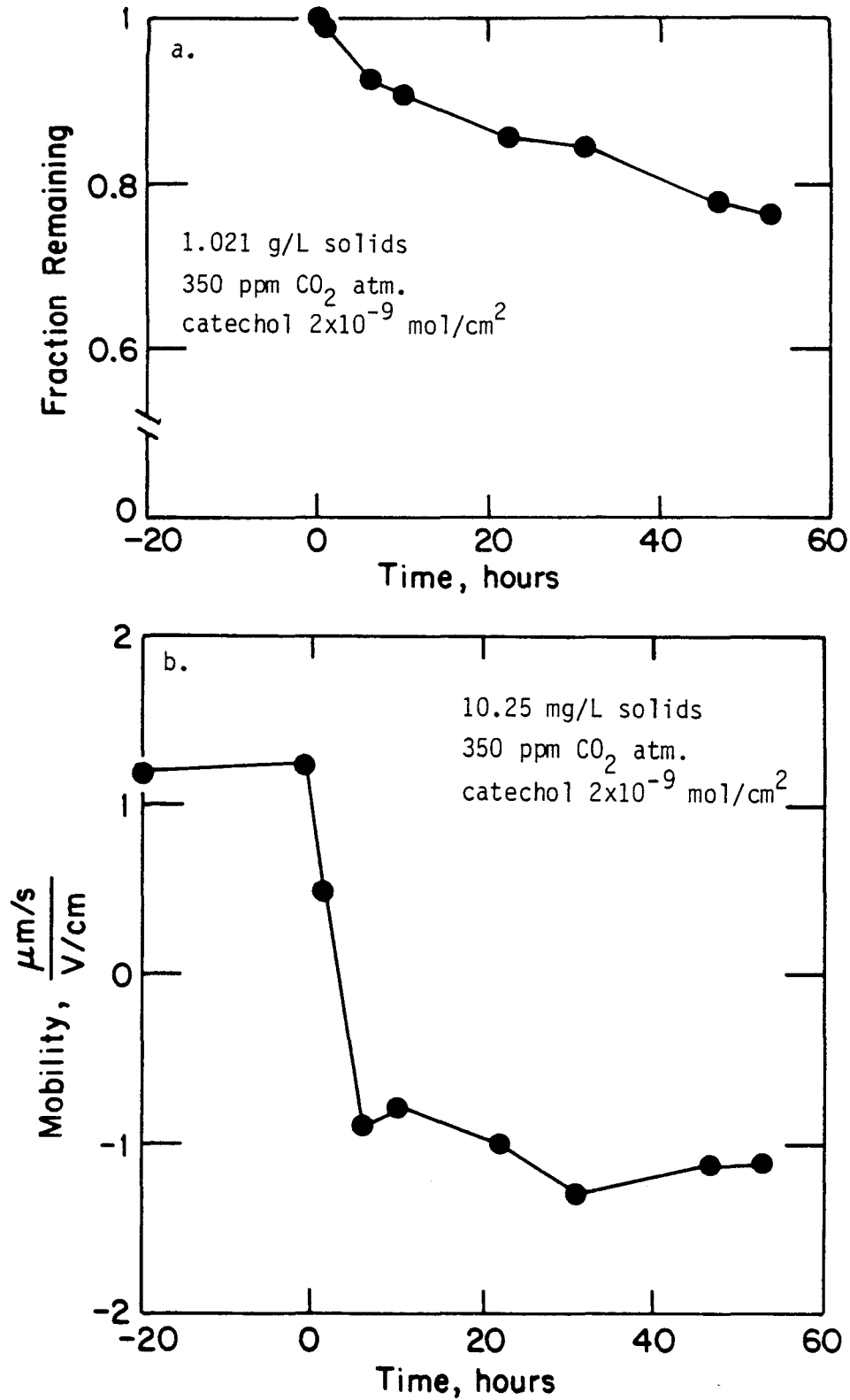
Fig. III.7.   Chrysotile mobility at pH 8 in 0.01 M NaCl.

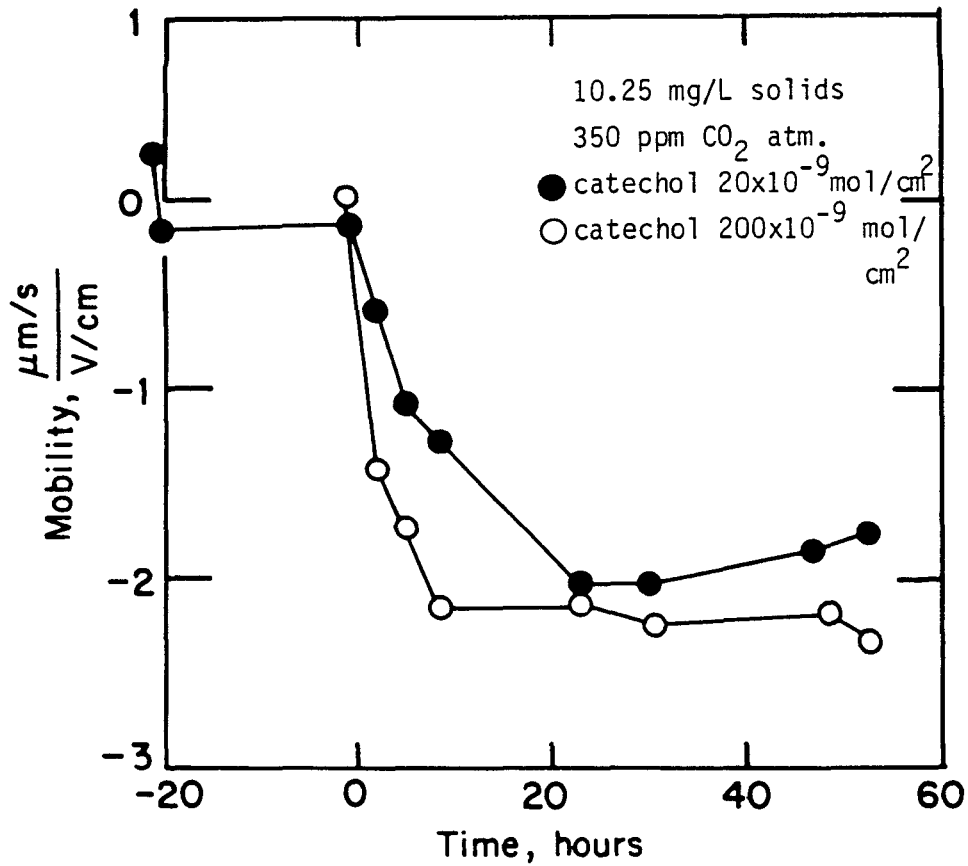Fig. III.8.   Chrysotile mobility at pH 8.2-8.3 in 0.01 M NaCl.

Fig. III.9. Chrysotile mobility at pH 8 in 0.01 M NaCl.

Fig. III.10. Chrysotile mobility at pH 7.5 in 0.01 M NaCl.

Fig. III.11. Chrysotile mobility at pH 8 in 0.01 M NaCl.

Fig. III.12. Chrysotile mobility at pH 8 in 0.01 M
NaCl; a) UV absorbance measurements of
solution concentration; b) mobility.
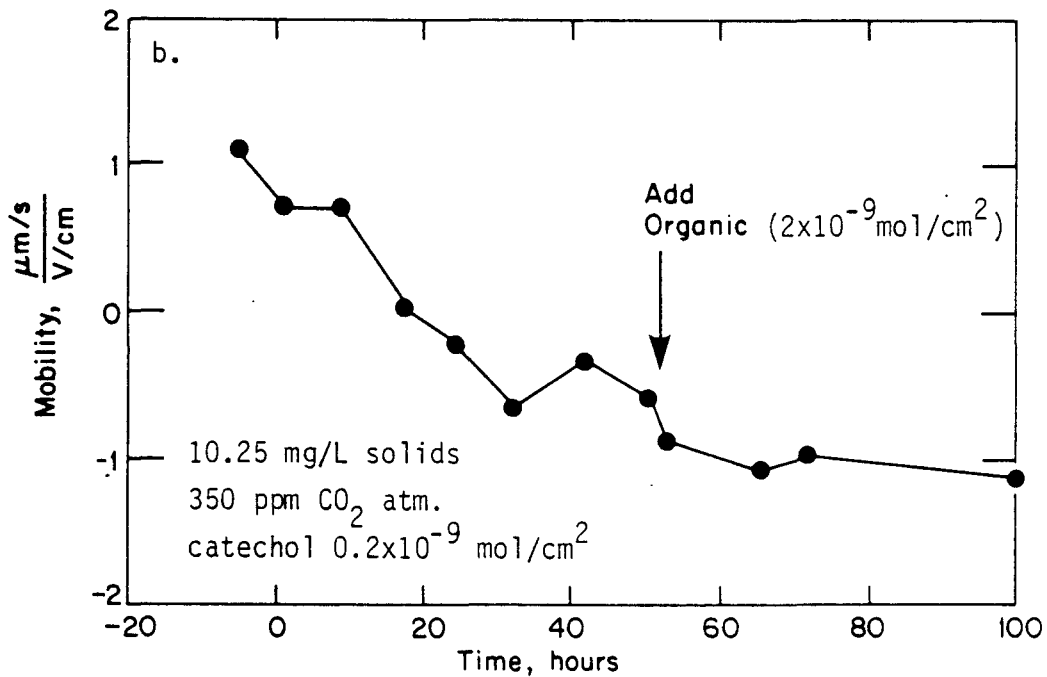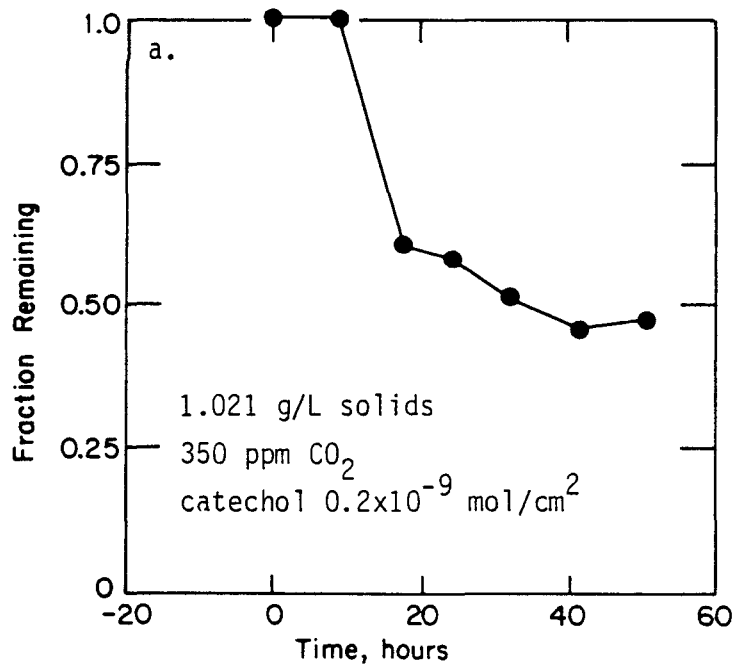
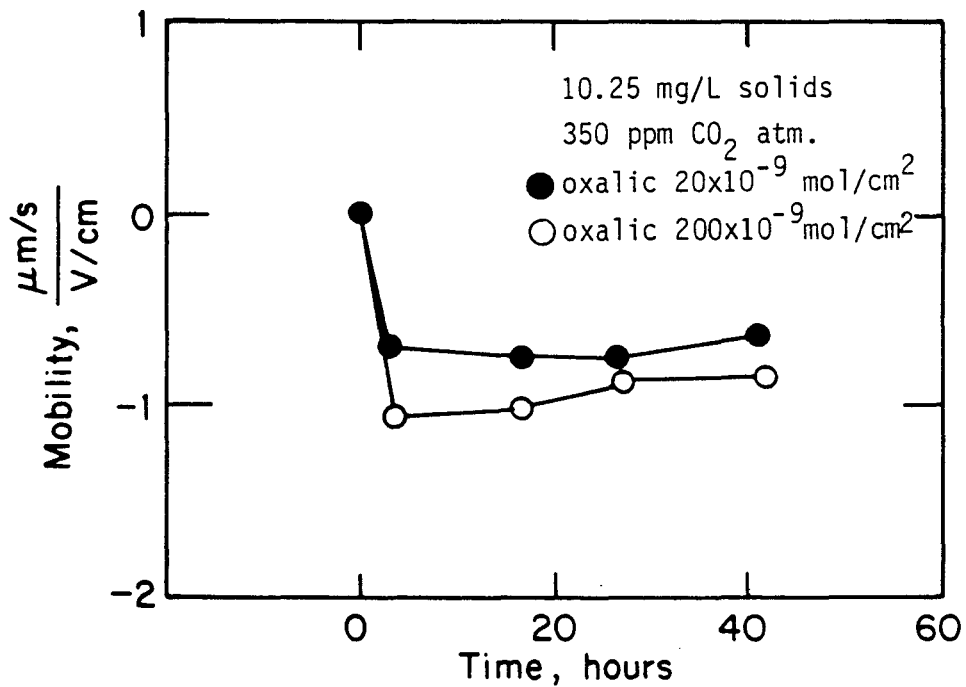Fig. III.13. Chrysotile mobility at pH 8 in 0.01 M NaCl.
a) UV absorbance measurements of solution
concentration;
b) mobility.

Fig. III.14. Chrysotile mobility at pH 8 in 0.01 M NaCl.

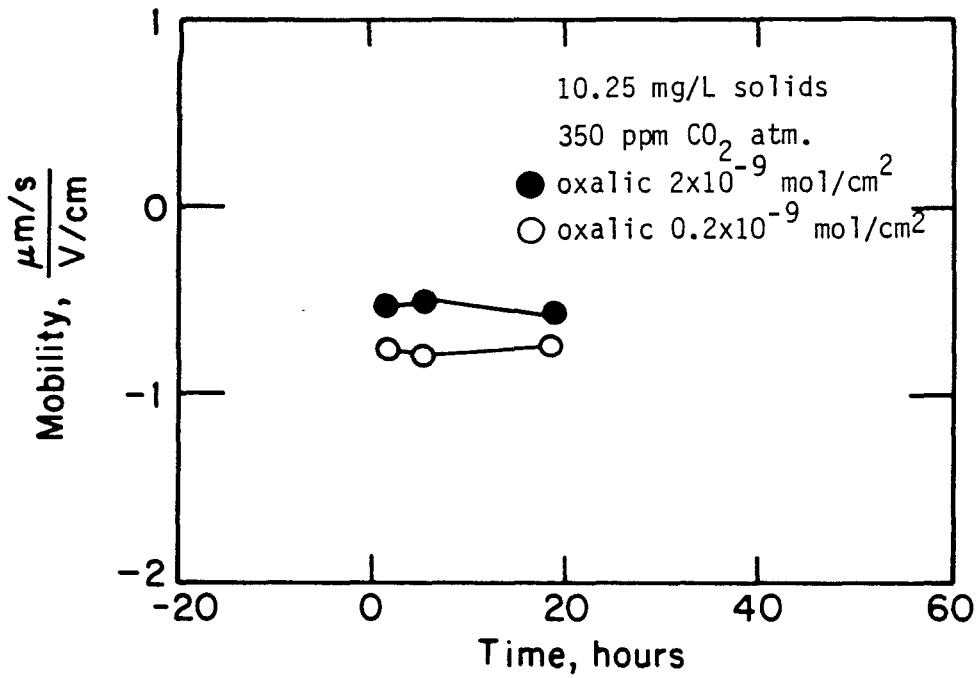Fig. III.15. Chrysotile mobility at pH 8 in 0.01 M NaCl.

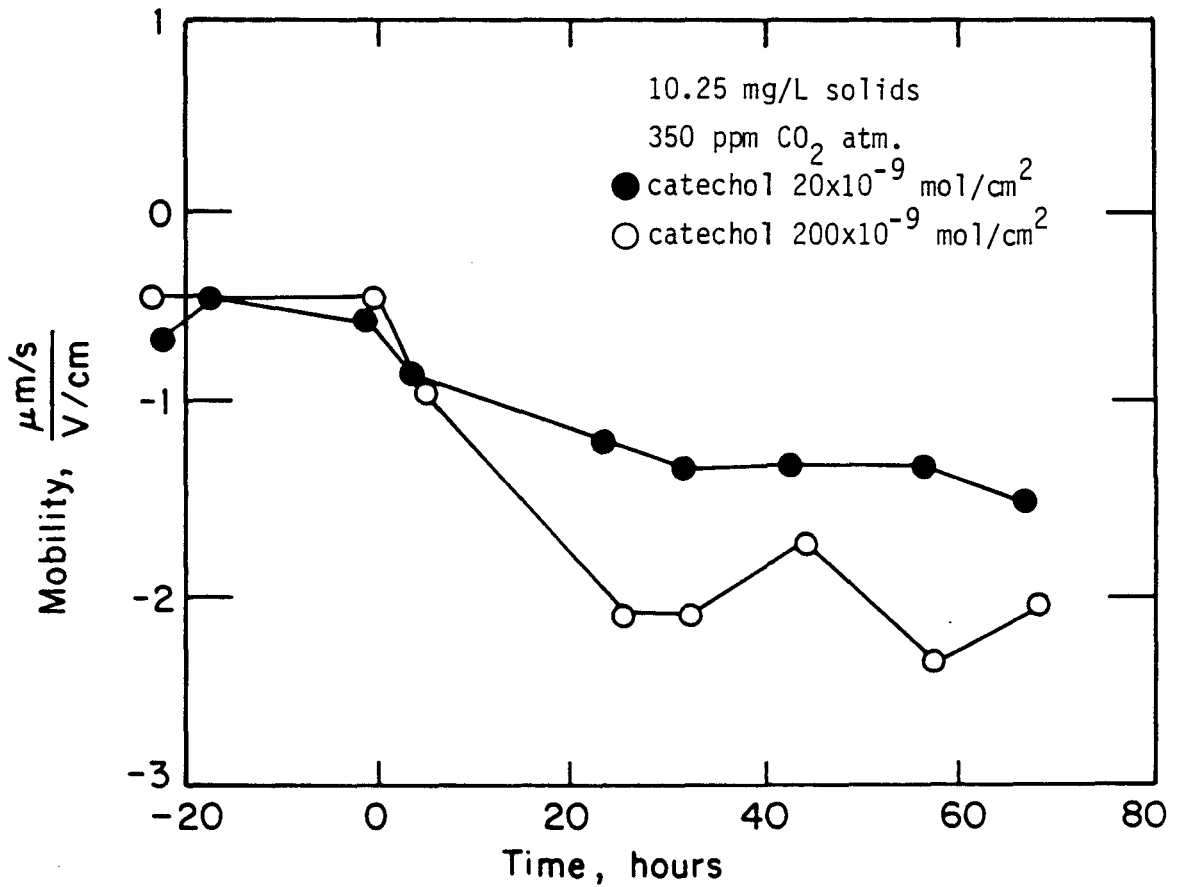Fig. III.16. Chrysotile mobility at pH 8 in 0.01 M NaCl.

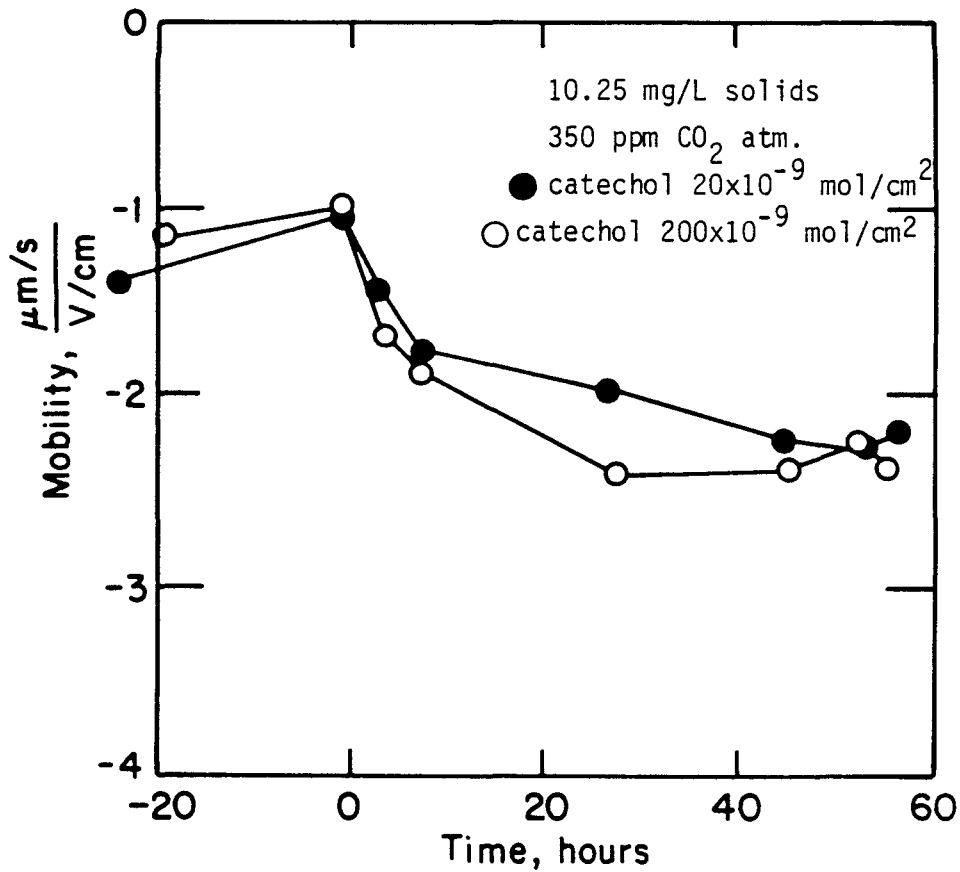Fig. III.17. Chrysotile mobility at pH 7.5 in 0.01 M NaCl.

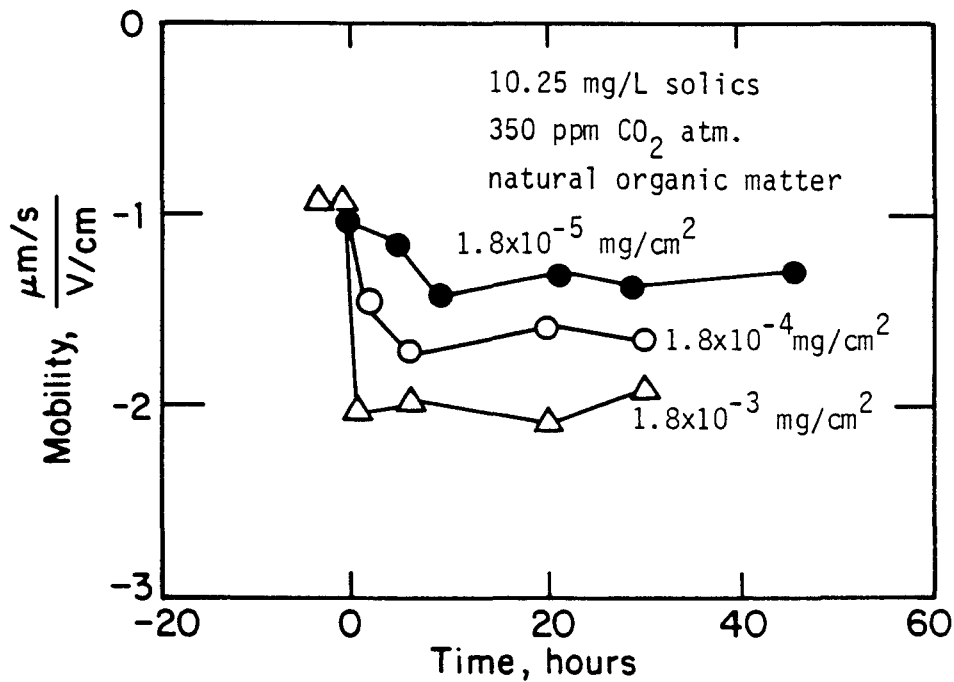Fig. III.18. Chrysotile mobility at pH 8.5 in 0.01 M NaCl.

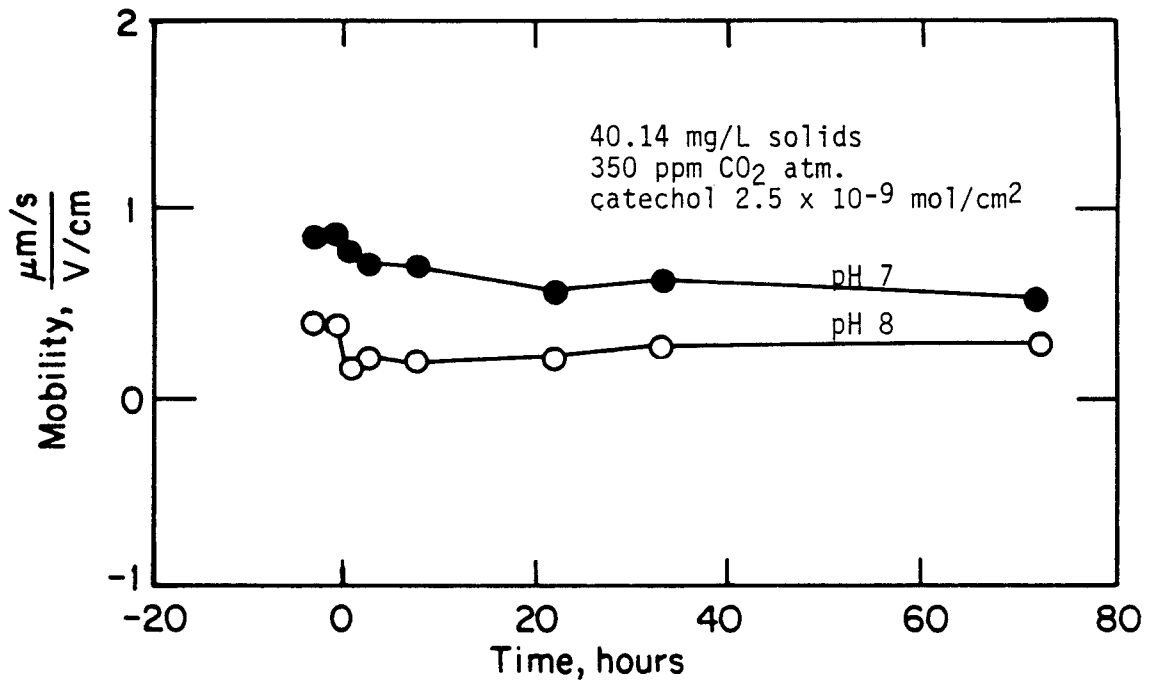Fig. III.19. Chrysotile mobility at pH 8 in 0.01 M NaCl.

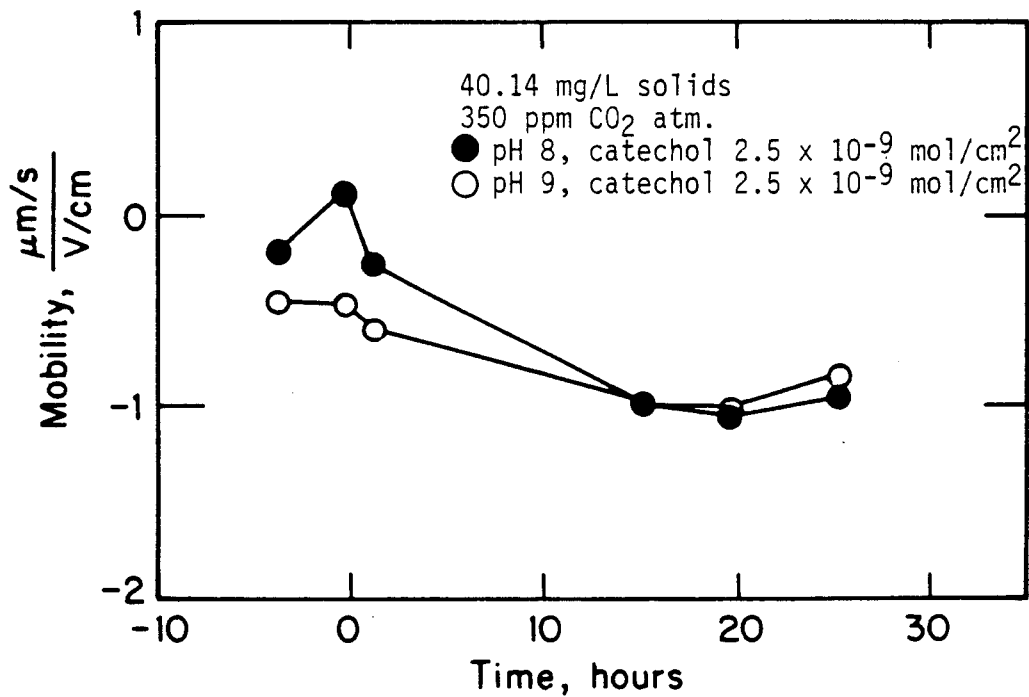Fig. III.20. Alox mobility at pH's 7 and 8 in 0.01 M NaCl.

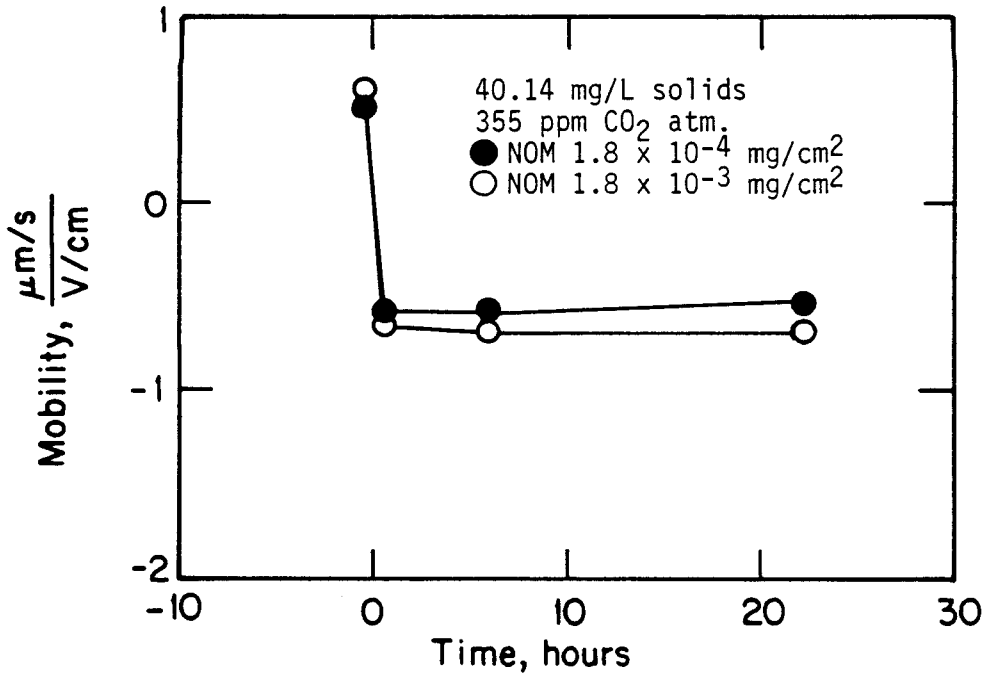Fig. III.21. Alox mobility at pH's 8 and 9 in 0.01 M NaCl.

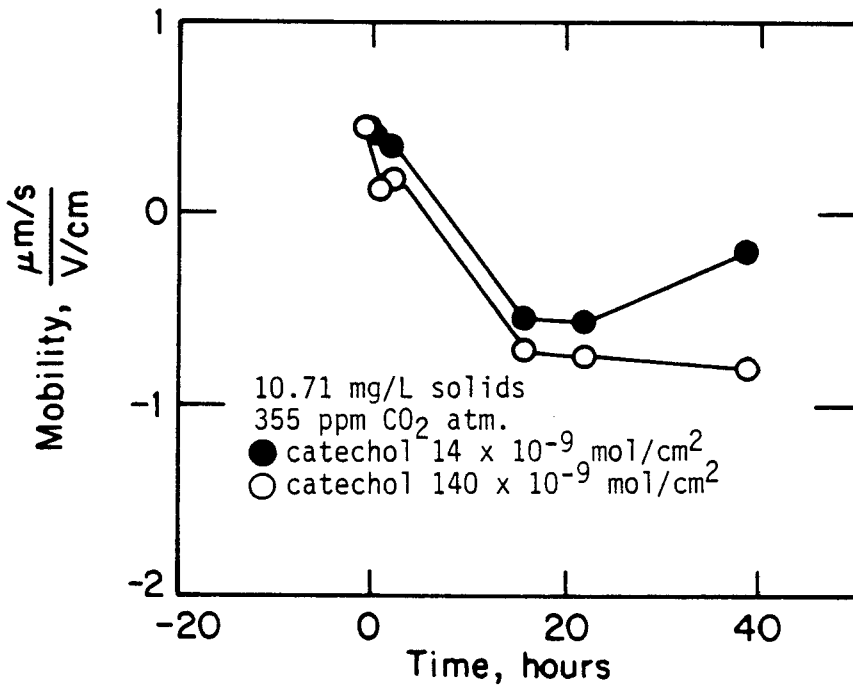Fig. III.22.   Alox mobility at pH 8 in 0.01 M NaCl.

Fig. III.23.   Alox mobility at pH 8 in 0.01 M NaCl.

APPENDIX IV

BRUCITE SURFACE TITRATIONS

A series of initial investigations was undertaken to determine the acid-base behavior of an >Mg-OH surface in a system with no silica present. These preliminary experiments were also designed to test the applicability of rapid acid-base titrations of the sort commonly used on >Fe-OH, >Al-OH, >Zn-OH, >Ti-OH and >Si-OH surfaces. It was hoped that results of these experiments should be used to predict the behavior of >Mg-OH sites on chrysotile.

Model

A constant-capacitance model of the surface was used to predict and interpret surface equilibria. Relations used are as follows:

$$K_{a1}{}^S = \frac{\{>Mg\text{-}OH\}\,[H^+]}{\{>Mg\text{-}OH_2{}^+\}}\;e^{-e\psi/kT} \tag{IV.1}$$

$$K_{a2}{}^S = \frac{\{>Mg\text{-}O^-\}\,[H^+]}{\{>Mg\text{-}OH\}}\;e^{-e\psi/kT} \tag{IV.2}$$

$$S_T = \{>Mg\text{-}OH_2\} + \{>Mg\text{-}OH^+\} + \{>Mg\text{-}O^-\} \tag{IV.3}$$

$$\sigma = F(\{>Mg\text{-}OH_2{}^+\} - \{>Mg\text{-}O^-\}) \tag{IV.4}$$

$$c = \sigma/\psi$$

$$\{Mg\text{-}OH_2\}^+ sa + [H^+] + C_B + [Mg^{2+}] + [MgOH^+] = \{>Mg\text{-}O^-\}sa + [OH^-] + C_A \tag{IV.5}$$

$$*K_{so} = \frac{[Mg^{2+}]}{[H^+]^2} \tag{IV.6}$$

$$^*K_1 = \frac{[MgOH^+][H^+]}{[Mg^{2+}]} \qquad (IV.7)$$

Surface concentrations are in mol/cm^2, σ is surface charge in $coul/cm^2$ and sa is the surface area concentration in cm^2/L. The electroneutrality condition (IV.5) includes dissolved magnesium species, given by (IV.6) and (IV.7). Otherwise terms have their standard definitions (Stumm & Morgan, 1981).

Materials and Methods

Titrations were done at 25 C in jacketed glass beakers through which nitrogen gas was bubbled to exclude carbon dioxide. This gas was first passed through a 1.0 M NaOH solution and two distilled water rinses to remove carbon dioide and humidify the gas. The electrolyte was reagent-grade 0.1 M KNO_3, which was filtered through a 0.22 μm Millipore filter prior to use. KOH and HNO_3 used to maintain constant pH were made from Dilut-it ampoules (J. T. Baker). Initial electrolyte OH^- concentrations were made by combining appropriate volumes of 0.1 M KNO_3 and 0.1 M KOH to make 500 ml of solution. The meter was calibrated against known OH^- concentrations, made by dilution of the KOH reagent.

The source of particles was $Mg(OH)_2$ powder from MC/B Chemicals. Atomic absorption spectrophotometry (AAS) analysis of three solutions of this powder gave a magnesium content that was 99.5 percent of that of a pure $Mn(OH)_2$ powder. Surface area determined by BET nitrogen adsorption was 45 m^2/g. Surface site density (S_T) was estimated to be 12 ion/mm^2, or 2×10^{-9} mol/cm^2.

Dissolved magnesium concentrations during these experiments were determined by AAS on 15 ml samples withdrawn and filtered through 0.22 μm Millipore filters that had been previously washed with acid and deionized distilled water.

Initial solutions (p^COH near 2.2) were allowed to equilibrate, $Mg(OH)_2$ powder was added, raising the p^COH to a value from 2.7-3.2, and allowed to equilibrate for 45 minutes. The suspension was then titrated with base to a p^COH of approximately 2.3. The suspension was then titrated with acid to a p^COH near 3. Acid and base additions were made at two minute intervals. The time required to reach a steady pH-meter reading between each titrant addition varied from 10 minutes at low p^COH to several hours at the higher p^COH's studied, however drifts were generally less than 0.1 mv per minute after about four minutes time. Only fast-titration adsorption and dissolution were studied in these experiments.

Experimental Results

Figure IV.1 shows fast-titration curves for a series of four experiments done with different solids concentrations. The observed small differences between forward and reverse titrations in each experiment are expected, as the system was not allowed to equilibrate at each step. Both adsorption of protons and dissolution of the particle may account for the difference. In the absence of dissolution, the four sets of data should yield a single curve. As Figure IV.2 illustrates, three sets of data fall close together and the fourth set, for 40 g/L, falls further away. Only the base-titration points are plotted. Difference in surface charge at a given p^COH are approximately ± 25 percent of the range measured, and
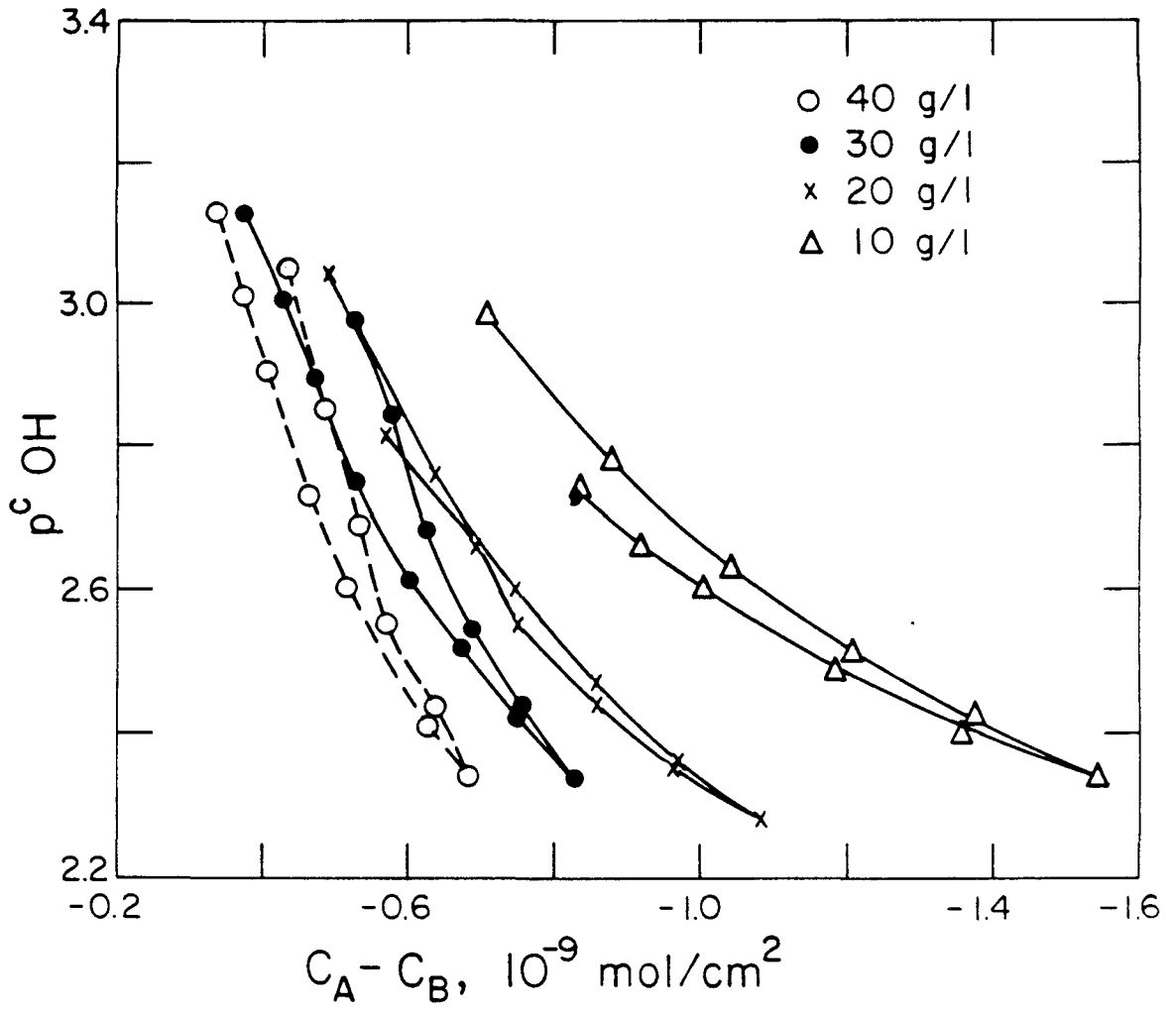
Fig. IV.1. Fast-titration curves of brucite suspensions; 0.1 M KNO_3, 25C, N_2 atm.; forward titration was from high to low p^cOH.
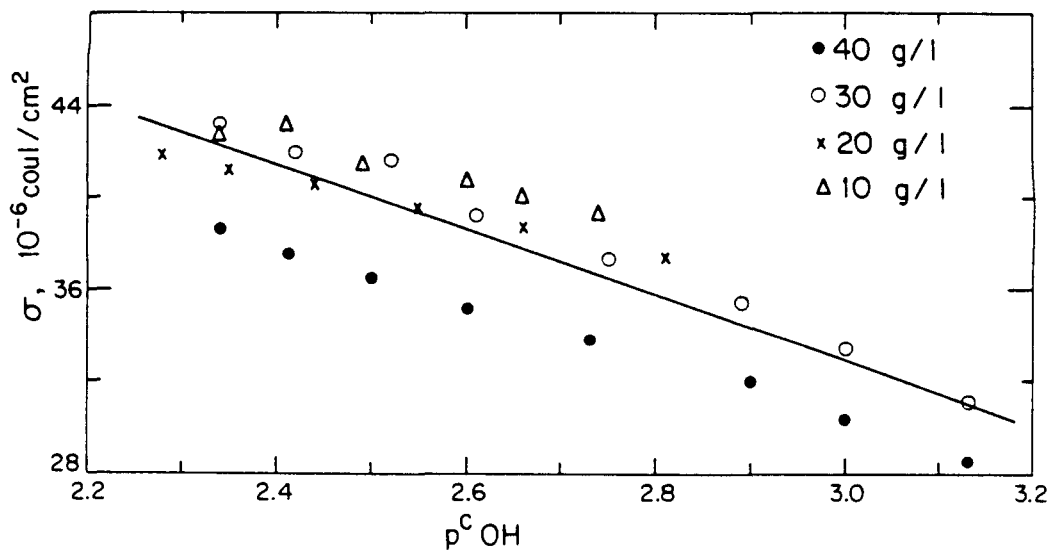
Fig. IV.2. Brucite surface charge as a function of $p^C OH$ for forward titration.
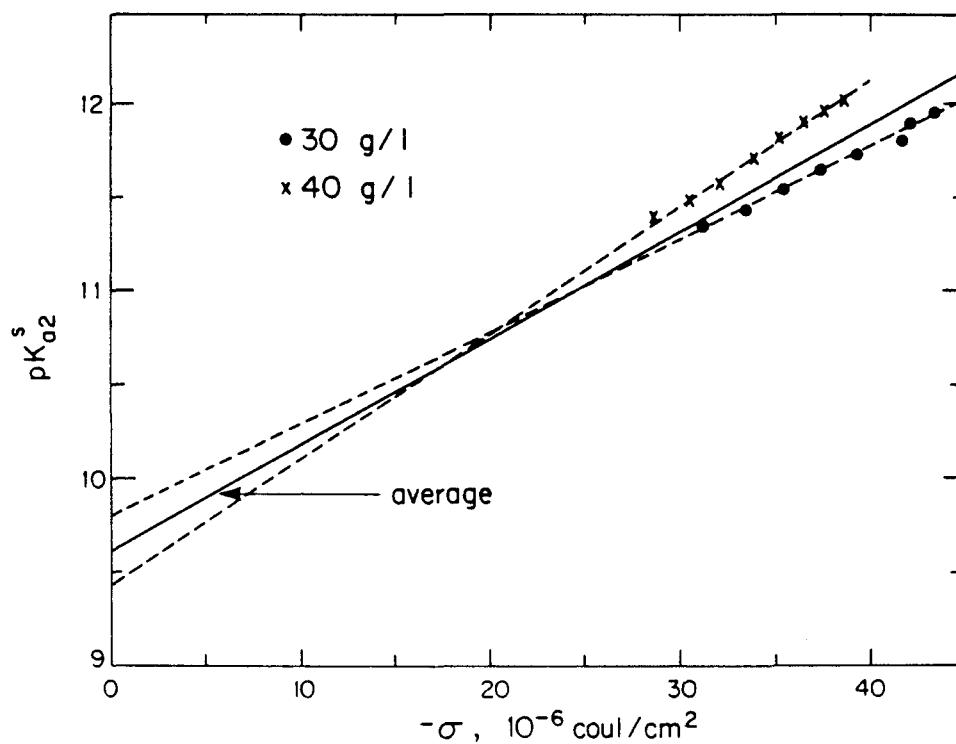
Fig. IV.3. Determination of surface equilibrium constant from forward titration of brucite.

could be due in part to a suspension effect at higher solids
concentration. A second possible error is in the magnitude of soluble
magnesium as measurements were made only at the lower solids
concentrations. K^S_{a2} is estimated to be $10^{-9.6}$ (Figure IV.3) based on
the 30 and 40 g/L data; other data cover a narrower range of surface
charge and no slope is estimated. The capacitance corresponding to
the average curve on Figure IV.3 is 3.1 farads. Model fit to the
titration data using these constants is illustrated on Figure IV.4.
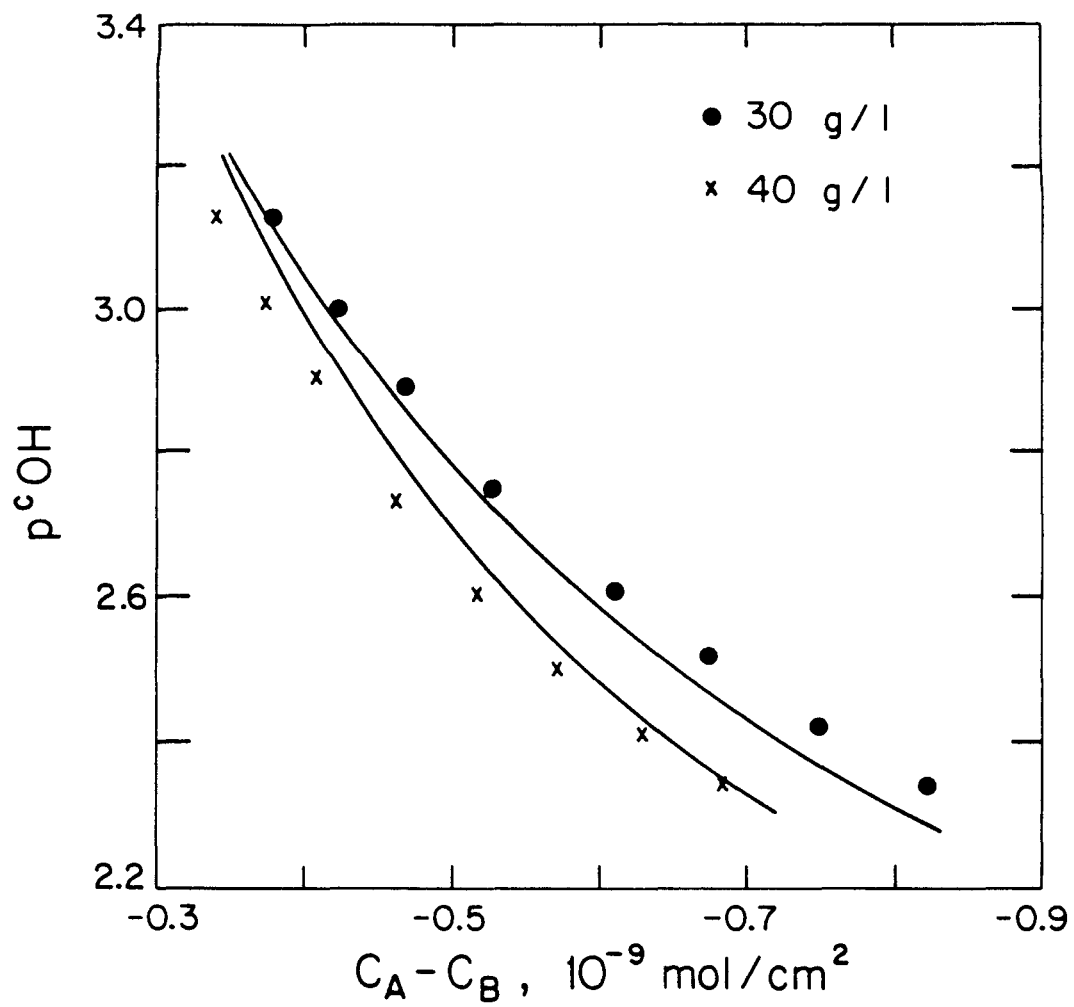
Fig. IV.4. Model fit to data for forward titration of brucite.

APPENDIX V

SCHEMATICS OF EXPERIMENTAL SETUP

AND COMPUTER PROGRAMS FOR EXPERIMENTAL CONTROL

Simple electronic circuits were used to interface pH and autoburette equipment with the Apple II+ computer. Figure V.1 shows the overall schematic that enabled using one of two possible control schemes: a) one pH meter connected to a switching box that allowed sequentially determining the pH in reactors 1 and 2 at about one minute intervals, and b) two pH meters, one connected to each reactor. In the second case, the switching obx was not used and the pH of each was determined at six-second intervals.

Figures V.2 and V.3 are circuit diagrams for the individual components. Section 3.4.1 is a functional description of the experimental setups.

The Apple II+ basic programs used for control are listed in Tables V.1 and V.2. The first program takes data from two pH meters and controls two ABUII autoburettes via the computer's game-paddle outputs. The second program uses the switching box to take data from two reactors with a single pH meter; two autoburettes are controlled via the game-paddle outputs. Slight modifications were necessary to use the John Bell 6522 parallel interface to control the ABUII autoburettes or the Slo-Syn stepping motors driving the micrometer syringes.
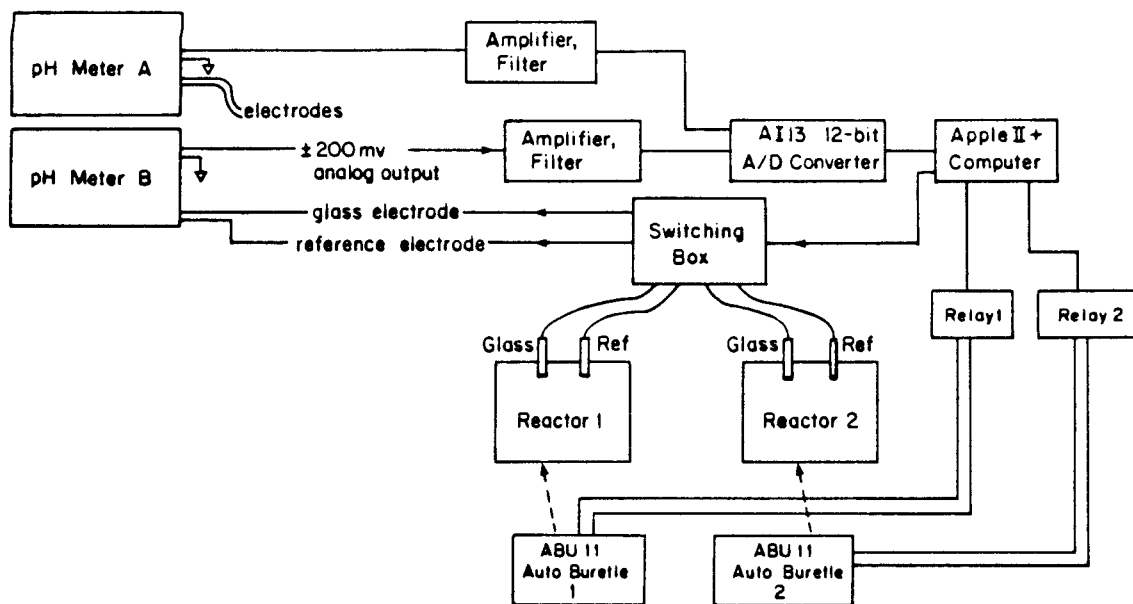
Fig. V.1. Schematic of pH measurement and autoburette control.

$$f_c = \frac{1}{2\pi RC}$$

$$f_c = \frac{1}{2\pi \times 30 \times 10^3 \times 0.1 \times 10^{-6}}$$

$$V_o = \left(1 + \frac{R_A}{1K}\right) V_{in}$$

$R_A \leq 50$ K (adjustable)
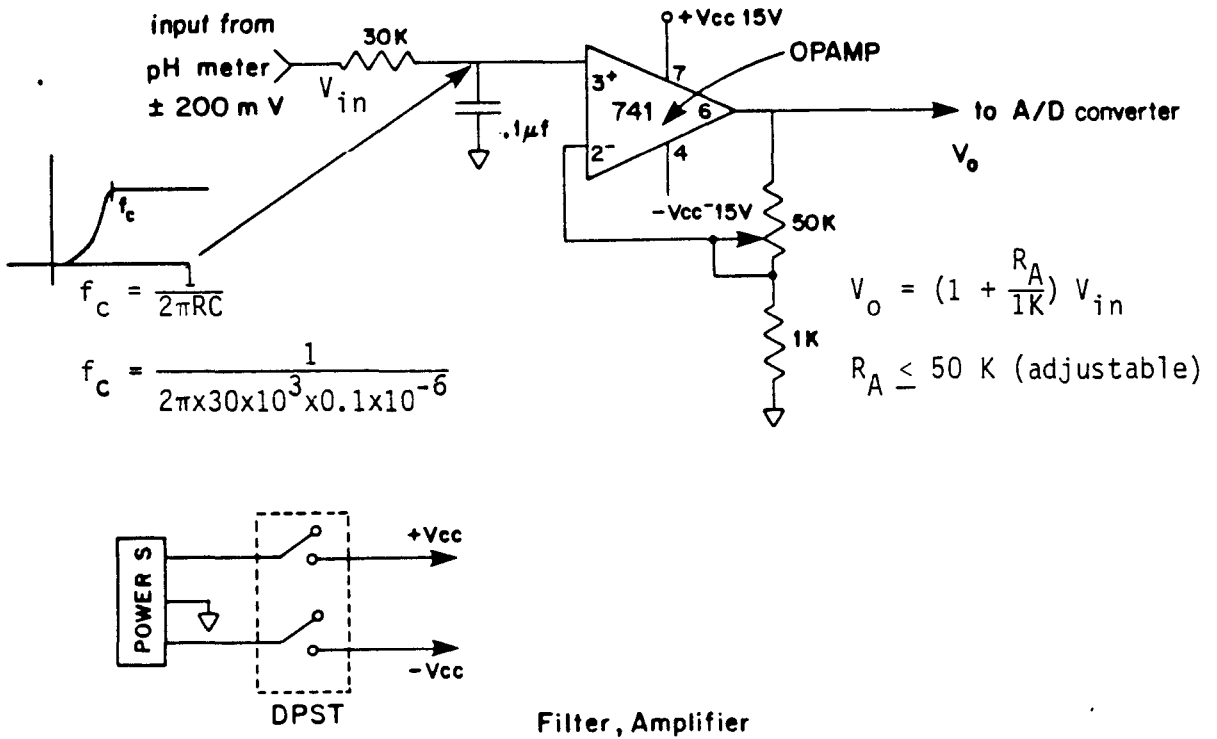
Filter, Amplifier

Fig. V.2. Schematic of amplifier, filter; typical of two; power supply 12-15 V, 0.7A, Standard Power, Inc.

a) Relay
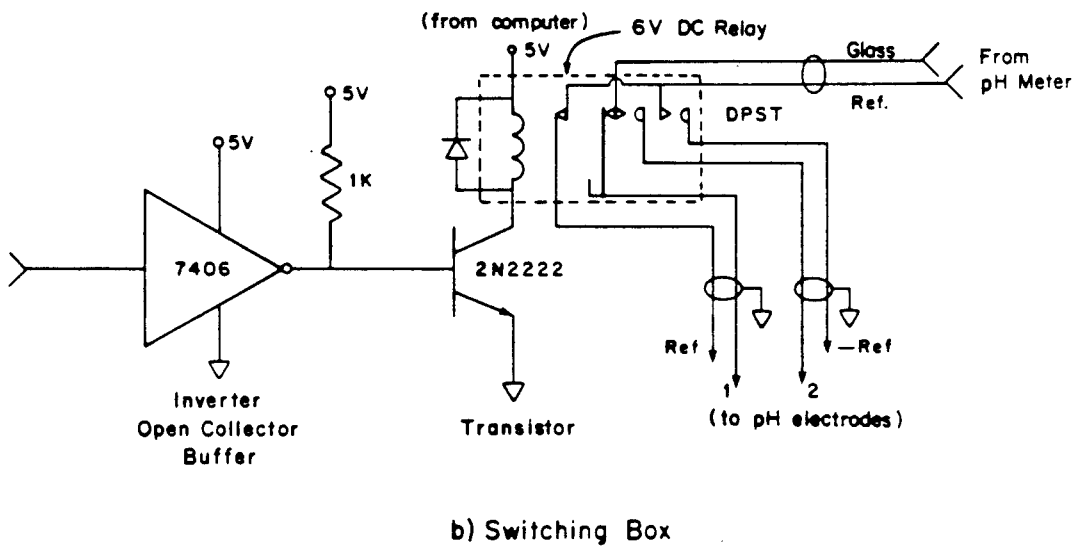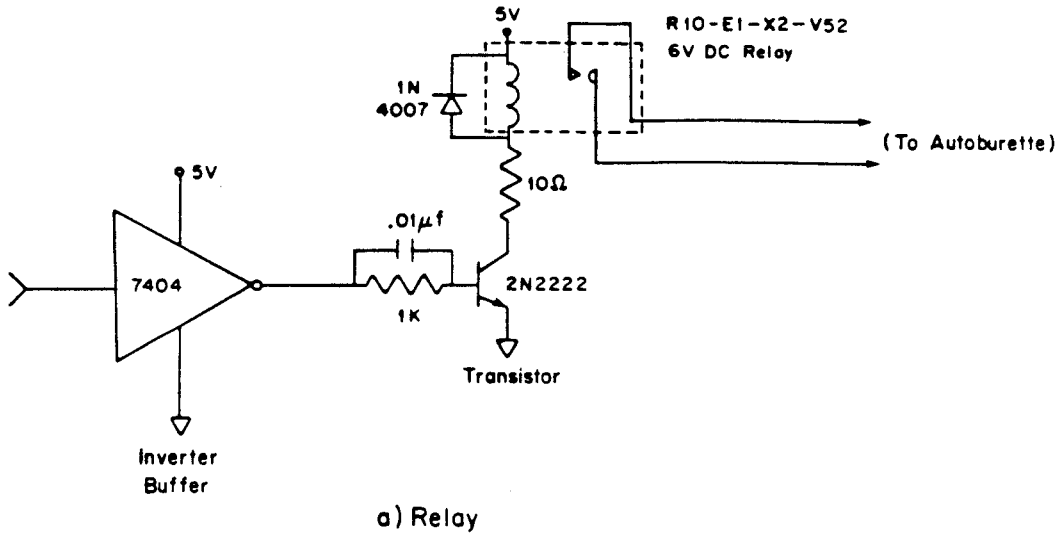
b) Switching Box

Fig. V.3. Schematic of a) relay to toggle autoburettes, typical of two; and b) switching box for pH electrodes.

Table V.1. Basic program for two pH meters and ABUII's.

```
90   HIMEM: 38144
100  F =   - 16384: REM  KEYBOARD S
     TROBE
110  B = 256:BX = B * B
120  D$ =  CHR$ (4)
137   PRINT D$;"BLOAD GET5"
138  Y = 6.651701:X = 1933.91
139  Y1 = 6.437056:X1 = 2143.20
150  L = 10
170  R1 =   - 16295:R2 =   - 16296
180  R3 =   - 16293:R4 =   - 16294
200  E1$ = " ":E2$ = " "
232  N = 5000
234  N1 = 19
235   POKE 27,N1 + 1
236  N2 = 155
240   INPUT "PRINT INTERVAL 0.1 1
     10 MIN ";P
241   IF P < > 0.1 AND P < > 1 AND
     P < > 10 THEN  GOTO 240
242   IF P = 0.1 THEN J = 18
243   IF P = 10 THEN J = 15
244   IF P = 1 THEN J = 16
251   INPUT "USING ABU11? ";Q$
252   IF  LEFT$ (Q$,1) < > "Y" THEN
      GOTO 300
253   INPUT "SET POINTS (MV) = ";C
     ,C1
254   INPUT "PRECISION (MV) = ";D
255   INPUT "(A)CID OR (B)ASE IN A
     BU11 #1, #2 ? ";E1$,E2$
256   IF E1$ < > "A" AND E1$ < >
     "B" OR E2$ < > "A" AND E2$ <
     > "B" THEN  GOTO 255
257  A1 = 100
260   INPUT "SET A1 & A2 (Y/N)";AC
     $
270   IF AC$ = "Y" THEN  INPUT "A1
     , A2 ";A1,A2
300   HOME
310   POKE  - 16368,0: REM  RESET
     KEYBOARD STROBE
320  FMT =  PEEK (50164): REM  GET
     CLOCK FORMAT
330   IF FMT < 16 THEN  POKE 50164
     ,FMT + 16
```

Table V.1. (cont.)

```
400   PRINT D$;"IN#3"
410   PRINT D$;"PR#3"
420   INPUT T$
430   PRINT D$;"IN#0"
440   PRINT D$;"PR#0"
445   VTAB 3: HTAB 1
450   POKE 26,N2
460   CALL 38144
480   V = (BX +  PEEK (3) + 5 +  PEEK
      (7) +  PEEK (6)) / N
500   S = (V - X) / Y
510   POKE 26,N2
520   CALL 38216
540   V1 = (BX +  PEEK (3) + 5 +  PEEK
      (7) +  PEEK (6)) / N
560   S1 = (V1 - X1) / Y1
600   M =  VAL ( MID$ (T$,J,1))
620   GOSUB 700
625   VTAB 5: HTAB 1
630   IF M < > L THEN  GOSUB 800
640   L = M:V = 0
642   V1 = 0
646   I1 = I1 + 1
648   IF I1 / 12 THEN  GOTO 660
650   IF E1$ = "A" THEN  GOSUB 200
      0
652   IF E2$ = "A" THEN  GOSUB 201
      0
655   IF E1$ = "B" THEN  GOSUB 210
      0
657   IF E2$ = "B" THEN  GOSUB 211
      0
660   K =  PEEK (F): REM  CHECK KEY
      BOARD STROBE
670   IF K < = 127 THEN  GOTO 400
680   INPUT "(E) EXIT, (C) CHANGE,
      (R) RESTART ";Q$
690   IF  LEFT$ (Q$,1) = "E" THEN
      END
692   IF  LEFT$ (Q$,1) = "R" THEN
      GOTO 300
695   GOTO 200
700   PRINT T$
710   VTAB 6: HTAB 12
712   PRINT "AI13 INT     MV"
713   PRINT "            ";
714   PRINT " --------    ----"
715   VTAB 6: HTAB 14
720   PRINT  INT (V);
730   PRINT "       ";
```

Table V.1. (cont.)

```
740 S = ( INT (S * 10)) / 10
741  PRINT S
742  PRINT "                "; 
744  PRINT  INT (V1);
746  PRINT "        ";
748 S1 = ( INT (S1 * 10)) / 10
749  PRINT S1
750  RETURN
800  PRINT D$;"PR#1"
810  PRINT T$;
820  PRINT "     ";
825  PRINT  INT (V);
830  PRINT "      ";
840 S = ( INT (S * 10)) / 10
841  PRINT S;
850  PRINT "                ";
860  PRINT  INT (V1);
870  PRINT "       ";
880 S1 = ( INT (S1 * 10)) / 10
881  PRINT S1
890  PRINT D$;"PR#0"
892  HOME
895  RETURN
2000  IF S + D < C THEN  GOSUB 22
     00
2005 I1 = 0
2006  RETURN
2010  IF S1 + D < C1 THEN  GOSUB
     2300
2015 I1 = 0
2020  RETURN
2100  IF S - D > C THEN  GOSUB 22
     00
2105 I1 = 0
2106  RETURN
2110  IF S1 - D > C1 THEN  GOSUB
     2300
2115 I1 = 0
2120  RETURN
2200  POKE R2,1
2210  FOR I = 1 TO H1
2220  NEXT I
2230  POKE R1,0
2240  PRINT D$;"PR#1"
2250  PRINT T$;
2260  PRINT "     ";.
```

Table V.1. (cont.)

```
2270    PRINT "ABU11 #1";
2271 A1 = A1 + 1
2272    PRINT "         ";
2275    PRINT A1
2280    PRINT D$;"PR#0"
2285    HOME
2290    RETURN
2300    POKE R4,1
2310    FOR I = 1 TO H1
2320    NEXT I
2330    POKE R3,0
2340    PRINT D$;"PR#1"
2350    PRINT T$;
2360    PRINT "        ";
2370    PRINT "ABU11 #2";
2371 A2 = A2 + 1
2372    PRINT "         ";
2375    PRINT A2
2380    PRINT D$;"PR#0"
2385    HOME
2390    RETURN
```

Table V.2. Basic program for two reactors and ABUII's with a
single pH meter and a switching box.

```
90   HIMEM: 38144
100  F = - 16384: REM  KEYBOARD S
     TROBE
110  B = 256:BX = B * B
120  D$ = CHR$ (4)
137  PRINT D$;"BLOAD GETS"
138  Y = 5.940607:X = 1945.78
139  Y1 = 5.940340:X1 = 1945.84
150  L = 10
170  R1 = - 15872
180  R3 = - 16295:R4 = - 16296
190  R5 = - 16293:R6 = - 16294
195  H1 = 100
200  E1$ = " ":E2$ = " "
210  R7 = 0
232  N = 5000
234  N1 = 19
235  POKE 27,N1 + 1
236  N2 = 155
240  INPUT "PRINT INTERVAL 0.1 1
     10 MIN ";P
241  IF P < > 0.1 AND P < > 1 AND
     P < > 10 THEN  GOTO 240
242  IF P = 0.1 THEN J = 18
243  IF P = 10 THEN J = 15
244  IF P = 1 THEN J = 16
251  INPUT "USING ABU11? ";Q$
252  IF  LEFT$ (Q$,1) < > "Y" THEN
     GOTO 300
253  INPUT "SET POINTS (MV) = ";C
     ,C1
254  INPUT "PRECISION (MV) = ";D
255  INPUT "(A)CID OR (B)ASE IN A
     BU11 #1, #2 ? ";E1$,E2$
256  IF E1$ < > "A" AND E1$ < >
     "B" OR E2$ < > "A" AND E2$ <
     > "B" THEN  GOTO 255
260  INPUT "SET A1 & A2 (Y/N)";AC
     $
270  IF AC$ = "Y" THEN  INPUT "A1
     , A2 ";A1,A2
300  HOME
310  POKE - 16368,0: REM  RESET
     KEYBOARD STROBE
320  FMT = PEEK (50164): REM  GET
     CLOCK FORMAT
330  IF FMT < 16 THEN  POKE 50164
     ,FMT + 16
390  POKE - 15870,255
```

Table V.2. (cont.)

```
400    POKE R1,R7
405    IF R8 > 100 THEN   GOSUB 1100

410  R8 = R8 + 1
420    GOSUB 1200
450    POKE 26,N2
460    CALL 38216
470    IF R7 = 0 THEN   GOTO 500
480  V = (BX *   PEEK (8) +  B *    PEEK
     (7) +   PEEK (6)) / N
490  S = (V - X) / Y
495    GOTO 600
500  V1 = (BX *   PEEK (8) +  B *   PEEK
     (7) +   PEEK (6)) / N
510  S1 = (V1 - X1) / Y1
600  M =   VAL ( MID$ (T$,J,1))
620    GOSUB 700
625    VTAB 5: HTAB 1
630    IF M < > L THEN   GOSUB 800
640  L = M
646  I1 = I1 + 1
648    IF I1 < 12 THEN   GOTO 660
649    IF R7 = 0 THEN   GOTO 655
650    IF E1$ = "A" THEN   GOSUB 200
     0
652    IF E1$ = "B" THEN   GOSUB 210
     0
653    GOTO 660
655    IF E2$ = "A" THEN   GOSUB 201
     0
657    IF E2$ = "B" THEN   GOSUB 211
     0
660  K =   PEEK (F): REM   CHECK KEY
     BOARD STROBE
670    IF K < = 127 THEN   GOTO 400

680    INPUT "(E) EXIT, (C) CHANGE,
     (R) RESTART ";Q$
690    IF   LEFT$ (Q$,1) = "E" THEN
     END
692    IF   LEFT$ (Q$,1) = "R" THEN
     GOTO 300
695    GOTO 200
700    PRINT T$,R8
710    VTAB 6: HTAB 12
712    PRINT "AI13 INT      MV"
713    PRINT "            ";
714    PRINT " --------    ----"
715    VTAB 8: HTAB 14
720    PRINT   INT (V);
730    PRINT "         ";
```

Table V.2.   (cont.)

```
740 S = ( INT (S * 10)) / 10
741  PRINT S
742  PRINT "                "  ;
744  PRINT  INT (V1);
746  PRINT "         " ;
747 S1 = ( INT (S1 * 10)) / 10
749  PRINT S1
760  RETURN
800  PRINT D$;"PR#1"
810  PRINT T$;
820  PRINT "       " ;
825  PRINT  INT (V);
830  PRINT "      " ;
840 S = ( INT (S * 10)) / 10
841  PRINT S;
850  PRINT "               " ;
860  PRINT  INT (V1);
870  PRINT "       " ;
875 S1 = ( INT (S1 * 10)) / 10
881  PRINT S1
890  PRINT D$;"PR#0"
892  HOME
895  RETURN
1100 R9 = 0
1110  IF R7 = 1 THEN  GOTO 1140
1120 R7 = 1
1130  GOTO 1160
1140 R7 = 0
1160  RETURN
1200  PRINT D$;"IN#3"
1210  PRINT D$;"PR#3"
1220  INPUT T$
1230  PRINT D$;"IN#0"
1240  PRINT D$;"PR#0"
1250  VTAB 3: HTAB 1
1260  RETURN
2000  IF S + D < C THEN  GOSUB 22
     00
2005 I1 = 0
2006  RETURN
2010  IF S1 + D < C1 THEN  GOSUB
     2300
2015 I1 = 0
2020  RETURN
2100  IF S - D > C THEN  GOSUB 22
     00
2105 I1 = 0
2106  RETURN
2110  IF S1 - D > C1 THEN  GOSUB
     2300
```

Table V.2.   (cont.)

```
2115  I1 = 0
2120  RETURN
2200  POKE R4,1
2210  FOR I = 1 TO H1
2220  NEXT I
2230  POKE R3,0
2240  PRINT D$;"PR#1"
2250  PRINT T$;
2260  PRINT "     ";
2270  PRINT "ABU11 #1";
2271  A1 = A1 + 1
2272  PRINT "       ";
2275  PRINT A1
2280  PRINT D$;"PR#0"
2285  HOME
2290  RETURN
2300  POKE R6,1
2310  FOR I = 1 TO H1
2320  NEXT I
2330  POKE R5,0
2340  PRINT D$;"PR#1"
2350  PRINT T$;
2360  PRINT "     ";
2370  PRINT "ABU11 #2";
2371  A2 = A2 + 1
2372  PRINT "       ";
2375  PRINT A2
2380  PRINT D$;"PR#0"
2385  HOME
2390  RETURN
```

Table V.3. Assembly listing of program to take data from
pH meters and store average of 5000 data points
in memory.

```
        LDA     #0                      LDA     #0
        TAY                             TAY
        TAX                             TAX

        STA     06                      STA     06
        STA     07                      STA     07
        STA     08                      STA     08

        LDA     #50                     LDA     #52
        STA     0C0D0                    STA     0C0D0
CC  LDA     0C0D1               GG  LDA     0C0D1
        CLC                             CLC
        AND     #0F                     AND     #0F
        ADC     07                      ADC     07
        STA     07                      STA     07
        BCC     AA                      BCC     EE
        INC     08                      INC     08

AA  LDA     0C0D0               EE  LDA     0C0D0
        CLC                             CLC
        ADC     06                      ADC     06
        STA     06                      STA     06
        BCC     BB                      BCC     FF
        CLC                             CLC
        LDA     07                      LDA     07
        ADC     #01                     ADC     #01
        STA     07                      STA     07
        BCC     BB                      BCC     FF
        INC     08                      INC     08

BB  INX                         FF  INX
        CPX     1A                      CPX     1A
        BNE     CC                      BNE     GG

        INY                             INY
        CPY     18                      CPY     18
        BEQ     DD                      BEQ     HH
        LDA     #0FF                    LDA     #0FF
        STA     1A                      STA     1A
        LDA     #0                      LDA     #0
        TAX                             TAX
        CLC                             CLC
        BCC     CC                      BCC     GG

DD  RTS                         HH  RTS
```

Chrysotile Asbestos in California Surface Waters: From Upstream Rivers Through Water Treatment

Roger C. Bales, Dale D. Newkirk, and Steven B. Hayward

Concentrations of chrysotile asbestos fibers in surface waters in California are estimated from a mass-balance model that takes into consideration natural weathering of serpentine rock in the Sierra Nevada and coastal mountains and removal of fibers by coagulation in reservoirs. Fiber concentrations range from 10^8/L in waters from the western slope of the Sierra Nevada foothills in the central part of the state to 10^{12}/L in rivers in the northwest part of the state. As predicted, fiber removals of from 90 to 99.8 percent were observed in reservoirs with detention times of from 0.5 to 3 years. Removal of submicron-sized fibers in water treatment plants also ranged from 90 to 99.8 percent, depending on the degree of coagulation prior to filtration.

As a result of the natural weathering of serpentine rock, chrysotile asbestos fibers are found in some surface waters originating in the western slopes of the Sierra Nevada and in the coastal mountains of California. Individual fibers are typically 0.03–0.04 μm in diameter, and fiber bundles are often up to 0.1 μm in width. Fiber length depends on source; deposits in California yield short fibers, 90 percent of which are from 0.1 to 3.0 μm long. This small size results in chrysotile fibers passing through reservoirs and through water treatment plants that are designed for turbidity removal.

This article describes the input, transport, and removal of chrysotile fibers delivered to Southern California through the State Water Project. Comparisons are made with other water sources. The input of fibers to natural waters is estimated from the areal distribution of chrysotile deposits in specific river basins and from the apparent physical weathering rate for rock in those basins. Fiber removal occurs by coagulation with larger particles during transport through rivers, reservoirs, and the Cali-

fornia Aqueduct. Further removal takes place in water filtration plants. Model predictions are compared with field data that had been accumulated by the Air and Industrial Hygiene Laboratory (AIHL) of the State of California Department of Health Services and The Metropolitan Water District of Southern California (Metropolitan).

Background

The term asbestos is applied to the fibrous forms of two chemically and structurally different classes of naturally occurring silicate minerals: amphiboles and serpentines. These fibrous minerals are important commercially because of their strength and resistance to fire. Amphiboles are less common in California than serpentines. Further, most commercial asbestos used in the United States originates from serpentine.

Chrysotile is a magnesium silicate serpentine mineral that is structurally similar to the clay kaolinite. In California, the serpentine group of minerals (chrysotile, lizardite, and antigorite) are found primarily in magnesium silicate ultramafic rocks. Ultramafic rocks form

elongate bodies within and adjacent to major fault zones of the western Sierra Nevada foothills: the most abundant component of these bodies is serpentine.[1] In the Klamath Mountains of northwest California, ultramafic rocks generally crop out as bodies that follow the contour of the mountain range. These rocks are serpentinized and in many places are highly sheared.[2] The largest ultramafic body in that area is virtually continuous for 160 km. Occurrences in other coastal mountains in Northern California are similar. The chrysotile deposit of greatest commercial importance is in the coastal mountains of central California near Coalinga (New Idria area). Major ultramafic bodies in California are shown in Figure 1.

Of the serpentine minerals, only chrysotile is commonly fibrous; however, not all chrysotile is fibrous. Some fibrous material may be antigorite.[3] Serpentine layers can intergrow closely with talc, a structurally similar magnesium silicate. Other asbestos forms are less common in the Sierra Nevada and the mountains of the Pacific coast than chrysotile, but they also may be found associated with ultramafics. For example, one sample from the Cascade Mountains consisted of four minerals—anthophyllite (an amphibole variety of asbestos), talc, chrysotile, and lizardite—in contact or within a few tens of angstroms of each other.[4] Brucite, a magnesium hydroxide mineral, may occur in fibrous form closely associated with chrysotile or as platey irregular grains.

The highly sheared chrysotile ore found in the New Idria area consists of friable masses of matted chrysotile surrounding other rock fragments,[5] which are most commonly lizardite, brucite, and magnetite in these alpine-type ultramafics.[5] Most other chrysotile ores consist of veins within massive serpentine rocks. Thirty-five to 75 percent of the fiber in the New Idria ore is recoverable; in most ores containing veins of chrysotile, recoverability is less than 10 percent. Chrysotile deposits in the Klamath Mountains commonly consist of a small zone of closely spaced veins up to 1 in. thick, with the fibers oriented perpendicularly to the vein walls.[7] Antigorite is the predominant serpentine type in other areas of the mountains of California, with little or no lizardite and chrysotile present.[6,8,9] However, it has recently been suggested that the majority of California's serpentine rocks are composed of lizardite only or of lizardite plus chrysotile.[10,11]

Occurrences of ultramafic rock in selected river basins in California are shown in Figure 2; the quantities of ultramafic rock in north coast and central valley river basins are summarized in Table 1.

The chrysotile content of the principally serpentine, ultramafic areas in California varies from near 0 to 100 percent. Ultramafic bodies vary in area from a few square metres to several square kilometres. Only the larger occurrences are shown in Figures 1 and 2. Most serpentine in California does not contain sufficient chrysotile to warrant mining. Historically, most mining claims contained less than 5 percent recoverable chrysotile in the serpentine ore,[12] the notable exception being chrysotile in the Coalinga area.[13]

Since all serpentine contains some chrysotile, naturally occurring chrysotile will be found in soils, streams, and lakes in many localities.[14]

Mass-balance model

The transport of chrysotile particles in natural waters can be represented by a mass-balance model, such as that depicted in Figure 3. In any well-mixed stream or reservoir, the mass flux of fibers leaving (advection out) equals advection in, plus input by weathering, plus deposition of airborne particles, less coagulation and sedimentation, plus resuspension.

In an upstream river, advection in and resuspension are zero at first approximation. Deposition of airborne particles may be important in certain cases, such as in areas with large deposits of exposed, sheared chrysotile. High rates of asbestos deposition, on the order of 1 mg/m²/d, would be required to influence the total fiber flux, even in downstream channels such as the California Aque-
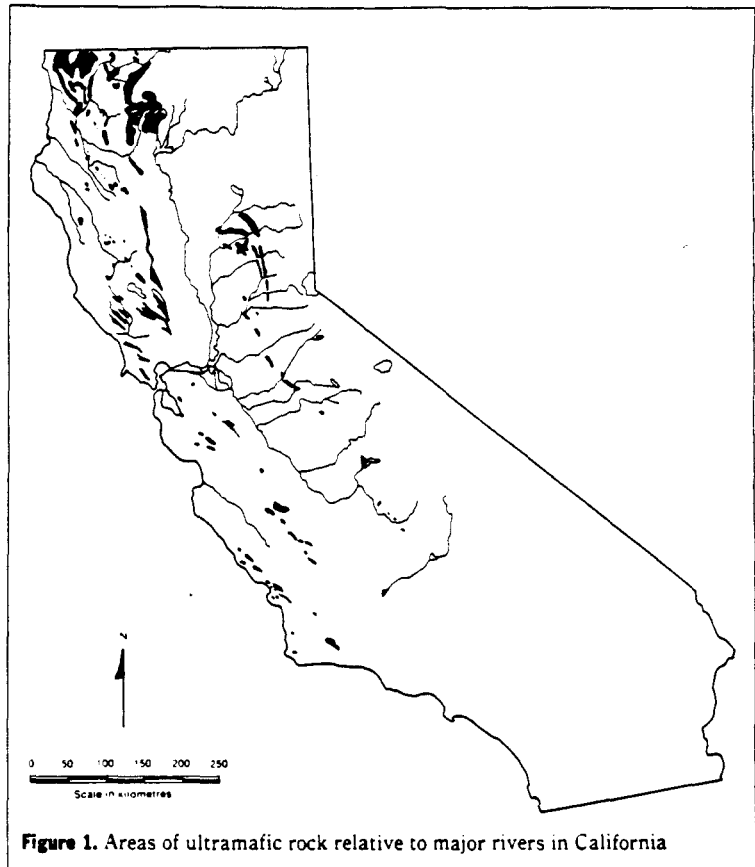

Figure 1. Areas of ultramafic rock relative to major rivers in California

duct. Deposition also depends on short-term climatic variations and is neglected in the long-term averages estimated in the present model. The observed chrysotile flux should thus equal the input by weathering less removal by coagulation and sedimentation. Fiber concentration is assumed to equal fiber flux divided by the flux of the water. Owing to the short travel times (order of days), coagulation in upstream rivers is small and, therefore, neglected. In a slowly flowing river or an aqueduct below upstream storage reservoirs, resuspension will also contribute to the fiber concentration. The amount of resuspension depends on flow velocity. For long-term estimates, it is assumed that resuspension is due to relatively constant scouring of sediment deposited by high flows. The change in fiber concentration during water treatment is due to coagulation with larger suspended flocs and deposition onto sand grains during filtration.

Methods of calculation

Input by weathering. Suspended sediment is introduced into a river both by weathering of soils in the tributary basin during rainfall and subsequent

runoff and by erosion of the river bank. For long-term estimates of serpentine weathering, it is assumed that only the former process is important. Insufficient data are available to allow calculation of seasonal or even annual variations. The equation used to estimate the long-term average input by weathering of chrysotile to a river is:

$$n_1 = \frac{WR \times A \times F \times Y}{WD} \qquad (1)$$

where n_1 = fiber concentration in number/L, WR = weathering rate in tons/km²/year, A = area of ultramafic rock in km², F = fraction of chrysotile in serpentine, Y = fiber yield in number/ton, and WD = water discharge in L/year. The parameters in this model are estimated from field data for drainage basins in California.

Coagulation and sedimentation. Particles with settling velocities greater than the hydraulic loading of a reservoir should settle out and be retained in the reservoir sediment. Submicron-sized particles, which have a much lower settling velocity, should pass through a reservoir without settling, unless they coagulate with larger particles and then settle out.

It is assumed that chrysotile fibers are characteristically 0.5 μm long: fibers observed in natural waters in California are typically 0.05-0.10 μm in width and 0.5-1.0 μm in length (Figure 4). The settling velocity for random orientation. calculated using Stokes law for a fiber of 0.5-μm length suspended in water at 20°C, is on the order of 10^{-2} m/year.

In reservoirs with detention times of approximately one year. mineral particles larger than about 2-5 μm in size should be removed to a large extent. Analyses of two sets of four samples taken from the Feather River in May and August 1983 showed that particles in the 2- to 4-μm range are more abundant than larger particles (Figure 5). with about 5 percent of the particles being larger than 10 μm. The total number of particles in the 2- to 100-μm range was on the order of 10^7 L. In the size range below 2 μm. only asbestos fibers were counted (by electron microscopy). For these model calculations it is assumed that fibers are removed by coagulation with a constant number of larger spherical particles. This assumption implies that although larger particles are removed by sedimentation and coagulation, the number and size distribution of these particles are at steady state. The rapid (relative to reservoir detention times) achievement of steady state for coagulating particles in the 2- to 100-μm range can be seen from the experiments of Hunt[15] and the recent calculations of Valioulis.[16] For model calculations. the concentration of 2- to 100-μm particles is assumed to be 10^7 L, with the size distribution that is shown on Figure 5 and a density of 2.6 g/cm³, corresponding to a high mineral fraction in the suspended matter. On a mass basis this is approximately 1-2 mg/L.

The rate $(L \cdot s)^{-1}$ at which chrysotile particles aggregate with larger particles can be expressed as:

$$R = \alpha n_1 \sum_i k_i n_i \qquad (2)$$

where α is the coagulation efficiency (the fraction of collisions that result in aggregation) and k_i is the coagulation rate constant (L/s). The number of fibers per litre is n_1, and the number of larger particles of size i per litre is n_i. The rate constants illustrated in Figure 6. together with the size distribution data of Figure 5. show that collisions between 0.5-μm particles and larger particles should occur primarily by sedimentation of the larger particles rather than by fluid shear or Brownian diffusion. In this case the rate coefficient is given by:

$$k_i = \frac{\pi g(\rho_p - \rho)(d_2 - d_1)^2(d_2^2 - d_1^2)}{72 \times 10^3 \mu} \qquad (3)$$

where ρ_p and ρ are the densities (g/cm³) of the particles and the water. respec-
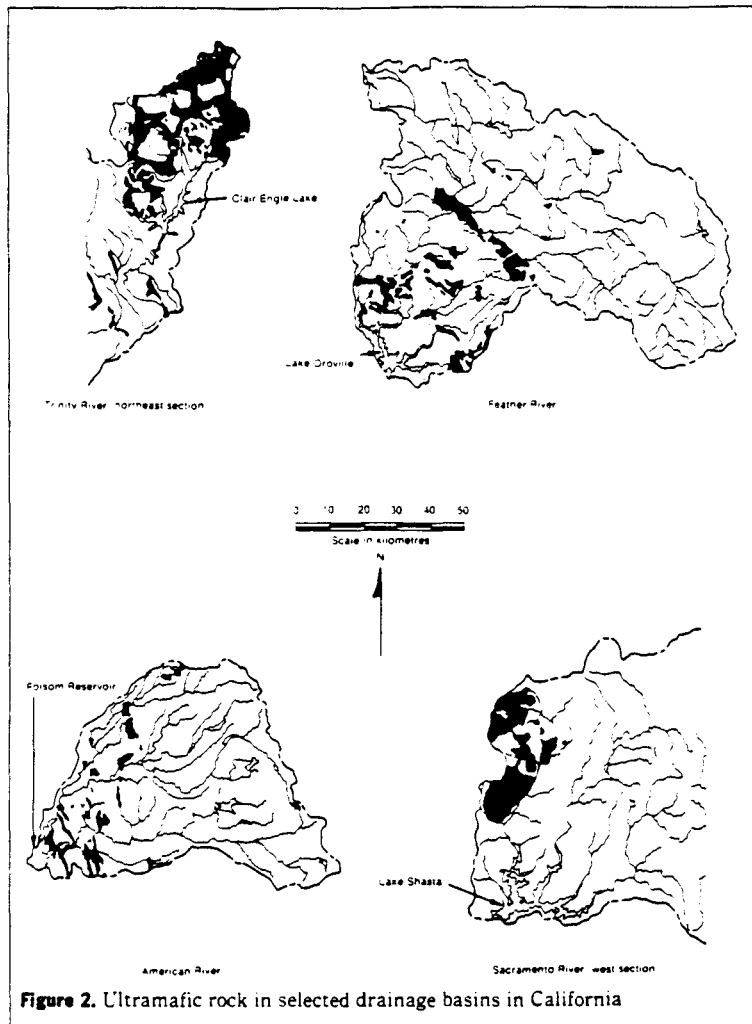
Figure 2. Ultramafic rock in selected drainage basins in California

tively: μ is viscosity (0.010 g/cm/s for water at 20°C): and d_1 and d_2 are fiber length (cm) and larger-particle diameter (cm), respectively. Fiber length rather than fiber diameter is used for coagulation if rotational diffusion is faster than transitional diffusion. If this is not the case. some smaller length or distribution of lengths should be used. For the present calculations. the highest rates occur for $d_2 >> d_1$, where k_i in Eq 3 is insensitive to fiber length.

For $d_2 >> d_1$. substitution of Eq 3 into Eq 2 and integration yield:

$$n_1/n_1' = \exp\left[\frac{-\pi g(\rho_p - \rho)}{72 \times 10^3 \mu} \alpha t \sum_i n_i d_i^2\right] \qquad (4)$$

where t is time in seconds. For completely destabilized particles (α = 1.0), essentially complete removal is expected over a one-year detention time. However. for like-charged particles that repel each other

on approach. α may be substantially lower. For α = 0.001. a removal of 90 percent is expected in one year: for α ≤ 10^{-4}. fiber removal is insignificant. In laboratory coagulation experiments. α values up to 0.5 have been reported:[17] however. values of 0.01-0.1 are more common.[18-21] Many of these reports are for seawater and estuarine waters. which have a much higher ionic strength than the waters being considered here (≤0.7 versus ≤0.01). suggesting that a lower α value may be appropriate.

No measurements of coagulation efficiency for fibers in natural waters are available. In natural waters. suspended particles adsorb dissolved organics and thus acquire surfaces of like charge. Limited electrophoretic mobility measurements of chrysotile fibers suspended in Feather River water suggest that the magnitude of the surface charge is relatively low (mobility -1 to -2 [μm/s]/

TABLE 1
Characteristics of selected river basins

River	Location	Drainage Area km²	Discharge km³/year	Reservoir Volume km³	Reservoir Detention Time year	Area of Ultramafic Rock km²	Area of Ultramafic Rock percent
North Coast							
Trinity River	Clair Engle Lake	1790	1.52	1.79	1.18	680	38
Trinity River	At Hoopa	7390	4.67			940	13
Klamath River	At Orleans§	21950	7.19			1120	5
Mad River	At Arcata	1260	1.32			1	<1
Eel River	Lake Pillsbury	750	0.48	0.11	0.23	11	2
Eel River	At Scotia	8060	6.49			118	1
Russian River	At Guerneville	3470	2.01			116	3
Northern and western Sacramento Valley							
Sacramento River	Above Lake Shasta	1100	1.03			359	33
Sacramento, McCloud, and Pit rivers	Lake Shasta	16630	7.57	5.47	0.72	359	2
Clear Creek	Whiskeytown Reservoir	520	0.41	0.30	0.17**	0	0
Cottonwood Creek	At Cottonwood	2400	0.75			76	3
Stony Creek	Black Butte Reservoir	1910	0.55	0.17	0.31	149	4
Cache Creek	Clear Lake	1370	0.31	0.39	1.26	27	2
Cache Creek	At Rumsey	2500	0.60			199	4
Putah Creek	Lake Berryessa	1490	0.46	1.96	4.26	301	21
Eastern Sacramento Valley							
Feather River	Lake Oroville	9340	5.22	3.31	0.63	300	3
North Yuba River	New Bullards Reservoir	1270	1.27	0.90	0.71	43	4
Yuba River	At Marysville	3470	2.19			44	2
Bear River	New Camp Far West Reservoir	730	0.41	0.12	0.30	19	3
American River	Folsom Reservoir	4820	3.34	1.25	0.37	133	3
Eastern San Joaquin Valley							
Cosumnes River	At McConnell	1880	0.47			33	2
Mokelumne River	Pardee Reservoir	1500	0.99	0.24	0.34	21	1
Calaveras River	New Hogan Reservoir	940	0.19	0.39	2.05	18	2
Stanislaus River	New Melones Reservoir	2430	1.19	2.98	2.50	7	<1
Stanislaus River	Tulloch Lake	2540	1.19			49	2
Tuolumne River	Hetch Hetchy Reservoir	1180	0.89	0.44	0.50	0	0
Tuolumne River	Don Pedro Reservoir	3970	1.72	2.50	1.46	30	1
Merced River	Lake McClure	2690	1.19	1.26	1.06	22	1
San Joaquin River	Millerton Reservoir	4250	2.11	0.62	0.29	0	0
Kings River	Pine Flat Reservoir	4000	2.01	1.23	0.61	39	1
Kaweah River	Kaweah Reservoir	1450	0.57	0.18	0.32	0	0
Kern River	Lake Isabella	5380	0.82	0.70	0.86	0	0

*Source: USGS Water-Data Repts. CA-81-2, CA-81-3, CA-81-4; discharge includes diversions
†2.6 km² = 1.0 sq mi, 1.23 km³ = 1.0 acre-ft
‡Source: Calif. Div Mines Geol., Geol. Maps of Calif., scale 1:250 000
§Includes Klamath, Salmon, Scott, and Shasta rivers
**Includes diversion from Trinity River

[V/cm]) in the pH range 7.5–8.0. Stumm[22] has suggested that α values on the order of 10^{-3}–10^{-4} may apply to rivers and of 10^{-4}–10^{-5} may apply to lakes. In the following analysis, it is assumed that α = 0.001 and that coagulation of fibers with larger particles occurs at the rate predicted by Eq 4.

Resuspension. During periods of heavy runoff, water from Arroyo Pasajero, near Coalinga, enters the California Aqueduct. Large quantities of asbestos-containing sediments are introduced into the aqueduct during these times.[23] The sediments are deposited and remain on the bed of the aqueduct until scoured and resuspended by passing water.

In principle, given the channel characteristics (dimensions, material, slope, roughness), the nature of the bed material (size, weight), and the flow rate, the extent of scouring and resuspension can be predicted. However, because of the uncertainty and variability of these factors, no predictions are made as part of this model. Rather, attention is drawn to the fact that the relatively abundant field data indicate an increase in chrysotile concentration of from two- to tenfold for flows passing through the aqueduct. For example, the more than 160 samples collected by the California Department of Water Resources (DWR), Division of Operation and Maintenance, as part of its sediment-removal project (August 1980–October 1982) show chrysotile asbestos levels in the aqueduct above Coalinga to be on the order of 5×10^6 fibers/L and levels in the aqueduct below Coalinga on the order of 2×10^9 fibers/L.[24] The concentration depends on the flow rate (scouring velocity) in the aqueduct. The geometric mean of 12 different samples removed (July 1981–June 1982) from the Delta and Tracy pumping plants at the head ends of the California Aqueduct and the Delta–Mendota Canal, respectively, and analyzed by AIHL is 1.8×10^9 fibers/L.[25] However, several samples taken upstream and downstream of Coalinga in the same month show statistically significant increases. Based on these observations, an increase by a factor of four is assumed in the model.

Water treatment. Particle removal during water filtration is estimated by using the spherical-collector model of O'Melia.[26,27] In this model, removal in a packed bed is related to the efficiency of a single spherical collector:

$$\frac{dn_1}{dL} = -\frac{3}{2} \frac{(1-f)}{d_2} \alpha \eta n_1 \qquad (5)$$

where L is bed depth (cm), d_2 is grain (collector) diameter (cm), and f is bed porosity; n_1 and α are as noted previously; and η is contact efficiency (dimensionless), given for Brownian diffusion in

terms of the Peclet number. Integrating Eq 5 yields:

$$n_1/n_1^0 = \exp\left[-\frac{3}{2}(1-f)\alpha\eta\frac{L}{d_2}\right] \quad (6)$$

where η can be calculated from the hydraulic characteristics of the bed; however, experimental results by Yao[27] suggest that a value on the order of 2.6×10^{-3} is applicable for submicron-sized particles. It is assumed that for water filtration $\alpha = 1$: i.e., particles are fully destabilized by addition of chemicals. Filters at Metropolitan contain 50 cm of anthracite ($d_1 = 1.0$ mm) underlain by 20 cm of sand ($d_2 = 0.5$ mm). Using these values and $f = 0.40$, n_1/n_1^0 is predicted to be 0.1. Coagulation of fibers into particles larger than $1 \mu m$ in size will improve the efficiency of fiber capture in a packed bed. For example, Yao[27] observed $\eta = 0.01$ for 7.6-μm latex spheres. Applying this value of η to Eq 6 for the conditions stated above, n_1/n_1^0 would be 3×10^{-4}. Significant coagulation preceding filtration would be required to incorporate all fibers into coagulant particles on the order of 7-10 μm in size. In addition, single fibers have been observed in finished waters from filtration plants. Because of the relatively low coagulant dosages applied (3-7 mg alum/L) and short coagulation times (20 min), it is assumed that fiber removal is by a combination of individual-fiber deposition onto sand grains and capture by larger flocs; the removal efficiency is expected to be within the predicted range of 80-99.97 percent. The larger values correspond to greater coagulation before or during filtration.

Results

Weathering. Table 2 summarizes weathering rates for selected river basins in Northern California. These estimates were determined from sediment gauging stations on rivers, as sedimentation rates in reservoirs have not been measured. Based on these data, values of 0.1 ± 0.05 mm/year (265 metric tons/ km^2/year and 0.5 ± 0.2 mm/year (1320 metric tons/km^2/year) are used for the central-valley river basins and the north-coast river basins, respectively.

It is assumed that the relative areas of ultramafic rock in different river basins are accurately reflected by these values and that the actual area is within 20 percent of that shown in Table 1. The areas were reproducibility-measured from 1:250 000-scale maps; uncertainty varies and is in general not known. In addition, it is assumed that ultramafic rock is 100 percent serpentine and that serpentine in the areas covered by this analysis is 5 ± 3 percent chrysotile.

The estimated long-term input by weathering of chrysotile to selected rivers, using Eq 1, is noted in Table 3. Concentrations are based on 10^{11} fi-

TABLE 2
Weathering rates for selected river basins

River	Location	Area* km^2	Discharge* km^3/year	Weathering Rate mm/year	Period of Record
North Coast					
Trinity River	Clair Engle Lake	1 790	1.52	0.138†	
Mad River	At Arcata	1 260	1.32	0.605‡	1957–64
Redwood Creek	At Orick	720	1.00	0.39§	1973–81
Eel River	At Scotia	8 060	6.49	0.69**	1958–67
Eel River	At Scotia	8 060	6.49	0.37§	1975–80
Dry Creek	At Russian River	420	0.28	0.20§	1975–81
Central Valley					
Sacramento River	Lake Shasta	16 630	7.57	0.119†	
Cottonwood Creek	At Cottonwood	2 400	0.75	0.116††	1956–67
Stony Creek	Black Butte Reservoir	1 910	0.55	0.100††	1957–62
Feather River	Lake Oroville	7 810	5.16	0.052‡‡	1902–62
American River	Folsom Lake	4 820	3.34	0.181†	
Cosumnes River	At McConnell	1 880	0.46	0.0288§§	1900–66

*Source: USGS Water-Data Repts. CA-81-2, CA-81-3, CA-81-4
†Reservoir design value: source: US Bureau of Reclamation, Denver, Colo., period of record not given
‡USGS Water-Resources Investigation 26-75
§USGS Water-Data Repts. CA-75-2 through CA-81-2
**USGS Water-Supply Paper 1986 (1971)
††USGS Water-Supply Paper 1798-J (1972)
‡‡USGS Water-Resources Investigation 78-20
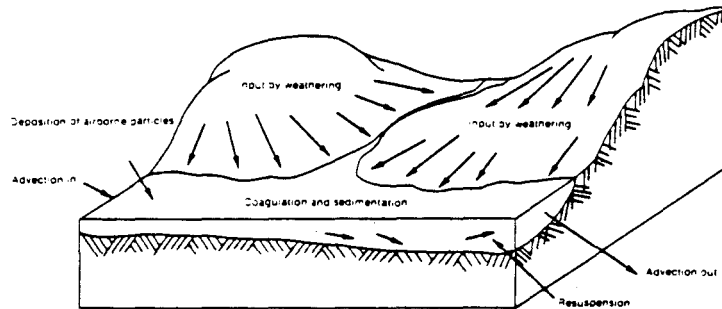§§USGS Water-Resources Investigation 80-64

Figure 3. Mass-balance model showing transport of chrysotile particles in natural waters

bers/mg (average fiber size 0.05-0.1-μm diameter, 0.5-1.0-μm length, and specific gravity of 2.6) and the flow volumes given in Table 1.

Coagulation. Coagulation removal is estimated by using Eq 4 and the detention times (Table 1) for upstream reservoirs. Short-circuiting of flow into and out of a reservoir results in less than the estimated removal. Coagulation may also be less if particles are not as fully destabilized as assumed ($\alpha < 0.001$).

The resulting fiber concentrations are also shown in Table 3. For the uncertainties noted above, the input of fibers by weathering should be within a factor of five at the values stated. Results from the AIHL monitoring program for surface waters for which fiber concentrations could be predicted are summarized in Table 3.[25] Overall, estimates are at least 10 times higher than observations. Higher predicted values suggest that weathering estimates are too high, coagulation estimates are too low, or both.

The only reservoir for which comparable upstream and downstream values are available is Lake Oroville. Two sets of four grab samples—three above the reservoir and one below—showed little difference between upstream and downstream fiber concentrations. The first set was taken during spring runoff in early May 1983 and the second in August 1983. Total particles in the 2-100-μm range were also similar. This suggests that removal of fibers by coagulation in upstream reservoirs is small.

Fiber concentrations in water delivered through the California Aqueduct to Metropolitan are reduced three to four orders of magnitude by coagulation in source-water reservoirs, by filtration, and, in some cases, by dilution with Colorado River water (Figure 7). Further dilution, with local groundwater, occurs in distribution pipelines and reservoirs.

Observed removals in reservoirs, shown in Table 4 and Figure 8, agree well with the predicted experimental
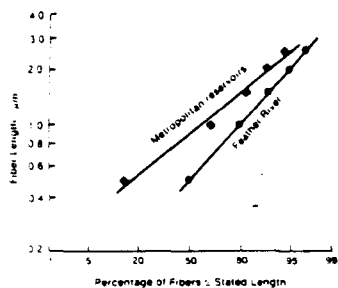
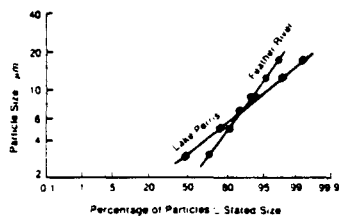**Figure 4.** Distribution by size of chrysotile fibers in natural waters

Figure 5. Distribution by size of particles in the 2-40-μm range *(particle-size instrument with multichannel capability was used for analysis; points are average counts of 8 samples from the Feather River and 15 samples from Lake Perris)*
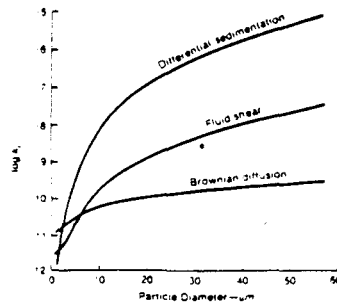
Figure 6. Rate constants for coagulation of chrysotile fibers (0.05-μm diameter, 0.5-μm length) with larger spherical particles in water with low fluid shear and high density *(k, in cm^3/s; water temperature = 20°C; G = 1 s^{-1}; ρ_p = 2.6 g/cm^3; calculated after Hunt[15] and O'Melia[26])*
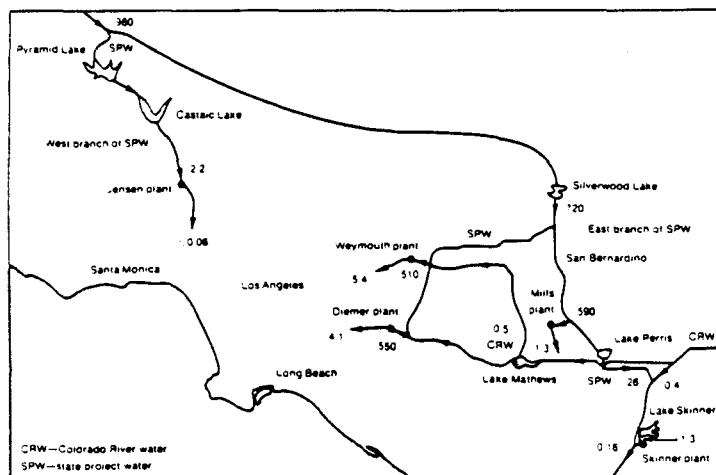
Figure 7. Concentrations of asbestos fibers in source-water reservoirs and filtration plants of The Metropolitan Water District of Southern California *(fiber concentrations given in 10^6 fibers/L)*
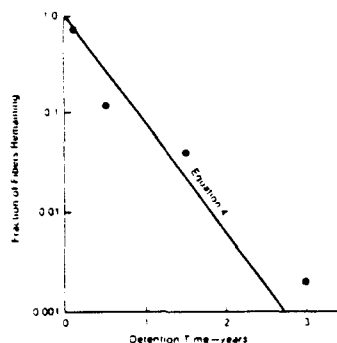
Figure 8. Predicted and actual fiber removal in reservoirs *(data points from Table 4)*

relationship (Eq 4). A coagulation efficiency (α) of 0.001 characterizes these observations for the coagulation rate constants of Figure 6 and the particle-size distribution of Figure 5. One possible explanation for the deviation between observed and predicted removal is that the number of larger particles available to coagulate with fibers changes seasonally owing to runoff and decreases with time owing to sedimentation. However, both the total number (10^7/L) and the size distribution (log-normal) of 2-100-μm particles in Lake Perris influent and effluent remain fairly constant throughout the year (Figure 5). Variations of fiber concentrations and total 2-100-μm-particle concentrations with depth in Lake Silverwood were noted previously.[28] These limited observations do not provide a sufficient basis for suggesting a depth-dependent coagulation model. Dissolution is another factor that may cause some reduction in fiber concentrations in reservoirs with

detention times of several years. Measured dissolution rates indicate that it takes 5-10 years to completely dissolve fibers suspended in water at pH 8.[29] Therefore, size reduction of most fibers and dissolution of only the small fiber fragments are expected in the waters studied in this research.

Fiber concentrations in waters entering and leaving the reservoirs follow a log-normal distribution (Figure 9). Geometric means are shown in Figure 7 and in Table 5 when sufficient data exist. In other cases, the median is used. For Lake Perris, the median and geometric mean differ by about 7 and 32 percent for effluent and influent, respectively.

Treatment plant. Fiber removal in water treatment plants, determined from the ratio of influent to effluent concentrations, ranged from near 0 to more than 99.9 percent (Figure 10). Three plants showed mean removals of approximately 99 percent; one had nearly 99.9 percent removal (Table 5). Model predictions

suggest that removals ≥99.9 percent can only be achieved as a result of significant coagulation of fibers with larger floc either before or during filtration. The lower removals may correspond to less effective coagulation. Over the two-year period of the study, the plants were operated for optimum turbidity removal, with an objective of 0.1 ntu for the finished water. Limited sampling prior to this period indicated that better fiber removal was often, but not always, associated with the optimized conditions.[28]

Conclusions

Weathering. Input of chrysotile fibers by weathering results in concentrations of from 10^{10} to 10^{12} fibers/L in upstream rivers and reservoirs (Table 6). Coagulation in upstream reservoirs should reduce that fiber concentration by one to three orders of magnitude, depending on detention time. Fiber levels observed in the Feather, American, and nearby rivers are from 30 to 100 times lower than

TABLE 3
Estimated and observed chrysotile fiber concentrations for selected river basins

River	Location	Estimated Input by Weathering			Estimated Removal by Coagulation percent	Estimated Concentration fibers·L	Observed Concentration fibers·L		Number of Observations
		metric tons/year	mg/L	fibers/L			Median	Range	
North Coast									
Trinity River	Clair Engle Lake	44 900	29.5	2.9×10^{12}	94.9	1×10^{11}			
Klamath River	At Orleans	72 400	10.1	1.0×10^{12}	0	1×10^{12}	2×10^{11}	7×10^{10}-3×10^{11}	4*
Eel River	Lake Pillsbury	990	2.1	2.1×10^{11}	44	1×10^{11}			
Russian River	At Guernyville	6 900	3.4	3.4×10^{11}	0	3×10^{11}			
Northern and western Sacramento Valley									
Sacramento River	Lake Shasta	24 000	3.2	3.2×10^{11}	84	5×10^{10}			
Stony Creek	Black Butte Reservoir	2 000	3.7	3.7×10^{11}	54	2×10^{11}			
Cache Creek	Clear Lake	360	1.2	1.2×10^{11}	95.8	5×10^{7}			
Putah Creek	Lake Berryessa	4 100	9.0	9.0×10^{11}	>99.9	9×10^{8}	3×10^{10}		1*
Eastern Sacramento–San Joaquin Valley									
Feather River	Lake Oroville	3 700	0.71	7.1×10^{10}	80	1×10^{10}	3×10^{8}	2×10^{8}-4×10^{8}	3‡
North Yuba River	New Bullards Reservoir	500	0.90	4.0×10^{10}	83	7×10^{9}	1×10^{8}		1§
Bear River	New Camp Far West Reservoir	290	0.71	7.1×10^{10}	53	3×10^{10}	1×10^{9}		1**
American River	Folsom Reservoir	1 900	0.57	5.7×10^{10}	61	2×10^{10}	2×10^{8}	5×10^{7}-6×10^{9}	5**
Mokelumne River	Pardee Reservoir	200	0.20	2.0×10^{10}	58	1×10^{10}	3×10^{7}		1‡‡

*Various samples taken near Ukonom ranger station. April 1982
**Water treatment plant raw water. April 1982
‡Below Lake Oroville. September 1982. May 1983. and August 1983
§At Marysville. September 1982
**At Highway 70. April 1982
**Various samples taken below Folsom Reservoir. December 1980–January 1982
‡‡Mokelumne Aqueduct. March 1982; fiber removal may occur between reservoir and sampling point.

TABLE 4
Fiber removal in downstream source-water reservoirs

Reservoir	Volume km³	Detention Time year	Concentration of Fibers* 10^6 fibers·L		Number of Observations†	Removal of Fibers‡ percent	
			Influent	Effluent		Observed	Predicted§
Lake Pyramid–Castaic**	0.83	3.0	980 (500–1900)	2.2 (0.19–45)	3. 16	99.8	99.9
Lake Silverwood	0.096	0.1	980 (500–1900)	720 (210–1700)	3. 14	27	22
Lake Perris	0.15	1.5	720 (210–1700)	26 (3.2–150)	14. 15	96	97.7
Lake Skinner	0.055	0.5	26 (3.2–150)	3.1** (≤1.5–30)	15. 16	88	72

*Upper value is geometric mean. range is in parentheses.
†Influent. effluent. for Lake Perris and Lake Skinner. influent and effluent were sampled on same day
‡Based on geometric mean of influent and effluent
§From Eq 4
**Considered as a single unit because water is periodically pumped from Castaic to Pyramid
**Calculated values. corrected for dilution with Colorado River water

predicted. This difference could be due to either lower-than-predicted inputs or greater-than-predicted coagulation. Single samples taken in these rivers. above the reservoirs. showed concentrations approximately 100 times lower than predicted. suggesting that weathering estimates are too high. The weathering model may thus provide only a relative estimate of concentrations in these rivers. Insufficient data are available to draw conclusions about predictions in other areas. Some of this difference could be due to uncertainty in the fiber counts. The precision of analysis is

35–65 percent;[5] accuracy is thought to be within an order of magnitude for the lower counts in natural waters.

The prediction of input of fibers by weathering could be improved by focusing on the field monitoring of upstream rivers at a few representative locations. Intensive sampling of this sort would allow the use of the relative model estimates to establish order-of-magnitude concentrations for other surface waters. These order-of-magnitude estimates would provide a level of certainty commensurate with a more extensive but less frequent field-monitoring program.

Coagulation. Improvements in the coagulation portion of the model for upstream waters are possible in three areas. First. coagulation of all particle sizes could be considered. rather than assuming that larger particles are in steady state. Second. measurement of α values for submicron-sized particles in well-characterized systems is needed to reinforce the value observed here ($\alpha = 0.001$). Third. field sampling and laboratory analyses to determine the identity. size. and surface properties of suspended particles would improve knowledge of actual reservoir conditions. As more

TABLE 5

Fiber removal in water treatment plants

| Facility | Concentration of Fibers*—10^6 fibers/L | | Removal of Fibers percent |
	Influent	Effluent	
Jensen	2.2 (0.19-45)	≤0.06⁺ (≤0.057-5.6)	≥97.7‡
Weymouth	510 (27-1300)	5.4 (0.37-31)	99.0
Diemer	550 (150-1300)	4.1 (0.14-200)	99.2
Mills	590 (230-1900)	1.3 (0.11-58)	99.8
Skinner	1.3 (≤0.11-8.8)	≤0.16⁺ (≤0.071-2.3)	≥86‡

*Upper value is geometric mean, or median where noted. of 14 or 15 observations. range is in parentheses.
⁺Median lies at or below this detection limit.
‡Median at or above this value. some effluent samples were below detection limit.

TABLE 6

Predicted and observed fiber concentrations

| Sampling Location | Concentration of Fibers in Water Leaving Sampling Location* fibers/L | |
	Predicted	Observed
North-coast rivers	10^{11}-10^{12}	10^{11}
Northern and western Sacramento Valley rivers	10^9-10^{11}	10^{10}
Eastern Sacramento Valley rivers	10^6-10^{10}	10^6-10^7
Eastern San Joaquin Valley rivers	0-10^4	10^2
Delta pumping plants	10^6-10^{10}	10^6-10^7
California Aqueduct	10^6-10^{10}	10^6
Metropolitan source water	10^6-10^4	10^3-10^4
Metropolitan water treatment plants	10^3-10^4	10^3-10^4

*The range of values reported reflects both variability between different locations and times and uncertainty in the precision and accuracy of fiber analyses.
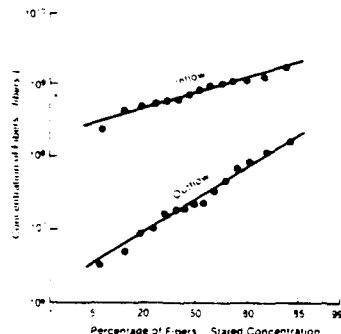

Figure 9. Distribution of observed fiber concentrations in Lake Perris
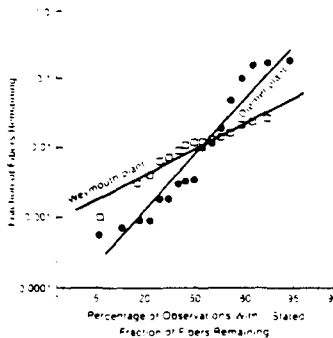

Figure 10. Distribution of observed fiber removal in water treatment plants

research is carried out, it is possible that chrysotile could be used as an indicator of the behavior of other mineral particles.

Fiber concentrations increase approximately fourfold as water passes through the California Aqueduct. However, most fibers are later removed by coagulation with larger particles and subsequent sedimentation in downstream source-water reservoirs. Residence times of about one year result in an almost 10-fold reduction in fiber concentration; longer residence times, about three years, result in a 1000-fold reduction.

Treatment plant. Water treatment

plants that are designed for turbidity removal consistently achieved about 99 percent fiber removal by a combination of coagulation and filtration. Higher removals, ≥99.9 perent, were observed in only a few cases, which represent enhanced coagulation before or during filtration. The filtration model was used only to estimate the range of removals possible, as it fails to capture the physical nucleation and coagulation processes that accompany deposition of particles onto sand grains. However, it does illustrate the importance of coagulation in removing submicron-sized asbestos fib-

ers during filtration. To design operating conditions for the removal of submicron-sized chrysotile fibers during filtration, three levels of investigation are needed—laboratory-scale, pilot-scale, and full-scale. Questions such as the efficiency and means of fiber capture in coagulant floc and the deposition of fibers on filter media for various chemical and physical conditions could be addressed by a program of research integrated with field-testing and monitoring.

References

1. CLARK, L.D. Foothills Fault System, Western Sierra Nevada, California. *Bull. Geol. Soc. Amer.*, 71:483 (1960).
2. IRWIN, W.P. Geology of the Klamath Mountains Province. *Bull. Calif. Div. Mines Geol.*, 190:19 (1966).
3. WICKS, F.S. Mineralogy, Chemistry and Crystallography of Chrysotile Asbestos. *Short Course in Mineralogical Techniques of Asbestos Determination*. Sect. 1, Part B, 4:35. Mineral. Assoc. Canada (1979).
4. VEBLEN, D.R. & BUSECK, R. Serpentine Minerals: Intergrowths and New Combination Structures. *Science*, 206:1398 (1979).
5. MUMPTON, F.A. & THOMPSON, C.S. Mineralogy and Origin of the Coalinga Asbestos Deposit. *Clays & Clay Minerals*, 23:131 (1975).
6. COLEMAN, R.G. Petrologic and Geophysical Nature of Serpentinites. *Bull. Geol. Soc. Amer.*, 82:897 (1971).
7. ALBERS, J.P. Economic Deposits of the Klamath Mountains. *Bull. Calif. Div. Mines Geol.*, 190:51 (1966).
8. SPRINGER, R.K. Contact Metamorphosed Ultramafic Rocks in the Western Sierra Nevada Foothills, California. *Jour. Petrol.*, 15:160 (1974).
9. OLMSTED, F.A. Pre-Cenozic Geology of the Southern Half of the Auburn 15-Minute Quadrangle. California. Bull. 1341. USGS. Washington, D.C. (1971).
10. MOODY, J.B. Serpentinization: A Review. *Lithos*, 9:125 (1976).
11. EVANS, B.W. Metamorphism of Alpine Peridotite and Serpentinite. *Ann. Rev. Earth Planetary Sci.*, 5:397 (1977).
12. RICE, S.J. Asbestos. *Bull. Calif. Div. Mines Geol.*, 176:49 (1957).
13. WIEBELT, F.J. & SMITH, C.M. A Reconnaissance of Asbestos Deposits in the Serpentine Belt of Northern California. Information Circular 7860. US Bureau of Mines. Washington, D.C. (1959).
14. WICKS, F.J. Introduction: Serpentine

Mineralogy, Petrology and Paragenesis Symposium. *Canadian Mineralogist,* 17:673 (1979).

15. HUNT, J.R. Coagulation in Continuous Particle Size Distributions: Theory and Experimental Verification. Rept. AC-5-80. W.M. Keck Lab. Envir. Engrg. Sci., Calif. Inst. Technol., Pasadena, Calif. (1980).

16. VALIOULIS, I.A. Particle Collisions and Coalescence in Fluids. Rept. KH-R-44. W.M. Keck Lab. Hydr. & Water Resources. Calif. Inst. Technol., Pasadena, Calif. (1983).

17. BIRKNER, F.B. & MORGAN, J.J. Polymer Flocculation Kinetics of Dilute Colloidal Suspensions. *Jour. AWWA,* 60:175 (1968).

18. HAHN, H.H. & STUMM, W.J. Kinetics of Coagulation with Hydrolyzed Al(III). *Jour. Colloid Interface Sci.,* 28:134 (1968).

19. EDZWALD, J.K.; UPCHURCH, J.B.; & O'MELIA, C.R. Coagulation in Estuaries. *Envir. Sci. & Technol.,* 8:58 (1974).

20. GIBBS, R.J. Effect of Natural Organic Coatings on the Coagulation of Particles. *Envir. Sci. & Technol.,* 17:237 (1983).

21. EPPLER, B.; NEIS, U.; & HAHN, H.H. Engineering Aspects of the Coagulation of Colloidal Particles in Natural Waters.

Progr. Water Technol., 7:2:207 (1975).

22. STUMM, W. Chemical Interaction in Particle Separation. *Envir. Sci. & Technol.,* 11:1066 (1977).

23. McGUIRE, M.G.; BOWERS, A.E.; & BOWERS, D.A. Asbestos Analysis Case History: Surface-Water Supplies in Southern California. *Jour. AWWA,* 74:471 (1982).

24. FARRELL, C. & QUALLEY, G. Evaluation of Sediment-Removal Project. Calif. Dept. of Water Resources Internal Rept. (Dec. 1982).

25. HAYWARD, S.B. Field Monitoring of Chrysotile Asbestos in California Waters. *Jour. AWWA,* 76:3:66 (Mar. 1984).

26. O'MELIA, C.R. Aquasols: The Behavior of Small Particles in Aquatic Systems. *Envir. Sci. & Technol.,* 14:1052 (1980).

27. YAO, K.; HABIBIAN, M.T.; & O'MELIA, C.R. Water and Wastewater Filtration: Concepts and Applications. *Envir. Sci. & Technol.,* 5:1105 (1971).

28. McGUIRE, M.J.; BOWERS, A.E.; & BOWERS, D.A. Optimizing Large-Scale Water Treatment Plants for Asbestos-Fiber Removal. *Jour. AWWA,* 75:7:364 (July 1983).

29. BALES, R.C. & MORGAN, J.J. Surface Chemistry of Chrysotile Asbestos in Natural Waters. Proc. AWWA Ann. Conf. Las Vegas, Nev. (1983).

About the authors: *Roger C. Bales* is a graduate research assistant in the Department of Environmental Engineering Science, California Institute of Technology, Pasadena, CA 91125. For the past four years he has conducted research on surface chemistry in natural water systems, with emphasis on the chemical and physical behavior of chrysotile asbestos. Bales was a water quality engineer at Brown and Caldwell for five years. Dale D. Newkirk is a water purification engineer with The Metropolitan Water District of Southern California, 700 N. Moreno Ave., La Verne, Calif. Steven B. Hayward is a research specialist and microscopy unit supervisor at the Air and Industrial Hygiene Laboratory, California Department of Health Services, 2151 Berkeley Way, Berkeley, Calif.*

*To whom correspondence should be addressed